Wall Teichoic Acid Glycosylation of *Staphylococcus epidermidis* and the Interaction of *Staphylococci* with the Human Host

Dissertation

der Mathematisch-Naturwissenschaftlichen Fakultät

der Eberhard Karls Universität Tübingen

zur Erlangung des Grades eines

Doktors der Naturwissenschaften

(Dr. rer. nat.)

vorgelegt von

Christian Roland Beck

aus Stuttgart

Tübingen

2023

Gedruckt mit Genehmigung der Mathematisch-Naturwissenschaftlichen Fakultät der Eberhard Karls Universität Tübingen.

Tag der mündlichen Qualifikation:	07.11.2023
Dekan:	Prof. Dr. Thilo Stehle
1. Berichterstatter/-in:	Prof. Dr. Andreas Peschel
2. Berichterstatter/-in:	Prof. Dr. Christiane Wolz

Table of contents

Abstract

Staphylococcus epidermidis colonizes the human skin microbiome of healthy individuals, but due to its ability to produce biofilms and to acquire antibiotic resistances, it can become an opportunistic pathogen and a frequent cause of foreign body related infections (FBRIs). As for most coagulase-negative *Staphylococci* (CoNS), *S. epidermidis* wall teichoic acid is composed of a long chain of glycerol-phosphate (GroP) repeating units linked to the cell wall peptidoglycan. While *Staphylococcus aureus* ribitol-phospate (RboP) wall teichoic acid (WTA) is glycosylated with n-acetylglucosamine (GlcNAc) and was shown to be involved in several cellular functions, including cell separation, binding to endothelial cells and immune activation, the composition and function of GroP-WTA is less well understood. We analyzed the WTA of *S. epidermidis* in detail and confirmed that GroP-WTA of *S. epidermidis* is mainly glycosylated with glucose by an enzyme with similarity to *Bacillus subtilis* TagE. This glucose residue determines the binding pattern of different types of bacteriophages, increasing adsorption of siphoviruses, while decreasing adsorption of podoviruses to the *S. epidermidis* host. We demonstrate that the presence of *tagE* in different CoNS determines horizontal gene transfer by *Rockefellervirus* ΦE72 and show that rare expression of *S. aureus* type RboP-WTA in *S. epidermidis* sequence type (ST) 23 can prevent binding of this phage. Additionally, we show that this RboP-WTA in *S. epidermidis* ST23 is also glycosylated with glucose by the enzyme TarM(*S.e.*) in a processive manner. As opposed to glycosylation with GlcNAc, glucose modified RboP-WTA shows reduced binding of human IgG and helps *S. epidermidis* to evade the immune system. Priming of neutrophils with acetate via the GPR43 receptor increases the immune response and inhibition of the ATP synthase sensitizes *S. aureus* towards antimicrobial peptides expressed by neutrophils and keratinocytes. Additionally, *S. aureus* releases pro-inflammatory membrane vesicles containing phenol soluble modulins (PSMs) and lipoproteins, which can activate formyl peptide receptors (FPRs) and toll-like receptors (TLRs), leading to increased neutrophil phagocytosis and cytokine release. Wall teichoic acid modulates the immune response as an important antigen and is the only described receptor for staphylococcal bacteriophages employed in phage therapy approaches. Understanding the wall teichoic acid of all potentially pathogenic CoNS is essential for treatment of infections with drug resistant *Staphylococci.*

Zusammenfassung

Staphylococcus epidermidis ist ein Kommensale der normalen Hautflora, kann aber aufgrund seiner Fähigkeit Biofilme zu bilden und Antibiotikaresistenzen zu erwerben, medizinische Fremdkörper besiedeln, und somit schwer behandelbare Infektionen verursachen. Wie bei den meisten Koagulase-negativen Staphylokokken (KNS) besteht die Zellwand gebundene Teichonsäure, die Wandteichonsäure (WTA), bei *S. epidermidis* aus einer langen Kette von Glycerol-Phosphat (GroP) Einheiten, während die WTA von *Staphylococcus aureus* in der Regel aus Ribitol-Phosphat (RboP) Einheiten besteht, welche mit n-Acetylglucosamin (GlcNAc) glykosyliert sind. Diese RboP-WTA ist an mehreren zellulären Funktionen beteiligt, darunter der Zellteilung, der Bindung an Endothelzellen und der Aktivierung des Immunsystems. Im Gegensatz dazu, ist die Zusammensetzung und Funktion der GroP-WTA von KNS weit weniger gut bekannt. In unserer vorgelegten Forschung zeigen wir, dass die WTA von *S. epidermidis* hauptsächlich mit Glukose durch ein Enzym glykosyliert wird, das Ähnlichkeit mit *Bacillus subtilis* TagE aufweist. Diese Modifikation mit Glukose bestimmt das Bindungsmuster verschiedener Gruppen von Bakteriophagen, wobei die Adsorption von Siphoviren an *S. epidermidis* erhöht, aber die Adsorption von Podoviren an *S. epidermidis* verringert wird. Expression von Genen mit Homologie zu TagE in verschiedenen KNS bestimmt ob horizontaler Gentransfer durch *Rockefellervirus* ΦE72 stattfinden kann, und die Expression von RboP-WTA in *S. epidermidis* Sequenztyp (ST) 23 kann die Bindung dieses Phagen blockieren. Darüber hinaus zeigen wir, dass diese RboP-WTA in *S. epidermidis* ST23 durch das Enzym TarM(*S.e.*) prozessiv mit Glukose glykosyliert wird. Im Gegensatz zur WTA-Glykosylierung mit GlcNAc, wird Glukose-modifizierte WTA schlechter durch humanes Serum-IgG gebunden, wodurch eine Erkennung von *S. epidermidis* durch das Immunsystem verhindert wird. Eine Voraktivierung von Neutrophilen mittels Stimulation des GPR43 Rezeptors mit Acetat verstärkt die Effektorfunktionen von Neutrophilen und eine Inhibition der ATP-Synthase verstärkt die Wirkung von antimikrobiellen Peptiden, die von Neurophilen und Keratinozyten freigesetzt werden. Zudem setzt *S. aureus* pro-inflammatorische Membranvesikel frei, die Phenol-lösliche Moduline (PSMs) und Lipoproteine beinhalten, wodurch Formylpeptid-Rezeptoren (FPRs) und Toll-like Rezeptoren (TLRs) aktiviert werden. Dies führt zu einer erhöhten Freisetzung von Zytokinen und einer erhöhten Phagozytose durch Neutrophile. Da die WTA ein wichtiges Antigen für menschliche oder rekombinante

Antikörper, und der einzig beschriebene Rezeptor für Staphylokokken-infizierende Bakteriophagen ist, ist das Verständnis der WTA aller potenziell pathogener KNS für die Phagen-Therapie und die Behandlung von Infektionen durch arzneimittelresistente Staphylokokken von wesentlicher Bedeutung.

Chapter 1

General introduction

Staphylococcus epidermidis

With approximately 30 m^2 of total surface area, skin offers one of the largest habitats for microorganisms with both follicular and interfollicular niches(1). It is colonized by a diverse set of microorganisms, among which bacteria are most frequent, and *Propionibacteria*, *Corynebacteria* and *Staphylococci* are representing the most abundant genera (2, 3). At the species level, one of the most common skin colonizers is *Staphylococcus epidermidis,* a coagulase-negative Staphylococcus (CoNS) with the ability to colonize most skin sites and a tendency for moist areas (2-6). While *Staphylococcus aureus* has long been described as a highly pathogenic, invasive cause of soft tissue infection, endocarditis and sepsis, CoNS were usually described as rather beneficial members of the skin microbiome. But many CoNS can become hospital-associated, especially in case of immunocompromised or chronically ill patients (5). Infections associated with medical devices are a large problem in the clinical environment, and *S. epidermidis* is the major cause of foreign body-related infections (FBRIs) (5, 7). The major invasive *S. epidermidis* clones seem to pursue two different virulence strategies. The sequence type 2 (ST2) strains are particularly strong biofilm formers (8). In contrast, ST10, ST23, and ST87 clones are only week biofilm formers but express an additional surface molecule that alters their host interaction capacities and leads to a shift from commensal to pathogen behavior (9). The biofilm producers either rely on the *icaADBC* locus for production of the exopolysaccharide polysaccharide intercellular adhesin (PIA) or on polysaccharide-independent biofilm formation, which protects them from desiccation, antibiotics, or components of the immune system (7). Interestingly, a wall teichoic acid (WTA) deletion mutant was reported to have decreased biofilm formation (10). For *ica*-negative biofilm formation, the accumulation associated protein (Aap) seems to be important due to its ability to polymerize and form fibrils, in addition to being a cell-wall bound adhesin important for binding to corneocytes (4).

In addition, *S. epidermidis* expresses several other adhesins like the microbial surface components recognizing adhesive matrix molecules (MSCRAMMs), represented by the keratin and type I collagen binding SdrF, and the fibrinogen binding SdrG (4). The bifunctional lipase GehD was also reported to bind collagen, and the autolysin AtlE was described to bind vitronectin (4, 11). In addition, Embp, a giant surface protein of *S. epidermidis,* and teichoic acids, were reported to be involved in binding of fibronectin (4, 12). But no teichoic acid (TA) modification mutants were used, and only crude TA isolation was performed, without distinguishing between wall teichoic acid (WTA) and lipoteichoic acid (LTA) (12). Furthermore, old studies using *S. aureus* and its TA, reported similar binding to fibronectin (13), while experiments with a WTA knockout mutant could not show any effect on fibronectin binding, but instead discovered WTA dependent binding to human endothelial cells (14).

Wall teichoic acid of *Staphylococci*

Teichoic acids are long chains of alditol-phosphates, either linked to the peptidoglycan as wall teichoic acids (WTA), or membrane anchored as lipoteichoic acids (LTA), and mostly modified by different sugars and D-alanine. While *S. aureus* type WTA usually consist of ribitol-phosphate (RboP) repeating units, both the WTA and the LTA of most *S. epidermidis* strains are formed of glycerol-phosphate (GroP) repeating units (15). But many variations in different strains exist. The *S. epidermidis* multi-locus sequence types (ST) 10, 23 and 87 were shown to express *S. aureus* type poly(RboP)-WTA in addition to poly(GroP)-WTA (9), while *S. aureus* ST395 expresses an unusual poly(GroP)-WTA modified with n-acetylgalactosamine (GalNac) (16, 17). *Bacillus subtilis* 168 expresses a major WTA built of GroP repeating units, equivalent to the WTA of CoNS, but also a minor WTA composed of glucosyl-N-acetylgalactosamine 1-phosphate (GlcGalNAcP) repeating units (18, 19). In contrast, *B. subtilis* strain W23 expresses a poly(RboP)-WTA similar to most *S.aureus* (20, 21), but while *S. aureus* glycosylates its poly(RboP)-WTA with n-acetylglucosamine (GlcNac) either in β1,4-, β1,3- or α1,4-confirmation by the glycosyltransferases TarS, TarP or TarM (22-26), respectively, *B. subtilis* W23 uses the TarQ enzyme to attach β-glucose to the RboP (26). *B. subtilis* strain 168 instead uses the TagE enzyme to glycosylate its major GroP-WTA with α-glucose, using UDP-glucose as precursor substrate (27, 28). The WTA modifications of *S.*

epidermidis and other CoNS have not been studied in detail but were suggested to contain GlcNac or glucose modified poly-(GroP) with rare exceptions like *Staphylococcus saprophyticus* and *Staphylococcus xylosus* expressing RboP-WTA (15). Still, no enzymes have been identified, and further analysis of the WTA composition of CoNS (like *S. epidermidis*) is needed, since WTA fulfills several important biological functions.

WTA is important for normal cell growth, septum formation during cell separation, and autolysis (26, 29-31), but also interacts with several effectors of the human immune system. Binding to scavenger receptor SREC-1 was recently shown to increase adhesion of *S. aureus* to the epithelium, while it is also involved in binding to the human C-type lectin receptor langerin on Langerhans cells (LC) and the macrophage galactose-type lectin (MGL) on monocyte-derived dendritic cells (32, 33). In addition, WTA is bound by soluble serum components, mostly by immunoglobulins and lectins such as the mannose-binding lectin (MBL), thereby increasing the effector functions of several immune cells (32, 34-36).

Bacteriophage nomenclature, morphology, and isolation source

WTA also functions as the only known host receptor for bacteriophages infecting *Staphylococci* (32). Historically, most staphylococcal bacteriophages were grouped according to morphological criteria into three main groups belonging to the order of *Caudovirales* (37). The myovirus-morphology group with a contractile tail and a genome size of more than 120 kb, the short-tailed podovirus-morphology with below 20 kb genomes, and the long-tailed siphovirus-morphology with ca. 40 kb or 90 kb genomes (38, 39). This system has recently been revised, and the morphology-based families belonging to the order *Caudovirales* have been replaced by the order *Caudoviricetes* to contain all tailed bacterial and archaeal viruses with icosahedral capsids and double-stranded DNA, with *Staphylococcal* myoviruses now forming part of the *Herelleviridae* family (40-42). But since the new phylogeny proposed by the International Committee on Taxonomy of Viruses (ICTV) remains incomplete and was only introduced recently, use of the morphological identifiers podovirus, myovirus and siphovirus as non-taxonomic units remains acceptable (40).

Staphylococcal phages were additionally clustered into 4 major groups according to average nucleotide identity (ANI), and average shared gene content determined by

protein phamily (pham) membership (39). They cluster like their morphological groups into cluster A podoviruses, cluster C myoviruses and cluster B and D siphoviruses, with cluster B comprising the abundant, lysogenic group with 39-48 kb genomes, while cluster D comprises rare lytic siphoviruses with approximately 90 kb genomes (39).

The NCBI Virus Resource Database hosted by the National Center for Biotechnology Information (NCBI) listed 753 bacteriophage sequences in the nucleotide database to infect Staphylococci (43-45) (by 15.09.2023). Of these bacteriophages, most were assigned to use *S. aureus* as host species, in contrast to only 63 infecting *S. epidermidis.* Genomic data on phages infecting other CoNS including *Staphylococcus pseudintermedius* (35 genomes) and *Staphylococcus carnosus* (22 genomes) is even more scarce (43-45). More Staphylococcal phages have been isolated, but the sequences have not yet been deposited in the Virus Resource Database. A collection of the phages with available genomic data, and which are assigned to *S. epidermidis,* or which use *S. epidermidis* as the primary host, are shown in Table 1. Only 8 sequenced phages with podovirus morphology are available (blue), while 33 sequenced phages likely have siphovirus morphology (green) and 18 have myovirus morphology (orange). 4 phage sequences cannot be clearly assigned since they were not analyzed in detail, lack annotation, and show unusual sequence length (grey). Interestingly, the genera of the phages fit to the clusters according to ANI and pham membership as assigned by Oliveira, et al. (39). Cluster A is represented by the *Andhraviridae*, cluster B by *Rockefellerviridae*, cluster C by *Sepunaviridae*, and cluster D by *Sextaecviridae* (Table 1). Of the phages, to which an isolation source can be clearly assigned, most were isolated from wastewater, some from the skin and few from the nares (Table 1). Siphoviruses were additionally acquired by prophage induction, mostly from clinical *S. epidermidis* isolates (Table 1). Additionally, siphoviruses can be grouped into main integrase types, since integrases are well conserved and allow prediction of the chromosomal location of prophages (46). For the *S. epidermidis* siphoviruses, three main integrase types can be identified, here named according to one important representative of each group (ΦE72, ΦIPLA5, ΦSEP9; Table 1). For some siphoviruses, the integrases did not cluster with these three groups and were therefore assigned to individual types (Table 1). ΦE72-type integrases have about 50% amino acid identity compared to Sa7 integrases of *S. aureus* phages, while ΦIPLA5-type integrases have about

70% amino acid identity compared to Sa9 integrases of *S. aureus* phages. No homology to *S. aureus* phage integrases could be found for the ΦSEP9-type integrases. Surprisingly, even though this integrase type is frequently present in *Sextaecviridae*, the well described representatives of this integrase type seem to be unable to lysogenize (47, 48). Furthermore, cluster B siphoviruses with similarity to Lacachita seem to lack an integrase altogether (49, 50), but Andrews, et al. (49) claim that phage Lacachita might be maintained within its host as extrachromosomal plasmid prophage.

Host range of *S. epidermidis* infecting bacteriophages

Even though phages are often species or even strain specific, some phages infect several closely related species, which makes it difficult to clearly assign a phage to a specific host (51). Especially myoviruses have a broad host range, infecting both CoPS and CoNS, which is particularly well understood for the bacteriophages K and ISP (52-54). A recent study on 94 staphylococcal bacteriophages isolated from wastewater, showed that 90 phages replicated on more than one of 117 staphylococcal strains from 29 species, and by average every phage infected 7.8 different species (51). Myoviruses were able to replicate by average on 9.8 of the tested staphylococcal species, while siphoviruses were only able to replicate by average on 2.5 species including both cluster B and D siphoviruses (51). Another study investigated 5 related cluster B siphoviruses formerly belonging to the genus *Phietavirus* but now grouped in the genus *Rockefellervirus*. These phages were only analyzed for infection of different *S. epidermidis* strains, of which between 17% and 34% were infected depending on the phage (55). Cluster D siphoviruses seem to have a slightly broader host range than cluster B siphoviruses (51, 56).

The host range of staphylococcal podoviruses is not well defined. One study isolated 6 *S. epidermidis* specific phages from the human skin microbiome, one of which being a podovirus (56). This podovirus (vB_SepP_BE03) only replicated in one of 44 tested *S. epidermidis* strains, but replicated on 4 of 10 different *S. capitis* and 2 of 3 different *S. caprae* isolates (56). Nonetheless, compared to the tested myoviruses, it showed a rather small host range, especially for the different *S. epidermidis* strains (56). Interestingly, none of the *S. epidermidis* infecting myoviruses analyzed in this study was able to also infect *S. aureus,* possibly showing a specificity for GroP-WTA (56). Less than 10 *S. epidermidis* specific podoviruses have been isolated and

published up to now, with phage Andhra of the *Rountreeviridae* family being the first and most well studied representative (57, 58). Of the 9 analyzed Staphylococci, including 3 *S. epidermidis* strains, podovirus Andhra only infected *S. epidermidis* RP62A (57). Interestingly, when the receptor binding proteins (RBPs) of phage Andhra and two related *S. epidermidis* infecting podoviruses (JBug18 and Pontiff) were compared with three *S. aureus* infecting podoviruses (Pabna, 44AHJD, P68), high RBP sequence similarity within the *S. epidermidis* phages, but low sequence similarity between both groups was observed (58). The same was true for siphoviruses of *S. epidermidis* compared with *S. aureus* siphovirus 80α. While all *S. epidermidis* infecting *Rockefellerviruses* showed more than 97% identity of their RBPs, these RBPs exhibited only 25% identity to *S. aureus* infecting *Phietavirus* 80α. This strong conservation of RBPs within the *S. epidermidis* infecting phage group, and the low homology to *S. aureus* infecting phage RBPs, most likely developed due to the differences in the phage receptors (WTA) of *S. aureus* and S*. epidermidis*, even though the podoviruses of *S. aureus* and *S. epidermidis* share a very similar genome organization (58).

In *S. aureus*, mutation of the *tarM* gene result in loss of α-GlcNAc modified WTA which causes resistance and reduced adsorption of siphoviruses (22, 59), while podoviruses, except for some exceptions (60), depend on ß-GlcNAc modification of WTA, and complete absence of WTA results in resistance to all phages including myoviruses (22, 23). Very little research was done on bacteriophage receptors of CoNS. Holland et al reported a bacteriophage resistant WTA deletion mutant of *S. epidermidis*, but did not show the data in the publication (10). Based on results of enzymatic and chemical detachment of glucose from WTA, Schleifer et al. suspected WTA-glucose involvement in bacteriophage adsorption to *S. epidermidis* cells, but denied an independent receptor function of teichoic acids (61). Since phage therapy approaches are considered for CoNS, research on CoNS bacteriophage receptors is urgently needed.

Table 1: Bacteriophages infecting *S. epidermidis*. Most sequence data were recovered from the NCBI Virus resource database (44, 45). (Podophage (P), Siphophage (S), Myophage (M), Phage-like element (PLE), Prophage (PP), Phage-related island (PRI))

Accession-Number/DSM-Number	Staphylococcus phage	Morphology	Length (bp)	Genus	Isolation source	Integrase type	Reference
MT596500.1	vB_SepP_BE03	P	18271	Andhravirus	skin[2]	-	(56)
KY471386.1	St 134	P	18275	Andhravirus	unknown	-	-[14]
MZ152915.1	SeAlphi	P	18292	Andhravirus	unknown	-	-[14]
MH972262.1	Pontiff	P	18364	Andhravirus	wastewater	-	(62)
MH972261.1	Pike	P	18376	Andhravirus	wastewater	-	(62)
DSM 108058[17]	vB_SepP_UKE3	P	18476	unclassified	wastewater[11]	-	(63)
KY442063.1	Andhra	P	18546	Andhravirus	wastewater	-	(57, 62)
MH972263.1	JBug18	P	18547	Andhravirus	wastewater	-	(62)
CP018841.1	HOB 14.1.R1	PLE	18659	unclassified	not isolated[3]	ΦE72	(64)
MT880870.1	PhiSepi-HH1	PP	34053	unclassified	not isolated[4]	XerC	(65)
MT880871.1	PI-Sepi-HH2	PRI	36164	unclassified	not isolated[4]	XerD	(65)
KT429161.1	StB20-like	-	40670	unclassified	unknown	ΦIPLA5[12]	-[14]
JN192401.1	Ipla7	S	42123	Rockefellervirus	mastitis isolate[5]	ΦE72	(66, 67)
MZ417352.1	PG-2021_91	S	42188	Rockefellervirus	wastewater[6]	ΦIPLA5	(51)
KY653120.1	IME1348_01	-	42371	Rockefellervirus	unknown	ΦE72	-[14]
MW364972.1	vB_SepS_48	S	42460	Rockefellervirus	clinical isolate[7]	ΦE72[13]	(55)
MW364974.1	vB_SepS_459	S	42498	Rockefellervirus	clinical isolate[7]	ΦE72[13]	(55)
MT596498.1	vB_SepS_BE01	S	42718	Rockefellervirus	skin[2]	ΦIPLA5	(56)
OQ355704.1	vB_SepS_BE28	S[1]	42841	Rockefellervirus	skin	ΦIPLA5	-[14]
MW364971.1	vB_SepS_27	S	42935	Rockefellervirus	clinical isolate[8]	ΦE72[13]	(55)
MZ417349.1	PG-2021_89	S	43039	Rockefellervirus	wastewater[6]	ΦE72	(51)
MW364973.1	vB_SepS_456	S	43266	Rockefellervirus	clinical isolate[7]	ΦE72[13]	(55)
KU598975.1	CNPx	S	43293	Rockefellervirus	unknown	ΦE72	(68)
NC_008722.1	CNPH82	S	43420	Rockefellervirus	unknown	ΦE72	(69)
MZ417353.1	PG-2021_93	S	43459	Rockefellervirus	wastewater[6]	ΦE72	(51)
OQ355699.1	vB_SepS_BE20	S[1]	43521	Rockefellervirus	skin	ΦE72	-[14]
OQ355700.1	vB_SepS_BE21	S[1]	43563	Rockefellervirus	skin	ΦIPLA5	-[14]
JN192400.1	Ipla5	S	43581	Rockefellervirus	mastitis isolate[9]	ΦIPLA5	(66, 67)
NC_008723.1	PH15	S	44041	Rockefellervirus	unknown	ΦE72	(69)
MZ417351.1	PG-2021_90	S	44493	Rockefellervirus	wastewater[6]	ΦIPLA5	(51)
MW364975.1	vB_SepS_E72	S	44592	Rockefellervirus	clinical isolate[6]	ΦE72[13]	(55)
ON325435.2	CUB-EPI_14	S	46098	unclassified	wastewater[11]	none	(50)
ON550478.1	Sazerac	-	46428	unclassified	wastewater	none	-[14]
OP142323.1	Lacachita	S	46473	unclassified	wastewater	none	(49)
OQ623150.1	Southeast	-	47272	unclassified	wastewater	none	-[14]
MZ417343.1	PG-2021_74	S	85762	Sextaecvirus	wastewater	ΦSEP9	(51)
MZ417336.1	PG-2021_46	S	86018	Sextaecvirus	wastewater	ΦSEP9	(51)
MZ417339.1	PG-2021_5	S	92222	Sextaecvirus	wastewater	ΦSEP9	(51)
MZ417348.1	PG-2021_88	S	92222	Sextaecvirus	wastewater	ΦSEP9	(51)
KF929199.1	vB_SepS_SEP9	S	92417	Sextaecvirus	wastewater	ΦSEP9	(47)
OQ355701.1	vB_SepS_BE22	S[1]	92847	Sextaecvirus	skin	ΦSEP9	-[14]
KJ804259	6ec	S	93794	Sextaecvirus	nares[10]	ΦSEP9	(48)

MT596499.1	vB_SepS_BE02	S	95233	Sextaecvirus	skin[2]	ΦSEP9	(56)
KT429160.1	SPbeta-like	S	127726	unclassified	unknown	ΦSPbeta-like	-[14]
MZ417327.1	PG-2021_29	M	131570	unclassified	wastewater	-	(51)
OQ448193.1	80A (COP-80A)	M	139772	Sepunavirus	wastewater	-	(70)
OQ448194.1	80B (COP-80A)	M	139772	Sepunavirus	wastewater	-	(70)
KF021268.1	phiIBB-SEP1	M	139928	Sepunavirus	wastewater	-	(71)
MT596502.1	vB_SepM_BE05	M[1]	140271	Sepunavirus	unknown	-	-[14]
OQ355703.1	vB_SepM_BE25	M[1]	140292	Sepunavirus	skin	-	-[14]
OQ355702.1	vB_SepM_BE24	M[1]	140570	Sepunavirus	skin	-	-[14]
MZ417332.1	PG-2021_38	M	140647	unclassified	wastewater	-	(51)
MT596503.1	vB_SepM_BE06	M	140659	Sepunavirus	skin[2]	-	(56)
MT596504.1	vB_SepM_BE07	M	140661	Sepunavirus	skin[2]	-	(56)
MT596506.1	vB_SepM_BE09	M	140668	Sepunavirus	skin[2]	-	(56)
KP027447	phiIPLA-C1C	M	140961	Sepunavirus	wastewater	-	(72)
MH542234.1	Terranova	M	141288	Sepunavirus	wastewater	-	(73)
MH321490.1	Quidividi	M	141446	Sepunavirus	wastewater	-	(73)
OQ448195.1	110 (COP-110)	M	141874	Sepunavirus	wastewater	-	(70)
MT596501.1	vB_SepM_BE04	M	142331	Sepunavirus	skin[2]	-	(56)
MH321491.1	Twillingate	M	142592	Sepunavirus	wastewater	-	(73)
MZ417323.1	PG-2021_1	M	143764	Sepunavirus	wastewater	-	(51)
MT880872.1	PhiSepi-HH3	-	147057	unclassified	unknown	ΦSPbeta-like	(65)

[1] inferred from systematic name

[2] skin of the forehead

[3] in *S. epidermidis* 14.1.R1 (isolated from human skin)

[4] in *S. epidermidis* PJI isolates (e.g. ST2 and ST83)

[5] prophage induction of human mastitis isolate (*S. epidermidis* AEA1)

[6] induction

[7] prophage induction from isolate from nasal swab cultures, from settle plates exposed during the operations in the operating theatre, or from clinical specimen (74)

[8] cross-culturing of isolates from nose and skin of hospital staff and patient 'clinical' specimens (75)

[9] lytic variant of Staphylococcus phage IPLA6 (isolated by prophage induction of human mastitis isolate; *S. epidermidis* DD2Laa)

[10] anterior nares of humans

[11] clinical wastewater

[12] 46% query coverage only

[13] integrates into a FAD-dependent oxidoreductase in *S. epidermidis* 1457

[14] unpublished; information recovered from NCBI database (44, 45, 76)

Horizontal gene transfer by transduction

Transduction is a process, in which bacterial DNA is mis-packaged during replication of a phage, and subsequently transferred to a new bacterial cell (46).

Transduction between *Staphylococci* usually relies on cluster B siphoviruses, and the recipient strain does not necessarily need to be susceptible for lysis by the transducing phage (46, 77). General transduction from *S. aureus* to different *Staphylococci* and even into *Listeria monocytogenes* has been reported (17, 78), and *S. epidermidis* infecting siphoviruses can transduce mobile genetic elements at least between *S. epidermidis* strains of different STs (55). Surprisingly, interspecies transduction, including non-aureus *Staphylococci* like *S. epidermidis*, *S. felis*, *S. sciuri*, and *S. pseudintermedius*, is also facilitated by a giant myovirus (46, 79).

Phage defense systems of *S. epidermidis*

Mechanisms other than the WTA receptor are known to limit the bacteriophage host range. While superinfection exclusion after genome integration of temperate phages is a limiting factor for further phage infection, very little is known about the exclusion mechanisms of lysogenic phages infecting *Staphylococci* (59). One recent study identified a phage-encoded phage defense protein of *S. aureus* (pdp_{Sau}), which prevents infection of Staphylococci form *Kayviruses* by encoding a transmembrane protein which causes membrane permeability and leads to abortive infection (Abi) (80). CRISPR-Cas systems are rare in Staphylococci, but restriction-modification (RM) systems are quite common, and all four types of bacterial RM systems have been found in *Staphylococci* (59). A recent study investigating 89 *S. epidermidis* RefSeq genomes found 40% of them carrying RM systems, but less than 10% carrying CRISPR-Cas systems (81, 82). In addition, several anti-phage systems have orthologues in staphylococcal genomes, even though they are rarely found in *S. epidermidis* (59, 81, 83). Furthermore, the serine/threonine kinase Stk2 has been described to induce abortive infection (Abi) in *S. epidermidis* RP62a and other *Staphylococci* upon infection with siphoviruses, via modification of several essential cellular pathways (68). Other Abi systems, especially Abi2 seem to be common in *S. epidermidis,* but further research considering its function and mode of action is needed (81, 84). Recently, a single enzyme with nuclease and helicase activity was described in *S. epidermidis* RP62a and named Nhi (nuclease-helicase immunity) (85). This enzyme prevents infection of all three phage morphotypes of

Staphylococcal phages and is dependent on the presence of certain single-stranded DNA-binding proteins (SSBs) (85). Even though Nhi is widespread among different phyla, including *Firmicutes*, *Bacteroidetes*, and *Proteobacteria*, less than 1% of all bacteria and less than 5% of *S. aureus* or *S. epidermidis* genomes contain an Nhi gene (81, 85). Surprisingly, many staphylococcal anti-phage defense systems are encoded near, or within, the staphylococcal cassette chromosome (SCC*mec*) and can be mobilized by SCCmec-encoded recombinases (81, 86).

Phage therapy for treatment of *S. epidermidis* infections

Due to their ability to integrate into the genome and their lysogenic potential, previous research on staphylococcal viruses has been focused on temperate phages (cluster B) (41, 46). Many of which harbor fitness or virulence factors which benefit the host, facilitate horizontal gene transfer via transduction (41, 46), or cause immune evasion via unstable chromosome rearrangements and formation of small-colony variants (SCVs) (87). Phage therapy targeting *Staphylococci* has therefore focused on strictly lytic bacteriophages, mostly of the *Kayvirus* genus (88-91), and most of the effort to determine bacteriophages useful in treating infections with *Staphylococci* are exclusively focused on *S. aureus* (91). Several reports on animal models confirmed the use of *in vivo* phage applications against *S. aureus*, both alone, and in combination with antibiotic treatment (92). Treatment of vertebrates with different phages, alone or in combination, were effective against systemic infection, skin and soft tissue infections, bone and joint infections, and heart and pulmonary infections (92). Several case studies proved similarly effective (92), but only 10 clinical trials (13.07.2023) involving treatment of staphylococcal infections with bacteriophages are currently listed at the clinicaltrials.gov website (5 in active status). A first study with phage cocktail WPP-201 in patients with venous leg ulcers (VLUs) showed no serious side effects (92), and other trials currently investigate the safety of topical application of bacteriophages to treat infections with multiple pathogens (including *S. aureus*), for diabetic foot ulcers (93, 94), pressure ulcers (95) and burn wounds (92, 96). One trial investigated the safety of topical administration of the well-known phage cocktail AB-SA01, which contains three *S. aureus* specific myoviruses, and was previously show to target about 95% of all tested *S. aureus* strains with considerable reduction of bacterial burden in a murine acute lung infection model (91, 97). This cocktail showed promising results for safety and treatment of chronic

rhinosinusitis, or for endocarditis and bacteremia in combination with antibiotics (98-100). Another trial currently investigates the safety, tolerability, and efficacy of intravenous phage cocktail AP-SA02 in subjects with *S. aureus* bacteremia (101, 102). And one trial investigates the influence of bacteriophages on *S. aureus* Prosthetic Joint Infection, which has already been successfully treated with myovirus SaGR51ø1 in a case study (103, 104). Altogether, phage application of *S. aureus* infecting phages, generally seems to be safe, but treatment results are dependent on individual case reports, and CoNS are neglected for now (92).

References

1. Gallo, R. L. (2017) Human Skin Is the Largest Epithelial Surface for Interaction with Microbes. *J Invest Dermatol* **137**, 1213-1214
2. Byrd, A. L., Belkaid, Y., and Segre, J. A. (2018) The human skin microbiome. *Nat Rev Microbiol* **16**, 143-155
3. Oh, J., Byrd, A. L., Deming, C., Conlan, S., Program, N. C. S., Kong, H. H., and Segre, J. A. (2014) Biogeography and individuality shape function in the human skin metagenome. *Nature* **514**, 59-64
4. Severn, M. M., and Horswill, A. R. (2023) Staphylococcus epidermidis and its dual lifestyle in skin health and infection. *Nat Rev Microbiol* **21**, 97-111
5. Becker, K., Heilmann, C., and Peters, G. (2014) Coagulase-negative staphylococci. *Clin Microbiol Rev* **27**, 870-926
6. Kloos, W. E., and Schleifer, K. H. (1975) Isolation and Characterization of Staphylococci from Human Skin II. Descriptions of Four New Species: Staphylococcus warneri, Staphylococcus capitis, Staphylococcus hominis, and Staphylococcus simulans1. *International Journal of Systematic and Evolutionary Microbiology* **25**, 62-79
7. Otto, M. (2018) Staphylococcal Biofilms. *Microbiol Spectr* **6**
8. Schilcher, K., and Horswill, A. R. (2020) Staphylococcal Biofilm Development: Structure, Regulation, and Treatment Strategies. *Microbiol Mol Biol Rev* **84**
9. Du, X., Larsen, J., Li, M., Walter, A., Slavetinsky, C., Both, A., Sanchez Carballo, P. M., Stegger, M., Lehmann, E., Liu, Y., Liu, J., Slavetinsky, J., Duda, K. A., Krismer, B., Heilbronner, S., Weidenmaier, C., Mayer, C., Rohde, H., Winstel, V., and Peschel, A. (2021) Staphylococcus epidermidis clones express Staphylococcus aureus-type wall teichoic acid to shift from a commensal to pathogen lifestyle. *Nat Microbiol* **6**, 757-768
10. Holland, L. M., Conlon, B., and O'Gara, J. P. (2011) Mutation of tagO reveals an essential role for wall teichoic acids in Staphylococcus epidermidis biofilm development. *Microbiology (Reading)* **157**, 408-418
11. Heilmann, C., Hussain, M., Peters, G., and Gotz, F. (1997) Evidence for autolysin-mediated primary attachment of Staphylococcus epidermidis to a polystyrene surface. *Mol Microbiol* **24**, 1013-1024
12. Hussain, M., Heilmann, C., Peters, G., and Herrmann, M. (2001) Teichoic acid enhances adhesion of Staphylococcus epidermidis to immobilized fibronectin. *Microb Pathog* **31**, 261-270

13. Raza, A., and Steve, L. (1987) Adherence of Staphylococcus aureus to Squamous Epithelium: Role of Fibronectin and Teichoic Acid. *Reviews of Infectious Diseases* **9**, S341-S350
14. Weidenmaier, C., Peschel, A., Xiong, Y.-Q., Kristian, S. A., Dietz, K., Yeaman, M. R., and Bayer, A. S. (2005) Lack of Wall Teichoic Acids in Staphylococcus aureus Leads to Reduced Interactions with Endothelial Cells and to Attenuated Virulence in a Rabbit Model of Endocarditis. *The Journal of Infectious Diseases* **191**, 1771-1777
15. Endl, J., Seidl, H. P., Fiedler, F., and Schleifer, K. H. (1983) Chemical composition and structure of cell wall teichoic acids of staphylococci. *Arch Microbiol* **135**, 215-223
16. Winstel, V., Sanchez-Carballo, P., Holst, O., Xia, G., and Peschel, A. (2014) Biosynthesis of the unique wall teichoic acid of Staphylococcus aureus lineage ST395. *mBio* **5**, e00869
17. Winstel, V., Liang, C., Sanchez-Carballo, P., Steglich, M., Munar, M., Bröker, B. M., Penadés, J. R., Nübel, U., Holst, O., Dandekar, T., Peschel, A., and Xia, G. (2013) Wall teichoic acid structure governs horizontal gene transfer between major bacterial pathogens. *Nat Commun* **4**, 2345
18. Freymond, P. P., Lazarevic, V., Soldo, B., and Karamata, D. (2006) Poly(glucosyl-N-acetylgalactosamine 1-phosphate), a wall teichoic acid of Bacillus subtilis 168: its biosynthetic pathway and mode of attachment to peptidoglycan. *Microbiology (Reading)* **152**, 1709-1718
19. Shibaev, V. N., Duckworth, M., Archibald, A. R., and Baddiley, J. (1973) The structure of a polymer containing galactosamine from walls of Bacillus subtilis 168. *Biochemical Journal* **135**, 383
20. Brown, S., Meredith, T., Swoboda, J., and Walker, S. (2010) Staphylococcus aureus and Bacillus subtilis W23 make polyribitol wall teichoic acids using different enzymatic pathways. *Chem Biol* **17**, 1101-1110
21. Lazarevic, V., Abellan, F. X., Möller, S. B., Karamata, D., and Mauël, C. (2002) Comparison of ribitol and glycerol teichoic acid genes in Bacillus subtilis W23 and 168: identical function, similar divergent organization, but different regulation. *Microbiology (Reading)* **148**, 815-824
22. Xia, G., Corrigan, R. M., Winstel, V., Goerke, C., Gründling, A., and Peschel, A. (2011) Wall teichoic Acid-dependent adsorption of staphylococcal siphovirus and myovirus. *J Bacteriol* **193**, 4006-4009
23. Li, X., Gerlach, D., Du, X., Larsen, J., Stegger, M., Kühner, P., Peschel, A., Xia, G., and Winstel, V. (2015) An accessory wall teichoic acid glycosyltransferase protects Staphylococcus aureus from the lytic activity of Podoviridae. *Sci Rep* **5**, 17219
24. Gerlach, D., Guo, Y., De Castro, C., Kim, S.-H., Schlatterer, K., Xu, F.-F., Pereira, C., Seeberger, P. H., Ali, S., Codée, J., Sirisarn, W., Schulte, B., Wolz, C., Larsen, J., Molinaro, A., Lee, B. L., Xia, G., Stehle, T., and Peschel, A. (2018) Methicillin-resistant Staphylococcus aureus alters cell wall glycosylation to evade immunity. *Nature* **563**, 705-709
25. Xia, G., Maier, L., Sanchez-Carballo, P., Li, M., Otto, M., Holst, O., and Peschel, A. (2010) Glycosylation of wall teichoic acid in Staphylococcus aureus by TarM. *J Biol Chem* **285**, 13405-13415
26. Brown, S., Xia, G., Luhachack, L. G., Campbell, J., Meredith, T. C., Chen, C., Winstel, V., Gekeler, C., Irazoqui, J. E., Peschel, A., and Walker, S. (2012)

Methicillin resistance in Staphylococcus aureus requires glycosylated wall teichoic acids. *Proc Natl Acad Sci U S A* **109**, 18909-18914
27. Young, F. E. (1967) Requirement of glucosylated teichoic acid for adsorption of phage in Bacillus subtilis 168. *Proc Natl Acad Sci U S A* **58**, 2377-2384
28. Allison, S. E., D'Elia, M. A., Arar, S., Monteiro, M. A., and Brown, E. D. (2011) Studies of the genetics, function, and kinetic mechanism of TagE, the wall teichoic acid glycosyltransferase in Bacillus subtilis 168. *J Biol Chem* **286**, 23708-23716
29. Peschel, A., Vuong, C., Otto, M., and Götz, F. (2000) The D-alanine residues of Staphylococcus aureus teichoic acids alter the susceptibility to vancomycin and the activity of autolytic enzymes. *Antimicrob Agents Chemother* **44**, 2845-2847
30. Brown, S., Santa Maria, J. P., Jr., and Walker, S. (2013) Wall teichoic acids of gram-positive bacteria. *Annu Rev Microbiol* **67**, 313-336
31. Schlag, M., Biswas, R., Krismer, B., Kohler, T., Zoll, S., Yu, W., Schwarz, H., Peschel, A., and Götz, F. (2010) Role of staphylococcal wall teichoic acid in targeting the major autolysin Atl. *Mol Microbiol* **75**, 864-873
32. van Dalen, R., Peschel, A., and van Sorge, N. M. (2020) Wall Teichoic Acid in Staphylococcus aureus Host Interaction. *Trends Microbiol* **28**, 985-998
33. Mnich, M. E., van Dalen, R., Gerlach, D., Hendriks, A., Xia, G., Peschel, A., van Strijp, J. A. G., and van Sorge, N. M. (2019) The C-type lectin receptor MGL senses N-acetylgalactosamine on the unique Staphylococcus aureus ST395 wall teichoic acid. *Cell Microbiol* **21**, e13072
34. Kurokawa, K., Jung, D. J., An, J. H., Fuchs, K., Jeon, Y. J., Kim, N. H., Li, X., Tateishi, K., Park, J. A., Xia, G., Matsushita, M., Takahashi, K., Park, H. J., Peschel, A., and Lee, B. L. (2013) Glycoepitopes of staphylococcal wall teichoic acid govern complement-mediated opsonophagocytosis via human serum antibody and mannose-binding lectin. *J Biol Chem* **288**, 30956-30968
35. van Dalen, R., Molendijk, M. M., Ali, S., van Kessel, K. P. M., Aerts, P., van Strijp, J. A. G., de Haas, C. J. C., Codée, J., and van Sorge, N. M. (2019) Do not discard Staphylococcus aureus WTA as a vaccine antigen. *Nature* **572**, E1-E2
36. Park, K. H., Kurokawa, K., Zheng, L., Jung, D. J., Tateishi, K., Jin, J. O., Ha, N. C., Kang, H. J., Matsushita, M., Kwak, J. Y., Takahashi, K., and Lee, B. L. (2010) Human serum mannose-binding lectin senses wall teichoic acid Glycopolymer of Staphylococcus aureus, which is restricted in infancy. *J Biol Chem* **285**, 27167-27175
37. Dion, M. B., Oechslin, F., and Moineau, S. (2020) Phage diversity, genomics and phylogeny. *Nat Rev Microbiol* **18**, 125-138
38. Deghorain, M., and Van Melderen, L. (2012) The Staphylococci phages family: an overview. *Viruses* **4**, 3316-3335
39. Oliveira, H., Sampaio, M., Melo, L. D. R., Dias, O., Pope, W. H., Hatfull, G. F., and Azeredo, J. (2019) Staphylococci phages display vast genomic diversity and evolutionary relationships. *BMC Genomics* **20**, 357
40. Turner, D., Shkoporov, A. N., Lood, C., Millard, A. D., Dutilh, B. E., Alfenas-Zerbini, P., van Zyl, L. J., Aziz, R. K., Oksanen, H. M., Poranen, M. M., Kropinski, A. M., Barylski, J., Brister, J. R., Chanisvili, N., Edwards, R. A., Enault, F., Gillis, A., Knezevic, P., Krupovic, M., Kurtböke, I., Kushkina, A., Lavigne, R., Lehman, S., Lobocka, M., Moraru, C., Moreno Switt, A., Morozova, V., Nakavuma, J., Reyes Muñoz, A., Rūmnieks, J., Sarkar, B. L.,

Sullivan, M. B., Uchiyama, J., Wittmann, J., Yigang, T., and Adriaenssens, E. M. (2023) Abolishment of morphology-based taxa and change to binomial species names: 2022 taxonomy update of the ICTV bacterial viruses subcommittee. *Archives of Virology* **168**, 74

41. Hatoum-Aslan, A. (2021) The phages of staphylococci: critical catalysts in health and disease. *Trends Microbiol* **29**, 1117-1129
42. Barylski, J., Kropinski, A. M., Alikhan, N. F., Adriaenssens, E. M., and Ictv Report, C. (2020) ICTV Virus Taxonomy Profile: Herelleviridae. *J Gen Virol* **101**, 362-363
43. Hatcher, E. L., Zhdanov, S. A., Bao, Y., Blinkova, O., Nawrocki, E. P., Ostapchuck, Y., Schäffer, A. A., and Brister, J. R. (2017) Virus Variation Resource - improved response to emergent viral outbreaks. *Nucleic Acids Res* **45**, D482-d490
44. Sayers, E. W., Bolton, E. E., Brister, J. R., Canese, K., Chan, J., Comeau, D. C., Connor, R., Funk, K., Kelly, C., Kim, S., Madej, T., Marchler-Bauer, A., Lanczycki, C., Lathrop, S., Lu, Z., Thibaud-Nissen, F., Murphy, T., Phan, L., Skripchenko, Y., Tse, T., Wang, J., Williams, R., Trawick, B. W., Pruitt, K. D., and Sherry, S. T. (2022) Database resources of the national center for biotechnology information. *Nucleic Acids Res* **50**, D20-d26
45. Brister, J. R., Ako-Adjei, D., Bao, Y., and Blinkova, O. (2015) NCBI viral genomes resource. *Nucleic Acids Res* **43**, D571-577
46. Ingmer, H., Gerlach, D., and Wolz, C. (2019) Temperate Phages of Staphylococcus aureus. *Microbiol Spectr* **7**
47. Melo, L. D. R., Sillankorva, S., Ackermann, H.-W., Kropinski, A. M., Azeredo, J., and Cerca, N. (2014) Characterization of Staphylococcus epidermidis phage vB_SepS_SEP9 – a unique member of the Siphoviridae family. *Research in Microbiology* **165**, 679-685
48. Aswani, V. H., Tremblay, D. M., Moineau, S., and Shukla, S. K. (2014) Complete Genome Sequence of a Staphylococcus epidermidis Bacteriophage Isolated from the Anterior Nares of Humans. *Genome Announc* **2**
49. Andrews, T., Hoyer, J. S., Ficken, K., Fey, P. D., Duffy, S., and Boyd, J. M. (2023) A Transducing Bacteriophage Infecting Staphylococcus epidermidis Contributes to the Expansion of a Novel Siphovirus Genus and Implies the Genus Is Inappropriate for Phage Therapy. *mSphere* **8**, e0052422
50. Fanaei Pirlar, R., Wagemans, J., Ponce Benavente, L., Lavigne, R., Trampuz, A., and Gonzalez Moreno, M. (2022) Novel Bacteriophage Specific against Staphylococcus epidermidis and with Antibiofilm Activity. *Viruses* **14**
51. Göller, P. C., Elsener, T., Lorgé, D., Radulovic, N., Bernardi, V., Naumann, A., Amri, N., Khatchatourova, E., Coutinho, F. H., Loessner, M. J., and Gómez-Sanz, E. (2021) Multi-species host range of staphylococcal phages isolated from wastewater. *Nature Communications* **12**, 6965
52. O'Flaherty, S., Coffey, A., Edwards, R., Meaney, W., Fitzgerald, G. F., and Ross, R. P. (2004) Genome of staphylococcal phage K: a new lineage of Myoviridae infecting gram-positive bacteria with a low G+C content. *J Bacteriol* **186**, 2862-2871
53. O'Flaherty, S., Ross, R. P., Meaney, W., Fitzgerald, G. F., Elbreki, M. F., and Coffey, A. (2005) Potential of the polyvalent anti-Staphylococcus bacteriophage K for control of antibiotic-resistant staphylococci from hospitals. *Appl Environ Microbiol* **71**, 1836-1842

54. Walsh, S. K., Imrie, R. M., Matuszewska, M., Paterson, G. K., Weinert, L. A., Hadfield, J. D., Buckling, A., and Longdon, B. (2023) The host phylogeny determines viral infectivity and replication across Staphylococcus host species. *PLoS Pathog* **19**, e1011433
55. Fisarova, L., Botka, T., Du, X., Maslanova, I., Bardy, P., Pantucek, R., Benesik, M., Roudnicky, P., Winstel, V., Larsen, J., Rosenstein, R., Peschel, A., and Doskar, J. (2021) Staphylococcus epidermidis Phages Transduce Antimicrobial Resistance Plasmids and Mobilize Chromosomal Islands. *mSphere* **6**
56. Valente, L. G., Pitton, M., Fürholz, M., Oberhaensli, S., Bruggmann, R., Leib, S. L., Jakob, S. M., Resch, G., Que, Y.-A., and Cameron, D. R. (2021) Isolation and characterization of bacteriophages from the human skin microbiome that infect Staphylococcus epidermidis. *FEMS Microbes* **2**
57. Cater, K., Dandu, V. S., Bari, S. M., Lackey, K., Everett, G. F., and Hatoum-Aslan, A. (2017) A Novel Staphylococcus Podophage Encodes a Unique Lysin with Unusual Modular Design. *mSphere* **2**
58. Hawkins, N. C., Kizziah, J. L., Hatoum-Aslan, A., and Dokland, T. (2022) Structure and host specificity of Staphylococcus epidermidis bacteriophage Andhra. *Sci Adv* **8**, eade0459
59. Moller, A. G., Lindsay, J. A., and Read, T. D. (2019) Determinants of Phage Host Range in Staphylococcus Species. *Appl Environ Microbiol* **85**
60. Uchiyama, J., Taniguchi, M., Kurokawa, K., Takemura-Uchiyama, I., Ujihara, T., Shimakura, H., Sakaguchi, Y., Murakami, H., Sakaguchi, M., and Matsuzaki, S. (2017) Adsorption of Staphylococcus viruses S13' and S24-1 on Staphylococcus aureus strains with different glycosidic linkage patterns of wall teichoic acids. *J Gen Virol* **98**, 2171-2180
61. Schleifer, K. H., and Steber, J. (1974) Chemische Untersuchungen am Phagenreceptor von Staphylococcus epidermidis. *Archives of Microbiology* **98**, 251-270
62. Culbertson, E. K., Bari, S. M. N., Dandu, V. S., Kriznik, J. M., Scopel, S. E., Stanley, S. P., Lackey, K., Hernandez, A. C., and Hatoum-Aslan, A. (2019) Draft Genome Sequences of Staphylococcus Podophages JBug18, Pike, Pontiff, and Pabna. *Microbiol Resour Announc* **8**
63. Beck, C., Krusche, J., Notaro, A., Walter, A., Kränkel, L., Vollert, A., Stemmler, R., Wittmann, J., Schaller, M., Slavetinsky, C., Mayer, C., Castro, C. D., and Peschel, A. (2023) Wall teichoic acid substitution with glucose governs phage susceptibility of Staphylococcus epidermidis. *bioRxiv*, 2023.2007.2027.550822
64. Lassen, S. B., Lomholt, H. B., and Brüggemann, H. (2017) Complete Genome Sequence of a Staphylococcus epidermidis Strain with Exceptional Antimicrobial Activity. *Genome Announc* **5**
65. Both, A., Huang, J., Qi, M., Lausmann, C., Weißelberg, S., Büttner, H., Lezius, S., Failla, A. V., Christner, M., Stegger, M., Gehrke, T., Baig, S., Citak, M., Alawi, M., Aepfelbacher, M., and Rohde, H. (2021) Distinct clonal lineages and within-host diversification shape invasive Staphylococcus epidermidis populations. *PLOS Pathogens* **17**, e1009304
66. Gutiérrez, D., Martínez, B., Rodríguez, A., and García, P. (2010) Isolation and Characterization of Bacteriophages Infecting Staphylococcus epidermidis. *Current Microbiology* **61**, 601-608

67. Gutiérrez, D., Martínez, B., Rodríguez, A., and García, P. (2012) Genomic characterization of two Staphylococcus epidermidis bacteriophages with anti-biofilm potential. *BMC Genomics* **13**, 228
68. Depardieu, F., Didier, J. P., Bernheim, A., Sherlock, A., Molina, H., Duclos, B., and Bikard, D. (2016) A Eukaryotic-like Serine/Threonine Kinase Protects Staphylococci against Phages. *Cell Host Microbe* **20**, 471-481
69. Daniel, A., Bonnen, P. E., and Fischetti, V. A. (2007) First Complete Genome Sequence of Two Staphylococcus epidermidis Bacteriophages. *Journal of Bacteriology* **189**, 2086-2100
70. Štrancar, V., Marušić, M., Tušar, J., Praček, N., Kolenc, M., Šuster, K., Horvat, S., Janež, N., and Peterka, M. (2023) Isolation and in vitro characterization of novel S. epidermidis phages for therapeutic applications. *Front Cell Infect Microbiol* **13**, 1169135
71. Melo, L. D. R., Sillankorva, S., Ackermann, H. W., Kropinski, A. M., Azeredo, J., and Cerca, N. (2014) Isolation and characterization of a new Staphylococcus epidermidis broad-spectrum bacteriophage. *J Gen Virol* **95**, 506-515
72. Gutiérrez, D., Vandenheuvel, D., Martínez, B., Rodríguez, A., Lavigne, R., and García, P. (2015) Two Phages, phiIPLA-RODI and phiIPLA-C1C, Lyse Mono- and Dual-Species Staphylococcal Biofilms. *Appl Environ Microbiol* **81**, 3336-3348
73. Freeman, M. E., Kenny, S. E., Lanier, A., Cater, K., Wilhite, M. C., Gamble, P., O'Leary, C. J., Hatoum-Aslan, A., Young, R. F., 3rd, and Liu, M. (2019) Complete Genome Sequences of Staphylococcus epidermidis Myophages Quidividi, Terranova, and Twillingate. *Microbiol Resour Announc* **8**
74. Verhoef, J., Van Boven, C. P. A., and Winkler, K. C. (1971) Lysogeny In Coagulase-Negative Staphylococci. *Journal of Medical Microbiology* **4**, 405-412
75. Dean, B. A., Williams, R. E., Hall, F., and Corse, J. (1973) Phage typing of coagulase-negative staphylococci and micrococci. *J Hyg (Lond)* **71**, 261-270
76. Schoch, C. L., Ciufo, S., Domrachev, M., Hotton, C. L., Kannan, S., Khovanskaya, R., Leipe, D., McVeigh, R., O'Neill, K., Robbertse, B., Sharma, S., Soussov, V., Sullivan, J. P., Sun, L., Turner, S., and Karsch-Mizrachi, I. (2020) NCBI Taxonomy: a comprehensive update on curation, resources and tools. *Database (Oxford)* **2020**
77. Haaber, J., Penadés, J. R., and Ingmer, H. (2017) Transfer of Antibiotic Resistance in Staphylococcus aureus. *Trends Microbiol* **25**, 893-905
78. Chen, J., and Novick, R. P. (2009) Phage-mediated intergeneric transfer of toxin genes. *Science* **323**, 139-141
79. Uchiyama, J., Takemura-Uchiyama, I., Sakaguchi, Y., Gamoh, K., Kato, S., Daibata, M., Ujihara, T., Misawa, N., and Matsuzaki, S. (2014) Intragenus generalized transduction in Staphylococcus spp. by a novel giant phage. *Isme j* **8**, 1949-1952
80. Kuntová, L., Mašlaňová, I., Obořilová, R., Šimečková, H., Finstrlová, A., Bárdy, P., Šiborová, M., Troianovska, L., Botka, T., Gintar, P., Šedo, O., Farka, Z., Doškař, J., and Pantůček, R. (2023) Staphylococcus aureus Prophage-Encoded Protein Causes Abortive Infection and Provides Population Immunity against Kayviruses. *mBio* **14**, e0249022
81. Hossain, M., Aslan, B., and Hatoum-Aslan, A. (2023) Tandem mobilization of anti-phage defenses alongside SCC mec cassettes. *bioRxiv*

82. Li, Q., Xie, X., Yin, K., Tang, Y., Zhou, X., Chen, Y., Xia, J., Hu, Y., Ingmer, H., Li, Y., and Jiao, X. (2016) Characterization of CRISPR-Cas system in clinical Staphylococcus epidermidis strains revealed its potential association with bacterial infection sites. *Microbiol Res* **193**, 103-110
83. Doron, S., Melamed, S., Ofir, G., Leavitt, A., Lopatina, A., Keren, M., Amitai, G., and Sorek, R. (2018) Systematic discovery of antiphage defense systems in the microbial pangenome. *Science* **359**
84. Chopin, M.-C., Chopin, A., and Bidnenko, E. (2005) Phage abortive infection in lactococci: variations on a theme. *Current Opinion in Microbiology* **8**, 473-479
85. Bari, S. M. N., Chou-Zheng, L., Howell, O., Hossain, M., Hill, C. M., Boyle, T. A., Cater, K., Dandu, V. S., Thomas, A., Aslan, B., and Hatoum-Aslan, A. (2022) A unique mode of nucleic acid immunity performed by a multifunctional bacterial enzyme. *Cell Host & Microbe* **30**, 570-582.e577
86. Mikkelsen, K., Bowring, J. Z., Ng, Y. K., Svanberg Frisinger, F., Maglegaard, J. K., Li, Q., Sieber, R. N., Petersen, A., Andersen, P. S., Rostøl, J. T., Høyland-Kroghsbo, N. M., and Ingmer, H. (2023) An Endogenous Staphylococcus aureus CRISPR-Cas System Limits Phage Proliferation and Is Efficiently Excised from the Genome as Part of the SCCmec Cassette. *Microbiol Spectr*, e0127723
87. Guérillot, R., Kostoulias, X., Donovan, L., Li, L., Carter, G. P., Hachani, A., Vandelannoote, K., Giulieri, S., Monk, I. R., Kunimoto, M., Starrs, L., Burgio, G., Seemann, T., Peleg, A. Y., Stinear, T. P., and Howden, B. P. (2019) Unstable chromosome rearrangements in Staphylococcus aureus cause phenotype switching associated with persistent infections. *Proc Natl Acad Sci U S A* **116**, 20135-20140
88. Ajuebor, J., Buttimer, C., Arroyo-Moreno, S., Chanishvili, N., Gabriel, E. M., O'Mahony, J., McAuliffe, O., Neve, H., Franz, C., and Coffey, A. (2018) Comparison of Staphylococcus Phage K with Close Phage Relatives Commonly Employed in Phage Therapeutics. *Antibiotics* **7**, 37
89. Leskinen, K., Tuomala, H., Wicklund, A., Horsma-Heikkinen, J., Kuusela, P., Skurnik, M., and Kiljunen, S. (2017) Characterization of vB_SauM-fRuSau02, a Twort-Like Bacteriophage Isolated from a Therapeutic Phage Cocktail. *Viruses* **9**
90. Vandersteegen, K., Mattheus, W., Ceyssens, P. J., Bilocq, F., De Vos, D., Pirnay, J. P., Noben, J. P., Merabishvili, M., Lipinska, U., Hermans, K., and Lavigne, R. (2011) Microbiological and molecular assessment of bacteriophage ISP for the control of Staphylococcus aureus. *PLoS One* **6**, e24418
91. Lehman, S. M., Mearns, G., Rankin, D., Cole, R. A., Smrekar, F., Branston, S. D., and Morales, S. (2019) Design and Preclinical Development of a Phage Product for the Treatment of Antibiotic-Resistant Staphylococcus aureus Infections. *Viruses* **11**
92. Plumet, L., Ahmad-Mansour, N., Dunyach-Remy, C., Kissa, K., Sotto, A., Lavigne, J. P., Costechareyre, D., and Molle, V. (2022) Bacteriophage Therapy for Staphylococcus Aureus Infections: A Review of Animal Models, Treatments, and Clinical Trials. *Front Cell Infect Microbiol* **12**, 907314
93. Nīmes, C. H. U. d., and Pharma, P. (2022) Standard Treatment Associated With Phage Therapy Versus Placebo for Diabetic Foot Ulcers Infected by S. Aureus. https://classic.clinicaltrials.gov/show/NCT02664740

94. Nir-Paz, R., Onallah, H., Gellman, Y. N., Haze, A., Braunstein, R., Hazan, R., Leandro, C., Barbosa, R., Dordio, H., Wagner, A., Corte Real, S. V., and Garcia, M. (2022) 1690. Assessing the safety of TP-102 bacteriophage treatment in the management of diabetic foot infections. *Open Forum Infectious Diseases* **9**
95. Inc., P. (2022) Phage Therapy for the Prevention and Treatment of Pressure Ulcers. https://classic.clinicaltrials.gov/show/NCT04815798
96. Inc., P. (2022) Phage Therapy for the Prevention and Treatment of Wound Infections in Burned Patients. https://classic.clinicaltrials.gov/show/NCT04323475
97. Armata Pharmaceuticals, I. Individual Patient Expanded Access for AB-SA01, an Investigational Anti-Staphylococcus Aureus Bacteriophage Therapeutic. https://classic.clinicaltrials.gov/show/NCT03395769
98. Ooi, M. L., Drilling, A. J., Morales, S., Fong, S., Moraitis, S., Macias-Valle, L., Vreugde, S., Psaltis, A. J., and Wormald, P. J. (2019) Safety and Tolerability of Bacteriophage Therapy for Chronic Rhinosinusitis Due to Staphylococcus aureus. *JAMA Otolaryngol Head Neck Surg* **145**, 723-729
99. Fabijan, A. P., Ben Zakour, N. L., Ho, J., Lin, R. C. Y., and Iredell, J. (2019) Polyclonal Staphylococcus aureus Bacteremia. *Ann Intern Med* **171**, 940-941
100. Petrovic Fabijan, A., Lin, R. C. Y., Ho, J., Maddocks, S., Ben Zakour, N. L., and Iredell, J. R. (2020) Safety of bacteriophage therapy in severe Staphylococcus aureus infection. *Nat Microbiol* **5**, 465-472
101. Hitchcock, N. M., Devequi Gomes Nunes, D., Shiach, J., Valeria Saraiva Hodel, K., Dantas Viana Barbosa, J., Alencar Pereira Rodrigues, L., Coler, B. S., Botelho Pereira Soares, M., and Badaró, R. (2023) Current Clinical Landscape and Global Potential of Bacteriophage Therapy. *Viruses* **15**
102. Armata Pharmaceuticals, I., and Defense, U. S. D. o. (2022) Study Evaluating Safety, Tolerability, and Efficacy of Intravenous AP-SA02 in Subjects With S. Aureus Bacteremia. https://classic.clinicaltrials.gov/show/NCT05184764
103. Pharma, P. (2022) Phage Therapy in Prosthetic Joint Infection Due to Staphylococcus Aureus Treated With DAIR. https://classic.clinicaltrials.gov/show/NCT05369104
104. Ramirez-Sanchez, C., Gonzales, F., Buckley, M., Biswas, B., Henry, M., Deschenes, M. V., Horne, B., Fackler, J., Brownstein, M. J., Schooley, R. T., and Aslam, S. (2021) Successful Treatment of Staphylococcus aureus Prosthetic Joint Infection with Bacteriophage Therapy. *Viruses* **13**

Chapter 2

Wall teichoic acid substitution with glucose governs phage susceptibility of *Staphylococcus epidermidis*

Christian Beck[a,b,c], Janes Krusche[a,b,c], Anna Notaro[d], Axel Walter[a,e], Lara Kränkel[a,b,c], Anneli Vollert[f], Regine Stemmler[a,b,c], Johannes Wittmann[g], Martin Schaller[f], Christoph Slavetinsky[a,b,c,h], Christoph Mayer[a,e], Cristina De Castro[i], Andreas Peschel[a,b,c,#]

[a]Cluster of Excellence "Controlling Microbes to Fight Infections (CMFI)", University of Tübingen, Tübingen, Germany
[b]Interfaculty Institute of Microbiology and Infection Medicine Tübingen, Infection Biology, University of Tübingen, Tübingen, Germany
[c]German Centre for Infection Research (DZIF), Partner Site Tübingen, Tübingen, Germany
[d]Department of Agricultural Sciences, University of Naples, Naples, Italy
[e]Interfaculty Institute of Microbiology and Infection Medicine Tübingen, Organismic Interactions/Glycobiology, University of Tübingen, Tübingen, Germany
[f]Electron-Microscopy, Department of Dermatology, University Hospital Tübingen, Tübingen, Germany
[g]Leibniz Institute, DSMZ-German Collection of Microorganisms and Cell Cultures, Braunschweig, Germany
[h]Pediatric Surgery and Urology, University Children´s Hospital Tübingen, University of Tübingen, Germany
[i]Department of Chemical Sciences, University of Naples, Naples, Italy
[#]Correspondence to Andreas Peschel (andreas.peschel@uni-tuebingen.de)

submitted manuscript

Abstract

The species- and clone-specific susceptibility of *Staphylococcus* cells for bacteriophages is governed by the structures and glycosylation patterns of wall teichoic acid (WTA) glycopolymers. The glycocodes of phage-WTA interaction in the opportunistic pathogen *Staphylococcus epidermidis* and in other coagulase-negative staphylococci (CoNS) have remained unknown. We report a new *S. epidermidis* WTA glycosyltransferase TagE whose deletion confers resistance to siphoviruses such as ΦE72 but enables binding of otherwise unbound podoviruses. *S. epidermidis* glycerolphosphate WTA was found to be modified with glucose in a *tagE*-dependent manner. TagE is encoded together with the enzymes PgcA and GtaB providing uridine diphosphate-activated glucose. ΦE72 transduced several other CoNS species encoding TagE homologs suggesting that WTA glycosylation via TagE is a frequent trait among CoNS that permits inter-species horizontal gene transfer. Our study unravels a crucial mechanism of phage-*Staphylococcus* interaction and of horizontal gene transfer and it will help in the design of anti-staphylococcal phage therapies.

Importance

Phages are highly specific for certain bacterial hosts, and some can transduce DNA even across species boundaries. How phages recognize cognate host cells remains incompletely understood. Phages infecting members of the genus *Staphylococcus* bind to wall teichoic acid (WTA) glycopolymers with highly variable structures and glycosylation patterns. How WTA is glycosylated in the opportunistic pathogen *Staphylococcus epidermidis* and in other coagulase-negative *Staphylococcus* (CoNS) species has remained unknown. We describe that *S. epidermidis* glycosylates its WTA backbone with glucose and we identify a cluster of three genes, responsible for glucose activation and transfer to WTA. Their inactivation strongly alters phage susceptibility patterns, yielding resistance to siphoviruses but susceptibility to podoviruses. Many different CoNS species with related glycosylation genes can exchange DNA via siphovirus ΦE72 suggesting that glucose-modified WTA is crucial for interspecies horizontal gene transfer. Our finding will help to develop antibacterial phage therapies and unravel routes of genetic exchange.

Introduction

Staphylococcus epidermidis is one of the most abundant colonizers of mammalian skin and of nasal epithelia [1, 2]. Some nosocomial *S. epidermidis* clones also cause invasive infections, in particular biofilm-associated infections on catheters or artificial implants such as hip and knee joints or heart valves [3, 4]. Although *S. epidermidis* is not an as aggressive pathogen as *Staphylococcus aureus*, biofilm-associated infections are difficult to treat and cause a high burden of morbidity and costs for health care systems. Many *S. epidermidis* clones are resistant to beta-lactams and other antibiotics such as linezolid, which further complicates the treatment of *S. epidermidis* infections [1].

The major invasive *S. epidermidis* clones seem to pursue two different virulence strategies. The MLST type 2 (ST2) strains produce particularly strong biofilms [3, 5]. In contrast, ST10, ST23, and ST87 clones are only weak biofilm formers, but they express an additional surface molecule that alters their host interaction capacities and leads to a shift from commensal to pathogen behavior [6]. Surface properties and host interaction of staphylococci are governed not only by surface proteins but also by cell-wall anchored glycopolymers composed of alditolphosphate repeating units called wall teichoic acids (WTA) [7, 8]. The WTA polymers of *S. epidermidis* and other coagulase-negative *Staphylococcus* (CoNS) species have remained a neglected field of research despite their potentially critical role for host colonization and infection. Most *S. epidermidis* clones seem to express WTA composed of glycerolphosphate (GroP) repeating units [9]. A recent study has shown that ST10, ST23, and ST87 strains express an additional *S. aureus*-type WTA composed of ribitolphosphate (RboP) repeating units, which shapes their interaction with human epithelial and endothelial cells [6].

WTA is also crucial for binding of virtually all known *Staphylococcus* phages, which use differences in WTA structure to recognize their cognate host species [10]. Phages of the Sipho- and podovirus groups often not only discriminate between different WTA backbones but also between different types of backbone glycosylation. Most Firmicutes link D-alanine esters and sugar residues to GroP or RboP repeating units [7, 8]. Variation in glycosylation for instance by N-acetylglucosamine (GlcNAc) in alpha or beta configuration or N-acetylgalactosamine (GalNAc) has been found to govern the susceptibility patterns of *S. aureus* strains for different phages [11-14].

The group of broad-host range myoviruses, however, requires WTA for binding but does not discriminate between RboP and GroP WTA and does not require WTA glycosylation [15-17].

WTA-phage interaction is of importance for phage-therapeutic strategies, which have gained increasing attention recently [3, 18]. Moreover, they are critical for inter-species horizontal gene transfer via transducing bacteriophages [19]. Such transduction events have led to the transfer of resistance and virulence genes into the genomes of *S. aureus* and other species, thereby allowing, for instance, evolution of methicillin-resistant *S. epidermidis* (MRSE) and methicillin-resistant *S. aureus* (MRSA) [20, 21]. Despite the critical role of WTA in these processes, the biosynthesis, composition, and glycosylation of the canonical *S. epidermidis* WTA has not been studied.

Here we demonstrate, that *S. epidermidis* strain 1457 glycosylates its GroP-WTA with glucose and we identify the WTA glucosyltransferase gene *tagE*. *S. epidermidis tagE* mutants showed complex changes in phage susceptibility patterns including both, the loss, and the acquisition of susceptibility to certain phages, some of which we found to be capable of transducing plasmid DNA between different CoNS species.

Results

1. Disruption of a putative glycosyl transferase gene cluster confers resistance to phage ΦE72

Several new phages with the capacity to infect *S. epidermidis* have been reported recently [22, 23]. Some of them have the capacity to transduce DNA between different *S. epidermidis* lineages, raising the question, which bacterial target structures are recognized by the phages' binding proteins, and how universal these target structures may be among different clones of *S. epidermidis* and other CoNS. As most *S. aureus* phages recognize the sugar modifications of WTA [11-13, 24], it was tempting to speculate that glycosylated GroP-WTA is also required for binding of *S. epidermidis* phages. However, the enzymes responsible for WTA glycosylation in *S. epidermidis* have remained unknown and it has also remained elusive, which glycosylation patterns can be found on *S. epidermidis* GroP-WTA. To elucidate the

WTA glycosylation pathways of *S. epidermidis* and explore its impact on phage interaction we set out to identify and inactivate the responsible enzyme genes.

A library of transposon mutants of *S. epidermidis* 1457 was created using a xylose-inducible Himar1 transposase [25] and incubated with phage ΦE72, which is known to infect and multiply in strain 1457 [22]. Two mutants, which were resistant to ΦE72 were identified and found to have the transposon integrated in two adjacent genes of unknown function (Fig. 1a; Fig. 2a, d). The two genes were not in the vicinity of other WTA-biosynthesis related genes, but their gene products shared similarity with glycosylation-related enzymes. The gene B4U56_RS02220 product was 46% similar to TagE of *Bacillus subtilis*, which glycosylates GroP-WTA with glucose residues [26] and 48% similar to TarM of *S. aureus,* which glycosylates RboP-WTA with GlcNAc (Fig. 1b) [27]. The adjacent gene B4U56_RS02215 encodes a protein with 59% similarity to the phosphoglucomutase PgcA of *B. subtilis*, which isomerizes glucose-6-phosphate to yield glucose-1-phosphate [28]. In addition, the product of gene B4U56_RS02210, next to *pgcA,* was 85% similar to the GtaB enzyme of *B. subtilis* generating UDP-glucose from glucose-1-phosphate and UTP [29]. Both, PgcA and GtaB are required for glycosylation of GroP-WTA with glucose via TagE in *B. subtilis* [30], although the two genes are not encoded together with *tagE* in *B. subtilis* [31, 32]. We assumed that the three enzymes might cooperate in *S. epidermidis* to activate and attach glucose to GroP-WTA.

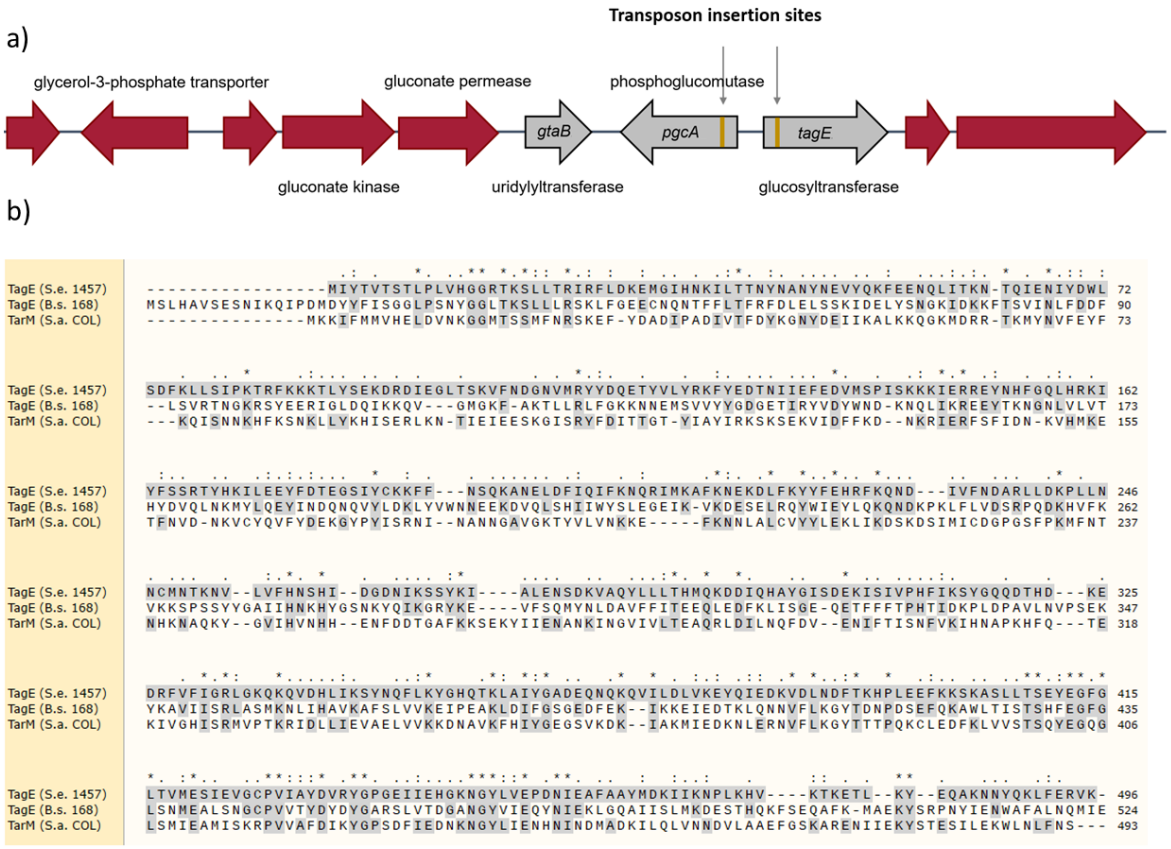

Figure 1: The *tagE* gene encodes a glycosyltransferase in *S. epidermidis*. a) Genetic locus identified by transposon mutagenesis contains the *S. epidermidis tagE, pgcA,* and *gtaB* homologues. Transposon insertion sites are labeled in gold. b) MUSCLE alignment of *S. epidermidis* TagE with *B. subtilis* TagE and *S. aureus* TarM protein sequences.

2. *S. epidermidis* TagE is responsible for glucose addition to GroP-WTA

The three *S. epidermidis* genes were renamed according to the corresponding *B. subtilis* genes *tagE*, *gtaB*, and *pgcA.* All three genes were inactivated by targeted deletion to confirm their roles in phage susceptibility. The three mutants were as resistant to ΦE72 infection as the transposon mutants, and complementation of the *tagE* mutant with a plasmid-encoded copy of the gene locus restored wild-type level ΦE72 susceptibility (Fig. 2 c,f). The various transposon and targeted deletion mutants were approximately 3-fold less susceptible to ΦE72 infection, but were not completely resistant, suggesting that the phage may have additional, albeit less effective ways to interact with *S. epidermidis* 1457. In a similar way, and even more pronounced, the mutants had retained only limited capacities to bind ΦE72 particles in liquid media (Fig. 2 d-f; Fig S1).

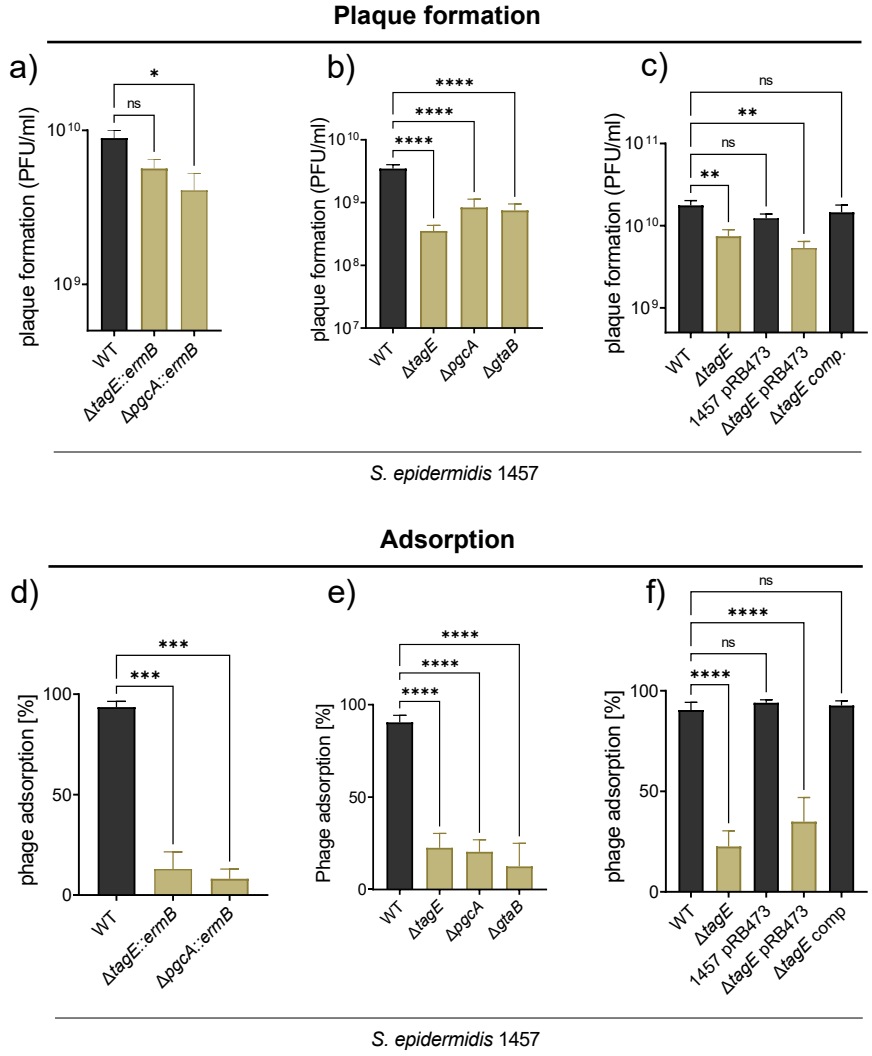

Figure 2: ΦE72 shows decreased infection (a,b) and binding (d,e) of the *tagE*, *pgcA,* and *gtaB* mutants. This deffect can be restored by complementing the *tagE* mutant with the genetic locus containing *tagE*, *pgcA,* and *gtaB* on plasmid pRB473 (c,f). The data represent the mean ± SEM of at least three independent experiments. Ordinary one-way ANOVA was used to determine statistical significance versus *S. epidermidis* 1457 wild type (WT), indicated as: not significant (ns), $^{*}P < 0.05$, $^{**}P < 0.01$, $^{***}P < 0.001$, $^{****}P < 0.0001$.

WTA isolated from 1457 wild type (WT) contained substantial amounts of glucose when analyzed by an enzymatic glucose assay indicating that ca. 50% of the GroP-WTA repeating units are modified with glucose (Fig. 3a). In contrast, none of the WTA samples of any of the *tagE*, *gtaB*, or *pgcA* mutants was found to contain glucose. High-performance liquid chromatography coupled to a mass spectrometry detector (HPLC-MS) and nuclear magnetic resonance (NMR) spectroscopy

confirmed the presence of glucose-substituted GroP repeating units in the wild type and the absence of glucose in the mutants (Fig. 3b,c; Fig. S2). These findings reflect earlier reports on the presence of glucose on *S. epidermidis* GroP-WTA [9] and they confirm that the PgcA-GtaB-TagE pathway is required for GroP-WTA glycosylation with glucose. NMR analysis indicated that the glucose units are α configured at the anomeric center and attached to the C2-position of GroP. About 15% of the glucose residues are modified with D-alanine at the O6-position of glucose (Fig. 3c; NMR extended description). The α-configuration is reminiscent of the configuration of GlcNAc on RboP-WTA introduced by the TagE-related TarM in *S. aureus* [27].

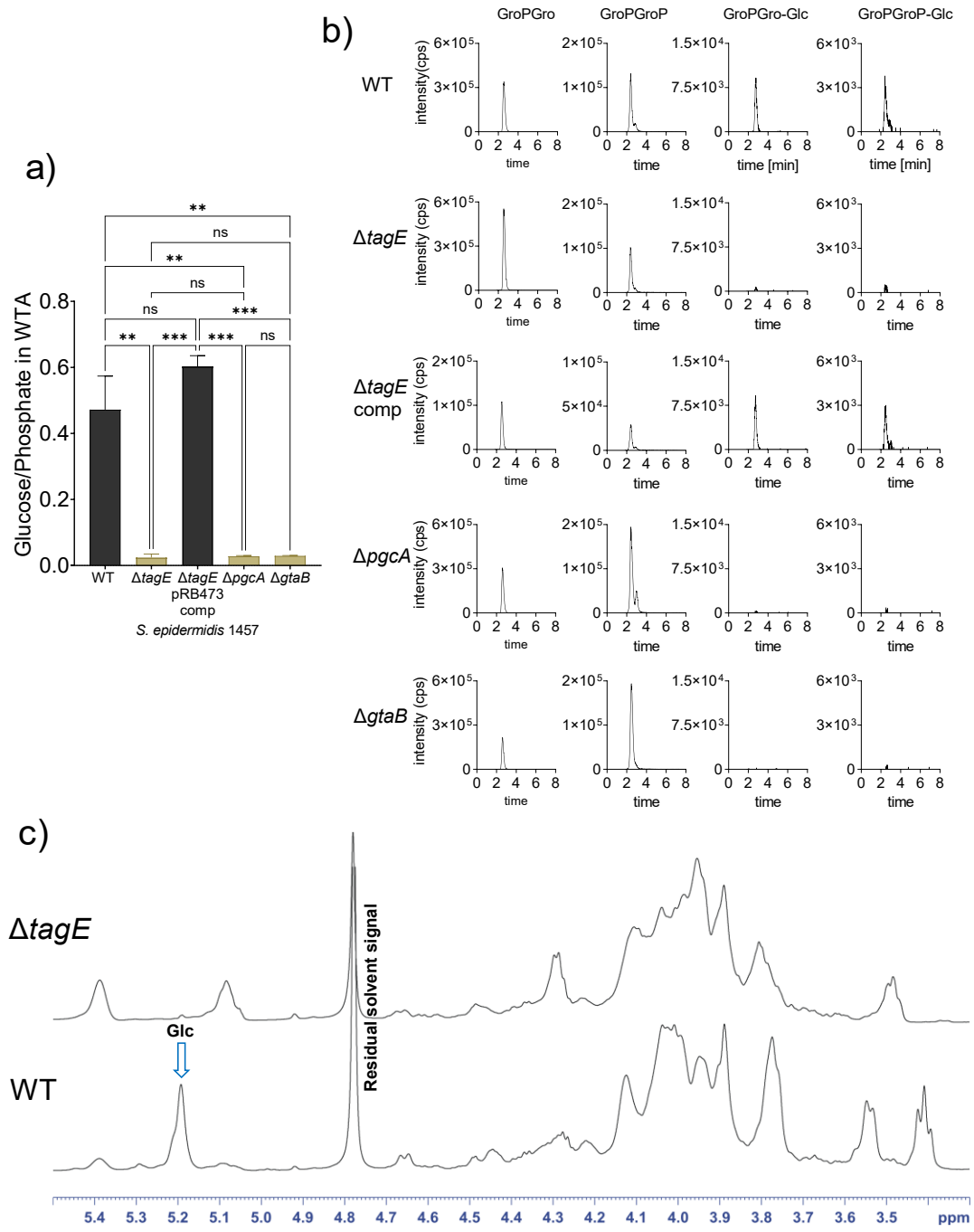

Figure 3: WTA analysis of the S. epidermidis mutants ΔtagE, ΔpgcA, ΔgtaB and of ΔtagE containing the pRB473 plasmid carrying tagE, pgcA, and gtaB genes for complementation. a) Ratio of glucose per phosphate content of WTA measured enzymatically. b) HPLC-MS: Extracted ion chromatograms (EIC) of GroP-Gro ([M - H]- = 245.0432) and GroP-GroP ([M - H]- = 325.0095) with (GroP-Gro-Glc; [M - H]- = 407.096) (GroP-GroP-Glc; [M - H]- = 487.0623) or without glucose substitution. c) 1H NMR spectra reveal D-glucose on WTA of the S. epidermidis 1457 wild type (WT) (at the C2-position of GroP), while deletion of tagE results in absence of glucose on WTA. For a) data represent the mean ± SEM of at least three independent experiments. Ordinary one-way ANOVA was used to determine statistical significance, indicated as: not significant (ns), **P < 0.01, ***P < 0.001.

The absence of glucose on GroP-WTA in the Δ*tagE* mutant did not alter biofilm formation by *S. epidermidis* 1457 (Fig. S3). Moreover, no differences in growth kinetics (Fig. S1), cell wall thickness, or cell shape (Fig. S4) were observed in the mutants, indicating that the absence of glucose on GroP-WTA has no major impact on overall cellular properties of the *S. epidermidis* surface.

UDP-glucose generated by PgcA and GtaB is also required for biosynthesis of the glycolipid diglucosyldiacylglycerol (DGlcDAG), which serves as anchor structure for lipoteichoic acid (LTA) polymers in *B. subtilis* and many other Firmicutes (Fig 4a) [33-35]. However, DGlcDAG is not essential for LTA biosynthesis because mutants lacking the glycolipids still produce LTA attached to phosphatidylglycerol lipids [35, 36]. The *S. epidermidis pgcA* and *gtaB* mutants, but not the *tagE* mutant, also lacked DGlcDAG, which was present in the parental strain (Fig. 4b), indicating that DGlcDAG is synthesized in *S. epidermidis* by the same pathway as in *B. subtilis* and *S. aureus*.

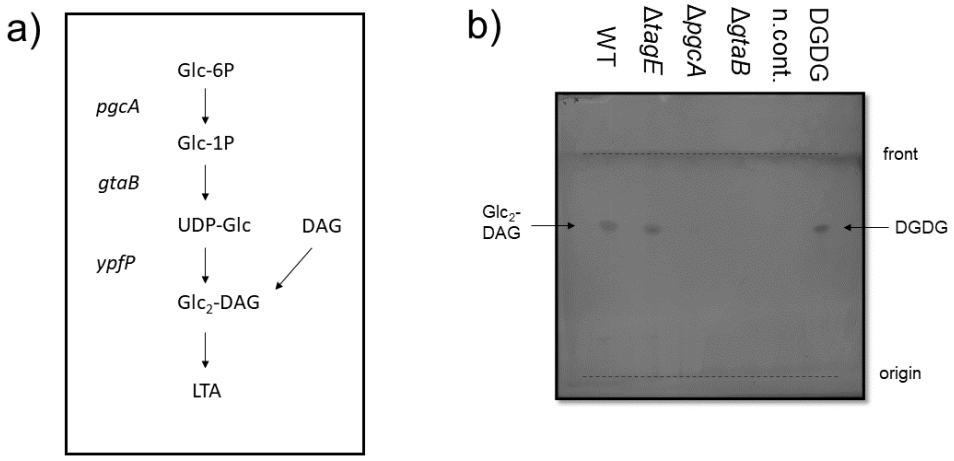

Figure 4: Glycolipid detection by TLC. a) LTA glycolipid biosynthesis pathway as described for S. aureus and B. subtilis (adapted from [36]). b) Glycolipid detection on a TLC plate stained with α-naphtol/sulfuric acid. 5 µg of digalactosyldiacylglycerol (DGDG) was used as positive control, the solvent methanol/chloroform (1:1) as negative control (n.cont.). One representative experiment of three independent experiments is shown.

3. Lack of WTA glucose impairs binding of known *S. epidermidis* siphoviruses but promotes binding of podoviruses

Several other phages in addition to ΦE72 were analyzed for an impact of GroP-WTA glucose modification on phage binding and infection. The ΦE72-related siphoviruses Φ456, Φ459, and Φ27, which are known to bind to *S. epidermidis* 1457 [22], showed reduced binding to the *pgcA, gtaB*, and *tagE* mutants compared to the wild type but the reduction was less pronounced as for ΦE72 (Fig. 5a,f). Φ459 was equally reduced in its capacities to propagate in the mutants as ΦE72 (Fig. 5b). Despite their capacity to bind *S. epidermidis* 1457, Φ27 and Φ456 did not form clear plaques on wild-type or mutant strains. Two recently isolated myoviruses of the genus sepunavirus, ΦBE04 and ΦBE06 [37], showed no reduction in their ability to bind and infect the mutants, suggesting that these myoviruses are not dependent on glucose-modified GroP-WTA (Fig. 5d,e). This behavior resembles the lacking impact of WTA glycosylation on myovirus ΦK infection of *S. aureus* [13].

Several other phages, which bind *S. epidermidis* 1457 but cannot replicate in this strain, behaved differently. Siphovirus Φ187, which is only distantly related to ΦE72 and requires GroP-WTA modified with GalNAc for infection of target cells [24], still bound efficiently to the GroP-WTA glucose-deficient mutants (Fig. 5a), indicating that the GroP-WTA glucose modifications are not necessary for Φ187 binding. Φ187 even showed higher plasmid transduction efficiency in the absence of GroP-WTA glucose residues (Fig. 6a). Furthermore, the podoviruses ΦUKE3, ΦSpree, and ΦBE03 [37] exhibited strongly increased binding to the *pgcA, gtaB,* and *tagE* mutants compared to the wild type (Fig. 5 c,f), indicating that these phages are attenuated for binding in the presence of glucose residues on GroP-WTA. Thus, the GroP-WTA glucose residues are important for most of the known *S. epidermidis* phages albeit in quite different ways, depending on the individual phage.

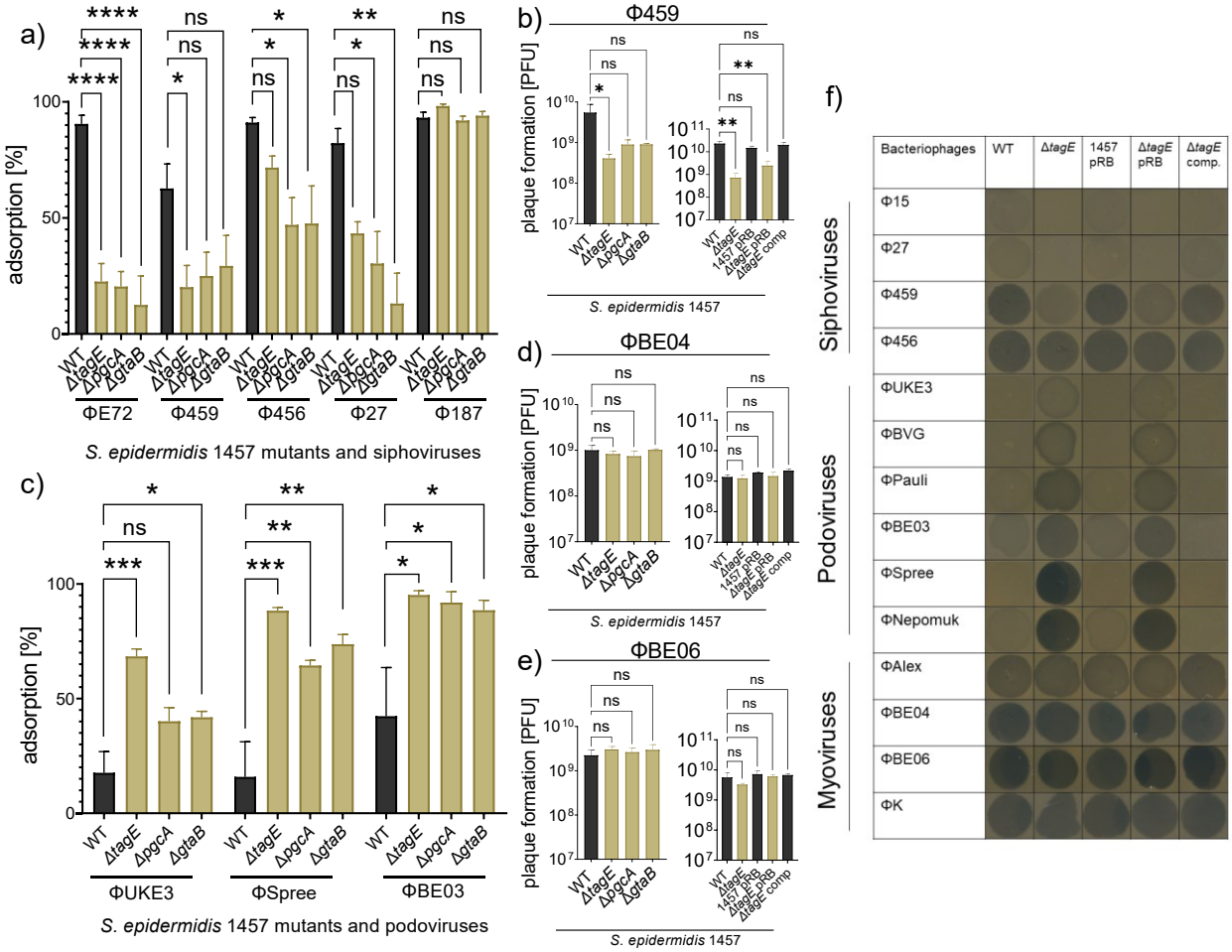

Figure 5: TagE-glycosylated WTA increases binding of siphoviruses but reduces podovirus binding. WTA glycosylation-deficient mutants of *S. epidermidis* show decreased binding of ΦE72-related siphoviruses Φ459, Φ456, and Φ27 (a), but increased binding of the podoviruses ΦUKE3, ΦSpree, and ΦBE03 (c), while the GroP-GalNAc-specific siphovirus Φ187 still shows strong binding (a). WTA glycosylation-deficient mutants of *S. epidermidis* show less plaque formation by ΦE72-related siphovirus Φ459 (b), while plaque formation by the myoviruses ΦBE04 (d) and ΦBE06 (e) remains unchanged. f) Lytic zones and "lysis from without" by siphoviruses decrease in the absence of *tagE* but increase for podoviruses. Myoviruses show formation of lytic zones independently of the presence or absence of *tagE*. (pRB= pRB473 (empty vector control); comp = complementation with *tagE*, *gtaB*, *pgcA* genes) The data represents the mean ± SEM of at least three independent experiments. Ordinary one-way ANOVA was used to determine statistical significance versus *S. epidermidis* 1457 wild type (WT), indicated as: not significant (ns), *P < 0.05, **P < 0.01, ***P < 0.001, ****P < 0.0001.

4. The presence of *tagE* in the genomes of CoNS species corresponds to the capacity of ΦE72 to transduce these species

The *tagE* gene was found in virtually all available *S. epidermidis* genomes suggesting that the substitution of GroP-WTA with glucose is a general trait in *S. epidermidis*. Accordingly, ΦE72 bound well to the tested *S. epidermidis* strains from at least two different sequence types (ST86, ST32) with one exception (Fig. 6b). Notably, ΦE72 did not bind to *S. epidermidis* E73 (ST23), which produces RboP-WTA in addition to GroP-WTA [6]. However, a E73 *tarIJLM2* mutant lacking RboP-WTA was effectively bound by ΦE72 indicating that the additional RboP-WTA shields the surface of *S. epidermidis* in a way that precludes binding of the phage.

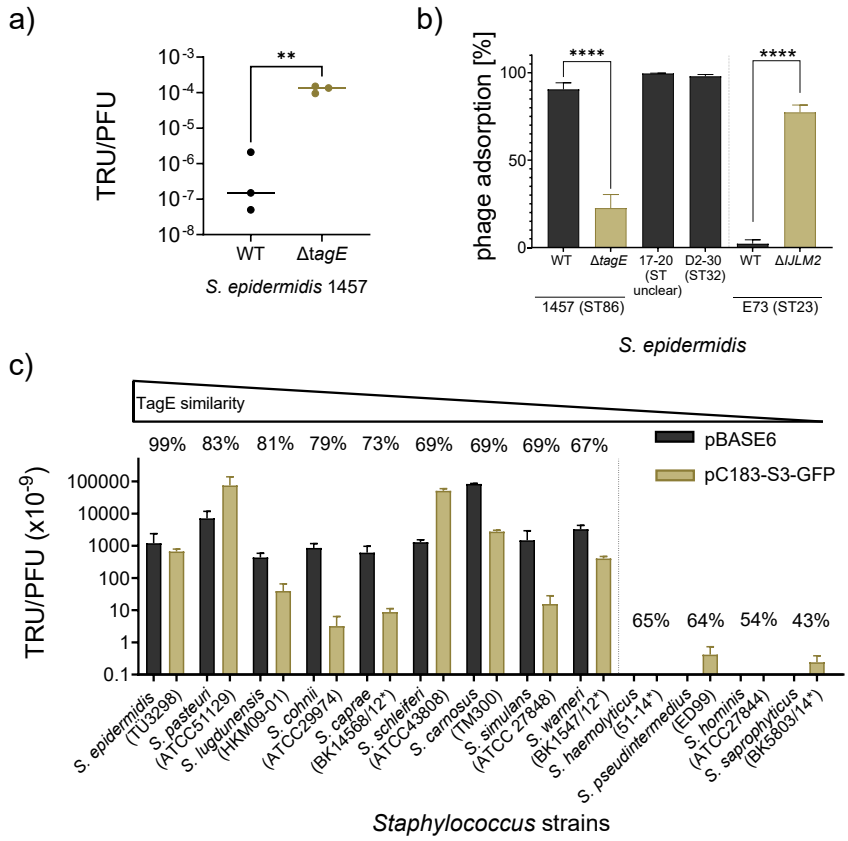

Figure 6: Correlation of TagE-related genes of CoNS species with phage transduction. a) Φ187 transduction of pRB473 is increased in the absence of glucosylated GroP-WTA. b) ΦE72 binds to different strains of *S. epidermidis* but binding is prevented by RboP expression of strain E73. c) ΦE72-mediated transduction of pBASE6 or pC183-S3-GFP to CoNS depends on high TagE homology. If type strains were used to determine sequence similarity of TagE homologues, strain names are marked with an asterisk. The data represents the mean ± SEM of at least three independent experiments. For a,b) unpaired t-test was used to determine statistical significance versus *S. epidermidis* 1457 wild type (WT), indicated as: **P < 0.01, ****P < 0.0001.

GroP-WTA has been reported in several other CoNS species. The nature of the sugar modifications in these species has remained largely unknown, but several CoNS have been reported to contain either glucose, GlcNAc or GalNAc attached to WTA [9]. We succeeded in transducing many different CoNS species via ΦE72 with either the staphylococcal shuttle vector pBASE or the green-fluorescent protein-expressing plasmid pC183-S3 GFP. Some of the available CoNS genomes were found to encode TagE homologs albeit with different degrees of sequence conservation, ranging from 43% to 83% similarity (Table 1). Those species with TagE similarities above 67% could be transduced by ΦE72, while those with less conserved TagE homologs did not take up DNA from ΦE72 (Fig. 6c), suggesting that only CoNS with highly conserved versions of TagE may glycosylate their GroP-WTA in a similar way as in *S. epidermidis* while the others may glycosylate either other WTA backbone types or may transfer other sugars. Among the tested species, *Staphylococcus pasteuri*, *Staphylococcus lugdunensis*, *Staphylococcus cohnii*, *Staphylococcus caprae*, *Staphylococcus schleiferi*, *Staphylococcus carnosus*, *Staphylococcus simulans,* and *Staphylococcus warneri* strains were transducible with ΦE72. Isolates of two of these species*, Staphylococcus cohnii* and *Staphylococcus warneri,* have indeed previously been described to produce GroP-WTA, which is modified with glucose [9]. In contrast to the varying degrees of conservation of *tagE*, the *pgcA* and *gtaB* genes are present in virtually all *Staphylococcus* genomes with high sequence similarity, including *S. aureus*, probably because UDP-glucose is required in all these species for DGlcDAG glycolipid synthesis [36]. Among the strains that encode highly conserved TagE homologues, *tagE* was encoded in the vicinity of both *pgcA* and *gtaB* only in *S. pasteuri* and *S. lugdunensis,* in addition to *S. epidermidis* (Table 1). Thus, phage ΦE72 represents a helpful tool for studying WTA properties and an attractive vehicle for interspecies transduction of DNA among members of the genus *Staphylococcus*.

Table 1: Conservation of TagE homologs in CoNS strains used for transduction.

Species	Strain name	Query cover [%]	Sequence identity [%]	Sequence similarity [%]	*tagE*, *pgcA*, *gtaB* encoded together
Staphylococcus epidermidis	TÜ3298	100%	99%	**99%**	Yes
Staphylococcus epidermidis	D2-30	100%	99%	**99%**	Yes
Staphylococcus pasteuri	ATCC51129	100%	69%	**83%**	Yes
Staphylococcus lugdunensis	HKU09-01	99%	64%	**81%**	Yes
Staphylococcus cohnii	ATCC29974	99%	61%	**79%**	No
Staphylococcus caprae	ATCC35538	100%	52%	**73%**	No
Staphylococcus schleiferi	ATCC43808	98%	50%	**69%**	No
Staphylococcus carnosus	TM300	99%	48%	**69%**	No
Staphylococcus simulans	ATCC27848	99%	46%	**69%**	No
Staphylococcus warneri	ATCC27836	99%	47%	**67%**	No
Staphylococcus haemolyticus	ATCC29970	99%	45%	**65%**	No
Staphylococcus pseudointermedius	ED99	100%	43%	**64%**	No
Staphylococcus hominis	ATCC27844	65%	28%	**54%**	No
Staphylococcus saprophyticus	ATCC15305	85%	24%	**43%**	No

Discussion

WTA structures are known to be highly diverse among Firmicutes, often with species- or even clone-specific composition [7, 38]. Most *S. epidermidis* produce a WTA type that is entirely different from that of *S. aureus* with a GroP rather than a RboP backbone. This study shows that *S. epidermidis* uses a GroP backbone with unmodified or with alanylated glucose. It remains unclear why *S. epidermidis* and *S. aureus* have developed such entirely different WTA types. The different structures may limit the number of bacteriophages that can infect and harm either one or both species. However, ΦK, one the most lytic bacteriophages, can lyse *Staphylococcus* cells irrespective of the WTA backbone structure and a recent study has demonstrated that several *Staphylococcus* phages can infect both, *S. aureus* and *S. epidermidis* [39]. The differences in WTA may limit infections and concomitant lysogenization or transduction events by specific members of the siphovirus group, which depend much more on a specific WTA backbone and glycosylation type than myoviruses. Notably, the presence of glucose on GroP-WTA prevented adsorption to *S. epidermidis* by all tested podoviruses (ΦUKE3, ΦSpree, and ΦBE03). The number of available *S. epidermidis*-targeting phages is still very limited, which impedes more extensive studies on the susceptibility of *S. epidermidis* wild-type and WTA mutant strains for different phage types. Discovery programs for identification of new phages that can infect *S. epidermidis* will help to clarify these questions in the future.

WTA is an important bacterial ligand for host receptors on mammalian immune cells with critical roles in innate immunity [8, 40]. WTA glycosylated with GlcNAc can activate the scavenger receptor langerin on skin Langerhans cells [41]. *S. aureus* is found on the skin of atopic dermatitis patients eliciting skin inflammation in a process that probably involves WTA-langerin interaction [8]. In contrast, *S. epidermidis* cannot activate langerin [41], probably because its GroP-WTA is glycosylated with glucose. It may be advantageous for *S. epidermidis*, one of the most abundant skin-colonizers [1], and for other CoNS, to avoid skin inflammation by producing a non-inflammatory WTA type decorated with glucose.

S. epidermidis uses the same pathway for GroP-WTA glycosylation with glucose residues as described for *B. subtilis* [28]. Activation of glucose via the PgcA and GtaB enzymes yields UDP-glucose as donor of glucose residues, which are subsequently transferred to the WTA backbone by TagE. Other WTA

glycosyltransferases apart for TarM [27], including those transferring glucose to RboP-WTA in *B. subtilis* W23 (TarQ) [7, 11], GlcNAc to RboP-WTA in certain *S. aureus* clones (TarS, TarP) [11, 42], or GalNAc to GroP-WTA in *S. aureus* ST395 (TagN) [24] share no or very low similarity with TagE. However, protein structure prediction with Alphafold 2 revealed that TagE most likely forms a symmetric, propeller-like homotrimer with each monomer divided into the characteristic glycosyltransferase domain and the β-sheets containing trimerization domain as previously described for the well-studied *S. aureus* glycosyltransferase TarM (Fig. S5) [43-45].

In addition to glucose, WTA is usually also modified with D-alanine [38]. Since GroP repeating units have only one free hydroxyl group for substitution with either D-alanine or glucose, it is not surprising that only ca. 50% of the repeating units carried glucose residues. The teichoic acid D-alanylation machinery attaches D-alanine to a variety of different molecules including LTA, RboP-WTA, and GroP-WTA [46]. Its limited specificity for acceptor substrates may explain why a minor portion of the glucose residues on *S. epidermidis* GroP-WTA are also alanylated. GroP repeating units are shorter than RboP repeating units, which may explain why the additional RboP-WTA polymers of *S. epidermidis* E73 are probably longer and precluded binding of ΦE72 to strain E73. The additional WTA may, therefore, represent a further strategy to interfere with phage infection and with interaction of other WTA-binding molecules.

Several other CoNS species appear to produce a similar WTA type as *S. epidermidis* because they encode potential TagE proteins and interact with ΦE72. Interspecies horizontal gene transfer via WTA-binding transducing phages appears to be rather common among these species and may have contributed to the import of the methicillin-resistance conferring *mecA* gene into *S. epidermidis* and, eventually, to *S. aureus* to create MRSE and MRSA clones [20]. It remains mysterious how the barrier for horizontal gene transfer between *S. epidermidis* and *S. aureus* that results from the substantial differences in WTA structure could be overcome. Specific *S. epidermidis* clonal lineages with both, GroP-WTA and *S. aureus*-type RboP-WTA such as ST10, ST23, and ST87 [6] or the *S. aureus* lineage ST395 producing CoNS-type GroP-WTA [14], may represent critical hubs for the exchange of genetic material between the species *S. epidermidis* and *S. aureus*. Several CoNS species encode

potential WTA glycosyltransferase homologs with only low or no similarity to TagE. They may produce other WTA backbones or glycosylate their WTA with other sugars. *S. epidermidis* often causes difficult-to-treat biofilm-based infections on implanted materials, which frequently require surgical replacement [4]. Treatment with lytic bacteriophages that could destroy *S. epidermidis* biofilms hold promise for the development of new therapeutic strategies [3, 18]. Understanding how phages detect suitable host bacteria and which *S. epidermidis* clones express corresponding phage-binding WTA motives will be important for the success of such strategies. The TagE-mediated WTA glycosylation with glucose might contribute to the narrow host range of lytic podoviruses like ΦBE03 [37]. Accordingly, finding podoviruses, which bind to GroP-WTA glucose might help to develop efficient therapeutic phage cocktails. Moreover, glycosylated WTA is a major antigen for protective antibodies against *S. aureus* [42, 47, 48] and, probably, also *S. epidermidis*. It represents therefore a particularly attractive antigen for vaccine development [48]. As for phage therapy, the success of such vaccination strategies will depend on in-depth knowledge on the structure and prevalence of WTA glycoepitopes among different *S. epidermidis* lineages. Our study may motivate more extensive investigations on WTA glycoepitopes in different staphylococcal pathogens and commensals.

Materials and Methods

Bacterial strains and growth conditions

S. epidermidis and *S. aureus* strains were cultivated in basic medium (BM) and incubated at 37°C on an orbital shaker. *E. coli* strains were cultivated in lysogeny broth (LB). Media were supplemented with appropriate antibiotics chloramphenicol (10 µg/ml), or ampicillin (100 µg/ml). *E. coli* DC10b and *S. aureus* PS187 Δ*sauUSI*Δ*hsdR* were used as cloning hosts, *S. epidermidis* 1457 was used for gene deletion studies. Bacteriophages and propagation strains used in this study are listed in Table S1.

Transposon mutagenesis of *S. epidermidis* strain 1457

The transposon plasmid pBTn described previously [25] was used to create a transposon library in *S. epidermidis* 1457. The features of this temperature-sensitive *E. coli/S. aureus* shuttle vector include a mini-transposon with an erythromycin

resistance cassette flanked by inverted repeats from the horn fly transposon and a xylose-inducible transposase Himar1, which can mobilize the mini-transposon and integrate it into the chromosome with no bias for any specific sequence. Transposon library construction has been described in detail before [27]. In short, *S. epidermidis* 1457 was transformed with pBTn followed by mobilization of the mini-transposon into the genome upon xylose induction of the transposase. The pBTn plasmid was cured via shifts to nonpermissive temperature.

Isolation of phage-resistant transposon mutants

To isolate phage-resistant mutants, the transposon mutant library was infected with ΦE72 at a MOI of at least 100. After incubation for up to 4 h, the cells were centrifuged at 5,000 × g for 10 min and plated on TSA agar containing erythromycin. Single colonies of surviving mutants were transferred to fresh TSA agar plates repeatedly. Phage resistance was confirmed by spot assays with ΦE72, and the phage-resistant mutants were treated with 1 µg/ml mitomycin to test for and to exclude lysogeny. To identify the site of transposon insertion, total DNA was isolated, purified with the NucleoSpin® tissue kit (Macherey-Nagel, Düren), digested, religated, multiplied with primers erm-For and erm-Rev (Table S2), which anneal to the erythromycin resistance cassette of the mini-transposon, and sequenced.

Molecular genetic methods

For the construction of the *tagE*, *pgcA,* and *gtaB* mutants in *S. epidermidis* 1457, the pBASE6 *E. coli/S.aureus* shuttle vector was used according to standard procedures [49]. For mutant complementation, plasmid pRB473 was used [50]. The primers for knockout and complementation plasmid construction are listed in (Table S2). Both pBASE6 and pRB473 containing either the respective up- and downstream fragments for knockout construction (pBASE6) or the complementation sequence (pRB473), were used to transform *E. coli* DC10b, and subsequently PS187 Δ*sauUSI*Δ*hsdR* by electroporation. The plasmids were subsequently transferred to *S. epidermidis* strain 1457 by transduction with Φ187 using *S. aureus* PS187 Δ*sauUSI*Δ*hsdR* as donor strain as described previously [51].

Phage binding, infection, and transduction assays

Phage spot assays were performed as described previously [14]. All applied bacteriophages (Table S1) were propagated in suitable bacterial host strains and phage lysates were filtered to yield sterile phage suspensions. Test bacteria were cultivated overnight in fresh BM. OD_{600} = 0.1 was adjusted in 5 ml LB soft agar for the preparation of bacterial overlay lawns. 10 µl of phage suspensions were spotted onto the bacterial lawns. After overnight incubation at 37°C for podoviruses and siphoviruses, and 30°C for myoviruses, phage clearing zones and individual plaques were observed and recorded.

Phage adsorption efficiency was determined as described previously with minor modifications [14]. Briefly, adsorption rates were analyzed by mixing approximately 10^6 PFU/ml in BM supplemented with 4 mM $CaCl_2$ with the tested bacteria at an OD_{600} of 0.5 and incubating for 15 min at 37°C. The samples were subsequently centrifuged, and the supernatants were spotted on indicator strains to determine the number of unbound phages in the supernatant. The adsorption rate was calculated by dividing the number of bound phages by the number of input phages.

Transduction experiments were performed as described previously [14]. Briefly, 1 ml of exponentially growing cultures of a recipient strain was adjusted to an OD_{600} of 0.5. The cells were sedimented by centrifugation and resuspended in 200 µl of phage buffer containing 0.1% gelatin, 1 mM $MgSO_4$, 4 mM $CaCl_2$, 50 mM Tris, and 0.1 M NaCl. 200 µl of bacteria in phage buffer were mixed with 100 µl of lysates obtained from *S. aureus* PS187 and *S. epidermidis* 1457 donor strains carrying plasmids of choice. Samples were then incubated for 15 min at 37°C, diluted, and plated on chloramphenicol-containing BM agar to count colonies.

Electron microscopy

S. epidermidis 1457 wild type, Δ*tagE*, Δ*pgcA*, and Δ*gtaB* were grown until stationary phase, and fixed at an OD_{600} of 10 in 200 µl Karnovsky's fixative (3% formaldehyde, 2.5% glutaraldehyde in 0.1 M phosphate buffer pH 7.4) for 24 h. Samples were then centrifuged at 1,400 x g for 5 min, supernatant was discarded, pellets were resuspended in approximately 20 µl agarose (3.9%) at 37°C, cooled to room

temperature, and cut into small pieces. Postfixation was based on 1.0% osmium tetroxide containing 2.5% potassium ferrocyanide (Morphisto) for 2 h. After following the standard methods, samples were embedded in glycide ether and cut using an ultramicrotome (Ultracut E, Reichert). Ultra-thin sections (30 nm) were mounted on copper grids and analyzed using a Zeiss LIBRA 120 transmission electron microscope (Carl Zeiss) operating at 120 kV.

WTA isolation

WTA was isolated as described previously [14, 52, 53] with minor modifications. Briefly, bacterial cells from two liters of overnight cultures were washed and disrupted with glass beads in a cell disrupter (Euler). Cell lysates were incubated at 37°C overnight in the presence of DNase and RNase. SDS was added to a final concentration of 2% followed by ultrasonication for 15 min. Cell walls were washed several times to remove SDS. To release WTA from cell walls, samples were treated with 5% trichloroacetic acid for 4 h at 65°C. Peptidoglycan debris was separated via centrifugation (10 min, 14,500 x g). Determination of phosphate amounts as described previously [53-55] was used for WTA quantification. Crude WTA extracts were further purified as already described [27]. Briefly, the pH of the crude extract was adjusted to 5 with NaOH and dialyzed against water with a Slide-A-Lyzer Dialysis Cassette (MWCO of 3.5 kDa; Thermo Fisher Scientific). For HPLC-MS analysis, 50 µl of 100 mM WTA sample were hydrolyzed with 100 mM NaOH at 60°C for 2 h. The remaining dialyzed WTA was further lyophilized for long-term storage at -20 °C or used for further analysis. 10-15 mg lyophilized WTA sample were used for NMR. Detailed explanations of the HPLC-MS and NMR methods can be found as extended descriptions of detailed methods.

Enzymatic determination of glucose in the WTA samples

The High Sensitivity Glucose Assay Kit (mak181, Sigma-Aldrich) was used to determine the glucose content in the WTA sample. 50 µl of dialyzed WTA samples and 50 µl of 1 mM glucose standard solution were dried in a vacuum concentrator at 60°C. 100 µl of 0.5 M HCl was added to the samples and the standard solution and cooked for 2 h in a water bath. The glucose standard was diluted 1:50 resulting in a 10 µM concentration and different volumes were used to cover a range of 0 - 100

pmol. Samples were also diluted at least 1:50 and different dilutions of the samples were tested in a 96-well plate. The assay was performed according to the manufacturer's instructions. The fluorescence intensity was measured at excitation wavelength 535 nm and emission wavelength 587 nm.

Glycolipid isolation, thin layer chromatography (TLC) and detection with α-naphthol

The detection of glycolipids was performed similar to a previously described method [36]. *S. epidermidis* 1457 and the respective mutants were grown to OD_{600} of 3.5. 5 ml of bacterial suspension were washed and resuspended in 500 µl of 100 mM sodiumacetate (pH 4.7) and transferred into glass vials. 500 µl chloroform and 500 ml methanol were added and the mixture was vortexed vigorously. The samples were centrifuged at 4,600 x g for 20 min at 4°C and the lower phase was dried overnight and resuspended in 25 µl methanol and chloroform in a 1:1 ratio. The whole sample was applied to a high-performance thin-layer chromatography (HPTLC) silica gel 60 plate (10 x 10 cm; Merck) with a Hamilton syringe. A positive control containing 5 µg digalactosyldiacylglycerol (DGDG, Sigma-Aldrich) was used. A Linomat 5 (Camag), and an auto developing chamber (Camag), were used to apply the sample to the TLC plate and to run it with a solvent containing 65:25:4 (v/v/v) chloroform/methanol/H_2O. The dried TLC plate was sprayed with 3.2% α-naphthol in methanol/H_2SO_4/H_2O 25:3:2 (v/v/v) and the glycolipids were visualized by heating the plate at 110°C for a few minutes.

***In silico* analysis**

All statistical analyses were performed with Graph Pad Prism 9.2.0 (GraphPad Software, La Jolla, USA). Multiple sequence alignment was performed with SnapGene® 5.3.2 using MUSCLE. Protein structure prediction was done using AlphaFold2 with ColabFold [44, 45].

Acknowledgements

We thank David Gerlach, Xin Du, and Bernhard Krismer for helpful discussions, Arnaud Kengmo Tchoupa and Ulrike Redel for help with TLC, and Y. Que and E. Baumgartner for supply of phages. This work was financed by grants from the

German Research Foundation to A.P. (TRR34; TRR165 project ID 246807620; PE 805/7-1 project ID 410190180; PE 805/8-1 project ID 410190180) and the German Center for Infection Research (DZIF) to A.P.
The authors acknowledge infrastructural support by the Cluster of Excellence EXC 2124 ‘Controlling Microbes to Fight Infections’ project ID 39083813.

References

1. Severn MM, Horswill AR. Staphylococcus epidermidis and its dual lifestyle in skin health and infection. Nat Rev Microbiol. 2022. Epub 20220830. doi: 10.1038/s41579-022-00780-3. PubMed PMID: 36042296.
2. Otto M. Staphylococcus epidermidis--the 'accidental' pathogen. Nat Rev Microbiol. 2009;7(8):555-67. doi: 10.1038/nrmicro2182. PubMed PMID: 19609257; PubMed Central PMCID: PMCPMC2807625.
3. Schilcher K, Horswill AR. Staphylococcal Biofilm Development: Structure, Regulation, and Treatment Strategies. Microbiol Mol Biol Rev. 2020;84(3). Epub 20200812. doi: 10.1128/mmbr.00026-19. PubMed PMID: 32792334; PubMed Central PMCID: PMCPMC7430342.
4. Becker K, Heilmann C, Peters G. Coagulase-negative staphylococci. Clin Microbiol Rev. 2014;27(4):870-926. doi: 10.1128/CMR.00109-13. PubMed PMID: 25278577; PubMed Central PMCID: PMCPMC4187637.
5. Otto M. Staphylococcal Biofilms. Microbiol Spectr. 2018;6(4). doi: 10.1128/microbiolspec.GPP3-0023-2018. PubMed PMID: 30117414; PubMed Central PMCID: PMCPMC6282163.
6. Du X, Larsen J, Li M, Walter A, Slavetinsky C, Both A, et al. Staphylococcus epidermidis clones express Staphylococcus aureus-type wall teichoic acid to shift from a commensal to pathogen lifestyle. Nat Microbiol. 2021;6(6):757-68. Epub 20210524. doi: 10.1038/s41564-021-00913-z. PubMed PMID: 34031577.
7. Brown S, Santa Maria JP, Jr., Walker S. Wall teichoic acids of gram-positive bacteria. Annu Rev Microbiol. 2013;67:313-36. doi: 10.1146/annurev-micro-092412-155620. PubMed PMID: 24024634; PubMed Central PMCID: PMCPMC3883102.

8. van Dalen R, Peschel A, van Sorge NM. Wall Teichoic Acid in Staphylococcus aureus Host Interaction. Trends Microbiol. 2020;28(12):985-98. Epub 20200612. doi: 10.1016/j.tim.2020.05.017. PubMed PMID: 32540314.
9. Endl J, Seidl HP, Fiedler F, Schleifer KH. Chemical composition and structure of cell wall teichoic acids of staphylococci. Arch Microbiol. 1983;135(3):215-23. doi: 10.1007/BF00414483. PubMed PMID: 6639273.
10. Ingmer H, Gerlach D, Wolz C. Temperate Phages of Staphylococcus aureus. Microbiol Spectr. 2019;7(5). Epub 2019/09/29. doi: 10.1128/microbiolspec.GPP3-0058-2018. PubMed PMID: 31562736.
11. Brown S, Xia G, Luhachack LG, Campbell J, Meredith TC, Chen C, et al. Methicillin resistance in Staphylococcus aureus requires glycosylated wall teichoic acids. Proc Natl Acad Sci U S A. 2012;109(46):18909-14. Epub 20121001. doi: 10.1073/pnas.1209126109. PubMed PMID: 23027967; PubMed Central PMCID: PMCPMC3503181.
12. Gerlach D, Sieber RN, Larsen J, Krusche J, De Castro C, Baumann J, et al. Horizontal transfer and phylogenetic distribution of the immune evasion factor tarP. Front Microbiol. 2022;13:951333. Epub 20221028. doi: 10.3389/fmicb.2022.951333. PubMed PMID: 36386695; PubMed Central PMCID: PMCPMC9650247.
13. Li X, Gerlach D, Du X, Larsen J, Stegger M, Kühner P, et al. An accessory wall teichoic acid glycosyltransferase protects Staphylococcus aureus from the lytic activity of Podoviridae. Sci Rep. 2015;5:17219. Epub 20151124. doi: 10.1038/srep17219. PubMed PMID: 26596631; PubMed Central PMCID: PMCPMC4667565.
14. Winstel V, Liang C, Sanchez-Carballo P, Steglich M, Munar M, Bröker BM, et al. Wall teichoic acid structure governs horizontal gene transfer between major bacterial pathogens. Nat Commun. 2013;4:2345. doi: 10.1038/ncomms3345. PubMed PMID: 23965785; PubMed Central PMCID: PMCPMC3903184.
15. Xia G, Corrigan RM, Winstel V, Goerke C, Gründling A, Peschel A. Wall teichoic Acid-dependent adsorption of staphylococcal siphovirus and myovirus. J Bacteriol. 2011;193(15):4006-9. Epub 20110603. doi: 10.1128/jb.01412-10. PubMed PMID: 21642458; PubMed Central PMCID: PMCPMC3147540.

16. O'Flaherty S, Ross RP, Meaney W, Fitzgerald GF, Elbreki MF, Coffey A. Potential of the polyvalent anti-Staphylococcus bacteriophage K for control of antibiotic-resistant staphylococci from hospitals. Appl Environ Microbiol. 2005;71(4):1836-42. doi: 10.1128/aem.71.4.1836-1842.2005. PubMed PMID: 15812009; PubMed Central PMCID: PMCPMC1082512.
17. Cerca N, Oliveira R, Azeredo J. Susceptibility of Staphylococcus epidermidis planktonic cells and biofilms to the lytic action of staphylococcus bacteriophage K. Lett Appl Microbiol. 2007;45(3):313-7. doi: 10.1111/j.1472-765X.2007.02190.x. PubMed PMID: 17718845.
18. Kilcher S, Loessner MJ. Engineering Bacteriophages as Versatile Biologics. Trends Microbiol. 2019;27(4):355-67. Epub 20181012. doi: 10.1016/j.tim.2018.09.006. PubMed PMID: 30322741.
19. Winstel V, Kühner P, Rohde H, Peschel A. Genetic engineering of untransformable coagulase-negative staphylococcal pathogens. Nat Protoc. 2016;11(5):949-59. Epub 20160421. doi: 10.1038/nprot.2016.058. PubMed PMID: 27101516.
20. Rolo J, Worning P, Nielsen JB, Bowden R, Bouchami O, Damborg P, et al. Evolutionary Origin of the Staphylococcal Cassette Chromosome mec (SCCmec). Antimicrob Agents Chemother. 2017;61(6). Epub 20170524. doi: 10.1128/AAC.02302-16. PubMed PMID: 28373201; PubMed Central PMCID: PMCPMC5444190.
21. Lee AS, de Lencastre H, Garau J, Kluytmans J, Malhotra-Kumar S, Peschel A, et al. Methicillin-resistant Staphylococcus aureus. Nat Rev Dis Primers. 2018;4:18033. Epub 2018/06/01. doi: 10.1038/nrdp.2018.33. PubMed PMID: 29849094.
22. Fisarova L, Botka T, Du X, Maslanova I, Bardy P, Pantucek R, et al. Staphylococcus epidermidis Phages Transduce Antimicrobial Resistance Plasmids and Mobilize Chromosomal Islands. mSphere. 2021;6(3). Epub 2021/05/14. doi: 10.1128/mSphere.00223-21. PubMed PMID: 33980677.
23. Fanaei Pirlar R, Wagemans J, Ponce Benavente L, Lavigne R, Trampuz A, Gonzalez Moreno M. Novel Bacteriophage Specific against Staphylococcus epidermidis and with Antibiofilm Activity. Viruses. 2022;14(6). Epub 20220620.

doi: 10.3390/v14061340. PubMed PMID: 35746811; PubMed Central PMCID: PMCPMC9230115.

24. Winstel V, Sanchez-Carballo P, Holst O, Xia G, Peschel A. Biosynthesis of the unique wall teichoic acid of Staphylococcus aureus lineage ST395. mBio. 2014;5(2):e00869. Epub 20140408. doi: 10.1128/mBio.00869-14. PubMed PMID: 24713320; PubMed Central PMCID: PMCPMC3993852.
25. Li M, Rigby K, Lai Y, Nair V, Peschel A, Schittek B, et al. Staphylococcus aureus mutant screen reveals interaction of the human antimicrobial peptide dermcidin with membrane phospholipids. Antimicrob Agents Chemother. 2009;53(10):4200-10. Epub 20090713. doi: 10.1128/aac.00428-09. PubMed PMID: 19596877; PubMed Central PMCID: PMCPMC2764178.
26. Allison SE, D'Elia MA, Arar S, Monteiro MA, Brown ED. Studies of the genetics, function, and kinetic mechanism of TagE, the wall teichoic acid glycosyltransferase in Bacillus subtilis 168. J Biol Chem. 2011;286(27):23708-16. Epub 20110510. doi: 10.1074/jbc.M111.241265. PubMed PMID: 21558268; PubMed Central PMCID: PMCPMC3129151.
27. Xia G, Maier L, Sanchez-Carballo P, Li M, Otto M, Holst O, et al. Glycosylation of wall teichoic acid in Staphylococcus aureus by TarM. J Biol Chem. 2010;285(18):13405-15. Epub 20100225. doi: 10.1074/jbc.M109.096172. PubMed PMID: 20185825; PubMed Central PMCID: PMCPMC2859500.
28. Lazarevic V, Soldo B, Médico N, Pooley H, Bron S, Karamata D. Bacillus subtilis alpha-phosphoglucomutase is required for normal cell morphology and biofilm formation. Appl Environ Microbiol. 2005;71(1):39-45. doi: 10.1128/aem.71.1.39-45.2005. PubMed PMID: 15640167; PubMed Central PMCID: PMCPMC544238.
29. Pooley HM, Paschoud D, Karamata D. The gtaB marker in Bacillus subtilis 168 is associated with a deficiency in UDPglucose pyrophosphorylase. J Gen Microbiol. 1987;133(12):3481-93. doi: 10.1099/00221287-133-12-3481. PubMed PMID: 2846750.
30. Yasbin RE, Maino VC, Young FE. Bacteriophage resistance in Bacillus subtilis 168, W23, and interstrain transformants. J Bacteriol. 1976;125(3):1120-6. doi: 10.1128/jb.125.3.1120-1126.1976. PubMed PMID: 815237; PubMed Central PMCID: PMCPMC236191.

31. Qian Z, Yin Y, Zhang Y, Lu L, Li Y, Jiang Y. Genomic characterization of ribitol teichoic acid synthesis in Staphylococcus aureus: genes, genomic organization and gene duplication. BMC Genomics. 2006;7(1):74. doi: 10.1186/1471-2164-7-74.
32. Swoboda JG, Campbell J, Meredith TC, Walker S. Wall teichoic acid function, biosynthesis, and inhibition. Chembiochem. 2010;11(1):35-45. doi: 10.1002/cbic.200900557. PubMed PMID: 19899094; PubMed Central PMCID: PMCPMC2798926.
33. Jorasch P, Wolter FP, Zähringer U, Heinz E. A UDP glucosyltransferase from Bacillus subtilis successively transfers up to four glucose residues to 1,2-diacylglycerol: expression of ypfP in Escherichia coli and structural analysis of its reaction products. Mol Microbiol. 1998;29(2):419-30. doi: 10.1046/j.1365-2958.1998.00930.x. PubMed PMID: 9720862.
34. Kiriukhin MY, Debabov DV, Shinabarger DL, Neuhaus FC. Biosynthesis of the glycolipid anchor in lipoteichoic acid of Staphylococcus aureus RN4220: role of YpfP, the diglucosyldiacylglycerol synthase. J Bacteriol. 2001;183(11):3506-14. doi: 10.1128/jb.183.11.3506-3514.2001. PubMed PMID: 11344159; PubMed Central PMCID: PMCPMC99649.
35. Fedtke I, Mader D, Kohler T, Moll H, Nicholson G, Biswas R, et al. A Staphylococcus aureus ypfP mutant with strongly reduced lipoteichoic acid (LTA) content: LTA governs bacterial surface properties and autolysin activity. Mol Microbiol. 2007;65(4):1078-91. Epub 20070719. doi: 10.1111/j.1365-2958.2007.05854.x. PubMed PMID: 17640274; PubMed Central PMCID: PMCPMC2169524.
36. Gründling A, Schneewind O. Genes required for glycolipid synthesis and lipoteichoic acid anchoring in Staphylococcus aureus. J Bacteriol. 2007;189(6):2521-30. Epub 20070105. doi: 10.1128/jb.01683-06. PubMed PMID: 17209021; PubMed Central PMCID: PMCPMC1899383.
37. Valente LG, Pitton M, Fürholz M, Oberhaensli S, Bruggmann R, Leib SL, et al. Isolation and characterization of bacteriophages from the human skin microbiome that infect Staphylococcus epidermidis. FEMS Microbes. 2021;2. doi: 10.1093/femsmc/xtab003.

38. Weidenmaier C, Peschel A. Teichoic acids and related cell-wall glycopolymers in Gram-positive physiology and host interactions. Nat Rev Microbiol. 2008;6(4):276-87. Epub 2008/03/11. doi: 10.1038/nrmicro1861. PubMed PMID: 18327271.

39. Goller PC, Elsener T, Lorge D, Radulovic N, Bernardi V, Naumann A, et al. Multi-species host range of staphylococcal phages isolated from wastewater. Nat Commun. 2021;12(1):6965. Epub 20211129. doi: 10.1038/s41467-021-27037-6. PubMed PMID: 34845206; PubMed Central PMCID: PMCPMC8629997.

40. Schade J, Weidenmaier C. Cell wall glycopolymers of Firmicutes and their role as nonprotein adhesins. FEBS Lett. 2016;590(21):3758-71. Epub 20160725. doi: 10.1002/1873-3468.12288. PubMed PMID: 27396949.

41. van Dalen R, De La Cruz Diaz JS, Rumpret M, Fuchsberger FF, van Teijlingen NH, Hanske J, et al. Langerhans Cells Sense Staphylococcus aureus Wall Teichoic Acid through Langerin To Induce Inflammatory Responses. mBio. 2019;10(3). Epub 20190514. doi: 10.1128/mBio.00330-19. PubMed PMID: 31088921; PubMed Central PMCID: PMCPMC6520447.

42. Gerlach D, Guo Y, De Castro C, Kim SH, Schlatterer K, Xu FF, et al. Methicillin-resistant Staphylococcus aureus alters cell wall glycosylation to evade immunity. Nature. 2018;563(7733):705-9. Epub 20181121. doi: 10.1038/s41586-018-0730-x. PubMed PMID: 30464342.

43. Koc C, Gerlach D, Beck S, Peschel A, Xia G, Stehle T. Structural and enzymatic analysis of TarM glycosyltransferase from Staphylococcus aureus reveals an oligomeric protein specific for the glycosylation of wall teichoic acid. J Biol Chem. 2015;290(15):9874-85. Epub 20150219. doi: 10.1074/jbc.M114.619924. PubMed PMID: 25697358; PubMed Central PMCID: PMCPMC4392284.

44. Jumper J, Evans R, Pritzel A, Green T, Figurnov M, Ronneberger O, et al. Highly accurate protein structure prediction with AlphaFold. Nature. 2021;596(7873):583-9. Epub 20210715. doi: 10.1038/s41586-021-03819-2. PubMed PMID: 34265844; PubMed Central PMCID: PMCPMC8371605.

45. Mirdita M, Schütze K, Moriwaki Y, Heo L, Ovchinnikov S, Steinegger M. ColabFold: making protein folding accessible to all. Nature Methods. 2022;19(6):679-82. doi: 10.1038/s41592-022-01488-1.
46. Schultz BJ, Snow ED, Walker S. Mechanism of D-alanine transfer to teichoic acids shows how bacteria acylate cell envelope polymers. Nat Microbiol. 2023. Epub 20230612. doi: 10.1038/s41564-023-01411-0. PubMed PMID: 37308592.
47. Kurokawa K, Jung DJ, An JH, Fuchs K, Jeon YJ, Kim NH, et al. Glycoepitopes of staphylococcal wall teichoic acid govern complement-mediated opsonophagocytosis via human serum antibody and mannose-binding lectin. J Biol Chem. 2013;288(43):30956-68. Epub 20130917. doi: 10.1074/jbc.M113.509893. PubMed PMID: 24045948; PubMed Central PMCID: PMCPMC3829409.
48. van Dalen R, Molendijk MM, Ali S, van Kessel KPM, Aerts P, van Strijp JAG, et al. Do not discard Staphylococcus aureus WTA as a vaccine antigen. Nature. 2019;572(7767):E1-e2. Epub 20190731. doi: 10.1038/s41586-019-1416-8. PubMed PMID: 31367020.
49. Geiger T, Francois P, Liebeke M, Fraunholz M, Goerke C, Krismer B, et al. The stringent response of Staphylococcus aureus and its impact on survival after phagocytosis through the induction of intracellular PSMs expression. PLoS Pathog. 2012;8(11):e1003016. Epub 20121129. doi: 10.1371/journal.ppat.1003016. PubMed PMID: 23209405; PubMed Central PMCID: PMCPMC3510239.
50. Brückner R. A series of shuttle vectors for Bacillus subtilis and Escherichia coli. Gene. 1992;122(1):187-92. doi: 10.1016/0378-1119(92)90048-t. PubMed PMID: 1452028.
51. Winstel V, Kühner P, Rohde H, Peschel A. Genetic engineering of untransformable coagulase-negative staphylococcal pathogens. Nature Protocols. 2016;11(5):949-59. doi: 10.1038/nprot.2016.058.
52. Weidenmaier C, Kokai-Kun JF, Kristian SA, Chanturiya T, Kalbacher H, Gross M, et al. Role of teichoic acids in Staphylococcus aureus nasal colonization, a major risk factor in nosocomial infections. Nat Med. 2004;10(3):243-5. Epub 20040201. doi: 10.1038/nm991. PubMed PMID: 14758355.

53. Peschel A, Otto M, Jack RW, Kalbacher H, Jung G, Gotz F. Inactivation of the dlt operon in Staphylococcus aureus confers sensitivity to defensins, protegrins, and other antimicrobial peptides. J Biol Chem. 1999;274(13):8405-10. doi: 10.1074/jbc.274.13.8405. PubMed PMID: 10085071.
54. Chen PS, Toribara TY, Warner H. Microdetermination of Phosphorus. Analytical Chemistry. 1956;28:1756-8.
55. Chen PS, Toribara TY, Warner H. Microdetermination of Phosphorus. Analytical Chemistry. 1956;28(11):1756-8. doi: 10.1021/ac60119a033.
56. Kontou EE, Walter A, Alka O, Pfeuffer J, Sachsenberg T, Mohite OS, et al. UmetaFlow: an untargeted metabolomics workflow for high-throughput data processing and analysis. Journal of Cheminformatics. 2023;15(1):52. doi: 10.1186/s13321-023-00724-w.
57. Speciale I, Notaro A, Garcia-Vello P, Di Lorenzo F, Armiento S, Molinaro A, et al. Liquid-state NMR spectroscopy for complex carbohydrate structural analysis: A hitchhiker's guide. Carbohydrate Polymers. 2022;277:118885. doi: https://doi.org/10.1016/j.carbpol.2021.118885.
58. Garcia-Vello P, Sharma G, Speciale I, Molinaro A, Im SH, De Castro C. Structural features and immunological perception of the cell surface glycans of Lactobacillus plantarum: a novel rhamnose-rich polysaccharide and teichoic acids. Carbohydr Polym. 2020;233:115857. Epub 20200110. doi: 10.1016/j.carbpol.2020.115857. PubMed PMID: 32059908.

Supplementary Figures

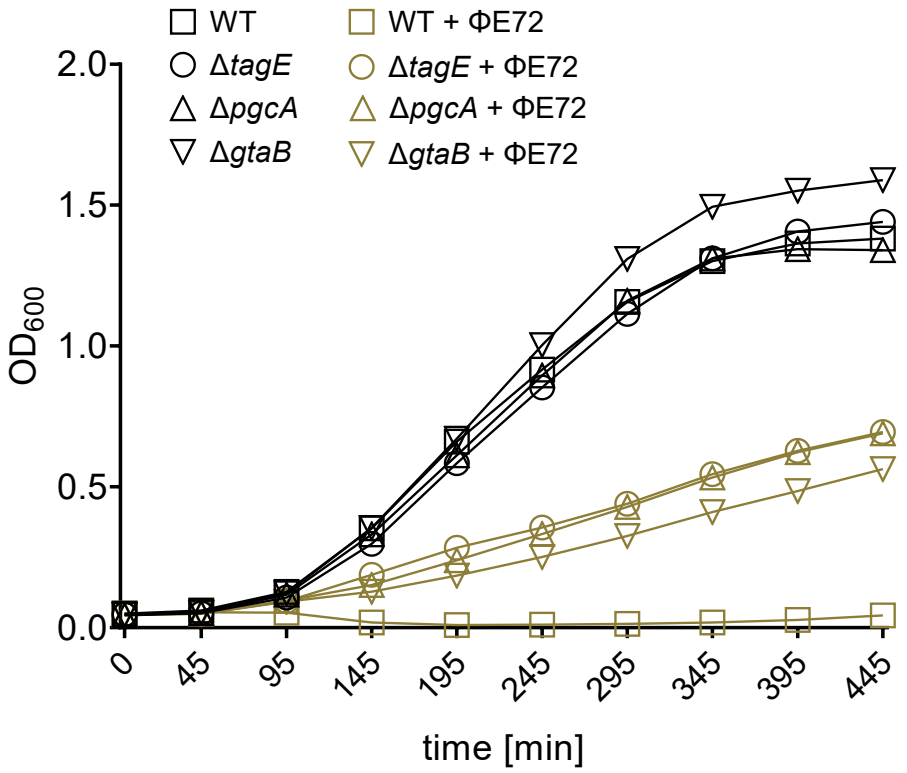

Fig. S1: ΦE72 prevents growth of *S. epidermidis* 1457 wild type (WT). Growth of the Δ*tagE*, Δ*pgcA,* Δ*gtaB* mutants is only partially reduced by ΦE72 compared to growth without addition of phage. Approximately 5x10^8 PFU/ml were used. Data represent mean ± SEM of three independent experiments.

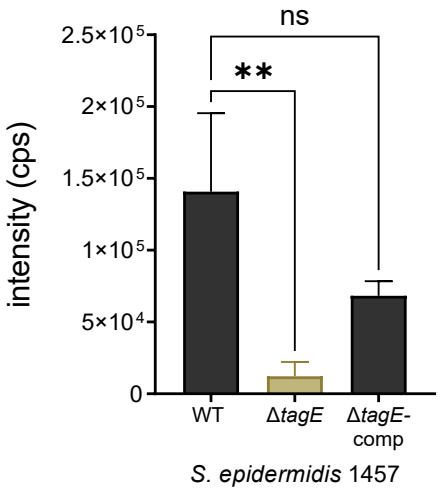

Fig. S2: Area-under-the-curve quantification of GroP-GroP-Glc residue ($[M-H]^-$ = 487.0623) total ion current (TIC) chromatogram measured by HPLC-MS after chemical digest of *S. epidermidis* WTA. Data represent mean ± SEM of three independent experiments. Ordinary one-way ANOVA was used

to determine statistical significance versus *S. epidermidis* 1457 wild type (WT), indicated as: not significant (ns), **P < 0.01.

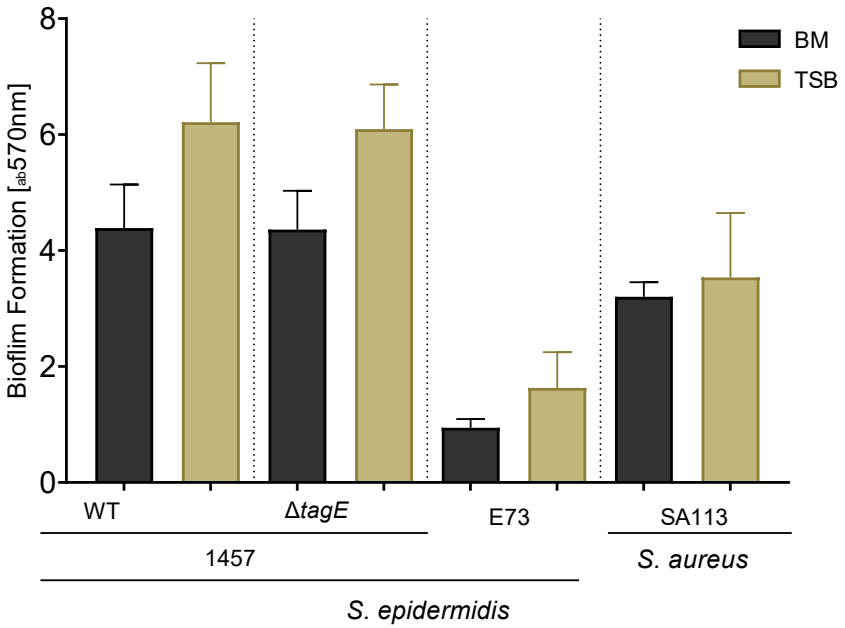

Fig. S3: *S. epidermidis* 1457 biofilm formation was measured in BM and TSB medium. Biofilm formation is unchanged in the Δ*tagE* deletion mutant.

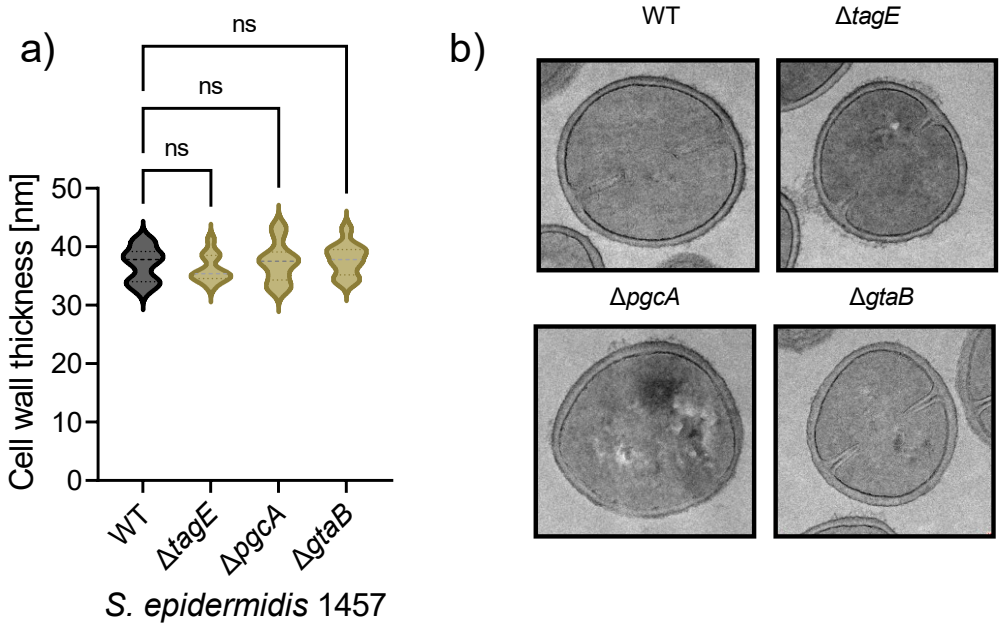

Fig. S4: Electron microscopy at 12,500 x magnification indicates that cell wall thickness (a), and cell shape (b), is unchanged in all mutants compared to the wild type. a) shows the mean cell wall thickness of at least 11 different bacterial cells of each mutant or the wild type (WT). Ordinary one-way ANOVA was used to determine statistical significance versus *S. epidermidis* 1457 wild type (WT), indicated as: not significant (ns).

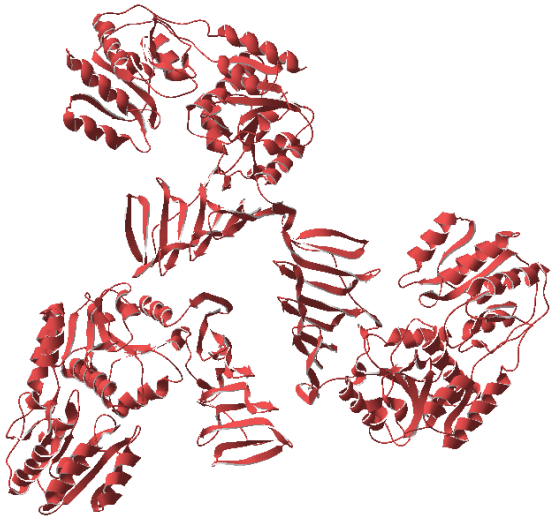

Fig. S5: Structural prediction of the *S. epidermidis* TagE trimer with Alphafold2 [44, 45].

Table S1: Bacteriophages and bacterial strains used in this study.

Bacteriophage	Propagation strain	Morphology	Reference or origin
ΦE72	*S. epidermidis* 1457	siphovirus	Fišarová et al
Φ459	*S. epidermidis* SE459	siphovirus	Fišarová et al
Φ456	*S. epidermidis* SE456	siphovirus	Fišarová et al
Φ27	*S. epidermidis* SE27	siphovirus	Fišarová et al
Φ15	*S. epidermidis* SE15	siphovirus	Fišarová et al
Φ187	*S. aureus* PS187	siphovirus	Pantůcek et al
ΦUKE3	*S. epidermidis* DSM18857	podovirus	DSMZ*
ΦSpree	*S. epidermidis* DSM18857	podovirus	DSMZ*
ΦBE03	*S. epidermidis* SKNA73	podovirus	Valente et al.**
ΦBVG	*S. epidermidis* DSM20608	podovirus	DSMZ*
ΦPauli	*S. epidermidis* DSM20608	podovirus	DSMZ*
ΦNepomuk	*S. epidermidis* DSM20044	podovirus	DSMZ*
ΦBE04	*S. epidermidis* SKNA34	myovirus	Valente et al.**
ΦBE06	*S. epidermidis* SKNA34	myovirus	Valente et al.**
ΦAlex	*S. epidermidis* DSM3269	myovirus	DSMZ*
ΦK	*S. epidermidis* RN4220	myovirus	O'Flaherty et al.

* DSMZ: German Collection of Microorganisms and Cell Cultures

** Department of Intensive Care Medicine, Inselspital, Bern University Hospital, Switzerland

Table S2: Primer sequences used for cloning and sequencing.

Primer name	Primer sequence	Application
tagE F1-For	ATCTGAATTCAGTAAATCAGCATCAATAAG	Deletion of *S. epidermidis tagE*
tagE F1-Rev	TTTGAGATCTGAAATTTTATAATGTGATTTAAGAAG	Deletion of *S. epidermidis tagE*
tagE F2-For	TATAAGATCTTAGGTATTCAGATGGTTTAGATGATC	Deletion of *S. epidermidis tagE*
tagE F2-Rev	ATTAGTCGACAATGCATTAGAAGTTAAATTCGAAC	Deletion of *S. epidermidis tagE*
pgcA F1-For	AAGGGAATTCCAAAAGAAATGTTACCAATATTAG	Deletion of *S. epidermidis pgcA*
pgcA F1-Rev	TTTGAGATCTTAATATCGAAATAGAATTAACATG	Deletion of *S. epidermidis pgcA*
pgcA F2-For	TACGAGATCTTTCGAAAACATAAAAAGTTCTTAG	Deletion of *S. epidermidis pgcA*
pgcA F2-Rev	TTTTGTCGACTTGAATGAAATCTAATTCATTTGC	Deletion of *S. epidermidis pgcA*
gtaB F1-For	GTCTTGGAATTCTAATACCACTCGTATTTACAG	Deletion of *S. epidermidis gtaB*
gtaB F1-Rev	ATATAAGATCTACAGACATCCACTGAAAAACACTAG	Deletion of *S. epidermidis gtaB*
gtaB F2-For	GTCAAGATCTTTTGATTATTAGAAAGGATAGTACCC	Deletion of *S. epidermidis gtaB*
gtaB F2-Rev	TATCTGTCGACAACTTTAATCAATTTGAGTTAGTTG	Deletion of *S. epidermidis gtaB*
TagE Locus Comp-For	TCATGGTACCTTACTTTACTCTCTCAAACAAC	Fragment synthesis for complementation of gene locus containing *tagE*, *pgcA,* and *gtaB*
TagE Locus Comp-Rev	TTCTGTCGACATTCTTGATTAAGTTAATGTTAATATTG	Fragment synthesis for complementation of gene locus containing *tagE*, *pgcA,* and *gtaB*
473 Eco	CCTCAAGCTAGAGAGTCATTACCCC	sequencing of pRB473 and pBASE shuttle vectors
473 Hind	CTGGATTTGTTCAGAACGCTCGG	sequencing of pRB473 shuttle vector
pBASE Hind	CTACTTCTTTCAAACTCTCTCTACG	sequencing of pBase shuttle vector
erm-For	CTATTATTTAACGGGAGGAAA	Sequencing from erythromycin cassette forward
erm-Rev	TAATCTAACGTATTTATCTGCGTA	Sequencing from erythromycin cassette reverse

Extended descriptions of detailed methods

WTA compositional analysis

HPLC-MS

Analysis of the WTA polymer composition was performed using an LTQ Orbitrap Velos mass spectrometer (Thermo Fisher Scientific), connected to an ACQUITY ultra-performance liquid chromatography (UPLC) system (Waters Corporation). Separation in the UPLC was carried out using a Phenomenex C18-Gemini® column (150 × 2 mm, 3 µm, 110 Å, Phenomenex) at 37°C with 0.1% formic acid and 0.05% HCO_2NH_4 (A) and CH_3CN (B) buffer system. A single run (injection volume of 5 µl) was performed with a flow rate of 0.2 ml/min and a two-step gradient: after 2.5 min of equilibration with 100% A, a 1-min gradient up to 5% B was followed by a 4-min gradient up to 70% B. After 2 min at 70% B, a re-equilibration step of 2.5 min followed with a flow rate of 4 ml/min. LC-MS data processing was done with UmetaFlow GUI ([56], https://github.com/axelwalter/streamlit-metabolomics-statistics) via extracted ion chromatograms with a mass tolerance of 10 ppm.

NMR

1H NMR spectra were recorded for both, wild-type and Δ*tagE S. epidermidis* strains, and they were carried out on a Bruker DRX-600 spectrometer equipped with a cryo-probe, at 298 K. Chemical shifts of spectra recorded in D_2O were calculated in ppm relative to internal acetone (2.225 and 31.45 ppm). 2D NMR spectra were acquired for *S. epidermidis* wild type only, the spectral width was set to 12 ppm and the frequency carrier placed at the residual HOD peak, suppressed by pre-saturation. Two-dimensional spectra (DQ-COSY, TOCSY, NOESY, gHSQC, and gHMBC) were measured using standard Bruker software. For all experiments, 512 FIDs of 2,048 complex data points were collected, 32 scans per FID were acquired for homonuclear spectra, and 100 and 200 ms of mixing time was used for the TOCSY and NOESY spectra, respectively. Heteronuclear ^{1}H-^{13}C spectra were measured in the ^{1}H-detected mode, gHSQC spectrum was acquired with 40 scans per FID, the GARP sequence was used for ^{13}C decoupling during acquisition; gHMBC scans doubled those of gHSQC spectrum. During processing, each data matrix was zero-filled in both dimensions to give a matrix of 4K × 2K points and was resolution-

enhanced in both dimensions by a cosine-bell function before Fourier transformation; data processing and analysis were performed with the Bruker Topspin 3 program.

NMR analysis of the WTA of the wild type (WT) strain of *Staphylococcus epidermidis*

NMR analyses of the spectra displayed several signals in the anomeric region (5.5 – 4.4 ppm, Fig. 3c) of the proton spectrum with the one at 5.20 ppm being more intense than the others. Then, inspection of the HSQC spectrum (Fig S6a) disclosed that only the signals at ~ 5.2 and ~ 5.1 ppm arose by the anomeric position of different monosaccharide residues, due to the characteristic values of the related carbon atoms (Table S3, [57]). The full assignment of both proton and carbon chemical shifts was possible with confidence only for the most abundant unit, labelled with **A.** Thus, the anomeric proton at 5.2 ppm was labelled $\mathbf{A_1}$, and the combined analysis of the TOCSY and COSY spectra determined that it was an α-glucose (Fig. S6b). Indeed, the TOCSY spectrum showed that $\mathbf{A_1}$ correlated to four other protons as occurs for *gluco* configured residues, and this information combined with those from the COSY spectrum enabled the sequence assignment from H-2 to H-5 (Fig. S6b, Table S3). Then, the identification of A6 was inferred by the finding of the H-4/H-6 cross peak in the TOCSY spectrum (Fig. S6b) while the position of the other H-6 proton, labelled A6’ was determined by the strong cross-peak in the COSY spectrum (Fig. S6b). Finally, the identification of the carbon chemical shifts was inferred by analysing the ^{1}H-^{13}C HSQC (Fig. S6a), which determined that **A** was a glucose unit that was not further substituted due to the similarity of its carbon chemical shifts to those reported for the reference glycoside [57]. The inspection of the HMBC spectrum (not shown) reported a cross peak connecting H-1 of **A** to a carbon at 76.7 ppm in turn correlated to a proton at 4.12 ppm, later assigned to H-2/C-2 of a glycerol (Gro) unit, labelled **b**.

Interestingly, H-1 of **A** was flanked by a second anomeric proton at 5.22 ppm (Fig. S6b, Table S3), labelled as **A’** and presenting a correlation pattern in the TOCSY spectrum very similar to that of **A**, except for the fact that the density analogue to $\mathbf{A_{1,5}}$ was missing while there was a new one relating H-1 to a proton at 4.21 ppm. The identification of the sequence between the protons of this second spin system was aided by the COSY spectrum and the additional signal at 4.21 was assigned to H-5,

in turn correlated to the two H-6 protons at 4.66 and 4.44 ppm (Fig. S6b), highly deshielded due to the O-acylation with an Ala residue as inferred by the long range correlation with a carbonyl group at 171.5 ppm (not shown).

Then, the anomeric region reported a proton signal at 5.39 ppm, attached to a carbon at 75.5 ppm with only one additional correlation in the COSY spectrum with a proton at ca. 4.1 ppm, assigned with a hydroxy-methyl carbon at 64.9 ppm in the HSQC spectrum (Figure S6a). The pattern of this unit, labelled **a**, was found to be consistent with that of a Gro unit, phosphorylated at both ends and acylated with an Ala unit at O-2, as described in the WTA polymers containing GroP motifs [42].

Finally, the HSQC spectrum contained three densities at $^{1}H/^{13}C$ 4.04/70.8, and 4.12/76.7, labelled as $\mathbf{c_2}$, and $\mathbf{b_2}$, respectively, all identified with the aid of the values reported in literature (Table S3). In detail, **c** was a glycerol unit not further substituted [42], while **b** had the glucose units (**A** and **A'**) linked to O-2 [58]. Of note, the HSQC spectrum contained other densities not related to the WTA polymer and presumably belonging to other compounds co-purified with it. In some cases, it was possible to recognize some amino acids, but it was never possible to establish the nature of the compound(s) due to the low intensities of the signals or to the lack of the proper correlations in the full set of NMR spectra acquired. The integration of the $\mathbf{A_{5,1}}$ and $\mathbf{A'_{5,1}}$ densities in the TOCSY spectrum (Figure S6b) revealed that about 15% of this monosaccharide was derivatized with an alanine at O-6.

Table S3: NMR chemical shifts. ^{1}H (600MHz) chemical shifts of WTA structural motifs found in *S. epidermidis* wild type. The sample was dissolved in deuterated water (HOD, 550 µl) and measured at 298 K. By convention, C-1 of the glycerol unit is placed at the left of the structural formula, P stands for phosphate.

Residue	motif	1;1' (for Gro)	2	3; 3' (for Gro)	4	5	6; 6'
a	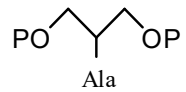	4.11 x 2	5.39	4.11 x 2	--	--	--
Gro		64.9	75.5	64.9	--	--	--
b	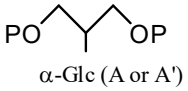	~ 4.02 x 2*	4.12	~ 4.05 – 4.00*	--	--	--
Gro		66.6	76.7	65.8	--	--	--
c		3.85;3.90	4.04	3.85;3.90	--	--	--
Gro		67.5	70.8	67.5	--	--	--
A	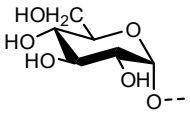	5.20	3.54	3.78	3.41	3.95	3.89; 3.77
t-α-Glc		98.9	72.8	74.3	71.0	73.1	61.9
A'	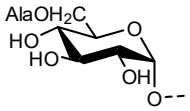	5.22	3.57	3.80	3.43	4.21	4.66; 4.44
t-α-Glc6Ala		96.2	72.6	74.1	71.2	71.0	66.5
Ala	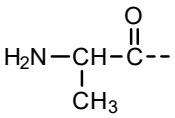	--	4.23	1.62	--	--	--
		171.5	50.1	16.6--	--	--	--

* These signals can be exchanged.

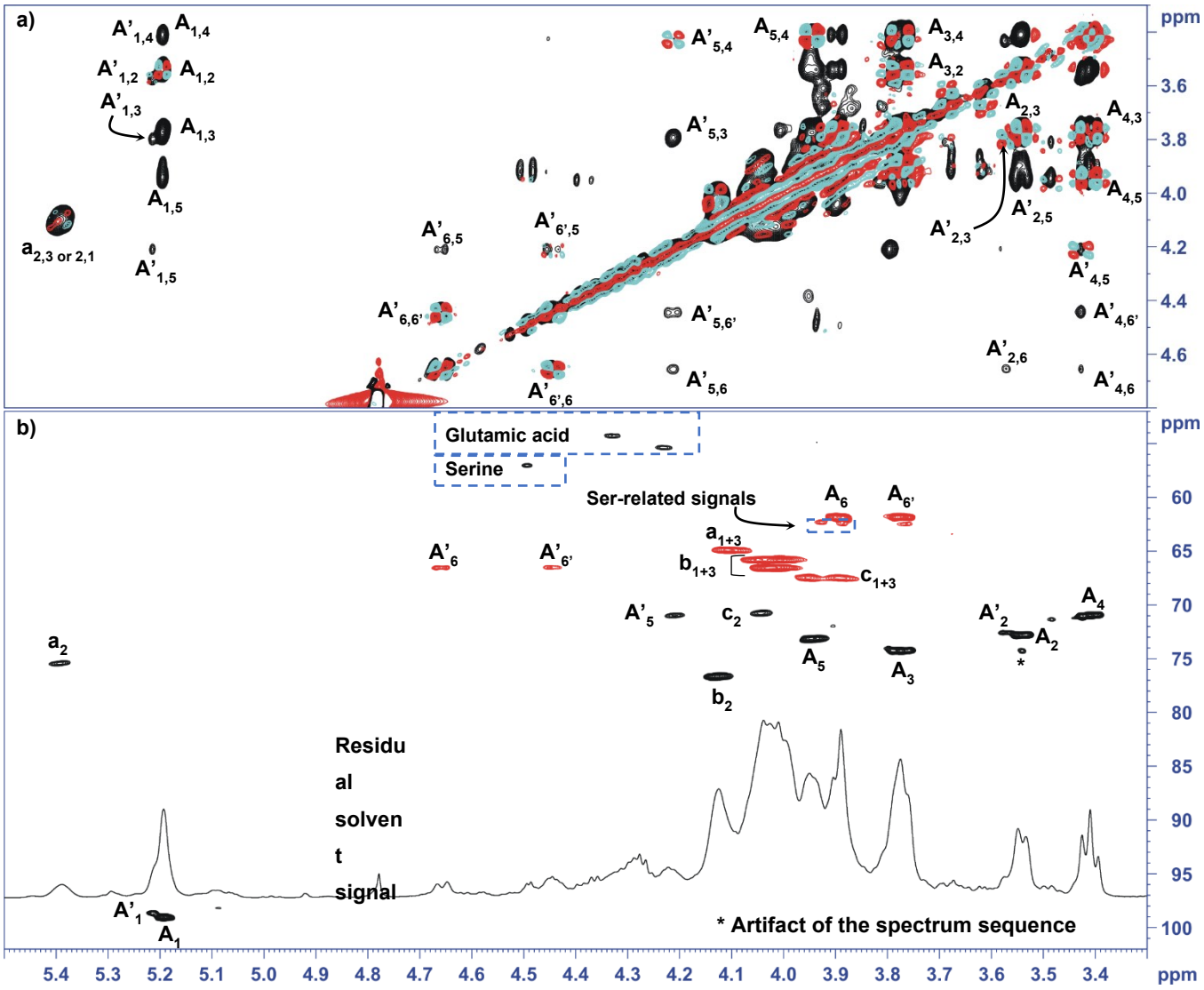

Fig. S6: NMR spectra recorded for WTA isolated from *S. epidermidis* wild type. a) Expansion of the HSQC spectrum detailing the anomeric and the carbinolic region. b) Overlap of the TOCSY (black) and COSY (cyan and red) spectra. In all the spectra, the most relevant densities are labelled with the letter used in Table S3; as for the carbohydrate units (**A** and **A'**), the anomeric signals are indicated with a capital letter, while the Gro units (**a**, **b**, and **c**) are labeled with small letters.

Chapter 3

Invasive *Staphylococcus epidermidis* use a unique processive wall teichoic acid glycosyltransferase to evade immune recognition

Yinglan Guo[1,2]†, Xin Du[2,3,4]†‡, Janes Krusche[2,3,4], Christian Beck[2,3,4], Sara Ali[5], Axel Walter[2,6], Volker Winstel[3,4 § ‖], Christoph Mayer[2,6], Jeroen D. C. Codée[5], Andreas Peschel[2,3,4]*, Thilo Stehle[1,2]*

[1]Interfaculty Institute of Biochemistry, University of Tübingen, Tübingen, Germany

[2]Cluster of Excellence "Controlling Microbes to Fight Infections (CMFI)", University of Tübingen, Tübingen, Germany

[3]Interfaculty Institute of Microbiology and Infection Medicine Tübingen, Infection Biology, University of Tübingen, Tübingen, Germany

[4]German Centre for Infection Research (DZIF), Partner Site Tübingen, Tübingen, Germany

[5]Leiden Institute of Chemistry, Leiden University, Leiden, The Netherlands

[6]Interfaculty Institute of Microbiology and Infection Medicine Tübingen, Organismic Interactions/Glycobiology, University of Tübingen, Tübingen, Germany

† Contributed equally

*Correspondence to Thilo Stehle (thilo.stehle@uni-tuebingen.de) and Andreas Peschel (andreas.peschel@uni-tuebingen.de)

Present address of Xin Du: ‡Department of Pediatrics, University of California, San Diego, CA 92093, USA.

Present address of Volker Winstel: §Research Group Pathogenesis of Bacterial Infections; TWINCORE, Centre for Experimental and Clinical Infection Research, a joint venture between the Hannover Medical School and the Helmholtz Centre for

Infection Research, Hannover, Germany; ‖Institute of Medical Microbiology and Hospital Epidemiology, Hannover Medical School, Hannover, Germany

submitted manuscript

Abstract

Staphylococcus epidermidis expresses glycerol-phosphate wall teichoic acid (WTA), but some healthcare-associated methicillin-resistant *S. epidermidis* (HA-MRSE) clones produce a second, ribitol-phosphate (RboP) WTA, resembling that of the aggressive pathogen *Staphylococcus aureus*. RboP-WTA promotes HA-MRSE persistence and virulence in bloodstream infections. We report here that the TarM enzyme of HA-MRSE (TarM(Se)) glycosylates RboP-WTA with glucose, instead of N-acetylglucosamine (GlcNAc) by TarM(Sa) in *S. aureus*. Replacement of GlcNAc with glucose in RboP-WTA impairs HA-MRSE detection by human IgG, which may contribute to the immune-evasion capacities of invasive *S. epidermidis*. Crystal structures of complexes with UDP-glucose, and with uridine diphosphate and glycosylated poly(RboP) reveal the binding and glycosylation mechanism of this enzyme and explain why TarM(Se) and TarM(Sa) link different sugars to poly(RboP). The structural data provide evidence that TarM(Se) is a processive WTA glycosyltransferase. Our study will support the targeted inhibition of TarM enzymes, and the development of RboP-WTA targeting vaccines and phage therapies.

Teaser

New immune-escape strategy based on alteration of major surface antigen in the opportunistic pathogen *Staphylococcus epidermidis*

Introduction

Staphylococcus epidermidis, a member of coagulase-negative staphylococci, is the most frequently isolated Gram-positive bacterium from the skin and mucous membranes of all humans(*1, 2*). The differences in skin features (thickness, folds, lipid content, densities of hair follicles and glands) define the habitats of a large number of clonal lineages(*3, 4*), as well as age-related dynamics of colonization(*5*). *S. epidermidis* lineages colonize the skin of virtually every human as commensals(*6, 7*), maintaining the commonly benign relationship with their host. For instance, the resident *S. epidermidis* is necessary for optimal skin immune fitness(*8, 9*). Many *S. epidermidis* isolates can stimulate nasal epithelia to produce antimicrobial peptides, killing pathogenic competitors(*10*), and Esp-secreting *S. epidermidis* strains are able

to inhibit biofilm formation and nasal colonization of *Staphylococcus aureus*(*11*), an aggressive pathogen that causes life-threatening infections in humans(*12, 13*).

In recent decades, however, some *S. epidermidis* clones have emerged as a major cause of hospital-acquired infections, including bloodstream infections and infections of indwelling medical devices, such as central intravenous catheters, prosthetic joint, vascular grafts, surgical site, central nervous system shunt and cardiac devices(*1, 14, 15*). A major percentage of invasive *S. epidermidis* clones displays resistance to methicillin and other antibiotics, which poses a substantial clinical burden due to broad and severe treatment difficulties(*5, 16-18*). Such invasive infections are largely caused by specific healthcare-associated methicillin-resistant *S. epidermidis* (HA-MRSE) lineages, which are usually not found on human skin or mucous membranes. While many of these clones have strong capacities to form biofilms on artificial surfaces that protect them from antibiotics and host defenses(*19*), the emerging ST10, ST23, and ST87 clones are poor biofilm formers but alter their surfaces in a way that promotes their invasiveness(*20*). These clones produce an additional, *S. aureus*-type wall teichoic acid (WTA), a glycopolymer governing interactions with host cell receptors, immune effectors, and bacteriophages(*21*).

WTA is the most abundant peptidoglycan-linked glycopolymer presented on the cell surface of most Bacillota (formerly known as Firmicutes), serving essential functions in cell wall integrity, susceptibility to bacteriophages, and resistance to antimicrobial molecules and host proteins(*21, 22*). *S. epidermidis* usually produces glycerol 3-phosphate (GroP) WTA, which is modified with D-alanine and variable sugar residues. In contrast, most clones of the aggressive pathogen *S. aureus* express ribitol 5-phosphate (RboP) WTA, which is modified by D-alanine and N-acetylglucosamine (GlcNAc)(*21, 22*). GlcNAc can be linked to the RboP repeating units in three different ways, which shape host and phage interactions differently(*23*). The housekeeping glycosyltransferase TarS catalyzes β-O-GlcNAcylation of poly(RboP) backbone at C4 position(*24, 25*). Some *S. aureus* clones also encode TarM, which modifies WTA the same position, albeit with α-O-GlcNAc(*26*). Recently, we identified a third glycosyltransferase, TarP, which is encoded on a prophage in some *S. aureus* clones, and which is responsible for C3-β-O-GlcNAcylation(*27*). WTA glycosylation with GlcNAc is essential for the *S. aureus* host colonization

capacities(*28*). The type of RboP-WTA GlcNAc linkages shapes the immunogenicity and interaction with certain groups of bacteriophages(*23*).

The emerging HA-MRSE clones, ST10, ST23 and ST87, produce in addition to GroP-WTA, a second, RboP-WTA using the *tarIJLM2* gene cluster(*20*). This cluster encodes TarI, TarJ, and TarL enzymes that assemble the poly(RboP) backbone, as well as a WTA glycosyltransferase, TarM. These genes are closely related to the corresponding genes in *S. aureus* and have probably been acquired by horizontal gene transfer. Production of RboP-WTA impairs *S. epidermidis* nasal colonization, but promotes persistence in the bloodstream, leading to increased mortality in a mouse sepsis model(*20*). Thus, RboP-WTA can alter the lifestyle of *S. epidermidis* from commensal to pathogenic and enable *S. epidermidis* to exchange DNA with *S. aureus* via Siphoviruses that bind to RboP-WTA and are major vehicles for horizontal gene transfer in staphylococci(*20, 29, 30*).

Here we report that TarM of *S. epidermidis* (TarM(Se)) incorporates glucose, instead of GlcNAc into RboP-WTA, which disables *S. aureus*-specific human IgG to detect *S. epidermidis* and is probably used by HA-MRSE to remain partially undetectable in the bloodstream. Extensive structural characterization of $TarM(Se)_{G117R}$ with donor and acceptor substrates, in particular, with product uridine diphosphate (UDP) and glycosylated poly(RboP) explains the binding model of poly(RboP) and the catalytic mechanism of a retaining WTA glycosyltransferase. Moreover they provide an explanation for the enzymatic differences between TarM(Se) and the corresponding *S. aureus* enzyme TarM(Sa). Our structures demonstrate that TarM(Se) is a processive WTA glycosyltransferase and provide an excellent basis for the development of TarM inhibitors that could help to impede the virulence and immune-evasion capacities of HA-MRSE and of methicillin-resistant *S. aureus* (MRSA) clones.

Results

RboP-WTA synthesized by the *S. epidermidis tarIJLM2* cluster differs in its antigenic properties from those of RboP-WTA from *S. aureus*

The *tarM(Se)* gene encodes a protein, TarM(Se), with 83% sequence similarity to the *S. aureus* TarM(Sa), which has been shown earlier to catalyze the α-O-GlcNAcylation of RboP-WTA backbone at C4 position utilizing UDP-GlcNAc as donor substrate(*26, 31, 32*) (fig. S1). *S. epidermidis* E73, a clinical isolate that harbors the

tarIJLM2 gene cluster, was therefore assumed to produce the same type of glycosylated WTA as *S. aureus* strains with *tarM(Sa)*. Although most *S. aureus* also carry the *tarS* gene, TarM(Sa) has been shown to be dominant over TarS leading to RboP-WTA, which is α-glycosylated with GlcNAc(*33*). Since WTA is a major surface antigen of *S. aureus* and the WTA GlcNAc residues are essential components of the antigenic epitope(*27, 34*), we compared binding of human IgG to *S. aureus* RN4220 and *S. epidermidis* E73 with or without *tarM(Se)* (Fig. 1A). Human IgG pooled from several healthy donors was used as virtually every human has abundant anti-*S. aureus* IgG antibodies as a consequence of previous *S. aureus* infections(*35*). *tarM(Se)*, the last gene of the *tarIJLM2* operon was deleted in E73, yielding mutant E73 Δ*tarM(Se)* with unaltered growth behavior, biofilm formation, or amount of WTA (fig. S2).

The E73 wild-type strain bound substantially lower amounts of human IgG than RN4220, a *tarM(Sa)*-expressing *S. aureus* strain (Fig. 1A). It should be noted that an RN4220 mutant lacking protein A (Spa), which binds IgG unspecifically via the Fc part(*36*), was used to monitor only antigen-specific IgG binding. While a moderate difference was expected because of differences between *S. aureus* and *S. epidermidis* surface protein antigens, the difference in IgG binding was much more substantial (Fig. 1A), suggesting that the dominant WTA antigen epitopes may differ between the two strains. Moreover, deletion of *tarM(Se)* in E73 did not further reduce IgG binding. To exclude potential contributions of non-WTA antigens we analyzed the binding of a previously described monoclonal IgG1 (mAb 4461) directed against RboP-WTA with α-GlcNAc(*37*). Notably, E73 wild type bound mAb 4461 in a dose-dependent manner but much less effectively as RN4220. In contrast, E73 Δ*tarM(Se)* did not bind mAb 4461. Thus, TarM(Se) is essential for binding of mAb 4461 to *S. epidermidis* E73 RboP-WTA but its glycosylation product may differ from that of TarM(Sa).

To further analyze if TarM(Sa) and TarM(Se) differ in their activities, binding of pooled human IgG and mAb 4461 to E73 Δ*tarM(Se)* complemented with a plasmid-encoded copy of either *tarM(Sa)* or *tarM(Se)* was compared (Fig. 1B). Complementation with *tarM(Sa)* led to a strong and dose-dependent increase of IgG and mAb 4461 binding that exceeded by far the binding capacity of E73 wild type. In contrast, complementation with *tarM(Se)* only restored wild-type level binding of IgG

and mAb 4461 but led to no further increase. These data indicate that TarM(Se) is functional and shapes the immunogenicity of *S. epidermidis* but that its glycosylation product may differ from that of TarM(Sa) in its capacity to bind human IgG and mAb 4461.

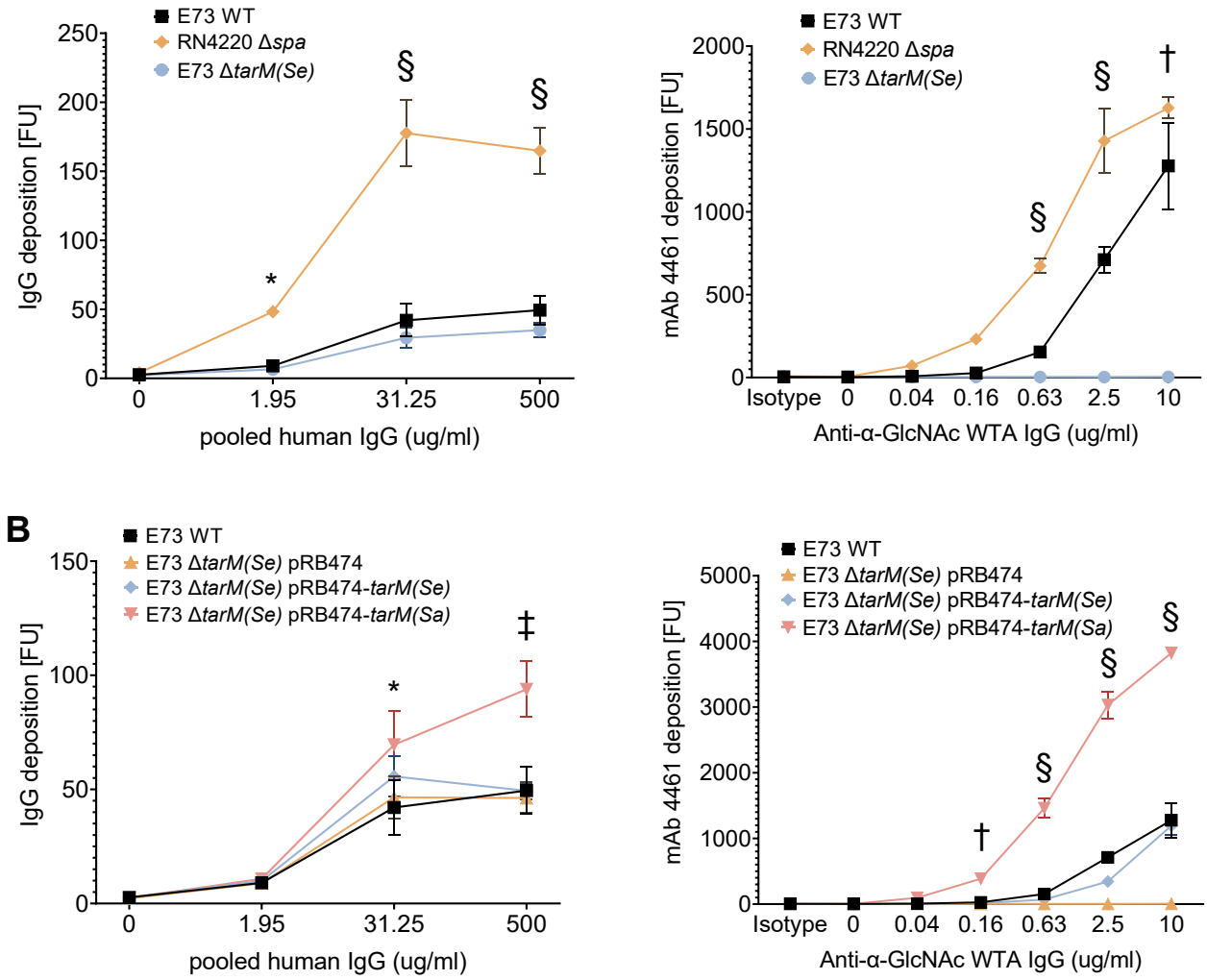

Fig. 1. TarM(Se) decreases binding of IgG to S. epidermidis or S. aureus with RboP-WTA. (A) S. aureus RN4220 binds much higher amounts of IgG from pooled human serum or of monoclonal IgG1 (mAb 4461) directed against RboP-WTA with α-GlcNAc than S. epidermidis E73. Inactivation of tarM(Se) does not further reduce pooled IgG binding to E73. (B) Complementation of E73 ΔtarM(Se) with tarM(Sa) leads to much higher IgG binding than complementation with tarM(Se). The data represents the mean ± SEM of at least 3 independent experiments. Two-way ANOVA was used to determine statistical significance. *P < 0.05, †P < 0.01, ‡P < 0.001, §P < 0.0001, significantly different versus S. epidermidis E73 wild type.

S. epidermidis TarM(Se) incorporates glucose instead of GlcNAc into RboP-WTA

While the composition of the E73 RboP-WTA backbone has recently been reported(*20*), the type of backbone glycosylation has not been analyzed yet. WTA isolated from E73 with or without *tarM(Se)* was analyzed by mass spectroscopy-coupled high-performance liquid chromatography (HPLC-MS) to detect sugar-modified RboP repeating units (Fig. 2). Notably, GlcNAc was absent from E73 RboP-WTA while it could be detected in the WTA of *S. aureus* RN4220. Instead, E73 wild type contained glucose-modified RboP repeating units, which were absent from those of RN4220. Deletion of *tarM(Se)* led to absence of glucose but complementation with a *tarM(Se)* copy restored the wild-type phenotype, demonstrating that TarM(Se) is required for RboP modification with glucose. RboP units lacking glycosylation were also prominent in E73 wild type suggesting that TarM(Se) glycosylates only a subfraction of the RboP polymers or of the RboP repeating units of a given polymer (Fig. 2A). RN4220 lacking all WTA glycosyltransferases (Δ*tarM(Sa)*Δ*tarS)* complemented with *tarM(Se)* also lacked GlcNAc but contained glucose-modified RboP units (Fig. 2B). Overall, complementation with *tarM(Se)* led to a smaller degree of RboP glycosylation compared to complementation with *tarM(Sa)*.

Figures and Figure Legends

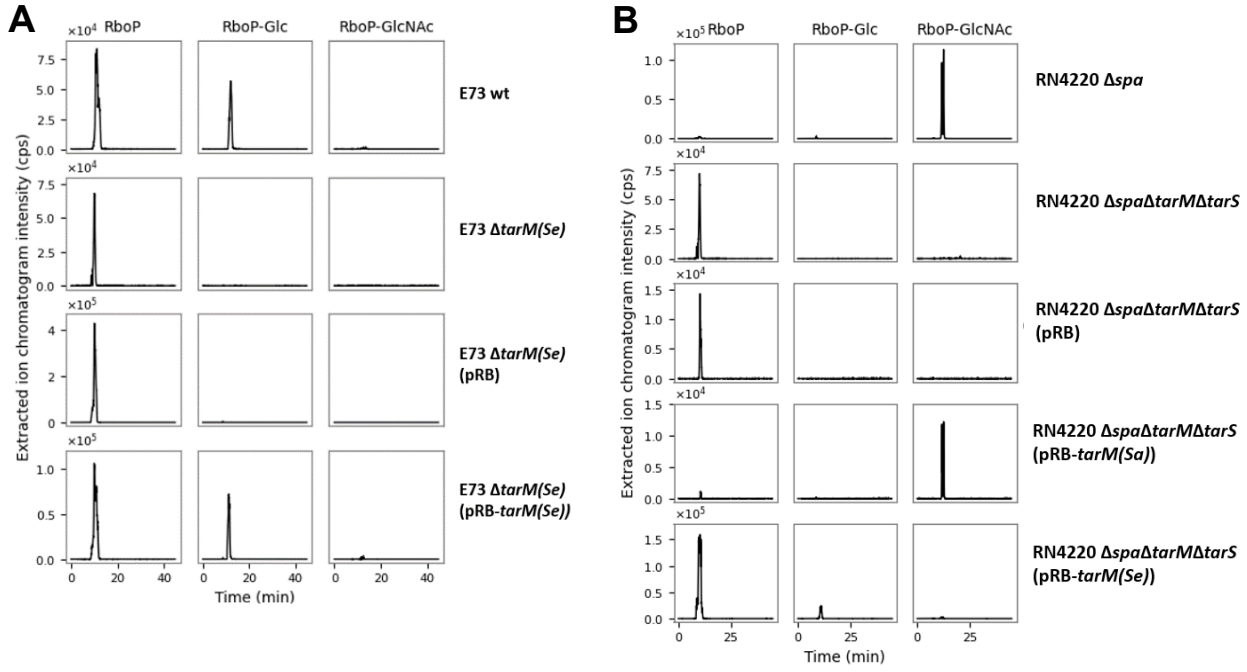

Fig. 2. TarM(Se) glycosylates RboP-WTA with glucose rather than GlcNAc. (A) Mass spectroscopy-coupled high-performance liquid chromatography (HPLC-MS) demonstrates the *tarM(Se)*-dependent presence of RboP-glucose but absence of RboP-GlcNAc in *S. epidermidis* E73 WTA. **(B)** Complementation of *S. aureus* RN4220 Δ*tarM(Sa)*Δ*tarS* with *tarM(Sa)* restores the presence of RboP-GlcNAc but complementation with *tarM(Se)* allows synthesis of RboP-glucose. Shown are extracted ion chromatograms.

In order to confirm that TarM(Sa) and TarM(Se) use different donor substrates, we set out to define the substrate specificity of TarM(Se). Four UDP-activated sugars, UDP-glucose, UDP-galactose, UDP-N-acetylgalactosamine, and UDP-GlcNAc were used as donors for glycosylation. TarM(Se) was able to glycosylate purified poly(RboP) in a UDP-glucose dependent manner, confirming that the enzyme has α-O-glucose transferase activity. However, TarM(Se) does not exclusively accept UDP-glucose as donor substrate, it can also use UDP-galactose, although the latter is less efficient than UDP-glucose (table S1A). When purified poly(GroP) was used as acceptor substrate, the activity of TarM(Se) was reduced to 2 - 30% compared with that for poly(RboP), indicating that TarM(Se) binds GroP-WTA less well (table S1B). Thus, *S. epidermidis* strains with *tarIJLM2* may use TarM(Se) with its altered glycosylation pattern to generate a WTA polymer that is less immunogenic and may support the bacteria in the evasion of host defense and, potentially, of phage infections.

Phage Φ11 binds to glucose-modified RboP-WTA with similar efficacy as to GlcNAc-modified RboP-WTA.

Glycosylated WTA represents the receptor structure for most of the known *Staphylococcus* phages, some of which can also discriminate between bacterial hosts with different glycosylation types(*27, 33, 38*). The currently known *S. epidermidis* phages only use GroP-WTA as receptor and a *S. epidermidis* phage binding to RboP-WTA has never been found(*39*). To analyze how the replacement of GlcNAc by glucose on RboP-WTA may change the susceptibility to phages, the *S. aureus* RN4220 strain panel with or without *tarM(Sa)* or *tarM(Se)* was tested for susceptibility to a variety of *S. aureus*-specific phages (Fig. 3). The Myovirus ΦK infected all strains, which confirms previous studies, which showed that ΦK requires only the WTA backbone for binding, irrespective of WTA glycosylation. The

Podovirus Φ68, which only infect *S. aureus* with RboP-WTA glycosylated by TarS with β-GlcNAc(*33*), and the Siphoviruses Φ187 and ΦE72, which infect only the *S. aureus* lineage CC395 with GroP-WTA(*40*) or GroP-WTA producing *S. epidermidis(39)*, respectively, did not infect any of the other strains. Siphovirus Φ11, however, which infects *S. aureus* strains with α-GlcNAc or β-GlcNAc glycosylation(*33*), also infected RN4220 with *tarM(Se)* as its only WTA glycosyltransferase gene (Fig. 3A). Likewise, *tarM(Se)* expression allowed Φ11 to bind to and to transduce RN4220 Δ*tarM(Sa)*Δ*tarS* lacking its own WTA glycosyltransferases (Fig. 3B, 3C). Thus, the receptor-binding protein of Φ11 can accommodate either RboP-GlcNAc or RboP-glucose.

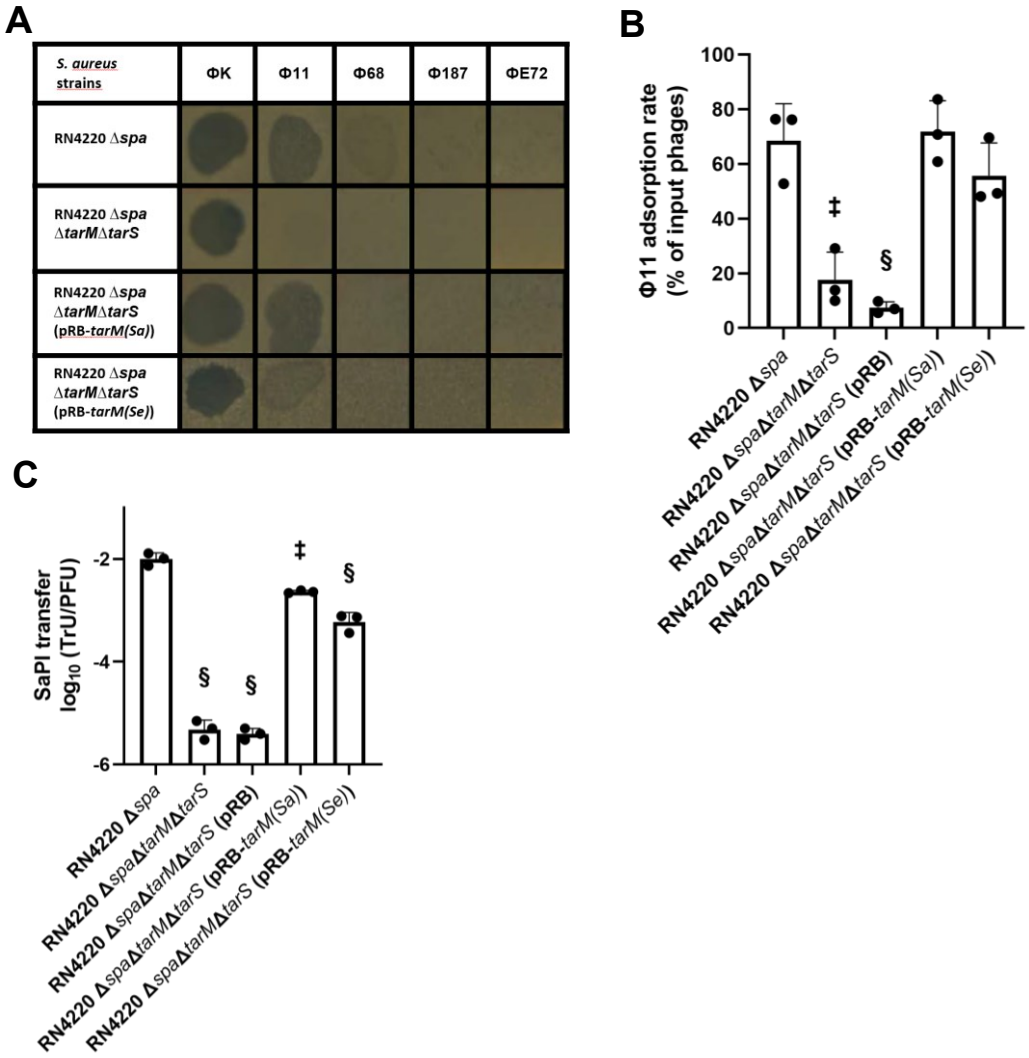

Fig. 3. *S. aureus* phage Φ11 does not discriminate between RboP-WTA with GlcNAc or glucose. **(A)** RboP-WTA glycosylation with glucose does not affect replication of Myovirus ΦK or Podovirus Φ68 in *S. aureus* RN4220 but allows replication of Siphovirus Φ11 in a similar way as glycosylation with GlcNAc. **(B)** and **(C)**, RboP-WTA glycosylation with glucose permits binding **(B)** and DNA transduction (**C**) by Φ11 in a similar way as glycosylation with GlcNAc. Means ± s.d. of three independent experiments are shown. Significant differences vs. RN4220Δ*spa* ($^{‡}P < 0.001$, $^{§}P < 0.0001$) were calculated by one-way ANOVA with Dunnett's post-test (two-sided).

Overall structure and domain organization of TarM(Se) homotrimer and TarM(Se)$_{G117R}$ monomer

In order to understand why the closely related TarM(Sa) and TarM(Se) proteins use different donor substrates, we solved the structure of unliganded full-length TarM(Se) from *S. epidermidis* at 3.2 Å resolution (Fig. 4A, table S2). Like its homolog TarM(Sa)(*31, 32*), TarM(Se) forms a symmetric, propeller-like homotrimer, with three blades projecting from the central hub that mediates trimerization via its trimerization domain(*31, 32*) (TD, residues 69 – 201, Fig. 4A, B). Each blade of the homotrimer contains a catalytic domain with a canonical GT-B fold, consisting of an N-terminal acceptor substrate-binding domain (ABD, residues 1 – 68, and 202 - 302) and a C-terminal nucleotide-binding domain (NBD, residues 303 – 492, Fig. 4B). In line with this property, the elution profile of TarM(Se) from size exclusion chromatography corresponds to a molecular weight of 162 kDa (Fig. 4C), suggesting that it exists as homotrimer in solution.

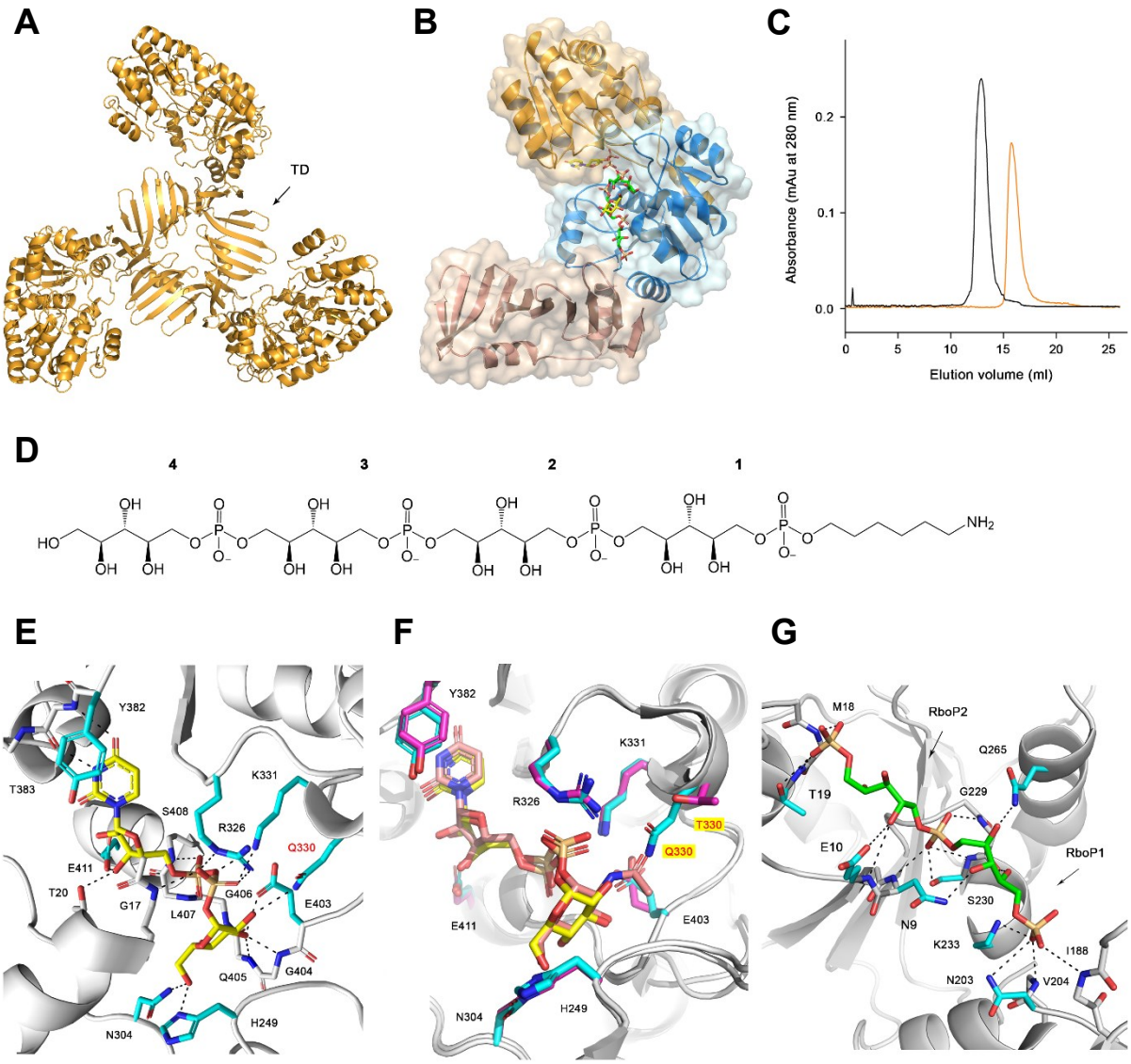

Fig. 4. Overall structure of TarM(Se) and interactions of TarM(Se)$_{G117R}$ with UDP-glucose or 4RboP-(CH$_2$)$_6$-NH$_2$. (A) Crystal structure of TarM(Se) homotrimer. Trimerization domain (TD) is indicated. **(B)** Crystal structure of TarM(Se)$_{G117R}$ monomer with product UDP (yellow) and 4RboP-glucose (4RboP, green, glucose at C4 position of the second unit of 4RboP, yellow). The nucleotide-binding domain (orange), acceptor-binding domain (blue), and TD (boron) are indicated. **(C)** Size exclusion chromatography elution profiles of TarM(Se) homotrimer (black) and TarM(Se)$_{G117R}$ monomer (orange). Based on calibration of the column, TarM(Se) wild type and TarM(Se)$_{G117R}$ mutant proteins have estimated molecular weights of 162 kDa (n = 6) and 55 kDa (n = 8), respectively, in agreement with the calculated molecular weights of 180 kDa for a TarM(Se) homotrimer and 60 kDa for monomeric TarM(Se)$_{G117R}$. **(D)** Chemical structure of synthetic 4RboP-(CH$_2$)$_6$NH$_2$. The unit numbers are indicated. **(E)** The binding site of UDP-glucose (yellow) in the TarM(Se)$_{G117R}$-UDP-glucose complex structure with key amino acids (cyan), Q330 was highlighted in red. Hydrogen bonds and salt bridges are shown as black dashed lines. **(F)** Superposition of TarM(Se)-UDP-glucose complex structure with TarM(Sa)-UDP-GlcNAc (PDB code 4X7M). Residues of TarM(Se) and TarM(Sa) are shown as cyan and magenta, respectively. UDP-glucose in TarM(Se) is colored yellow

and UDP-GlcNAc in TarM(Sa) salmon. The identical residues are labelled as black, Q330 in TarM(Se) and T330 in TarM(Sa) are highlighted in red with yellow background. **(G)** Interactions of TarM(Se)$_{G117R}$ with 4RboP-$(CH_2)_6NH_2$ (green) in the binary structure, RboP1 and RboP2 are indicated.

Since the resolution of the native TarM(Se) structure was limited to 3.2 Å, we generated a G117R mutant (TarM(Se)$_{G117R}$). This mutation modifies an amino acid at the trimer interface and was designed to yield monomeric protein that might form better-diffracting crystals(*32*). Indeed, the mutant protein TarM(Se)$_{G117R}$ formed crystals that diffracted to 2.06 Å (Table 1). TarM(Se)$_{G117R}$ is monomeric both in the crystal (Fig. 4B) and in solution (Fig. 4C), and the activities of the native and mutant proteins are similar (table S3). In order to prepare complexes with reaction partners, a compound mimicking WTA, comprising four RboP repeating units (4RboP-$(CH_2)_6NH_2$), was synthesized and used for cocrystallization (Fig. 4D, Supplementary Fig. 1). We obtained binary structures of TarM(Se)$_{G117R}$ bound to either UDP-glucose or 4RboP-$(CH_2)_6NH_2$. Furthermore, we solved the structure of a ternary complex of TarM(Se)$_{G117R}$ bound to the product UDP and to glycosylated 4RboP-$(CH_2)_6NH_2$. Analysis of the electron density in the ligand binding site clearly shows that the glycosylation reaction has taken place. Collectively, the structures of the TarM(Se)$_{G117R}$ complexes provide detained insight into both ligand binding and the mechanism of catalysis.

Table 1. Data collection and refinement statistics for TarM(Se)$_{G117R}$, TarM(Se)$_{G117R}$-UDP-glucose and TarM(Se)$_{G117R}$-UDP-4RboP-glucose

	TarM(Se)$_{G117R}$* (PDB 7QD7)	TarM(Se)$_{G117R}$-UDP-glucose* (PDB 8P1X)	TarM(Se)$_{G117R}$-UDP-4RboP-glucose* (PDB 8P20)
Data collection			
Space group	$P2_12_12_1$	$P2_12_12_1$	P1
Cell dimensions			
a, *b*, *c* (Å)	58.68, 88.42, 97.49	58.65, 88.73, 98.05	58.62, 75.75, 129.40
α, β, γ (°)	90.00, 90.00, 90.00	90.00, 90.00, 90.00	90.01, 90.04, 90.03
Resolution (Å)	44.21-2.06 (2.11 -2.06)	49.03-2.03 (2.08-2.03)	49.23-2.85 (2.92-2.85)
R_{merge}	11.2 (165.6)	16.4 (198.4)	25.8 (181.9)
$I / \sigma (I)$	14.93 (1.55)	15.64 (1.42)	5.80 (0.88)
Completeness (%)	100.0 (100.0)	100.0 (100.0)	99.9 (100.0)
Redundancy	12.8 (12.5)	13.2 (13.1)	4.6 (4.2)
Refinement			
Resolution (Å)	43.71-2.06	49.03-2.03	49.21-2.85
No. reflections	32047	33765	51972
R_{work} / R_{free}	21.85/23.61	20.10/23.81	22.65/26.32
No. atoms			
Protein	3722	3847	14004
Ligand		36	356
Ions	9	18	3
other molecules	35	33	64
Water	218	293	734
B-factors			
Protein	49.7	38.5	59.6
Ligand		38.4	60.7
Ions	52.1	49.0	75.5
other molecules	54.6	48.1	72.4
Water	50.5	42.5	43.1
R.m.s. deviations			
Bond lengths (Å)	0.004	0.004	0.003
Bond angles (°)	1.081	1.143	1.094

Values in parentheses are for the highest-resolution shell. *Diffraction data from a single crystal were used to obtain the structure.

The UDP-glucose binding site

UDP-glucose is firmly held in a deep pocket through multiple contacts, leaving only the β-phosphate and glucose moiety exposed to the acceptor substrate (Fig. 4E, Fig. 6B, Table 1, fig. 3A). The backbone amide and carbonyl groups of Thr383 form two hydrogen bonds with the O2 and N3 atoms of the base, providing specificity for uridine, and the aromatic ring system of the base is stacked against the Tyr382 side chain. The ribose moiety forms three interactions with the protein. The C2 and C3 hydroxyls interact with the Glu411 side chain, and the C3 hydroxyl is additionally

hydrogen-bonded to the side chain of Thr20. The tandem backbone amide groups of Leu407 and Ser408 contact the α-phosphate of UDP-glucose and another main-chain amide group from Gly17 interacts with β-phosphate. In addition, the side chains of Arg326 and Lys331, each form two salt bridges with the β-phosphate. The glucose moiety contacts TarM(Se)$_{G117R}$ through multiple interactions. The side chains of Asn304 and His249 are hydrogen-bonded to the C6 hydroxyl group, the backbone amide group of Gly406 interacts with C4 hydroxyl, and the Glu403 side chain and backbone amide groups of Gly404 and Gln405 contact with the C3 hydroxyl group. The side chain of Gln330 is hydrogen-bonded to the C2 hydroxyl. Interestingly, the related enzyme TarM(Sa), which accepts UDP-GlcNAc as donor substrate, has a threonine at this position(*31*). Thus, the longer Gln330 side chain appears to allow TarM(Se) to distinguish UDP-glucose from UDP activated bulkier sugars, such as UDP-GalNAc and UDP-GlcNAc (table S1A). The binding site for UDP-glucose in TarM(Se) is composed of eight amino acids, seven of which are identical to that for UDP-GlcNAc in TarM(Sa)(*32*). The only difference is Gln330 in TarM(Se) and Thr330 in TarM(Sa), which clearly suggests a key role for this residue in allowing TarM(Se) to discriminate against the use of UDP-GlcNAc as a donor substrate (Fig. 4F). Analysis of all 13 HA-MRSE TarM(Se) sequences available in the BLAST database revealed that Gln330 is conserved in all copies of the gene, suggesting that all *S. epidermidis* strains with *tarIJLM2* can produce RboP-WTA carrying glucose.

The poly(RboP) binding site in the binary structure

The 4RboP-$(CH_2)_6NH_2$ compound was introduced into the TarM(Se)$_{G117R}$ crystals through cocrystallization. However, interpretable electron density was only observed for two RboP units and one phosphate group (Fig. 4G, fig. S3B, table S2), suggesting that the remainder of the molecule is not ordered. We were not able to identify the unit number of 4RboP-$(CH_2)_6NH_2$ due to the lack of the electron density. After we obtained the ternary complex structure of TarM(Se)$_{G117R}$ with product UDP and glycosylated 4RboP-$(CH_2)_6NH_2$, the RboP unit number in the binding site could be assigned. The side chain of Lys233 forms a salt bridge with phosphate group of RboP1 (the first RboP unit of 4RboP-$(CH_2)_6NH_2$), and the Asn203 side chain, the backbone amide groups of Val204 and Ile188 contact the same phosphate. The ribitol moiety of RboP1 forms three hydrogen bonds with the side chains of Asn9 and

Gln265, as well as the backbone carbonyl group of Gly229. Three main-chain amide groups interact with the phosphate group of RboP2. Two of these are from tandem backbone amide groups of Gly229 and Ser230, and the third one is contributed by Asn9; this phosphate group is also hydrogen-bonded to the side chain of Ser230. The ribitol moiety of RboP2 has only contacts with the side chain and backbone amide group of Glu10. The phosphate group of RboP3 interacts with tandem backbone amide groups of Met18 and Thr19, and is further hydrogen-bonded to the Thr19 side chain. We could not find any electron density for the ribitol moiety of RboP3, the entire RboP4 unit, and the linker region of the molecule.

The ternary complex structure of TarM(Se)$_{G117R}$ with product UDP and glycosylated 4RboP-(CH$_2$)$_6$NH$_2$

Although crystals of TarM(Se)$_{G117R}$ cocrystallized with 4RboP-(CH$_2$)$_6$NH$_2$ were used for soaking of UDP-glucose and 4RboP-(CH$_2$)$_6$NH$_2$, electron densitiy was only observed for the product UDP and glycosylated 4RboP were observed in the binding sites (Fig. 5C). This demonstrates that the reaction has taken place, confirming that the crystallized protein is enzymatically active(*41*). Most of the interactions between UDP and TarM(Se)$_{G117R}$ in the ternary complex are the same as in those seen in the binary structure. For the binding site of 4RboP-(CH$_2$)$_6$NH$_2$, the electron density for 4RboP is well defined and allows for unambiguous placement of the ligand, including its orientation. In the initial refinement, we noticed a disc-shaped, strong positive difference Fourier electron density that connected to C4-hydroxyl of RboP2 in all four copies of the TarM(Se)$_{G117R}$ ternary complex in the asymmetric unit. We used 4RboP-glucose instead of 4RboP, did further refinement, and concluded that our ternary structure represents a complex of TarM(Se)$_{G117R}$ with product UDP and glycosylated 4RboP that carries a glucose residue at C4 position of RboP2 (4RboP-glucose) (Fig. 5, Table 1). The interactions between RboP1 and TarM(Se)$_{G117R}$ are all conserved as in the binary structure. Four interactions for the phosphate group of RboP2 in the binary structure are present in the ternary complex structure, while the ribitol moiety of RboP2 contacts the side chain of Glu10 and the glucose at C4 position is hydrogen-bonded to the Gln265 side chain. The phosphate group of RboP3 is fixed by two tandem backbone amide groups of Gly16, Gly17, Met18, and Thr19, and its ribitol moiety is hydrogen-bonded to the side chains of Arg326 and

Gln330. The phosphate group of RboP4 forms a salt bridge with Lys263 and is further hydrogen-bonded to the side chain of Asn255, while the ribitol moiety also interacts with the Asn255 side chain (Fig. 5A, B). For convenience of description, the binding sites for the phosphate groups of RboP1, RboP2, RboP3, and RboP4 are referred to as P1, P2, P3, and P4, respectively. As shown in Fig. 5, the key interactions between TarM(Se)$_{G117R}$ and 4RboP-glucose are formed mainly by backbone amide groups that serve to anchor phosphate groups of 4RboP-glucose into the P1, P2, and P3 sites, while Arg326 and Gln330 side chains interact with the ribitol moiety of RboP3, with help from Lys263 and Asn255, leading the poly(RboP) fragment to adopt a V-shaped conformation, in which the phosphate group of RboP3 is located at the vertex. As a result of these interactions, 4RboP-glucose rests in an extended electropositive groove on the TarM(Se) surface (Fig. 6A). The observed binding mode for phosphate groups and the extended electropositive groove on the TarM(Se) surface is similar to that of 3RboP bound to TarP, a structure of an inverting WTA glycosyltransferase (Fig. 6C) that we have determined earlier(*27*). TarM(Se) is a retaining WTA glycosyltransferase, therefore, the relative positions of donor and acceptor substrates in TarM(Se) and TarP are different (Fig. 6B, C).

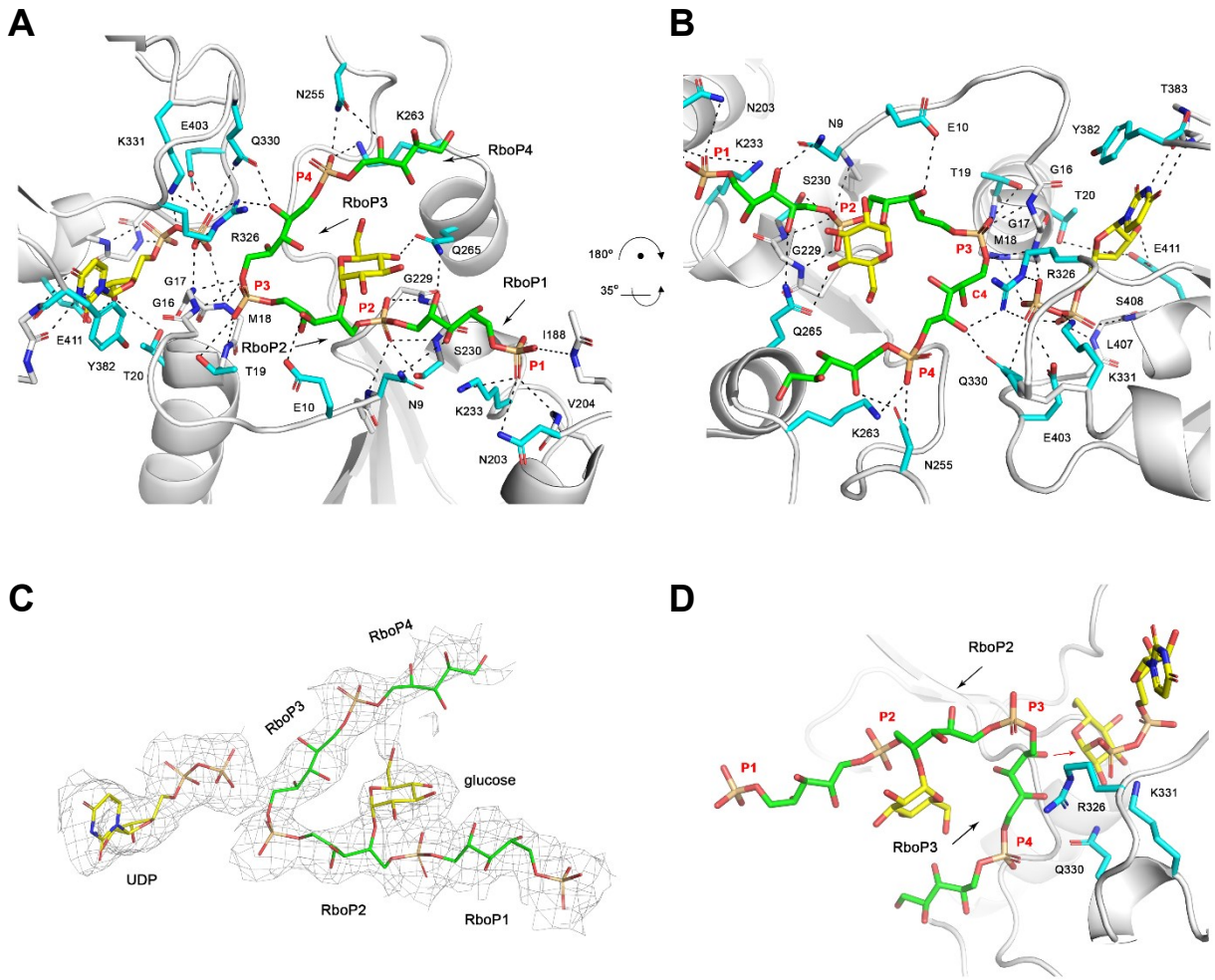

Fig. 5. Interactions of TarM(Se)$_{G117R}$ with product UDP and glycosylated 4RboP-(CH$_2$)$_6$NH$_2$ (4RboP-glucose) and reaction mechanism of TarM(Se). (A) The binding sites of product UDP (yellow) and 4RboP-glucose in TarM(Se)$_{G117R}$-UDP-4RboP-glucose complex structure with key amino acids (cyan), focuses on the binding site of 4RboP-glucose for clarity. The linker region is omitted due to no electron density for it. 4RboP is colored green and glucose on C4 of RboP2 colored yellow. D-ribitol 5-phosphate units, RboP1, RboP2, RboP3, and RboP4, are labelled. The binding sites for phosphate group of RboP1, RboP2, RboP3, and RboP4 are indicated as P1, P2, P3, and P4, respectively. Hydrogen bonds and salt bridges are shown as black dashed lines. **(B)** Upon 180° and 35° rotation of **(A)** focuses on the active center. P1, P2, P3, and P4 for phosphate binding sites and C4-hydroxyl of RboP3 in the active center are labeled. The unit numbers are omitted for clarity. **(C)** Simulated-annealing (mFo − DFc) omit map of UDP (yellow) and 4RboP-glucose in the TarM(Se)$_{G117R}$-UDP-4RboP-glucose complex structure (grey mesh, at 1.5 σ). 4RboP is colored green and glucose residue on 4RboP colored yellow. The product UDP, RboP unit numbers and glucose residue on 4RboP are indicated. **(D)** View into the active center of TarM(Se). RboP2 and RboP3 are labeled. The red arrow indicates how the C4-hydroxyl of RboP3 could nucleophilically attack C1 of UDP-glucose on the α-face.

Key residues for catalysis and reaction mechanism of TarM(Se)

As shown in Fig. 5, Arg326 and Lys331 both coordinate with β-phosphate of the donor substrate, so that the glucose moiety lies in a correct orientation for the attacking of the nucleophile. Simultaneously, they could stabilize negative charges on the leaving phosphate group. The side chains of Arg326 and Gln330 interact not only with the donor substrate, but also with 4RboP-glucose, with help from Lys263, enforcing the RboP unit in the active center to adopt a proper orientation for glycosylation. Our mutation analysis and previous studies show that substitution of Arg326, Lys331, and Gln330 into alanine renders the enzyme inactive(*31, 32*) (table S3). Thus, we propose that these three residues are essential for catalysis. Glu403 rests near the side chain of Lys331, the distances between the side chains of these two residues are similar in the TarM(Se)$_{G117R}$-UDP-glucose binary structure and the ternary structure of TarM(Se)$_{G117R}$-UDP-4RboP-glucose (2.76 and 3.03 Å, respectively), which indicates that the side chain of Glu403 could interact with Lys331, helping it in correct orientation during the catalytic cycle. In line with this assumption, the activities of E403A and K263A mutant proteins are severely reduced compared with that of the wild type protein (table S3). Therefore, Glu403 and Lys263 are both important for binding and catalysis. Asn9, Glu10, Asn203, Lys233, Asn255, and Gln265 are involved in the binding of 4RboP-glucose, as alanine mutant proteins of these residues are all well folded and homotrimeric (fig. S3C, D). K233A and E10A showed 21.7% and 30.9% remaining activities, respectively, while the other four mutant proteins displayed more than 50% activity, suggesting that a single mutation in this region is not sufficient to affect poly(RboP) binding due to the multiple interactions.

To interpret the catalytic mechanism of TarM(Se), we changed UDP in Fig. 5B into UDP-glucose and omitted most residues except Arg326, Gln330, and Lys331 (Fig. 5D). As Fig. 5D shows, the C4-hydroxyl of the unit RboP3 rests at the α-face of UDP-glucose, the distance between the C4-hydroxyl of RboP3 and the putative anomeric C1 of UDP-glucose is 2.64 Å. Furthermore, at 3.34 Å, β-phosphate O2B atom of UDP is well within hydrogen bonding distance of the C4-hydroxyl of RboP3 (Fig. 5B, C, Fig. 6B). The observed geometry and distances nicely support an internal nucleophilic substitution (S_Ni)-like mechanism(*42, 43*). In this mechanism, the phosphate group of UDP-glucose would serve as a base catalyst, activating the C4-

hydroxyl of RboP3 and the activated nucleophile could attack the anomeric C1 of UDP-glucose on the α-face, thus yielding an α-O-glycosylated RboP-WTA. The nucleoside diphosphate leaving group could be stabilized by the side chains of Arg326 and Lys331.

Fig. 6. Electrostatic potential surface representation of 4RboP-glucose binding site in TarM(Se)

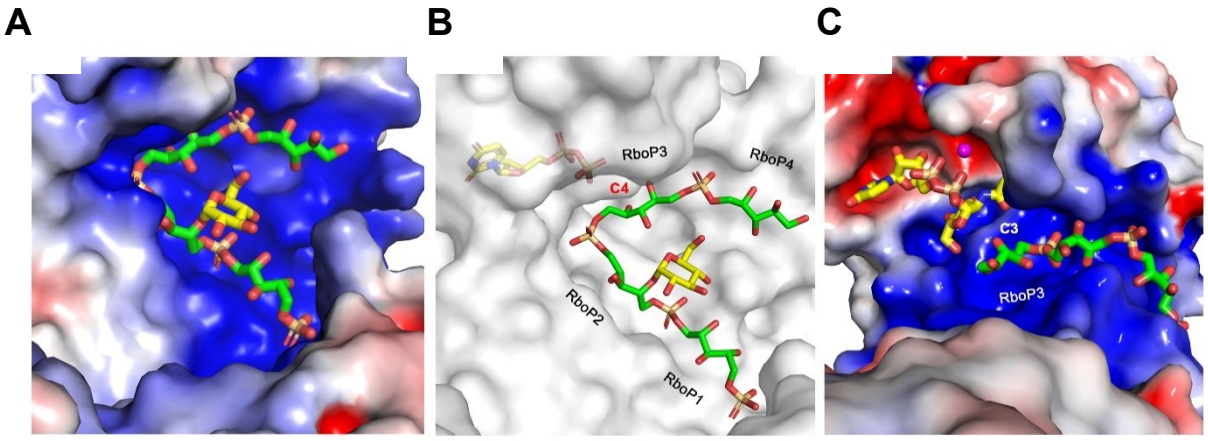

and relative positions of donor and acceptor substrates in TarM(Se) and TarP from *S.aureus* (PDB code 6H4M). (A) Electrostatic potential surface representation of 4RboP-glucose binding site in TarM(Se), with electrostatic potential +5 kcal/mole in blue to -5 kcal/mole in red. 4RboP is colored green and glucose residue on 4RboP yellow. **(B)** Relative position of product UDP (yellow) and 4RboP-glucose in TarM(Se)$_{G117R}$, a retaining WTA glycosyltransferase, in surface presentation (grey). 4RboP-glucose is colored as in **(A)**. The unit numbers and C4-hydroxyl of RboP3 in the active center are indicated. **(C)** Relative position of UDP-GlcNAc (yellow) and 3RboP (green) in TarP *from S.aureus*, an inverting WTA glycosyltransferase, in electrostatic potential surface representation, with +5 kcal/mole in blue to -5 kcal/mole in red. Mg^{2+} is shown as ball, colored magenta. RboP3 and C3-hydroxyl of RboP3 in the active center are indicated.

TarM(Se) is a processive WTA glycosyltransferase

In *S. aureus*, all three enzymes, TarM(Sa), TarS, and TarP, glycosylate RboP-WTA with GlcNAc, but at same or different positions in either α- or β-configuration(*24, 26, 27*). These glycosyltransferases are predicted to act as processive enzymes(*32, 44, 45*). However, so far, no structural evidence for this hypothesis is available. In our ternary complex structure, the UDP molecule occupies the binding site of UDP-glucose; the glucose residue is covalently bound at the C4 position of RboP2 in 4RboP-$(CH_2)_6NH_2$, the phosphate group of RboP2 occupies P2 site and the C4-hydroxyl of RboP3 is placed near to the β-phosphate of UDP (Fig. 5, Fig. 6B, Fig. 7C), suggesting at least three reaction steps have been completed during the crystal

soaking with UDP-glucose and 4RboP-$(CH_2)_6NH_2$. First, UDP-glucose docks into its position, the RboP1 phosphate group of 4RboP-$(CH_2)_6NH_2$ binds to the P2 site, and the phosphate groups of RboP2 and RBoP3 bind to P3 and P4 sites, respectively, putting the C4-hydroxyl of RboP2 at the active center for glycosylation (Fig. 7A). Second, glycosylation of the C4-hydroxyl of RboP2 occurs (Fig. 7B). Third, the glycosylated 4RboP-$(CH_2)_6NH_2$ chain moves forward through the active center for one unit, so that the phosphate group of RboP1 is shifted to the P1 site just as the crystal snapshot of the ternary complex structure shows. We do not know how many steps really take place in the whole catalytic cycle of TarM(Se), but we think it is likely that the crystallographic snapshot of the active center in the ternary structure of TarM(Se)$_{G117R}$-UDP-4RboP-glucose represents the rate-determining step of this cycle and this snapshot is just the step before the exchange of product UDP for UDP-glucose for the second catalytic cycle. Therefore, our ternary structure of TarM(Se)$_{G117R}$ with UDP and 4RboP-glucose demonstrates (i) that TarM(Se) is a processive enzyme; (ii) that TarM(Se) starts the processive reaction from the second unit of the poly(RboP) chain, here RboP2; (iii) that the glycosylated poly(RboP) chain moves forwards through the active center for one unit after each catalytic cycle; and (iv) that each RboP unit of the poly(RboP) chain except the first one is glycosylated, which is consistent with previous findings for *S aureus* RboP-WTA using NMR and MS analysis(*46*).

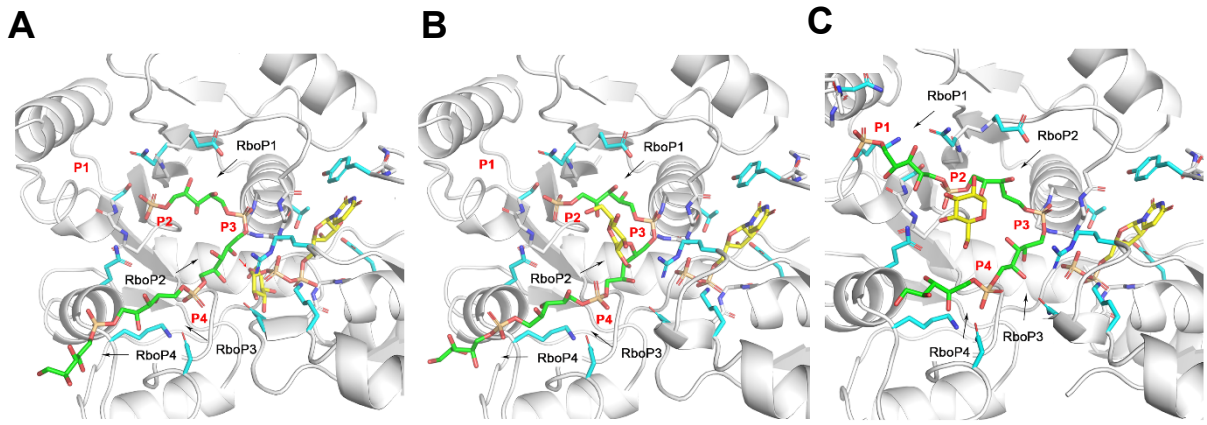

Fig. 7. TarM(Se) is a processive WTA glycosyltransferase. (A) Binding of UDP-glucose (yellow) and 4RboP (green) in proposed first step of the processive reaction (the linker region of 4RboP-$(CH_2)_6NH_2$ is omitted for clarity). The key amino acids in the ternary complex structure are shown (cyan). RboP1, RboP2, RboP3, and RboP4 are labeled. The binding sites of phosphate group of

RboP1, RboP2, RboP3, and RboP4 are labeled as P1, P2, P3, and P4, respectively, same as in Fig. 2. The phosphate group of RboP2 is located at P3. Red arrow indicates that the C4-hydroxyl of RboP2 attacks nucleophilically C1 of UDP-glucose. **(B)** Glycosylation of 4RboP in the proposed second step of the processive reaction. Product UDP is colored yellow, 4RboP green and glucose residue on 4RboP is colored yellow. P1, P2, P3, P4, and the unit numbers of 4RboP are indicated. **(C)** Crystal snapshot after sliding of 4RboP-glucose for one RboP unit. The phosphate group of RboP1 is shifted to P1 site from P2. UDP and 4RboP-glucose are colored as in **(B)**. P1, P2, P3, P4, and unit numbers are labeled.

Discussion

We demonstrate here that TarM(Se) modifies RboP-WTA with glucose, instead of with GlcNAc by TarM(Sa) from *S. aureus*. Invasive HA-MRSE clones with *tarIJLM2* may use the altered glycosylation pattern generated by TarM(Se) to support their immune evasion capacities. Our study also reveals phenotypic consequences of the replacement of GlcNAc with glucose on RboP-WTA. In order to decipher the reaction mechanism, we determined several structures of TarM(Se) in complex with ligands that together serve to outline the binding mode as well as the likely catalytic pathway of this glycosyltransferase. The ternary complex structure of TarM(Se)$_{G117R}$ bound to UDP and 4RboP-glucose provides, for the first time, clear evidence that a glycosyltransferase glycosylates WTA in a processive manner. This is in line with the observations that WTAs extracted from bacterial cells are heavily modified with sugars(*22, 46*), and the WTA chains contain sugars with exclusive α- or β-configuration(*47, 48*). The enzyme activity and theoretical potential for the processive ability of the TarM(Sa) homotrimer and TarM(Sa)$_{G11R}$ monomer are similar, suggesting the trimerization does not impact the substrate binding, catalysis, and processivity(*32*). In our ternary complex structure, the ribitol moiety of RboP4 rests in the center of the acceptor substrate-binding domain, while the phosphate group of RboP1 (P1 site) lies at the interface of acceptor substrate-binding and trimerization domains, indicating that the poly(RboP) chain moves into the active center from the entry site (E), and the glycosylated poly(RboP) chain leaves the TarM(Se) surface near the P1 site (Fig. 8A, B). The C1-hydroxyl group of RboP4 in molecule A is 33.7 Å away from molecule B in the homotrimer, which corresponds to a length of 3.7 RboP units. Therefore, it is not possible that three TarM(Se) molecules in the homotrimer glycosylate the same poly(RboP) chain at same time in the processive

reaction. This is consistent with the observation about similarities of the activity and processive ability of TarM(Sa) homotrimer and TarM(Sa)$_{G117R}$ monomer(*32*). Interestingly, the processive ability of the trimeric TarS wild-type protein is 18-fold higher than that of a C-terminally truncated enzyme that lacks the trimerization domain, suggesting a contribution of the trimerization domain or trimerization to the processivity of TarS(*44*).

To date, no complex structure of TarM(Sa) with its donor and acceptor substrates is available. The ternary structure of TarM(Se)-UDP-4RboP-glucose allows us to predict also how poly(RboP) binds to the homologous TarM(Sa) enzyme (Fig. 8C). The binding sites for the four phosphate groups of 4RboP-glucose in TarM(Se) are all conserved in TarM(Sa), the essential residues for catalysis Arg326 and Lys331 are present in both enzymes and the third one, Gln330, binds specifically the C2-hydroxyl of UDP-glucose in TarM(Se), while a threonine in TarM(Sa) accommodates the large volume of GlcNAc at C2 position(*32*). The other nine residues, which are in contact with 4RboP-glucose, eight are identical or conserved. Therefore, we conclude that the poly(RboP) chain adopts similar conformations in TarM(Sa) and in TarM(Se) and, thus, the *S. aureus* TarM(Sa) is expected to use the same S$_N$i-like mechanism for its catalytic reaction.

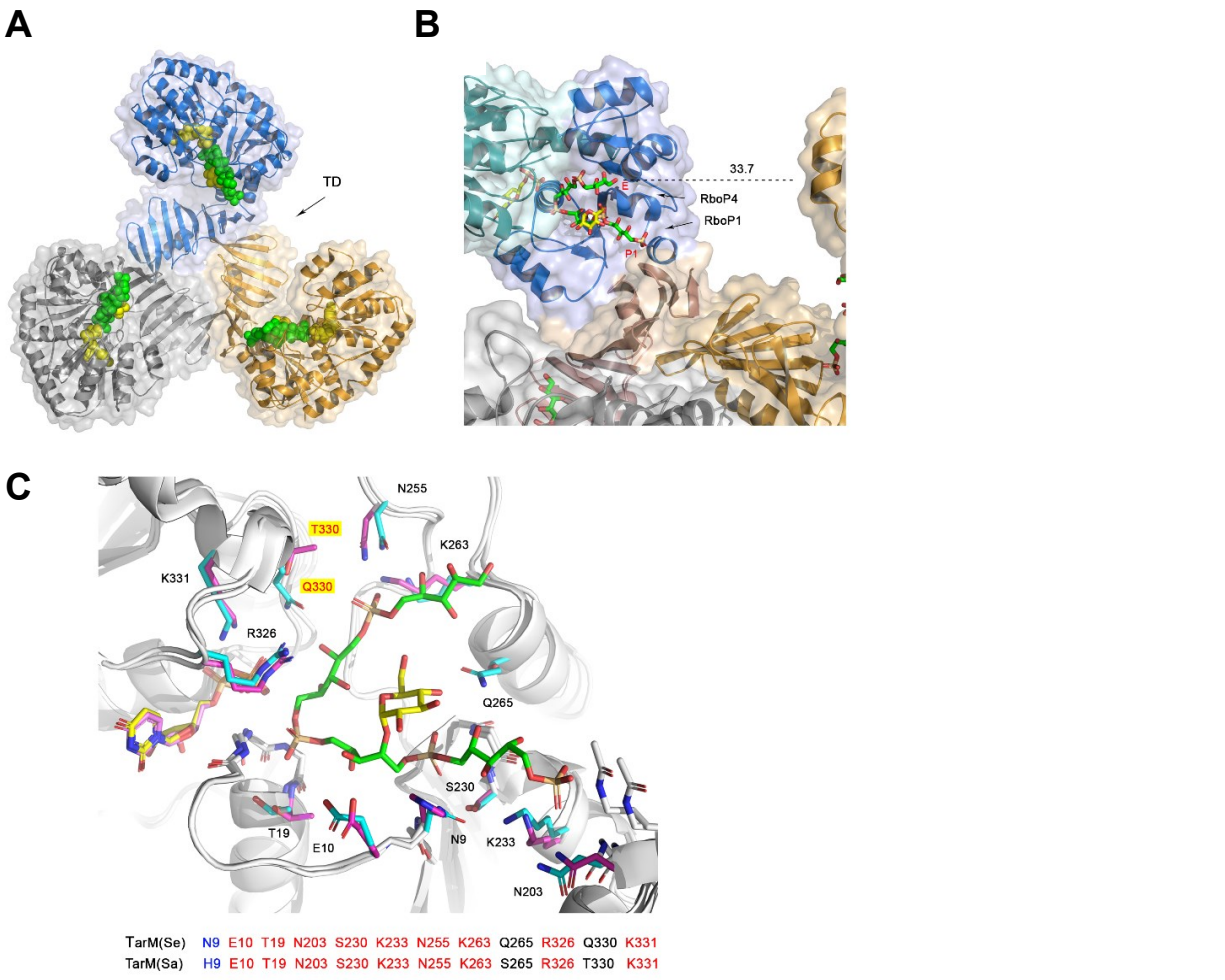

Fig. 8. UDP and 4RboP-glucose in TarM(Se) homotrimer and comparison of the essential residues for catalysis and poly(RboP) binding in TarM(Se) with the corresponding residues in TarM(Sa) from *S.aureus* (PDB code 4X7R). (A) UDP and 4RboP-glucose in TarM(Se) homotrimer (blue, molecule A; orange, molecule B; grey, molecule C). UDP and 4RboP-glucose are shown as full-atom models. UDP is colored yellow, 4RboP green, and glucose residue on 4RboP is colored yellow. Trimerization domains are indicated. **(B)** UDP and 4RboP-glucose in TarM(Se) homotrimer, focusses on molecule A. The nucleotide-binding domain (green), acceptor substrate-binding domain (blue) and trimerization domain (boron) of molecule A are labeled. RboP1, RboP4, the entry site (E) of poly(RboP) chain into the active center and the region of glycosylated poly(RboP) chain leaves TarM(Se) surface (near P1) are indicated. The distance (33.7 Å) from C1-hydroxyl of RboP4 in molecule A to the nearest point of molecule B is shown as black dashed line. **(C)** Comparison of the essential residues for catalysis and poly(RboP) binding in TarM(Se) with the corresponding residues in TarM(Sa) from *S.aureus*. Residues of TarM(Se), UDP and 4RboP-glucose are colored as in Fig. 2. TarM(Sa) residues are colored magenta and UDP violet. Only residues of TarM(Se) and T330 in TarM(Sa) are labelled for clarity. Q330 in TarM(Se) and T330 in TarM(Sa) are highlighted as red with yellow background. Key residues for catalysis and binding of 4RboP-glucose are shown at the bottom, with nine identical (red) and one conserved (blue).

Glycosylated RboP-WTA has been considered as a promising vaccine antigen against *S. aureus* because it is highly abundant on the bacterial surface and is largely invariant except for variation of the glycosidic linkages(*34, 37*). Accordingly, the majority of anti-*S. aureus* antibodies in human sera are directed against glycosylated RboP-WTA(*34*). Our recent report of nosocomial *S. epidermidis* clones with RboP-WTA has raised hopes that such a vaccine could also protect from *S. epidermidis* infections(*20*). Our study indicates that in addition to RboP-GlcNAc, a broadly active anti-*Staphylococcus* vaccine should also include RboP-glucose epitope to cover major invasive *S. epidermidis* clones such as ST10, ST23, and ST87. These emerging *S. epidermidis* lineages do usually not colonize the human nose or skin but are often found as the cause of invasive infections(*20*). As *S. epidermidis* infections are usually restricted to hospitalized and immunocompromised patients, the adaptive immune systems of the majority of the human population have probably not been exposed to *tarIJLM*-expressing *S. epidermdis* clones, which may explain the apparent absence of IgG specific for RboP-glucose epitopes in pooled human sera. In addition, the type of glycosylation is crucial for the immunogenicity of RboP-WTA(*27*). While TarP and TarM(Sa), which are found only in a minority of the *S. aureus* strains and are dominant over the housekeeping RboP-WTA glycosyltransferase TarS, lead already to a substantial reduction in the immunogenicity of WTA(*27, 37*), glycosylation by TarM(Se) may have the same or even a stronger impact on the immunogenic properties of RboP-WTA. In-depth immunological studies will unravel how the various glycosylation types affect the capacity of the human immune system to raise protective antibodies. Notably, coupling of TarP-modified RboP-WTA to an immunogenic carrier protein has been shown to restore full antigenicity of WTA(*49*), which opens attractive avenues for the development of anti-*Staphylococcus* vaccines directed against major WTA epitopes.

Nosocomial *S. epidermidis* clones have been shown to harness RboP-WTA because the additional polymer increases their invasiveness and persistence in the bloodstream(*20*). Future studies on the interaction of the various RboP-WTA glycosylation variants with human epithelial and endothelial receptors will reveal how WTA polymers with glucose contribute to the establishment of infection and evasion of immune responses. Interestingly, the replacement of GlcNAc with glucose on RboP-WTA did not alter the bacterial susceptibility to the Siphovirus Φ11 and,

potentially, other serogroup-B phages, which share similar receptor-binding proteins. This finding extends our knowledge on the receptor and host preferences of *Staphylococcus*-specific phages and it will help in the development of phage therapy approaches, which will become promising alternatives for the treatment of multi-resistant *S. aureus* and *S. epidermidis* infections(*50*). In addition, our ternary complex structure of TarM(Se)-UDP-4RboP-glucose, together with the structure of TarP-UDP-GlcNAc-3RboP*(27)*, can now serve as a solid platform for the development of new inhibitors that could render MRSA and MRSE susceptible to human host defenses, and attenuate their virulence.

Materials and Methods

Bacterial strains and growth conditions.

S. aureus strain RN4220 was used for phage propagation and as test strain for phage binding and transduction experiments. *S. aureus* JP1794 and PS187-H VW1 were used as donor strains for SaPI particle propagation as described below. *E. coli* DC10B was used as a cloning host. *E. coli* BL21(DE3) was used for protein expression. RN4220 and PS187 were used as donor strains for plasmid transduction. *S. epidermidis* and *S. aureus* strains were cultivated in tryptic soy broth (TSB) medium or Mueller-Hinton broth (MHB), or otherwise noted and incubated at 37°C on an orbital shaker. *E. coli* strains were cultivated in lysogeny broth (LB). Media were supplemented with appropriate antibiotics (tetracycline (5 µg/ml), chloramphenicol (10 µg/ml), or ampicillin (100 µg/ml)). Clinical *S. epidermidis* strain E73 was from the strain collection used in our previously published study(*20*) .

Molecular genetic methods.

For the construction of the Δ*tarM(Se)* mutant in *S. epidermidis* E73, the pBASE6-erm/lox1 shuttle vector was used according to standard procedures. For mutant complementation to *S. epidermidis* E73 and *S. aureus* RN4220, plasmid pRB474 was used. The primers for knockout and complementation plasmid construction are listed in table S4. The pRB474 with *tarM(Sa)* were constructed by the method and primers mentioned in a previous study. Plasmid transduction to *S. epidermidis* strains

was performed using Φ11 with *S. aureus* RN4220 as donor strain or Φ187 with *S. aureus* PS187 as donor strain as described previously(*51*).

For TarM(Se) overexpression, the DNA sequence containing the coding region of *tarM(Se)* was chemically synthesized, inserted into pET-11α at NdeI and BamHI sites, and single mutations were introduced from the synthesized *tarM(Se)* using the same restriction sites (GenScript Biotech, Netherlands, B.V.). Obtained amplicons were confirmed by sequencing and were used to transform *E. coli* B21(DE3) for expression.

IgG binding.

S. epidermidis and *S. aureus* were grown overnight, washed, and adjusted to an OD_{600} of 0.4 in PBS containing 0.1% BSA. 25 µl of the diluted bacteria were incubated with 25 µl serial dilutions of pooled human IgG (Merck, I4506) or mAb 4461 In a 96-well plate for 30 min at 4°C(*37, 52*). The samples were subsequently washed, centrifuged, and incubated with fluorescein thioisocyanat labeled goat anti-human IgG F(ab')2 FITC conjugate (2 ug/ml) (Merck, AQ112F) for 20 min at 4°C in the dark. Labeled bacteria were washed, centrifuged, and fixed with 1% paraformaldehyde for 20 min at room temperature in the dark. The bacteria were centrifuged again, resuspended in PBS and surface-bound IgG was measured by flow cytometry using a BD FACS Calibur. 10 µg/ml isotype control IgG directed against HIV protein gp120 (b12-IgG) was used in experiments with mAb 4461. The whole bacterial population was gated, and the mean FL-1 fluorescence was analyzed with FlowJo version 10.8.1. The WTA-specific mAb 4461 as well as the B12 isotype control were described previously(*53*).

Phage binding, infection, and transduction assays.

Phage spot assays to test the bacterial susceptibilities were performed as described previously(*40*). Myovirus FK, Siphoviruses F11, F187, and FE72, and Podovirus F68, were freshly propagated in suitable bacterial host strains and filtered to yield sterile phage suspensions. Final concentrations of the phages were adjusted to approximately 1×10^9 plaque-forming units (pfu) /ml. Test bacteria were cultivated overnight in fresh TSB to densities of OD_{600}=0.5. 100 µl of the suspensions were added to 5 ml soft-agar for the preparation of bacterial overlay lawns. 10 µl of each

phage suspension were spotted onto the bacterial lawns. After 37°C overnight incubation, phage clearing zones were observed and recorded.

SaPI transfer experiments were performed according to standard procedures(*40*). Briefly, approximately 8.0×10^7 cells of a recipient strain grown overnight were mixed with 100 µl of lysates obtained from *S. aureus* donor strain JP1794 or PS187-H VW1 bearing the tetracycline resistance marker-labelled SaPIbov1 (~1.0×10^6 PFU ml^{-1}) after addition of 100 µl transducing F11 lysate. Samples were then incubated for 15 min at 37°C, diluted, and plated on tetracycline-containing TSB agar to count transductant colonies.

The adsorption efficiency of FK, F11, F68, F187 and FE72 was determined as described previously with minor modifications(*40*). Briefly, adsorption rates were analyzed using a multiplicity of infection (MOI) of 0.1. The adsorption rate was elucidated by determining the number of unbound phages in the supernatant and dividing the number of bound phages by the number of input phages.

WTA isolation.

Cell walls and WTA were isolated and purified according to previously described methods(*54*). In brief, bacteria were grown in TSB (with 0.25% glucose) in a shaker at 37°C overnight. Bacterial cells were collected and disintegrated with a FastPrep-24 instrument (MP Biomedicals). The bacterial lysates were incubated with DNase I (Roche) and RNase A (Sigma) at 37°C overnight. Cell walls were then obtained by sonification of lysates and repeated washing of the insoluble cell walls with 2%-SDS solution. The WTA was released from peptidoglycan by treatment with 5% trichloroacetic acid and then dialyzed in water using a Spectra/Por3 dialysis membrane (MWCO of 3.5 kDa; VWR International GmbH). Obtained soluble WTA was quantified by determining the content of phosphate as previously described(*54*). To quantify the WTA amount per cell, 300 µl cell wall suspension was mixed with 300 µl 1-M NaOH and incubated at 60°C with constant shaking of 600 rpm for 2 hours. The phosphate content in supernatants of this mixture was then measured by phosphate assay(*54*). The same amount of 300 µl cell wall was dried in a Speedvac concentrator and weighted to determine the phosphate amount per cell wall dry mass.

WTA compositional analysis.

Identification of the WTA polymer type was performed using an Ultimate 3000RS HPLC system (Dionex) coupled to a micrOTOFII electrospray-ionization (ESI) TOF mass spectrometer (Bruker). Purified WTA was mixed 1:1 with 2-M NaOH and incubated at 60°C with constant shaking of 600 rpm for 2 hours and then used in the composition analysis. For HPLC, a Gemini C18 column (150 x 4.6 mm, 110 Å, 5 µM, Phenomenex) was used at 37°C with a flow rate of 0.2 ml/min. A 5-min equilibration step with 100% buffer A (0.1% formic acid, 0.05% ammonium formate) was applied, followed by a linear gradient of 0 to 40% buffer B (acetonitrile) for 30 min. A final washing step with 40% buffer B for 5 min and a re-equilibration step (100% buffer A) for 5 min completed the method. Samples were ionized via ESI in positive ion mode. Exact masses in positive ion mode were presented as extracted ion chromatograms with Data Analysis (Bruker). Base peak chromatograms were used for sample normalization.

Semiquantitative biofilm assay.

S. epidermidis biofilm formation was analyzed using 96-well delta microtiter plates (NUNC) as described previously(*20*) with the following modifications. Overnight cultures of bacterial cells were diluted in fresh TSB with 1% glucose and distributed into the 96-well plates with each well containing 200 µl diluted bacterial cells. After incubation at 37°C for 1 h, the bacterial cells in the plates were washed gently three times in PBS and then stained with 0.1% crystal violet solution. The stain was washed off gently under slowly-running water and plates were dried. Finally, 5% acetic acid was added to the wells to dissolve the staining. The absorbance was measured at 570 nm using a MicroELISA autoreader (Bio-Rad).

Synthesis of 4RboP-$(CH_2)_6NH_2$. 4RboP-$(CH_2)_6NH_2$ was synthesized according to the scheme described previously(*55*) (fig. S1). The analytic data can be found in Supplementary information.

Protein expression and purification.

E. coli BL21(DE3) were grown in LB or TB medium at 30°C. Expression of *tarM(Se)* was induced with 0.5 mM IPTG at 22°C at an OD_{600} of 0.6. After 15 hours cells were

harvested, washed with wash buffer (50 mM Tris-HCl, pH 8.0, 1 mM EDTA), and lysed by sonication in lysis buffer (70 mM NaH_2PO_4, pH 8.0, 1 M NaCl, 10 mM β-mercaptoethanol, 20% glycerol, 10 U/ml of benzonase nuclease). After centrifugation (15,000 g), the supernatant was filtered with a 0.45 µm filter, loaded onto a His Trap FF column (GE Healthcare, 5 ml), and washed with buffer A (50 mM NaH_2PO_4, pH 8.0, 1 M NaCl, 10 mM β-mercaptoethanol, 20% glycerol) supplemented with 42 mM imidazole and buffer B (buffer A with 60 mM imidazole). Finally, the protein was eluted with buffer C (buffer A with 500 mM imidazole), and the fractions were pooled and further purified by size-exclusion chromatography on a Superdex 200 increase 10/30 column equilibrated with buffer D (20 mM triethanolamine, pH 7.8 (for $TarM(Se)_{G117R}$), or 8.5 (for TarM(Se) and mutant proteins), 250 mM LiCl, 10 mM β-mercaptoethanol, 5% glycerol). The peak fractions were pooled and concentrated to 3.0 (for TarM(Se)) or 2.4 mg/ml (for $TarM(Se)_{G117R}$) for crystallization.

Glycosyltransferase activity assay.

The activity of TarM(Se) and mutated proteins was determined with the ADP Quest Assay kit (DiscoverRx). The reaction volume was 20 µl with 1 mM UDP-glucose or other UDP-activated sugars, 1.5 mM purified poly(RboP) WTA from RN4220 Δ*tarM(Sa)*Δ*tarS* or poly(GroP) WTA from *S. epidermidis* E73 Δ*tarM(Se)*. The reaction was started by addition of proteins and incubated at room temperature for 1 hour. Released UDP was converted into a fluorescence signal that was detected in a 384-well black assay plate with 530 nm excitation and 590 nm emission wavelengths using TECAN Infinite M200.

Circular dichroism (CD).

CD measurements were performed on a JASCO J-720 spectropolarimeter (Gross-Umstadt, Germany). Purified TarM(Se) and mutant proteins (1.4 - 3.2 mg/ml in buffer D) were diluted with H_2O to a final concentration of 0.2 mg/ml. A path length of 0.1 cm was used and the samples were scanned at a speed of 100 nm/min. Spectra were recorded at room temperature with an accumulation of 10 in the range of 250 – 190 nm and evaluated using the software Spectra Manager (Jasco).

Crystallization and data collection.

Crystals were obtained by hanging drop vapor diffusion. For native TarM(Se), 1 µl protein solution (3 mg/ml) was mixed with 1 µl reservoir solution containing 15% PEG 1,000, 6 mM hexaamminecobalt (III) chloride, 0.1 M Tris-HCl, pH 6.9 at 12°C. For TarM(Se)$_{G117R}$ mutant protein (2.4 mg/ml) the reservoir solution composed of 10% PEG 20,000, 25% PEG MME 550, 0.1 M MES/imidazole, pH 6.9, 0.03 M $NaNO_3$, 0.03 M Na_2HPO_4, 0.03 M $(NH_4)_2SO_4$ at 20°C. The crystals of TarM(Se)$_{G117R}$ were used for soaking of UDP-glucose (26 mM) for 5 min. For crystals of TarM(Se)$_{G117R}$ with 4RboP-$(CH_2)_6NH_2$, 30 mM 4RboP-$(CH_2)_6NH_2$ was introduced in the protein solution and 1 µl protein solution was mixed with 1 µl reservoir solution containing 10% PEG 20,000, 25% PEG MME 550, 0.1 M MES/imidazole, pH 6.9, 0.02 M sodium formate, 0.02 M ammonium acetate, 0.02 M trisodium citrate, 0.02 M sodium potassium tartrate (racemic), 0.02 M sodium oxamate. The crystals of TarM(Se)$_{G117R}$ with 4RboP-$(CH_2)_6NH_2$ were used for soaking of UDP-glucose (20 mM) and 4RboP-$(CH_2)_6NH_2$ (41 mM) together for 5 min.

For data collection the crystals were cryo-protected with 20% MPD in reservoir solution and flash-frozen in liquid nitrogen. Diffraction data were collected at beamline X06DA of Swiss Light Source in Villigen, Switzerland.

Structure solution and refinement.

All data were reduced using XDS/XSCALE software packages(*56*). The structure of native TarM(Se) was solved by molecular replacement using PHASER software and a version of TarM(Sa) (PDB code 4WAC) was modified by CHAINSAW and then used as search model(*31, 57, 58*). The final structure of native TarM(Se) was achieved by cycles of iterative model modification using COOT(*59*), and restrained refinement with BUSTER and REFMAC5(*60, 61*). One chain of TarM(Se) was then used as search model to solve the structure of TarM(Se)$_{G117R}$ by molecular replacement. The two binary structures and one ternary complex structure of TarM(Se)$_{G117R}$ with UDP-glucose or 4RboP-$(CH_2)_6NH_2$ or both together were solved by molecular replacement using PHASER and the unliganded TarM(Se)$_{G117R}$ structure was used as a search model. UDP-glucose in TarM(Se)$_{G117R}$-UDP-glucose structure, 4RboP-$(CH_2)_6NH_2$ in TarM(Se)$_{G117R}$-4RboP-$(CH_2)_6NH_2$ structure, as well as UDP and 4RboP-glucose in the ternary complex structure were removed from the

models to calculate the simulated annealing (mF_o – DF_c) omit maps using PHENIX(*62*). The coordinate and parameter files for 4RboP and 4RboP-glucose were calculated by the PRODRG server(*63*). All structure figures were generated by PyMOL and the models were evaluated using MolProbity(*64, 65*). Statistics for the data collection and refinement are reported in Table 1 and table S2.

Statistical information.

Statistical analysis was performed using the Prism 8.0 package (GraphPad Software). P values of ≤0.05 were considered significant.

References

1. M. Otto, Staphylococcus epidermidis--the 'accidental' pathogen. *Nat Rev Microbiol* **7**, 555-567 (2009).
2. M. M. Severn, A. R. Horswill, Staphylococcus epidermidis and its dual lifestyle in skin health and infection. *Nat Rev Microbiol* **21**, 97-111 (2023).
3. A. L. Byrd, Y. Belkaid, J. A. Segre, The human skin microbiome. *Nat Rev Microbiol* **16**, 143-155 (2018).
4. A. Kengmo Tchoupa, D. Kretschmer, B. Schittek, A. Peschel, The epidermal lipid barrier in microbiome-skin interaction. *Trends Microbiol*, (2023).
5. M. Li, X. Wang, Q. Gao, Y. Lu, Molecular characterization of Staphylococcus epidermidis strains isolated from a teaching hospital in Shanghai, China. *J Med Microbiol* **58**, 456-461 (2009).
6. E. A. Grice, J. A. Segre, The skin microbiome. *Nat Rev Microbiol* **9**, 244-253 (2011).
7. K. Becker, C. Heilmann, G. Peters, Coagulase-negative staphylococci. *Clin Microbiol Rev* **27**, 870-926 (2014).
8. S. Naik, N. Bouladoux, C. Wilhelm, M. J. Molloy, R. Salcedo, W. Kastenmuller, C. Deming, M. Quinones, L. Koo, S. Conlan, S. Spencer, J. A. Hall, A. Dzutsev, H. Kong, D. J. Campbell, G. Trinchieri, J. A. Segre, Y. Belkaid, Compartmentalized control of skin immunity by resident commensals. *Science* **337**, 1115-1119 (2012).
9. G. J. Christensen, H. Bruggemann, Bacterial skin commensals and their role as host guardians. *Benef Microbes* **5**, 201-215 (2014).

10. Q. Liu, Q. Liu, H. Meng, H. Lv, Y. Liu, J. Liu, H. Wang, L. He, J. Qin, Y. Wang, Y. Dai, M. Otto, M. Li, Staphylococcus epidermidis Contributes to Healthy Maturation of the Nasal Microbiome by Stimulating Antimicrobial Peptide Production. *Cell Host Microbe* **27**, 68-78 e65 (2020).
11. T. Iwase, Y. Uehara, H. Shinji, A. Tajima, H. Seo, K. Takada, T. Agata, Y. Mizunoe, Staphylococcus epidermidis Esp inhibits Staphylococcus aureus biofilm formation and nasal colonization. *Nature* **465**, 346-349 (2010).
12. S. Y. Tong, J. S. Davis, E. Eichenberger, T. L. Holland, V. G. Fowler, Jr., Staphylococcus aureus infections: epidemiology, pathophysiology, clinical manifestations, and management. *Clin Microbiol Rev* **28**, 603-661 (2015).
13. A. S. Lee, H. de Lencastre, J. Garau, J. Kluytmans, S. Malhotra-Kumar, A. Peschel, S. Harbarth, Methicillin-resistant Staphylococcus aureus. *Nat Rev Dis Primers* **4**, 18033 (2018).
14. W. Ziebuhr, S. Hennig, M. Eckart, H. Kranzler, C. Batzilla, S. Kozitskaya, Nosocomial infections by Staphylococcus epidermidis: how a commensal bacterium turns into a pathogen. *Int J Antimicrob Agents* **28 Suppl 1**, S14-20 (2006).
15. G. Meric, L. Mageiros, J. Pensar, M. Laabei, K. Yahara, B. Pascoe, N. Kittiwan, P. Tadee, V. Post, S. Lamble, R. Bowden, J. E. Bray, M. Morgenstern, K. A. Jolley, M. C. J. Maiden, E. J. Feil, X. Didelot, M. Miragaia, H. de Lencastre, T. F. Moriarty, H. Rohde, R. Massey, D. Mack, J. Corander, S. K. Sheppard, Disease-associated genotypes of the commensal skin bacterium Staphylococcus epidermidis. *Nat Commun* **9**, 5034 (2018).
16. M. Otto, Molecular basis of Staphylococcus epidermidis infections. *Semin Immunopathol* **34**, 201-214 (2012).
17. X. Du, Y. Zhu, Y. Song, T. Li, T. Luo, G. Sun, C. Yang, C. Cao, Y. Lu, M. Li, Molecular analysis of Staphylococcus epidermidis strains isolated from community and hospital environments in China. *PLoS One* **8**, e62742 (2013).
18. J. Y. H. Lee, I. R. Monk, A. Goncalves da Silva, T. Seemann, K. Y. L. Chua, A. Kearns, R. Hill, N. Woodford, M. D. Bartels, B. Strommenger, F. Laurent, M. Dodemont, A. Deplano, R. Patel, A. R. Larsen, T. M. Korman, T. P. Stinear, B. P. Howden, Global spread of three multidrug-resistant lineages of Staphylococcus epidermidis. *Nat Microbiol* **3**, 1175-1185 (2018).

19. K. Y. Le, M. D. Park, M. Otto, Immune Evasion Mechanisms of Staphylococcus epidermidis Biofilm Infection. *Front Microbiol* **9**, 359 (2018).
20. X. Du, J. Larsen, M. Li, A. Walter, C. Slavetinsky, A. Both, P. M. Sanchez Carballo, M. Stegger, E. Lehmann, Y. Liu, J. Liu, J. Slavetinsky, K. A. Duda, B. Krismer, S. Heilbronner, C. Weidenmaier, C. Mayer, H. Rohde, V. Winstel, A. Peschel, Staphylococcus epidermidis clones express Staphylococcus aureus-type wall teichoic acid to shift from a commensal to pathogen lifestyle. *Nat Microbiol* **6**, 757-768 (2021).
21. C. Weidenmaier, A. Peschel, Teichoic acids and related cell-wall glycopolymers in Gram-positive physiology and host interactions. *Nat Rev Microbiol* **6**, 276-287 (2008).
22. S. Brown, J. P. Santa Maria, Jr., S. Walker, Wall teichoic acids of gram-positive bacteria. *Annu Rev Microbiol* **67**, 313-336 (2013).
23. R. van Dalen, A. Peschel, N. M. van Sorge, Wall Teichoic Acid in Staphylococcus aureus Host Interaction. *Trends Microbiol* **28**, 985-998 (2020).
24. S. Brown, G. Xia, L. G. Luhachack, J. Campbell, T. C. Meredith, C. Chen, V. Winstel, C. Gekeler, J. E. Irazoqui, A. Peschel, S. Walker, Methicillin resistance in Staphylococcus aureus requires glycosylated wall teichoic acids. *Proc Natl Acad Sci U S A* **109**, 18909-18914 (2012).
25. Y. Guo, N. M. Pfahler, S. L. Volpel, T. Stehle, Cell wall glycosylation in Staphylococcus aureus: targeting the tar glycosyltransferases. *Curr Opin Struct Biol* **68**, 166-174 (2021).
26. G. Xia, L. Maier, P. Sanchez-Carballo, M. Li, M. Otto, O. Holst, A. Peschel, Glycosylation of wall teichoic acid in Staphylococcus aureus by TarM. *J Biol Chem* **285**, 13405-13415 (2010).
27. D. Gerlach, Y. Guo, C. De Castro, S. H. Kim, K. Schlatterer, F. F. Xu, C. Pereira, P. H. Seeberger, S. Ali, J. Codee, W. Sirisarn, B. Schulte, C. Wolz, J. Larsen, A. Molinaro, B. L. Lee, G. Xia, T. Stehle, A. Peschel, Methicillin-resistant Staphylococcus aureus alters cell wall glycosylation to evade immunity. *Nature* **563**, 705-709 (2018).
28. V. Winstel, P. Kuhner, F. Salomon, J. Larsen, R. Skov, W. Hoffmann, A. Peschel, C. Weidenmaier, Wall Teichoic Acid Glycosylation Governs Staphylococcus aureus Nasal Colonization. *mBio* **6**, e00632 (2015).

29. M. Otto, Coagulase-negative staphylococci as reservoirs of genes facilitating MRSA infection: Staphylococcal commensal species such as Staphylococcus epidermidis are being recognized as important sources of genes promoting MRSA colonization and virulence. *Bioessays* **35**, 4-11 (2013).
30. G. Meric, M. Miragaia, M. de Been, K. Yahara, B. Pascoe, L. Mageiros, J. Mikhail, L. G. Harris, T. S. Wilkinson, J. Rolo, S. Lamble, J. E. Bray, K. A. Jolley, W. P. Hanage, R. Bowden, M. C. Maiden, D. Mack, H. de Lencastre, E. J. Feil, J. Corander, S. K. Sheppard, Ecological Overlap and Horizontal Gene Transfer in Staphylococcus aureus and Staphylococcus epidermidis. *Genome Biol Evol* **7**, 1313-1328 (2015).
31. C. Koc, D. Gerlach, S. Beck, A. Peschel, G. Xia, T. Stehle, Structural and enzymatic analysis of TarM glycosyltransferase from Staphylococcus aureus reveals an oligomeric protein specific for the glycosylation of wall teichoic acid. *J Biol Chem* **290**, 9874-9885 (2015).
32. S. Sobhanifar, L. J. Worrall, R. J. Gruninger, G. A. Wasney, M. Blaukopf, L. Baumann, E. Lameignere, M. Solomonson, E. D. Brown, S. G. Withers, N. C. Strynadka, Structure and mechanism of Staphylococcus aureus TarM, the wall teichoic acid alpha-glycosyltransferase. *Proc Natl Acad Sci U S A* **112**, E576-585 (2015).
33. X. Li, D. Gerlach, X. Du, J. Larsen, M. Stegger, P. Kuhner, A. Peschel, G. Xia, V. Winstel, An accessory wall teichoic acid glycosyltransferase protects Staphylococcus aureus from the lytic activity of Podoviridae. *Sci Rep* **5**, 17219 (2015).
34. K. Kurokawa, D. J. Jung, J. H. An, K. Fuchs, Y. J. Jeon, N. H. Kim, X. Li, K. Tateishi, J. A. Park, G. Xia, M. Matsushita, K. Takahashi, H. J. Park, A. Peschel, B. L. Lee, Glycoepitopes of staphylococcal wall teichoic acid govern complement-mediated opsonophagocytosis via human serum antibody and mannose-binding lectin. *J Biol Chem* **288**, 30956-30968 (2013).
35. T. C. Meyer, S. Michalik, S. Holtfreter, S. Weiss, N. Friedrich, H. Volzke, T. Kocher, C. Kohler, F. Schmidt, B. M. Broker, U. Volker, A Comprehensive View on the Human Antibody Repertoire Against Staphylococcus aureus Antigens in the General Population. *Front Immunol* **12**, 651619 (2021).

36. H. K. Kim, V. Thammavongsa, O. Schneewind, D. Missiakas, Recurrent infections and immune evasion strategies of Staphylococcus aureus. *Curr Opin Microbiol* **15**, 92-99 (2012).
37. R. van Dalen, M. M. Molendijk, S. Ali, K. P. M. van Kessel, P. Aerts, J. A. G. van Strijp, C. J. C. de Haas, J. Codee, N. M. van Sorge, Do not discard Staphylococcus aureus WTA as a vaccine antigen. *Nature* **572**, E1-E2 (2019).
38. D. Gerlach, R. N. Sieber, J. Larsen, J. Krusche, C. De Castro, J. Baumann, A. Molinaro, A. Peschel, Horizontal transfer and phylogenetic distribution of the immune evasion factor tarP. *Front Microbiol* **13**, 951333 (2022).
39. L. Fisarova, T. Botka, X. Du, I. Maslanova, P. Bardy, R. Pantucek, M. Benesik, P. Roudnicky, V. Winstel, J. Larsen, R. Rosenstein, A. Peschel, J. Doskar, Staphylococcus epidermidis Phages Transduce Antimicrobial Resistance Plasmids and Mobilize Chromosomal Islands. *mSphere* **6**, (2021).
40. V. Winstel, C. Liang, P. Sanchez-Carballo, M. Steglich, M. Munar, B. M. Broker, J. R. Penades, U. Nubel, O. Holst, T. Dandekar, A. Peschel, G. Xia, Wall teichoic acid structure governs horizontal gene transfer between major bacterial pathogens. *Nat Commun* **4**, 2345 (2013).
41. J. L. Morgan, J. Strumillo, J. Zimmer, Crystallographic snapshot of cellulose synthesis and membrane translocation. *Nature* **493**, 181-186 (2013).
42. L. L. Lairson, B. Henrissat, G. J. Davies, S. G. Withers, Glycosyltransferases: structures, functions, and mechanisms. *Annu Rev Biochem* **77**, 521-555 (2008).
43. C. Breton, S. Fournel-Gigleux, M. M. Palcic, Recent structures, evolution and mechanisms of glycosyltransferases. *Curr Opin Struct Biol* **22**, 540-549 (2012).
44. S. Sobhanifar, L. J. Worrall, D. T. King, G. A. Wasney, L. Baumann, R. T. Gale, M. Nosella, E. D. Brown, S. G. Withers, N. C. Strynadka, Structure and Mechanism of Staphylococcus aureus TarS, the Wall Teichoic Acid beta-glycosyltransferase Involved in Methicillin Resistance. *PLoS Pathog* **12**, e1006067 (2016).
45. L. Yakovlieva, M. T. C. Walvoort, Processivity in Bacterial Glycosyltransferases. *ACS Chem Biol* **15**, 3-16 (2020).

46. E. Vinogradov, I. Sadovskaya, J. Li, S. Jabbouri, Structural elucidation of the extracellular and cell-wall teichoic acids of Staphylococcus aureus MN8m, a biofilm forming strain. *Carbohydr Res* **341**, 738-743 (2006).
47. S. I. Morse, Studies on the chemistry and immunochemistry of cell walls of Staphylococcus aureus. *J Exp Med* **116**, 229-245 (1962).
48. S. G. Nathenson, N. Ishimoto, J. S. Anderson, J. L. Strominger, Enzymatic synthesis and immunochemistry of alpha- and beta-N-acetylglucosaminylribitol linkages in teichoic acids from several strains of Staphylococcus aureus. *J Biol Chem* **241**, 651-658 (1966).
49. P. A. Driguez, U. wei, L. Peschel, D. Buch, t. wang, Q. li, B. Stehle. (2017), vol. WO/2017/064190, chap. WO/2017/064190.
50. S. Kilcher, M. J. Loessner, Engineering Bacteriophages as Versatile Biologics. *Trends Microbiol* **27**, 355-367 (2019).
51. V. Winstel, P. Kuhner, H. Rohde, A. Peschel, Genetic engineering of untransformable coagulase-negative staphylococcal pathogens. *Nat Protoc* **11**, 949-959 (2016).
52. S. M. Lehar, T. Pillow, M. Xu, L. Staben, K. K. Kajihara, R. Vandlen, L. DePalatis, H. Raab, W. L. Hazenbos, J. H. Morisaki, J. Kim, S. Park, M. Darwish, B. C. Lee, H. Hernandez, K. M. Loyet, P. Lupardus, R. Fong, D. Yan, C. Chalouni, E. Luis, Y. Khalfin, E. Plise, J. Cheong, J. P. Lyssikatos, M. Strandh, K. Koefoed, P. S. Andersen, J. A. Flygare, M. Wah Tan, E. J. Brown, S. Mariathasan, Novel antibody-antibiotic conjugate eliminates intracellular S. aureus. *Nature* **527**, 323-328 (2015).
53. A. Hendriks, R. van Dalen, S. Ali, D. Gerlach, G. A. van der Marel, F. F. Fuchsberger, P. C. Aerts, C. J. C. de Haas, A. Peschel, C. Rademacher, J. A. G. van Strijp, J. D. C. Codee, N. M. van Sorge, Impact of Glycan Linkage to Staphylococcus aureus Wall Teichoic Acid on Langerin Recognition and Langerhans Cell Activation. *ACS Infect Dis* **7**, 624-635 (2021).
54. C. Weidenmaier, J. F. Kokai-Kun, S. A. Kristian, T. Chanturiya, H. Kalbacher, M. Gross, G. Nicholson, B. Neumeister, J. J. Mond, A. Peschel, Role of teichoic acids in Staphylococcus aureus nasal colonization, a major risk factor in nosocomial infections. *Nat Med* **10**, 243-245 (2004).

55. S. Ali, A. Hendriks, R. van Dalen, T. Bruyning, N. Meeuwenoord, H. S. Overkleeft, D. V. Filippov, G. A. van der Marel, N. M. van Sorge, J. D. C. Codee, (Automated) Synthesis of Well-defined Staphylococcus Aureus Wall Teichoic Acid Fragments. *Chemistry* **27**, 10461-10469 (2021).
56. W. Kabsch, Integration, scaling, space-group assignment and post-refinement. *Acta Crystallogr D Biol Crystallogr* **66**, 133-144 (2010).
57. A. J. McCoy, R. W. Grosse-Kunstleve, P. D. Adams, M. D. Winn, L. C. Storoni, R. J. Read, Phaser crystallographic software. *J Appl Crystallogr* **40**, 658-674 (2007).
58. N. Stein, CHAINSAW: a program for mutating pdb files used as templates in molecular replacement. *J. Appl. Cryst.* **41**, 641-643 (2008).
59. P. Emsley, B. Lohkamp, W. G. Scott, K. Cowtan, Features and development of Coot. *Acta Crystallogr D Biol Crystallogr* **66**, 486-501 (2010).
60. G. N. Murshudov, P. Skubak, A. A. Lebedev, N. S. Pannu, R. A. Steiner, R. A. Nicholls, M. D. Winn, F. Long, A. A. Vagin, REFMAC5 for the refinement of macromolecular crystal structures. *Acta Crystallogr D Biol Crystallogr* **67**, 355-367 (2011).
61. O. S. Smart, T. O. Womack, C. Flensburg, P. Keller, W. Paciorek, A. Sharff, C. Vonrhein, G. Bricogne, Exploiting structure similarity in refinement: automated NCS and target-structure restraints in BUSTER. *Acta Crystallogr D Biol Crystallogr* **68**, 368-380 (2012).
62. P. D. Adams, P. V. Afonine, G. Bunkoczi, V. B. Chen, I. W. Davis, N. Echols, J. J. Headd, L. W. Hung, G. J. Kapral, R. W. Grosse-Kunstleve, A. J. McCoy, N. W. Moriarty, R. Oeffner, R. J. Read, D. C. Richardson, J. S. Richardson, T. C. Terwilliger, P. H. Zwart, PHENIX: a comprehensive Python-based system for macromolecular structure solution. *Acta Crystallogr D Biol Crystallogr* **66**, 213-221 (2010).
63. A. W. Schuttelkopf, D. M. van Aalten, PRODRG: a tool for high-throughput crystallography of protein-ligand complexes. *Acta Crystallogr D Biol Crystallogr* **60**, 1355-1363 (2004).
64. V. B. Chen, W. B. Arendall, 3rd, J. J. Headd, D. A. Keedy, R. M. Immormino, G. J. Kapral, L. W. Murray, J. S. Richardson, D. C. Richardson, MolProbity: all-

atom structure validation for macromolecular crystallography. *Acta Crystallogr D Biol Crystallogr* **66**, 12-21 (2010).

65. L. L. C. Schrodinger, The PyMOL Molecular Graphics System. Version 1.8 (2015).

Acknowledgments

Funding:

German Research Foundation TRR34 (TS, AP)
German Research Foundation TRR165 project ID 246807620 (AP)
German Research Foundation PE 805/7-1 project ID 410190180 (AP)
German Research Foundation PE 805/8-1 project ID 410190180 (AP)
German Center of Infection Research (AP)
Cluster of Excellence EXC 2124,
'Controlling Microbes to Fight Infections' project ID 390838134 (AP)

Author contributions:

Designed the study: YG, XD, AP, TS
Purified and crystallized proteins: YG
Solved the structures and performed in vitro analysis of TarM(Se): YG
Identified the tarM(Se) gene, constructed mutants and complements: XD, VW
Characterized mutant phenotypes and conducted phage assay: XD
Purified WTAs: XD
Studied IgG depostition: JK, CB
Analyzed WTA composition: AW, CM
Designed and synthesized 4RboP-$(CH_2)_6NH_2$: SA, JC
Analyzed the results: YG, XD, AP, TS
Wrote the manuscript: YG, XD, AP, TS

Competing interests:

Authors declare that they have no competing interests.

Data and materials availability:

The coordinates and structure factors were deposited in the RCSB Protein Data Bank under accession codes: 7QNT, 7QD7, 7QH9, 8P1X, and 8P20. Previously published structures that were used in this work for molecular replacement or structural comparisons were retrieved from the RCSB Protein Data Bank entries: 4WAC, 4X7M, 6H4M, and 4X7R. All data are available in the main text or the supplementary materials.

Supplementary Materials for

Invasive *Staphylococcus epidermidis* use a unique processive wall teichoic acid glycosyltransferase to evade immune recognition

Yinglan Guo *et al.*

*Corresponding author: Thilo Stehle (thilo.stehle@uni-tuebingen.de)
Andreas Peschel (andreas.peschel@uni-tuebingen.de)

This PDF file includes:

Tables S1 to S4
Figs. S1 to S3
Supplementary Information 1 and 2

Table S1. Substrate specificity of TarM(Se).

A, Donor substrate specificity of TarM(Se) using poly(RboP) WTA as acceptor substrate.

Sugar nucleotide	Enzymatic activity (nmol/mg*min)	Activity of UDP-glucose in %
UDP-glucose	1.85	100
UDP-galactose	0.98	53
UDP-GalNAc	0.53	29
UDP-GlcNAc	0.3	16

B, Donor substrate specificity of TarM(Se) using poly(GroP) WTA as acceptor substrate.

Sugar nucleotide	Enzymatic activity (nmol/mg*min)	Activity of UDP-glucose and poly(RboP) WTA in %
UDP-glucose	0.55	30
UDP-galactose	0.46	25
UDP-GalNAc	0.05	3
UDP-GlcNAc	0.04	2

Table S2. Data collection and refinement statistics for TarM(Se) and TarM(Se)$_{G117R}$-4RboP-(CH$_2$)$_6$NH$_2$

	TarM(Se) native* (PDB 7QNT)	TarM(Se)$_{G117R}$-4RboP-(CH$_2$)$_6$NH$_2$* (PDB 7QH9)
Data collection		
Space group	$P6_3$	P1
Cell dimensions		
a, *b*, *c* (Å)	154.01, 154.01, 207.72	58.87, 70.57, 137.38
α, β, γ (°)	90.00, 90.00, 120.00	89.97, 90.01, 90.02
Resolution (Å)	48.99-3.21 (3.29-3.21)	49.23-2.69 (2.76-2.69)
R_{merge}	20.9 (229.8)	6.1 (142.7)
I / $\sigma(I)$	15.57 (1.64)	9.98 (0.70)
Completeness (%)	100.0 (100.0)	95.2 (97.4)
Redundancy	20.6 (20.7)	2.5 (2.5)
Refinement		
Resolution (Å)	48.99-3.21	49.21-2.69
No. reflections	45535	58472
R_{work} / R_{free}	22.77/25.72	24.26/25.28
No. atoms		
Protein	13389	14001
Ligand		124
Ions	16	3
other molecules	12	4
Water	264	240
B-factors		
Protein	93.7	97.9
Ligand		99.7
Ions	77.4	38.4
other molecules	91.2	29.4
Water	52.8	42.5
R.m.s. deviations		
Bond lengths (Å)	0.002	0.004
Bond angles (°)	1.020	1.296

Values in parentheses are for the highest-resolution shell. *Diffraction data from a single crystal were used to obtain the structure.

Table S3. Enzymatic activities of mutated TarM(Se) proteins

Function	TarM(Se) variant	Activity of wild type in %
Trimer interface	G117R	96.0
Catalysis	R326A	Not active[31,32]
	Q330A	5.7
	K331A	Not active[31,32]
	E403A	Not active[31,32]
Poly(RboP) binding	N9A	51.0
	E10A	30.9
	N203A	64.7
	K233A	21.7
	N255A	100.1
	K263A	17.2
	Q265A	67.6

Table S4. Primers used in this study

Primer name	primer sequence
***tarM(Se)* knockout**	
tarM(Se) pBASE 1up	CGATGGTACCGCTTTATTTAAAAGAAATATATCTGATAGAAG
tarM(Se) pBASE 1dn	TAATATTACCTCATTATTTATTTCTTAAATGC
tarM(Se) pBASE 2up	TAAATAATGAGGTAATATTAGTATCCATTTTTCTATTATTCAGTTTCTATGTAC
tarM(Se) pBASE 2dn	GTCAGTCGACCTATTTGACTATTATCAACTTTCTTCGCTTTATG
***tarM(Se)* expression in pRB474**	
	GTCGGATCCAAAGGAGGTTATATA
*tarM(Se)*_F	ATGAAACAAACTTATATGATTGTAAATGAGTTGG
*tarM(Se)*_R	CCGATGAATTCTTAGTTAAACAATTGTTTCCATTTCACCATC

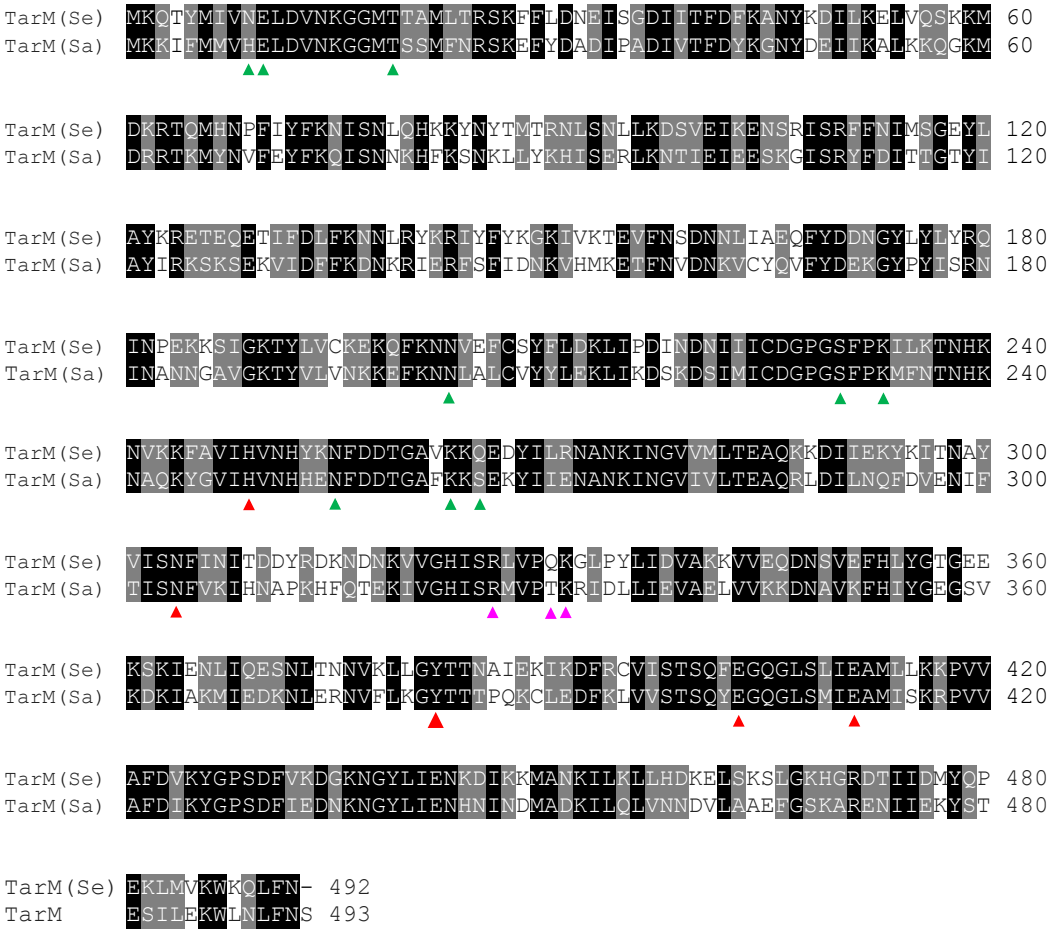

Fig. S1. Sequence alignment of TarM(Se) from *S. epidermidis* and TarM(Sa) from *S. aureus*. The alignment was calculated with pairwise sequence alignment tool GGSEARCH2SEQ[66]. Identical amino acids are shown in black boxes and similar amino acids are shaded in gray. The amino acids that are involved in binding of UDP-glucose (red), 4RboP-glucose (green) and catalysis (magenta) are indicated as filled triangle.

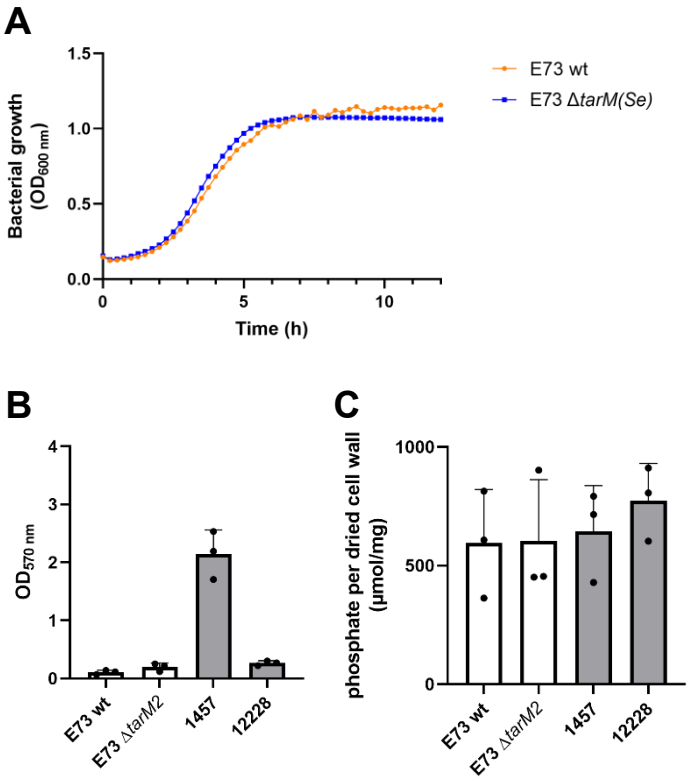

Fig. S2. TarM(Se) expression does not change the overall WTA amounts and does not affect *S. epidermidis* biofilm formation or growth behavior. (A), Growth curves of *S. epidermidis* E73 with or without *tarM(Se)* in TSB. Means of three independent experiments are shown. **(B)**, The characteristic of negative biofilm formation in E73 is not altered by deletion of *tarM(Se)*. The laboratory *S. epidermidis* strains ATCC12228 (biofilm negative) and 1457 (biofilm positive) were included as control strains. **(C)**, Total WTA phosphate amount per cell wall dry weight of the indicated *S. epidermidis* strains. None of the minor differences is significant. Means ± s.d. of three independent experiments are shown in **(B)** and **(C)**.

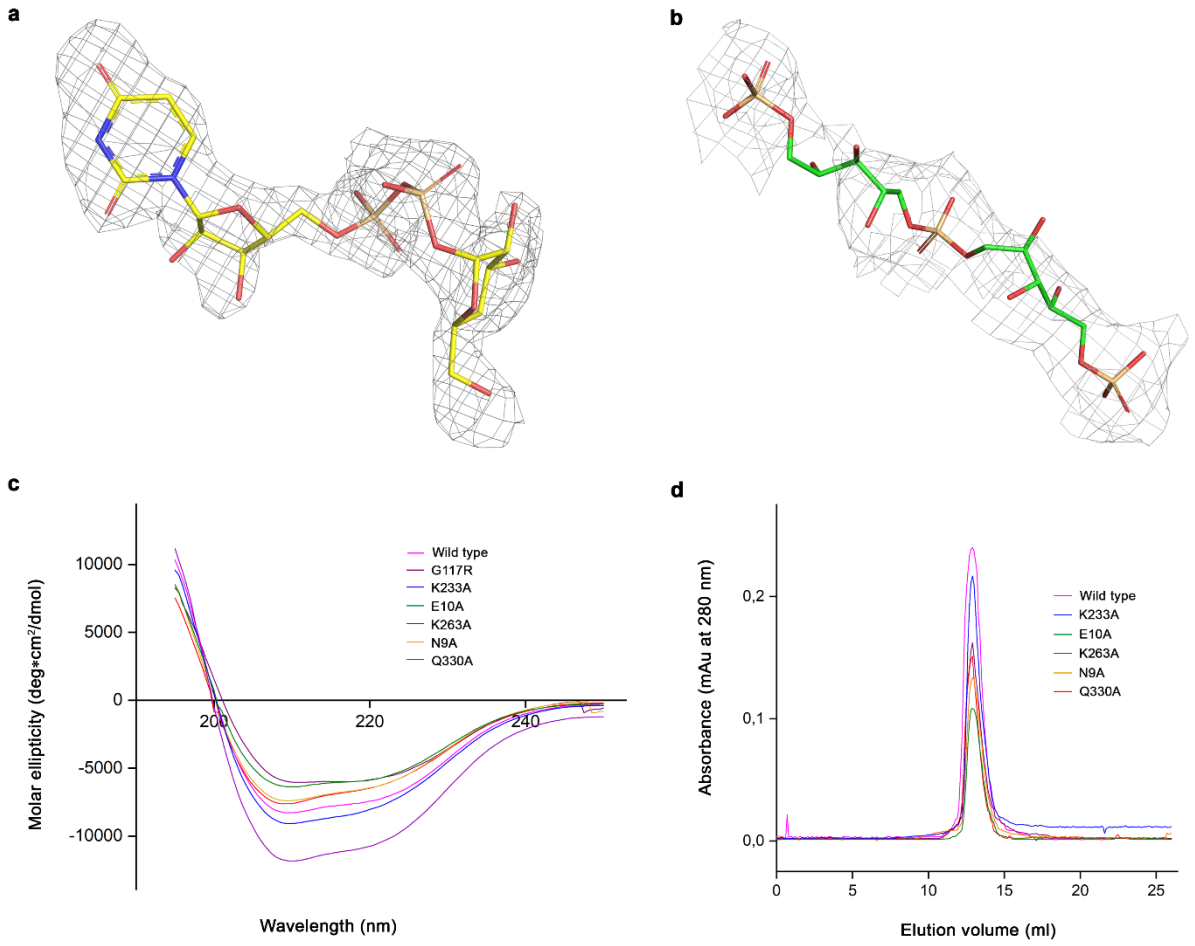

Fig. S3. Simulated-annealing (mFo − DFc) omit maps of UDP-glucose and 4RboP-$(CH_2)_6NH_2$ in the binary structures and characterization of TarM(Se) wild type and mutant proteins. **(A)**, Simulated-annealing (mFo − DFc) omit map of UDP-glucose (yellow) in TarM(Se)$_{G117R}$-UDP-glucose complex structure (grey mesh, at 2.0 σ). **(B)**, Simulated-annealing (mFo − DFc) omit map of 4RboP-$(CH_2)_6NH_2$ (green) in TarM(Se)$_{G117R}$-4RboP-$(CH_2)_6NH_2$ complex structure (grey mesh, at 1.5 σ). **(C)**, Circular dichroism spectra of wild type and mutant TarM(Se) proteins (for wild type, G117R, Q330A and K263A, n = 3; for N9A, E10A, and K233A, n = 2). **(D)**, Size exclusion chromatography elution profiles of wild-type and mutant TarM(Se) proteins (for wild type n = 6; for Q330A, K263A and E10A, n = 3; for N9A and K233A, n = 2). Mutant proteins N203A, N255A and Q265A showed similar circular dichroism spectra and size exclusion chromatography elution profiles (data not shown).

Supplementary Information 1

Synthesis of 4RboP-$(CH_2)_6NH_2$. The RboP tetramer was synthesized according to Fig. 1. as described previously[55].

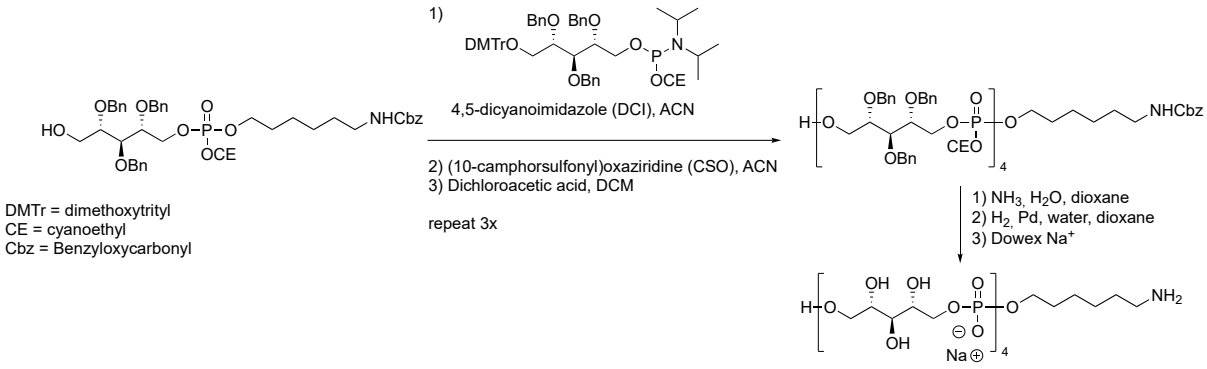

Supplementary Information 2

Analytical data of Fig. 1. Synthesis of 4RboP-$(CH_2)_6NH_2$:

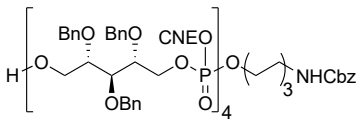

IR (neat, cm^{-1}): 3447, 2938, 2866, 1717, 1506, 1456, 1267, 1028, 1009, 746, 698; ^{1}H NMR (400 MHz, CD_3CN) δ = 1.27 (m, 4H, CH_2-hexyl spacer), 1.40 - 1.41 (m, 2H, CH_2-hexyl spacer), 1.58 - 1.59 (m, 2H, CH_2-hexyl spacer), 2.52 - 2.59 (m, 8H, 4x CH_2-cyanoethyl), 3.06 (q, 2H, J= 6.4 Hz, CH_2-N hexyl spacer), 3.67 - 3.79 (m, 3H, CH-Rbo, CH_2-Rbo), 3.84 - 4.13 (m, 22H, 12x CH-Rbo, CH_2-O hexyl spacer, 4x CH_2 cyanoethyl), 4.17 - 4.40 (m, 14H, 7x CH_2-Rbo), 4.50 - 4.69 (m, 24H, 12x CH_2-Bn), 5.05 (s, 2H, CH_2-Cbz), 5.72 (bs, 1H, N-H), 7.25 - 7.35 (m, 65H, H-arom); ^{13}C-APT NMR (101 MHz, CD_3CN) δ = 20.1, 20.2, 20.2 (CH_2 cyanoethyl), 25.7, 26.8, 30.4, 30.7, 30.8 (CH_2 hexyl spacer), 41.4 (CH_2-N hexyl spacer), 61.5 (CH_2-Rbo), 63.1, 63.1, 63.2 (CH_2 cyanoethyl), 66.6 (CH_2-Cbz), 67.5, 67.7, 67.8, 68.3 (CH_2-Rbo), 68.9, 69.0 (CH_2-O hexyl spacer), 72.7, 73.0, 73.1, 73.1, 74.5, 74.5, 74.6 (CH_2-Bn), 78.3, 78.6, 78.9, 78.9, 79.0, 79.1, 80.6 (CH-Rbo), 118.3 - 118.6 (C_q-cyanoethyl), 128.4, 128.6, 128.6, 128.7, 128.8, 128.9, 128.9, 129.3, 129.3, 129.4 (CH-arom), 139.1, 139.2, 139.3, 139.5, 139.7 (C_q-arom), 158.0 (C=O); ^{31}P NMR (162 MHz, CD_3CN) δ = 0.2, 0.2, 0.2, -0.0, -0.1, -0.1, -0.2, -0.2; HRMS: $[M+H]^+$ calculated for $C_{101}H_{119}N_4O_{24}P_3$ 2401.9343, found 2401.9241.

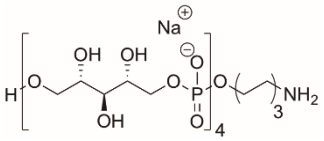

^{1}H NMR (600 MHz, D_2O) δ = 1.39 - 1.40 (m, 4H, 2x CH_2 hexyl spacer), 1.55 - 1.68 (m, 4H, 2x CH_2-hexyl spacer), 2.97 (t, 2H, J= 7.2 Hz, CH_2-N hexyl spacer), 3.62 (dd, 1H, J= 12.0 Hz, J= 7.2 Hz, CH_2-ribitol), 3.72 (t, 1H, J= 6.6 Hz, CH-ribitol), 3.76 - 3.82 (m, 4H, CH/CH_2-ribitol), 3.82 - 3.84 (m, 1H, CH/CH_2-ribitol), 3.85 - 3.96 (m, 16H, 14 CH/CH_2-ribitol, CH_2-O hexyl spacer), 3.97 - 4.06 (m, 7H, CH/CH_2-ribitol); ^{13}C-APT NMR (151 MHz, D_2O) δ = 25.4, 26.0, 27.5 (3x CH_2-hexyl spacer), 30.3 (d, J= 7.6 Hz, CH_2-hexyl spacer), 40.3 (CH_2-N hexyl spacer), 63.2 (CH_2-ribitol), 67.0 - 67.4 (7x CH_2-ribitol/CH_2-O hexyl spacer), 71.7 - 73.0 (10x CH-ribitol); ^{31}P NMR (162 MHz, D_2O) δ = 1.8, 1.6; HRMS: $[M+H]^+$ calculated for $C_{26}H_{60}NO_{29}P_4$ 974.2201, found 974.2202.

Chapter 4

From a Hsp90 - binding protein to a peptide drug

Aparna Viswanathan Ammanath[1], Anders Jarneborn[2], Minh-Thu Nguyen[3], Laura Wessling[4], Paula Tribelli[5], Mulugeta Nega[1], Christian Beck[6], Arif Luqman[7], Khaled A Selim[8,11], Hubert Kalbacher[9], Boris Macek[10], Sandra Beer Hammer[4], Tao Jin[2], Friedrich Götz[1,11*]

[1] Microbial Genetics, Interfaculty Institute of Microbiology and Infection Medicine Tübingen (IMIT), University of Tübingen, Tübingen, Germany

[2] Department of Rheumatology and Inflammation Research, Institute of Medicine, Sahlgrenska Academy, University of Gothenburg, Gothenburg, Sweden

[3] Section of Medical and Geographical Infectiology, Institute of Medical Microbiology, University Hospital of Münster, Münster, Germany

[4] Department of Pharmacology, Experimental Therapy and Toxicology, Institute of Experimental and Clinical Pharmacology and Pharmacogenomik and ICePhA, University of Tuebingen, Tuebingen, Germany

[5] Departamento de Química Biológica, FCEyN-UBA, Buenos Aires, Argentina

[6] Infection Biology, Interfaculty Institute for Microbiology and Infection Medicine Tübingen, University of Tübingen, Tübingen, Germany

[7] Biology Department, Institut Teknologi Sepuluh Nopember, Surabaya 60111, Indonesia

[8] Organismic Interactions Department, Interfaculty Institute for Microbiology and Infection Medicine, University of Tübingen, Tübingen, Germany.

[9] Interfacultary Institute for Biochemistry, Tübingen, Germany

[10] Proteome Center Tübingen, University of Tübingen, Germany

[11]Excellence Cluster 2124 'Controlling Microbes to Fight Infections' (CMFI), University of Tübingen, Germany

Running title: Anti-infective peptides protects from bacteremia

Key words: Hsp90-interaction, infection, Lpl-derived peptides, larvae/mouse Infection model, *Staphylococcus aureus*

*** Corresponding author:**

Prof. Dr. Friedrich Götz

Microbial Genetics

Interfaculty Institute of Microbiology and Infection Medicine (IMIT)

University of Tübingen, Germany

E-mail: friedrich.goetz@uni-tuebingen.de

Published: Ammanath, A. V., Jarneborn, A., Nguyen, M. T., Wessling, L., Tribelli, P., Nega, M., Beck, C., Luqman, A., Selim, K. A., Kalbacher, H., Macek, B., Hammer, S. B., Jin, T., and Götz, F. (2023) From an Hsp90 - binding protein to a peptide drug. *Microlife* **4**, uqac023

Abstract (241 words)

The Lpl proteins represent a class of lipoproteins that was first described in the opportunistic bacterial pathogen *Staphylococcus aureus*, where they contribute to pathogenicity by enhancing F-actin levels of host epithelial cells and thereby increasing *S. aureus* internalization. The model Lpl protein, Lpl1 was shown to interact with the human heat shock proteins Hsp90α and Hsp90ß, suggesting that this interaction may trigger all observed activities. Here we synthesized Lpl1-derived peptides of different lengths and identified two overlapping peptides, namely L13 and L15, which interacted with Hsp90α. Unlike Lpl1, the two peptides not only decreased F-actin levels and *S. aureus* internalization in epithelial cells but they also decreased phagocytosis by human $CD14^+$ monocytes. The well-known Hsp90 inhibitor, geldanamycin, showed a similar effect. The peptides not only interacted directly with Hsp90α, but also with the mother protein Lpl1. While L15 and L13 significantly decreased lethality of *S. aureus* bacteremia in an insect model, geldanamycin did not. In a mouse bacteremia model L15 was found to significantly decreased weight loss and lethality. Although the molecular bases of the L15 effect is still elusive, *in vitro* data indicate that simultaneous treatment of host immune cells with L15 or L13 and *S. aureus* significantly increase IL-6 production. L15 and L13 represent not antibiotics but they cause a significant reduction in virulence of multidrug-resistant *S. aureus* strains in *in vivo* models. In this capacity, they can be an important drug alone or additive with other agents.

Introduction

The opportunistic human pathogen *Staphylococcus aureus* can cause severe community acquired and nosocomial infections. Different proteins on the bacterial surface support its adherence to and/or internalization into host cells by either directly binding to a defined host cell receptor or by interacting with a matrix protein such as fibronectin which in turn binds to the α5β1 integrin on the host cell surface (1, 2).

Among the cell envelope-bound proteins, the bacterial lipoproteins (Lpp) represent a distinct class of proteins. They are anchored to the outer leaflet of the cytoplasmic membrane by an N-terminal lipid moiety (3); in Gram-negative bacteria they can in addition be anchored to the inner leaflet of the outer membrane (4). Many lipoproteins are part of an ABC transport system that takes up nutrients or have an essential role in respiration or protein folding (5).

S. aureus and few other species have so-called Lpl lipoproteins which are typically encoded in a cluster of paralogous genes on the pathogenicity island vSaα. Depending on the strain, 3 to 9 *lpl* genes may be encoded in this island (6, 7). As classical lipoproteins Lpl proteins have a typical lipo-box signal peptide and contribute to activation of the innate immune system *via* the toll like receptor 2 (TLR2) pathway. However, the function of their protein moiety has been long unknown. Only in the last few years it emerged that the *lpl* gene cluster is involved in the interaction of *S. aureus* with host cells and in the virulence of *S. aureus*.

When the entire *lpl* gene cluster was deleted, both, adherence to host cells and internalization of *S. aureus* by epithelial cells and keratinocytes were impaired (8, 9). Additionally, in a murine kidney abscess model, mice challenged with the *S. aureus lpl* mutant displayed a reduced bacterial burden in the kidneys, indicating that the *lpl* cluster contributes to virulence. Further interaction studies using purified Lpl1, that is, the first encoded Lpl protein in the cluster, revealed that Lpl1 acts as a cyclomodulin by delaying G2/M phase transition in HeLa cells (10). However, unlike other staphylococcal cyclomodulins, such as phenol-soluble modulins (PSM) (11), Lpl1 shows no cytotoxicity even at high concentrations. Since internalization and propagation of *S. aureus* within the host cells takes place in the G2 phase (12), an extension of the latter by the Lpl proteins could explain their contribution to host cell invasion on the molecular level (9).

A breakthrough in understanding the function of this subclass of lipoproteins was achieved when pull-down experiments revealed that the Lpl1 binds preferentially to the isoforms of the human heat shock proteins Hsp90α and Hsp90ß (13). Antibodies against Hsp90 decreased *S. aureus* invasion in primary human keratinocytes as well as in immortalized ones (HaCaT cells). Additionally, inhibition of the ATPase function of Hsp90 or silencing of Hsp90α expression by siRNA also decreased *S. aureus* invasion in HaCaT cells. While Hsp90ß is constitutively expressed, the Hsp90α isoform is heat inducible and appears to play a major role in the interaction with Lpl1. Pre-incubation of HaCaT cells at 39°C increased both Hsp90α expression and *S. aureus* invasion. Lpl1-Hsp90 interaction induces F-actin formation thus triggering an

endocytosis-like internalization (13). Such a mechanism based on Lpl-Hsp90 interaction represents a new strategy of host cell invasion.
Geldanamycin for example inhibits the essential ATPase activity of Hsp90, resulting in the inactivation, destabilization and degradation of Hsp90 client proteins. Since these processes play an important role in the regulation of cell cycle, cell growth, cell survival, apoptosis and oncogenesis, geldanamycin inhibits the proliferation of cancer cells and shows anti-cancer activity in animal studies (14). Nonetheless, its pharmaceutical application is limited by its high cytotoxicity (14, 15).

The aim of this study was to identify domain sequences of the Lpl1 protein that interact with Hsp90α. For this purpose, we synthesized peptides covering the entire Lpl1 protein. We identified two peptides, L13 and L15, which interacted with Hsp90α and Lpl1, inhibited the internalization of *S. aureus* by host cells, and provided partial protection against *S. aureus* infection in insect and mouse infection models.

Materials and Methods

Bacterial strains and cell lines. N/TERT-1 cells were a kind gift from Dr. J. Rheinwald, Harvard Medical School, Boston, USA (16). N/TERT-1 cells were cultured in 24 well plates with keratinocyte serum-free medium (K-SFM) (Gibco, Invitrogen Corp.), supplemented with bovine pituitary extract (BPE) (25 µg per ml), EGF (0.2 ng per ml), and $CaCl_2$ (0.4 mM). HaCaT cells were maintained in Dulbecco's Modified Eagle Medium (DMEM) (Thermo Fisher, Waltham, MA, USA) supplemented with 10% fetal bovine serum (FBS) (BiochromAG, Berlin, Germany) and 1% penicillin-streptomycin (Thermo Fisher, Waltham, MA, USA). MONO-MAC-6 (MM6) cell lines were maintained in Gibco Roswell Park Memorial Institute 1640 Medium (RPMI 1640) (Thermo Fisher, Waltham, MA, USA) supplemented with 10% FBS, 2 mM L-glutamine, non-essential amino acids, 1 mM sodium pyruvate and 10 µg/ml human insulin. *S. aureus* Newman and USA300 were cultured aerobically in Tryptic Soy Broth (TSB) at 37 °C. The bacterial strains were stored at -70°C. Upon aerobic culture, bacterial cells were washed with sterile phosphate-buffered saline (PBS), and adjusted to the desired concentration.

Peptide synthesis. The amino acid sequences of peptides used in this study are given in Table S1. The peptides were synthesised by Apeptide (Shanghai, China) with a purity of >95%, dissolved in water at 1 mg/ml and stored at −20°C. 20 µM of L15, 30 µM of L13 and 5 µM of geldanamycin were used in *in vitro* studies unless described otherwise.

Invasion studies in HaCaT and N/TERT-1 cells. The invasion protocol was adapted from our previous papers (13, 17). $5x10^5$ Keratinocytes were seeded in a 24 well plate (Greiner, Frickenhausen, Germany) to attain a monolayer of ~10^6 cells/well. *S. aureus* was grown overnight at 37°C, centrifuged and suspended in invasion medium (DMEM with 10% FBS for HaCaT and K-SFM for NTERT-1 cells). The adherent keratinocytes were washed with PBS and supplemented with invasion medium followed by treatment with 20 µM of L15, 30 µM of L13 or 5 µM geldanamycin (Sigma-Aldrich, Germany) or monoclonal antibodies specific against Hsp90α (α-Hsp90α, Abcam) for 1 h. After 1h, 100 µl of bacterial suspension was added to each well to attain a MOI (multiplicity of infection) of 30 and incubated with cells for 1.5 h. Subsequently, the extracellular bacteria were killed with treatment of 2.5 µg/ml lysostaphin (Sigma-Aldrich, Germany)) for 1.5 h. The cells were then washed, lysed, mechanically detached by scraping, diluted and enumerated on TSA (Tryptic Soy Agar) plates to quantify the intracellular bacteria.

$CD14^+$ monocyte isolation. Peripheral Blood Mononuclear cells (PBMCs) were isolated by density gradient centrifugation following the previous study (18). From the pool of PBMCs, monocytes were isolated by positive selection with anti-human CD14 microbeads (Miltenyi Biotech, Bergisch-Gladbach, Germany) following a previously reported protocol (18). The purity was analysed by flow cytometry on a BD Accuri C6 (BD Biosciences, Heidelberg, Germany) with anti-human CD14-FITC, CD45-PE and propidium iodide (BD Biosciences, Heidelberg, Germany) and ranged from 85% to 98%.

Phagocytosis assay. For the phagocytosis, 10^6 $CD14^+$ monocytes were seeded in 1 ml of medium (RPMI supplemented with L-Glutamine and 10% FCS) in a 12 well plate (Greiner, Germany). The cells were incubated with 20 µM of L15, 30 µM of L13 or 5 µM of Geldanamycin for 60 min at 37 °C and 5% CO2 before addition of

bacteria. For the phagocytosis assay, bacterial cells were resuspended in 100 µl RPMI medium at MOI of 30 and incubated with monocytes for 90 min. The cells were washed once with PBS and 0.5 ml of medium supplemented with 2.5 µg/ml of Lysostaphin was added for 90 min to remove the extracellular bacteria. Then, monocytes were washed twice with PBS and resuspended in 0.5 ml of milliQ dH2O. The cells were scraped, and the lysed solution was transferred into a new 1.5 ml Eppendorf tube for a 5 min sonication (frequency 80, power 100) at room temperature to prevent the bacterial cell clumping by using ultrasonic water bath Elmasonic P (Elma Schmidbauer Gmb, Singen, Germany). 10 µl fractions of undiluted, 10^{-1}, 10^{-2} and 10^{-3} dilutions were inoculated on tryptic soy agar (TSA) plates and incubated overnight at 37 °C. The numbers of internalized bacteria were determined based on the manual counting of bacterial colony forming units (cfu) recovered on the agar plates.

Bacterial Growth kinetics. S. aureus precultured in TSB overnight were inoculated to OD~0.01 into a 48 well plate and L15 and L13 were added to study the effect of peptides on bacterial growth using Varioskan LUX Multimode Microplate Reader. With this instrument, a kinetic measurement of OD578 nm was obtained every 1 h for a total of 24 h, at 37°C with continuous shaking.

Peptide - Hsp90α/Lpl1 interaction studies with immunoblotting. Two µg of each peptide was blotted (dot blot) directly on PDV nitrocellulose membrane and blocked with ROTI®Block (Carl Roth, Germany). After washing, the membrane was then incubated with 20 µg of recombinant Hsp90α (Abcam)/Lpl1-his protein at 4 °C overnight. In case of interaction studies with Hsp90α, α-Hsp90α (produced in mouse, Abcam) was used as the primary antibody and for interaction studies with Lpl1-his, Anti-6X His tag antibody (also produced in mouse, Sigma-Aldrich, Germany) was used. Alkaline phosphatase conjugated goat-α-mouse IgG (Sigma-Aldrich, Germany) served as the secondary antibody. Detection was done using BCIP®/NBT solution (Sigma, Germany). Lpl1-his was isolated and purified as described in our previous paper (13).

F-actin measurement. 5 x 10^4 cells were seeded in black flat bottom 96 well cell culture microplate (Greiner, Germany) and incubated overnight. The cells were then

incubated with peptides or geldanamycin for 1.5 h. After incubation, the cells were washed, permeabilised with 0.1% (v/v) Triton X-100 and stained with ActinGreen™ 488 ReadyProbes® (Thermo Fischer, Germany) for 30 min. After the staining, the cells were washed and measure for its fluorescence at Excitation/Emission: 495/518 nm (19).

Cytotoxicity studies. MTT (3-(4,5-dimethylthiazol-2-yl)-2,5-diphenyl tetrazolium bromide) assay was employed to analyze the cytotoxicity of peptides and geldanamycin to the cells. 5 x 10^5 cells were seeded in a 96 flat bottom well plate and incubated for 2.5h or 24 h at 37 °C with 5% CO_2. The cells were then treated with increasing concentration (0 to 200 µM) of peptides or geldanamycin for 24 h. After the incubation, 10 µl of the MTT labelling reagent is added to each well to attain a final concentration 0.5 mg/ml, followed by 4 h incubation. Metabolically active cells convert the yellow tetrazolium salt to purple formazan crystals, which were solubilized using the solubilization solution (DMSO) and measured for absorbance at $\lambda_{max}/\lambda_{ref}$ - 570/690 nm (20).

***Galleria mellonella* larvae studies**. *Galleria mellonella* larvae, purchased from Feeders & more GmbH, Germany, were sorted based on weight and used within one week. Ten larvae per group with weight average of 500 mg/larvae were injected with bacteria and/or peptides on its last proleg using a BD insulin syringe. The dosage used for the experiment were 60 mg/kg for peptides, 5 mg/kg of geldanamycin and 20 mg/kg for vancomycin. Each larva was injected with 10µl of L15 (last left proleg) 1h before administration of 10^6 cfu *S. aureus* (last right proleg). The larvae were maintained at 37 °C and observed for mortality every day over the course of 5 days.

Hemolysin activity. 6 mm Whatman empty Antibiotic Assay Discs were impregnated with L15 or L13 and allowed to dry. Once dried, the discs were placed on sheep blood agar plates, inoculated with *S. aureus* and incubated at 37 °C overnight. The halo obtained was measured and compared.

Mouse studies. Eight- to 10-week-old female NMRI mice were purchased from Envigo (Venray, Netherlands) and stored under standard temperature, light, and nutrition conditions in the animal facility of the Department of Rheumatology and Inflammation Research, University of Gothenburg. Due to its poor solubility in PBS,

L13 was not used in mouse experiments. To study the effect of L15 on *S. aureus* bacteremia two separate experiments were performed. The mice were treated intraperitoneally with L15 (10 mg/kg) in 200 µl of PBS every 12 hours, starting 2 hours before inoculation with bacteria and continuing until the animals were sacrificed. Mice were challenged with septic dose of 2 x 10^6 CFU/mouse of *S aureus* Newman. To induce the *S. aureus* systemic infection in NMRI mice, 0.2 ml of *S. aureus* Newman suspension was inoculated intravenously into the tail vein of the mice. During the course of the experiments, the mice were regularly weighed until the mice were sacrificed. After sacrificing the mice at day 7, kidneys from mice were aseptically removed, homogenised, serially diluted with PBS and enumerated to quantify the bacterial CFUs.

Immune stimulation. Human peripheral blood mononuclear cells (PBMCs) from buffy coat blood samples of healthy donors were stimulated with the indicated doses of L15 and L13 for 20 hours. For the subsequent bead-based immunoassay, the cell culture supernatants of a total of four buffy coats per immunoassay were used. Each of the stimulations was performed in biological duplicates. The secreted cytokines were then identified and quantified using the immunofluorescent bead-based immunoassay LEGENDplex® Human Macrophage/Microglia Panel (13-plex) and the corresponding Data Analysis Software from BioLegend. Muramyl Dipeptide (MDP) which activates the NOD-2 receptors was used as the positive control.

Bioinformatics analysis. The 3D structure of Lpl1 was predicted using the protein structure prediction server Robetta using RoseTTAFold modelling method (21). The obtained .pdb structure was then visualized in PyMOL (Schrödinger). The homologs of *S. aureus* USA300 Lpl1 in different bacteria were identified using the Protein BLAST tool on the NCBI server. The comparison of different lipoprotein homologs from different bacteria was done in Snapgene using Clustal Omega algorithm.

Statistical analysis. GraphPad Prism was employed for statistical analysis. Student's t tests or one-way analysis of variance (ANOVA) were used to check the statistical significance of different results. P value > 0.05 was considered as not significant (ns). In figures, significant differences are represented as follows: * $p < 0.05$; ** $p < 0.01$; *** $p < 0.001$; and **** $p < 0.0001$.

Ethical Statement. The use of human peripheral blood mononuclear cells (PBMCs) from buffy coats was approved by the Ethics Committee of the Medical Association of Westphalia-Lippe and the University of Münster (Approval number 2021-063-f-S) and the Ethics Committee of the Medical Faculty of the University of Tübingen and the Medical Clinic Tübingen (approval number 084/2021BO2). Buffy coats were obtained from the German Red Cross Blood transfusion west (Hagen, Germany) and the Transfusion Blood Bank of the Medical Clinic Tübingen. The Ethics Committee of Animal Research of Gothenburg approved all experiments conducted on mice. The mouse experiments were performed in accordance with the Swedish Board of Agriculture's regulations and recommendations on animal experiments.

Results

Lpl1-derived peptides L15 and L13 decrease *S. aureus* USA300 internalisation by keratinocytes in a Hsp90 mediated way. In our previous work, we demonstrated that the *lpl* cluster of *S. aureus* USA300 triggers invasion of *S. aureus* into HaCaT cells. In the USA300Δ*lpl* mutant, the rate of invasion was 2.5-fold lower compared with wild type (6). We identified two Lpl1-derived peptide sequences (L26 and L27) that boosted *S. aureus* internalization to the same extent as the whole Lpl1 protein (**blue-labeled peptide regions in Fig. 1A**).

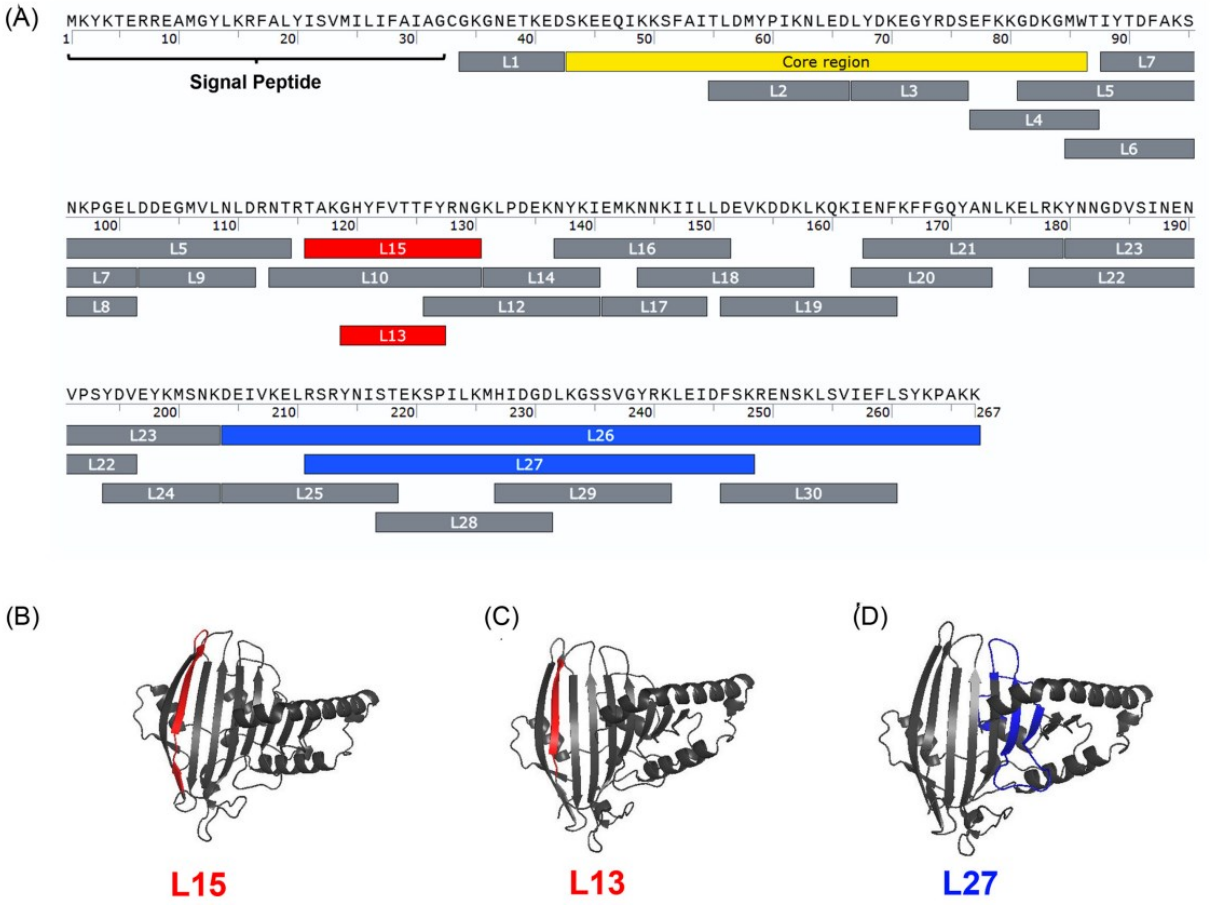

Fig. 1. Schematic overview of the smaller peptide fragments of Lpl1 and their invasion activity in host cells. (**A**) Representation of the peptide fragments used in the study. L15 and L13, labelled in red, reduced *S. aureus* internalization in HaCaT cells. L26 an L27, labelled in blue, increased *S. aureus* internalization. Most of the other synthesized peptides showed no effect in *S. aureus* internalization in HaCaT cells (labelled in grey). Localisation of (**B**) L15 (highlighted in red), (**C**) L13 (highlighted in red) and (**D**) L27 (highlighted in blue) in the Lpl1-protein. The 3D structure of Lpl1 was predicted using the protein structure prediction server Robetta using RoseTTAFold modelling method and visualized in PyMOL.

Here, we further dissected the Lpl1-protein into smaller peptide fragments and examined these for their invasive activity by host cells. All Lpl1-derived peptides tested are marked in **Fig. 1A**. Most of the synthesized peptides showed no effect (**grey-labeled peptide regions in Fig. 1A**). However, we found two small peptides that produced the opposite effect, namely, they decreased *S. aureus* internalization by host cells (**red-labeled peptide regions in Fig. 1A**). We named these two peptides L13 and L15. L13 is part of L15 and they are 9 and 15 amino acids long, respectively; (**Fig. 1A**). Both peptides are part of a beta-sheet region of the Lpl1-protein (**Fig. 1B**). Preincubation of HaCaT cells with L13 or L15 caused a 50-60 % decrease in uptake of *S. aureus* USA300 compared to untreated control (**Fig. 2A**). As an additional control we included the well-known Hsp90 inhibitor geldanamycin (5 µM), a benzoquinoid from *Streptomyces hygroscopicus* that is known to inhibit the ATPase activity of Hsp90. As expected, geldanamycin reduced the internalization of *S. aureus* USA300 by HaCaT cells by approximately 75% (**Fig. 2A**). As a positive control, we also tested the peptides L26 and L27, which increased invasion by approximately 1.5-fold (**see Table 1**). All other peptides had no effect on the internalization of *S. aureus* into HaCaT cells. (Please note, L26 and L27 were called P10 and P11 respectively in our previous paper (13))

Table 1: Effect of tested Lpl1-derived peptides on their invasion potential, F-actin levels in HaCaT cells and binding to Hsp90α. In all the studies, 35 µg/ml of peptides were tested for its effect on HaCaT cells

Name	Sequence	No of AA	Molarity (µM)	Relative Invasion in HaCaT	Interaction with Hsp90α	Relative F-actin level in HaCaT
L1	[34] GKGNETKED	9	35.82	1.02 ± 0.34	No	0.95 ± 0.49
L2	[55] TLDMYPIKNLED	12	24.14	1.12 ± 0.40	No	0.99 ± 0.13
L3	[67] LYDKEGYRDS	10	28	1.00 ± 0.11	No	1.03 ± 0.1
L4	[77] EFKKGDKGMWT	11	26.32	0.93 ± 0.12	No	0.94 ± 0.08
L5	(0:sup)81(/0: sup)GDKGMWTIYTDFAKSNKP GELDDEGMVLNLDRNTR	34	8.77	1.59 ± 0.76	No	0.97 ± 0.08
L6	[85] MWTIYTDFAKS	11	25.74	0.98 ± 0.68	No	0.91 ± 0.1
L7	[88] IYTDFAKSNKPGEL	14	22.15	1.10 ± 0.18	No	1.03 ± 0.08
L8	[96] NKPGEL	6	53.03	1.28 ± 0.34	No	0.96 ± 0.05
L9	[102] DDEGMVLNLD	10	31.25	1.0 ± 0.44	No	1.06 ± 0.07
L10	[113] NTRTAKGHYFVTTFYRNG	18	16.43	1.10 ± 0.17	Yes	0.99 ± 0.08
L13	[119] GHYFVTTFY	9	30.97	0.45 ± 0.08	Yes	0.87 ± 0.03
L15	[116] TAKGHYFVTTFYRNG	15	19.88	0.4 ± 0.09	Yes	0.83 ± 0.04
L12	[126] FYRNGKLPDEKNYKI	15	18.52	0.94 ± 0.11	No	0.98 ± 0.06
L14	[131] KLPDEKNYKI	10	28	0.78 ± 0.26	No	0.98 ± 0.08
L16	[137] NYKIEMKNNKIILLD	15	18.91	0.92 ± 0.37	Yes	1.08 ± 0.23
L17	[141] EMKNNKIIL	9	31.82	1.05 ± 0.26	No	1.09 ± 0.20
L18	[144] NNKIILLDEVKDDKL	15	19.77	1.05 ± 0.36	No	1.09 ± 0.22
L19	[151] DEVKDDKLKQKIENF	15	18.92	1.29 ± 0.37	No	0.97 ± 0.11
L20	[162] IENFKFFGQYAN	12	23.65	1.15 ± 0.20	No	1.03 ± 0.11
L21	[163]ENFKFFGQYANLKELRK	17	16.43	1.20 ± 0.25	Yes	1.09 ± 0.13
L22	[177]LRKYNNGDVSINENVPSYDV	20	15.22	1.29 ± 0.13	No	0.97 ± 0.09
L23	[180]YNNGDVSINENVPSYDVEYKMSNK	24	12.59	1.09 ± 0.46	No	0.96 ± 0.05
L24	[194]YDVEYKMSNK	10	27.34	0.95 ± 0.12	No	0.94 ± 0.08
L25	[204] DEIVKELRSRYNIST	15	19.23	1.0 ± 0.06	No	1.03 ± 0.16
L26	(0:sup)204(/0: sup)DEIVKELRSRYNISTEKSPILK MHIDGDLKGSSVGYRKLEI DFSKRENSKLSVIEFLSYKPAKK	64	4.72	1.50 ± 0.17	Yes	1.25 ± 0.13
L27	(0:sup)211(/0: sup)RSRYNISTEKSPILKMHIDG DLKGSSVGYRKLEIDFSKRENSK	38	7.03	1.55 ± 0.17	Yes	1.36 ± 0.12
L28	[217]STEKSPILKMHIDGD	15	20.96	1.0 ± 0.27	No	0.90 ± 0.04
L29	[227]HIDGDLKGSSVGYRK	15	21.47	1.21 ± 0.33	No	0.90 ± 0.05
L30	[246]FSKRENSKLSVIEFL	15	19.44	1.24 ± 0.32	No	0.96 ± 0.1
	Geldanamycin		5	0.25 ± 0.13	NA	0.88 ± 0.03
	Lpl1				Yes	
	BSA				No	

We also investigated whether L15 and L13 mediated internalization of *S. aureus* by the host cell is dependent on Hsp90α. For this purpose, we pretreated HaCaT cells with anti-Hsp90α (α-Hsp90α) antibody, which decreased *S. aureus* invasion by 89.3% (0.11 ± 0.09) (**Fig. 2A**). This suggested that the interaction of the peptide with Hsp90α plays a crucial role in host cell internalization.

Similar results were obtained with the N/TERT-1 keratinocyte cell line (**Fig. 2B**), which is often used as a substitute for primary keratinocyte cells because of the limited availability and high inter-donor variability of the latter. N/TERT-1 cells are immortalized and behave essentially like primary human keratinocytes in terms of host defense gene and protein expression and epidermal differentiation (22). It should be noted that the peptides/geldanamycin at the tested concentration and exposure time, didn’t cause any toxicity either to HaCaT or N/TERT-1 cells (**Fig. S1**).

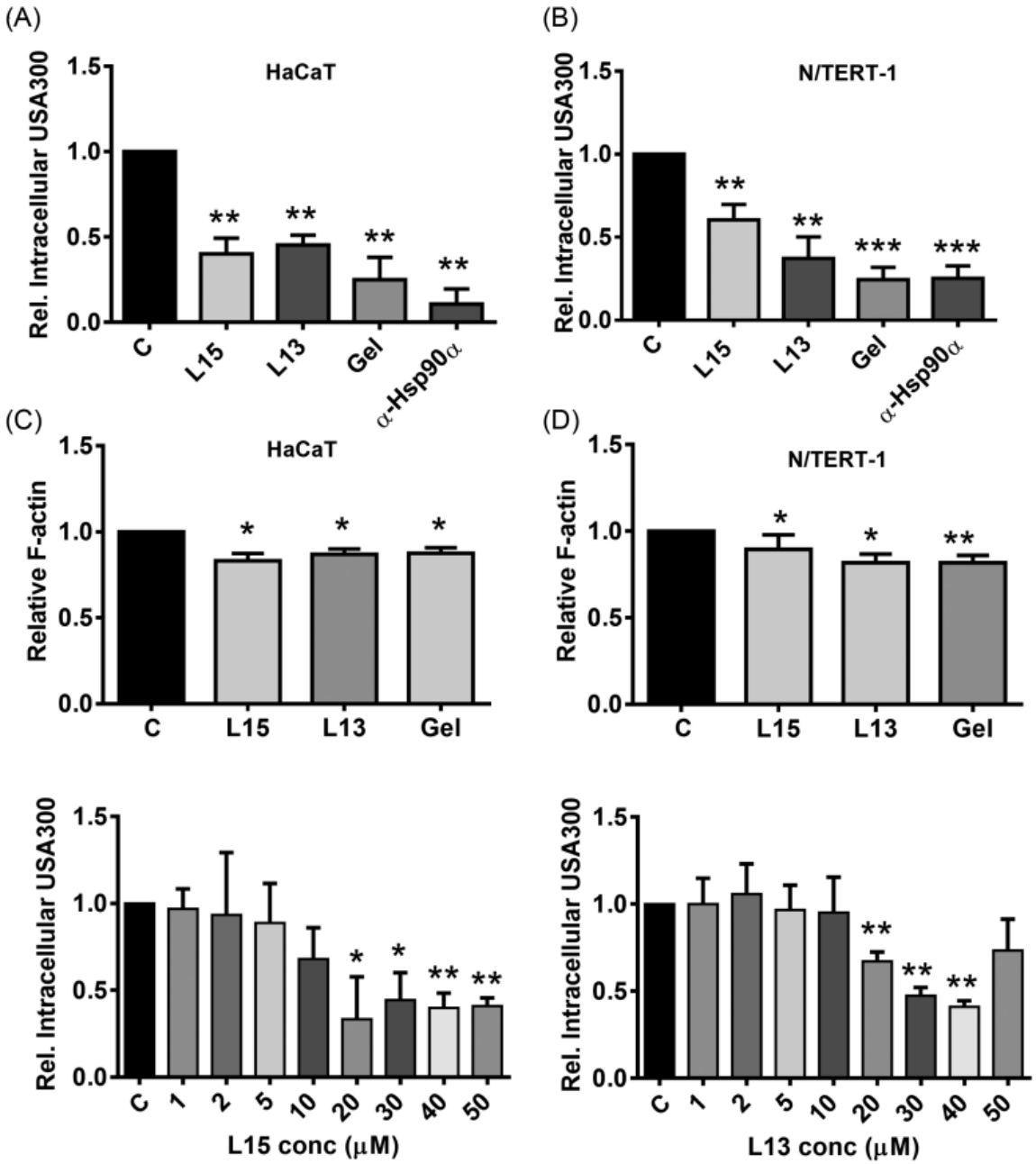

Fig. 2. **Bioactivity of L15 and L13 with respect to invasion and F-actin levels.** One-hour-half long pretreatment (1.5 h) with L15 and L13 inhibits the invasion of *S. aureus* USA300 into (**A**) HaCaT and (**B**) N/TERT-1 cell lines. Pretreatment of cells with geldanamycin (Gel), a known Hsp90 inhibitor, or with α-Hsp90α (Hsp90α) antibody also reduced USA300 invasion into the keratinocytes. L15, L13 and geldanamycin reduced F-actin levels in (**C**) HaCaT and (**D**) N/TERT-1 cells. The cells were treated with 20 μM of L15, 30 μM of L13 or with 5 μM of geldanamycin for these analyses. In (A) and (B) C indicates control; In (C) and (D) UT indicates untreated cells. Error bars show standard deviation of the mean of 3 biological replicates. P values were obtained by student's T-test: * $p < 0.05$; ** $p < 0.01$; *** $p < 0.001$; and **** $p < 0.0001$.

L15 and L13 reduced F-actin levels in keratinocytes and directly interact with Hsp90α. In our previous work, we showed that the parent protein, Lpl1, increased F-actin levels in HaCaT cells (13), whereas geldanamycin (17-AAG) decreased F-actin levels in breast cancer cells (Taiyab & Rao Ch, 2011). Here we investigated whether L15 and L13 influenced actin polymerization and found that both peptides, similarly to geldanamycin, caused a significant decrease in F-actin levels in both HaCaT and N/TERT-1 cell lines (**Fig. 2C and D**). In HaCaT cells L15 decreased the relative F-actin content to 0.83 ± 0.04, L13 to 0.87 ± 0.03, and geldanamycin to 0.88 ± 0.03. In N/TERT-1 cells we observed a similar decrease in F-actin levels for all three compounds, L13 (0.81±0.03), L15 (0.9±0.02) and geldanamycin (0.82±0.03). As expected, L26 and L27, which induced increased host cell invasion, caused an increase in F-actin levels (**Table 1**).

A concentration dependent effect of the peptides L15 and L13 on *S.aureus* USA300 invasion into HACaT cells were carried out (from 0 – 50 µM). A significant reduction of intracellular USA300 were observed from a concentration of 20 µM on for both L15 and L13 (**Fig. 2E and F)**. For L15, the relative invasion or intracellular bacterial count remained almost similar from concentration 20 to 50 µM (from 0.33 ± 0.24 to 0.40 ± 0.05) as compared to the untreated control (1.0 ± 0.0). In case of L13, a concentration dependent reduction in USA300 invasion into HaCaT were seen from 20 – 40 µM (0.67 ± 0.05 to 0.41 ± 0.03) as compared to the untreated group. At 50 µM L13, no significant change in the intracellular USA300 count was observed (0.73 ± 0.18).

In our previous work, we showed that Lpl1 interacts directly with Hsp90α (13). Here, we performed similar experiments with the synthetic peptides by blotting them directly onto PDV nitrocellulose membrane and testing for binding to Hsp90α *via* immunoblotting. The results are summarized in **Table 1**. Most of the Lpl1-derived peptides showed no binding to Hsp90α as exemplified by peptides L1 to L3. However, peptides that either promoted (L26 und L27) or inhibited (L13 and L15) invasion and F-actin levels also interacted with Hsp90α **(Fig. 3A)**.

L15 and L13 were also observed to interact directly with their mother protein Lpl1, when tested with dot blot method. Here, 2 µg L15, L13 or Hsp90α was blotted directly

on PDV nitrocellulose membrane and tested for their binding to Lpl1-His via immunoblotting. Hsp90α was used as positive and BSA as negative control (**Fig. 3B).**

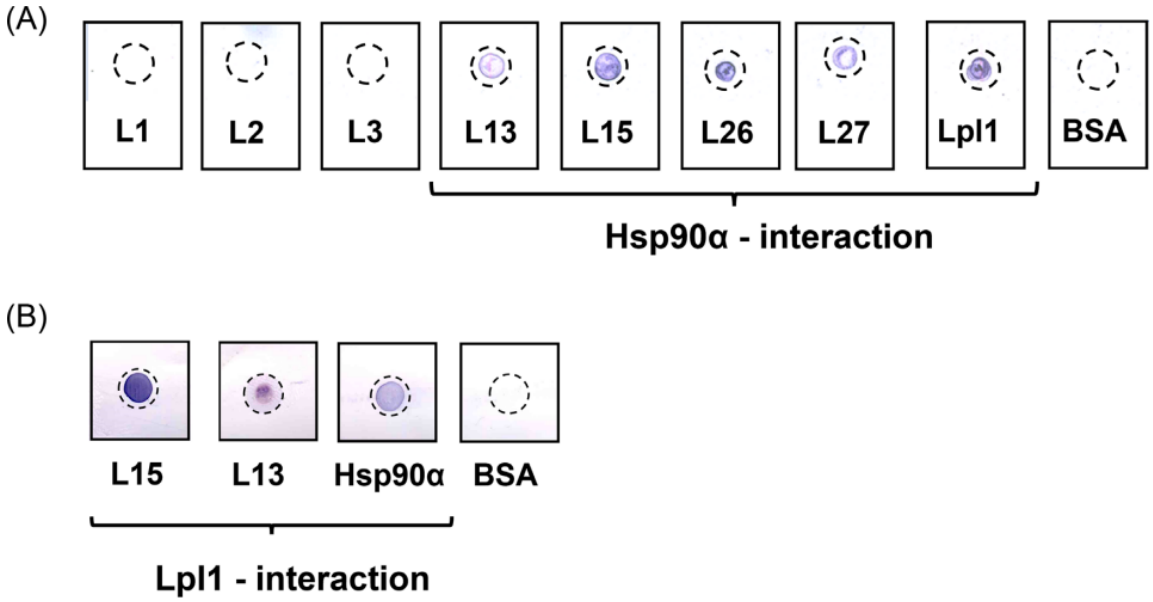

Fig. 3. L15 and L13 interacts with Hsp90α and Lpl1 (A) Interaction of Lpl1 and Lpl1-derived peptides with Hsp90α by dot blot analysis. Here we showed that most of the Lpl1-derived peptides do not interact with Hsp90 as exemplified with L1 to L3. The C-terminal localized peptides L26 and L27 bind to Hsp90, but like the parent Lpl1 they boost internalization and F-actin levels. The L13 and L15 peptides also bind to Hsp90 but show an opposite effect. BSA was used as another negative control. **(B)** Dot blot image showing the direct interaction of L15, L13 with Lpl1 *via* immunoblotting. Hsp90α and BSA was used as the positive and negative control respectively.

L15 and L13 are non-toxic to HaCaT and MM6 cells. Considering their potential as antimicrobials, we investigated whether L15, L13 and geldanamycin (as a control) are cytotoxic to human cells over a concentration range of 1 - 200 µM and for 24 h. Cytotoxicity was tested using the MTT assay in human keratinocytes (HaCaT cells) and human monocytic cells (MM6 cells). The percentage of viable cells after 24 hours of treatment with **L15** ranged from 94.95 ± 24.03 (200 µM) to 122.27 ± 20.79 (1 µM) for MM6 cells and 87.39 ± 7.84 (200 µM) and 100.76 ± 4.20 (1 µM) for HaCaT cells. Cell viability upon **L13** exposure ranged between 82.43 ± 8.59% (200 µM) and 106.71 ± 6.40% (1 µM) in MM6 cells and 83.79 ± 11.13 (200 µM) and 103.05 ± 10.06 (1µM) in HaCaT cells. Overall, it can be said that a slight reduction in viability was only observed at the highest concentration of 200 µM for both L13 and L15. In contrast, geldanamycin exhibited relatively high cytotoxicity also at lower

concentrations (**Fig. 4A and B**). In HaCaT cells, viability decreased gradually from a concentration of 50 µM, and in MM6 cells already from 10 µM.

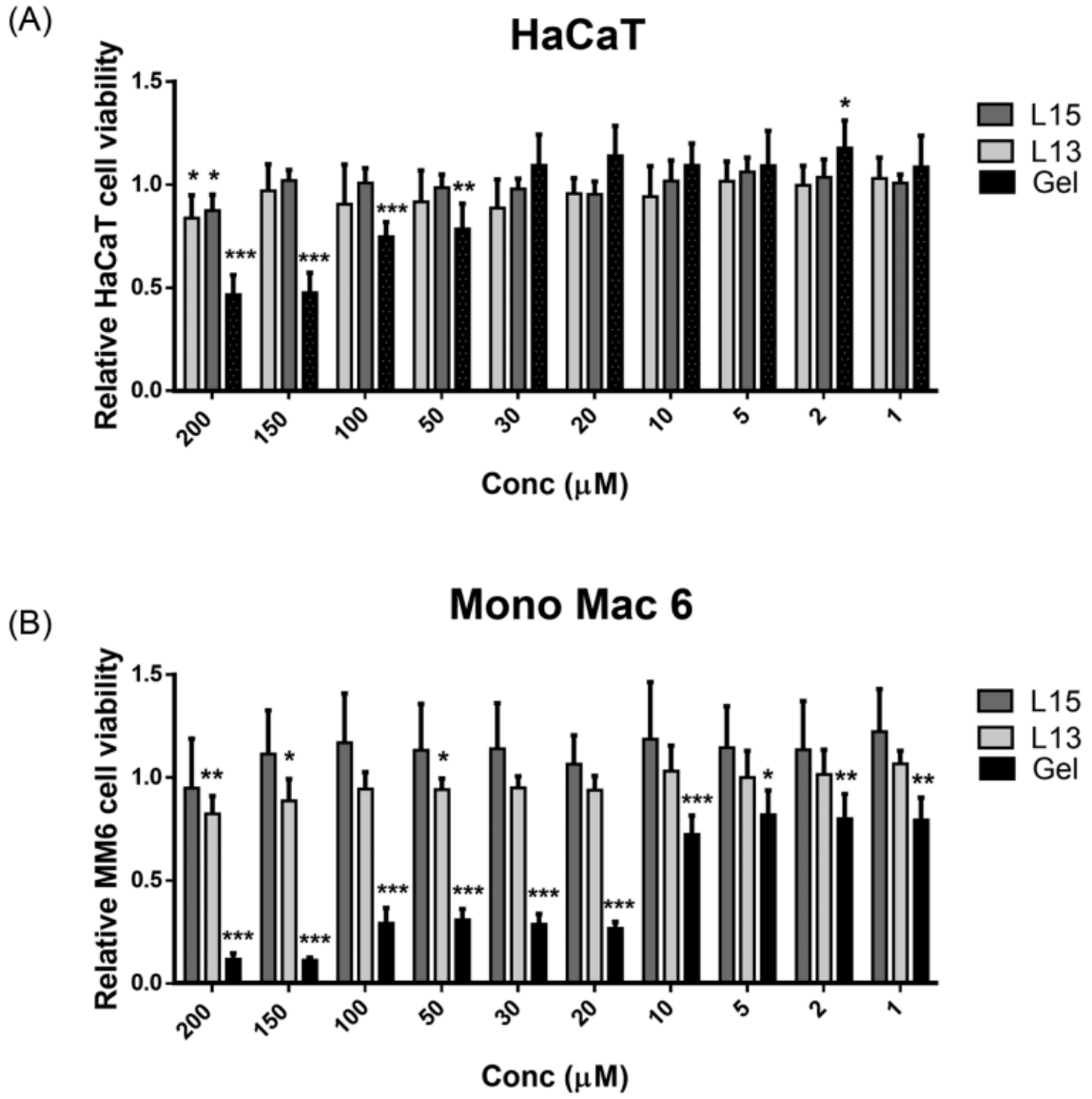

Fig. 4. **Unlike geldanamycin, L15 and L13 show little or no cytotoxicity.** (**A**) HaCaT keratinocytes and (**B**) Mono Mac 6 (MM6) cells were incubated with increasing concentration (0 to 200 µM) of peptides or geldanamycin for 24 h and the viability of cells was determined using MTT cytotoxicity assay. Error bars show standard deviation of the mean of 3 biological replicates. P values were obtained by student's T-test: * $p < 0.05$; ** $p < 0.01$; *** $p < 0.001$.

L15 and L13 significantly decrease lethality of *S. aureus* bacteremia in insect model but they do not affect growth or hemolytic activity of *S. aureus*. The larvae of *Galleria mellonella*, or *Greater Wax Moth*, are a recognized experimental model for studying the virulence of various pathogens and for evaluating the efficacy of antimicrobial

compounds. The large size of the larvae ensures easy handling and direct injection of a drug into the larval hemocoel. Ten microliters of L15 (60 mg/kg), L13 (60 mg/kg) or geldanamycin (5 mg/kg) were injected into their hemocoel of *G. mellonella* one hour prior to inoculation of *S. aureus* USA300 or *S. aureus* Newman, respectively. Larval survival was then followed for 5 days. Fig. 5A shows the killing rate of larvae infected with *S. aureus* USA300 alone and treated with L15 (20 μM), L13 (30 μM), or geldanamycin (5 μM). All infected untreated larvae died by the end of the third day. However, when the larvae were pretreated with L15 or L13, 30% and 23% of the larvae still survived on day 5, respectively. When the larvae were infected with *S. aureus* Newman, the picture was similar. When pretreated with L15 or L13, 36% or 46% of the larvae, respectively, survived on day 5 (Fig. 5B). When pretreated with vancomycin (20 mg/kg), 100% of the larvae survived, whereas geldanamycin had no or rather a negative effect on survival. The tested doses of peptides, geldanamycin, and vancomycin were not toxic to larvae.

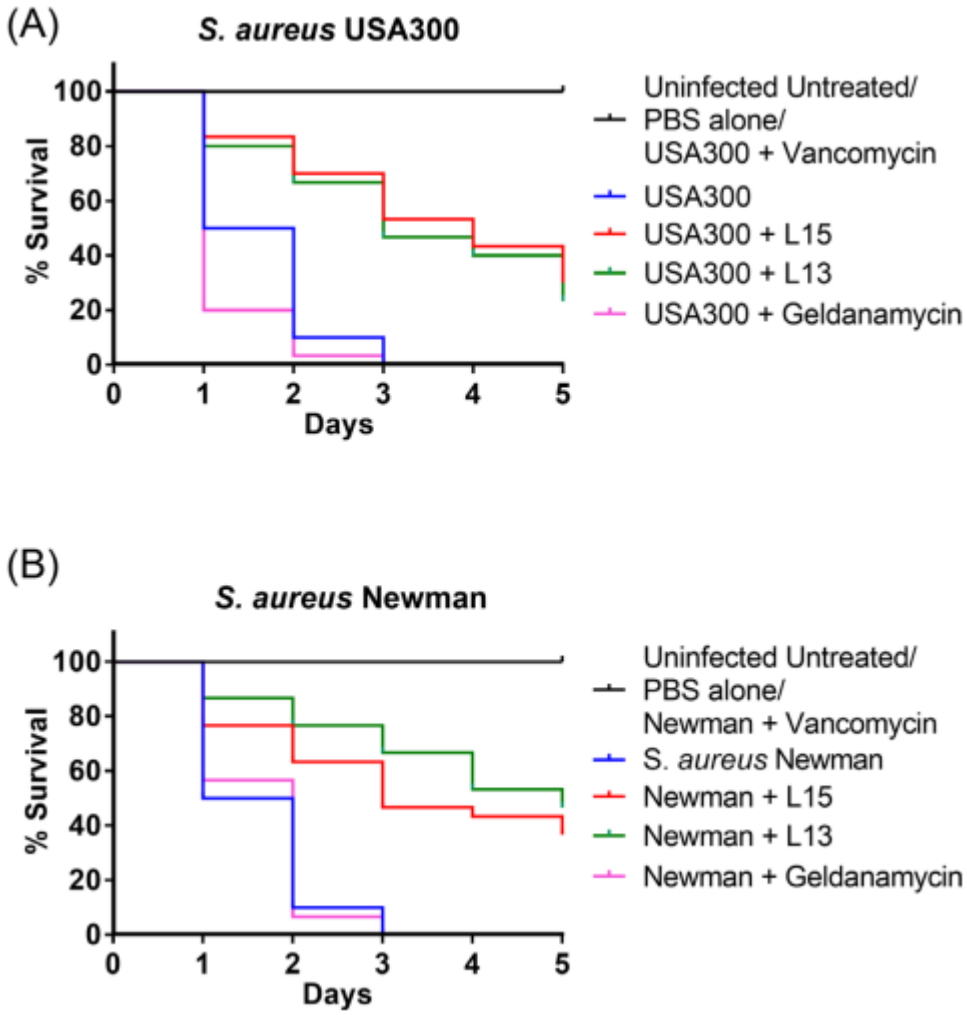

Fig. 5. **L15 and L13 rescue larvae from *S. aureus* infection**. Ten *Galleria mellonella* larvae per group, with average weight of 500 mg/larvae, were injected with bacteria and/or peptides on their last proleg using a BD insulin syringe. Each larva was injected with 10 µl of either of the two peptides, or geldanamycin or vancomycin (last left proleg) 1h before administration of 10^6 colony forming units (cfu) *S. aureus* (last right proleg) (**A**) USA300 and (**B**) Newman. The dosages used for the experiment were 60 mg/kg for peptides, 5 mg/kg of geldanamycin and 20 mg/kg for vancomycin. The larvae were maintained at 37 °C and observed for mortality every day over the course of 5 days. A total of three biological replicates are represented in the graph.

Since L15 and L13 could partially protect larvae from *S. aureus* infection, we then investigated whether they affected growth or the expression of virulence markers such as hemolysis. However, we did not detect any effect on growth (**Fig. S2A**), nor was hemolysis activity markedly affected (**Fig. S2B**).

L15 significantly decrease lethality of *S. aureus* bacteremia in mice. The results seen in larvae infection model encouraged us to test the same protective effect in mice. Here we chose the better soluble peptide, L15. To test this, NMRI mice were intravenously infected with *S. aureus* Newman. The clinical outcomes were monitored during the course of a 7-day infection. L15 treated mice were compared with the control mice receiving PBS.

The mice infected with *S. aureus* Newman began to lose weight after infection. In the L15-treated mice, weight loss was significantly reduced in L15 treated compared to control mice (**Fig. 6A**). No significant difference was observed with regard to the bacterial load in the kidneys (**Fig. 6B**). Regarding the mortality rate, 40 % of the animals in the control group died, whereas all mice treated with L15 survived during the 7-day observation period (**Fig. 6C**), indicating that L15 treatment significantly decreased lethality of *S. aureus* bacteremia.

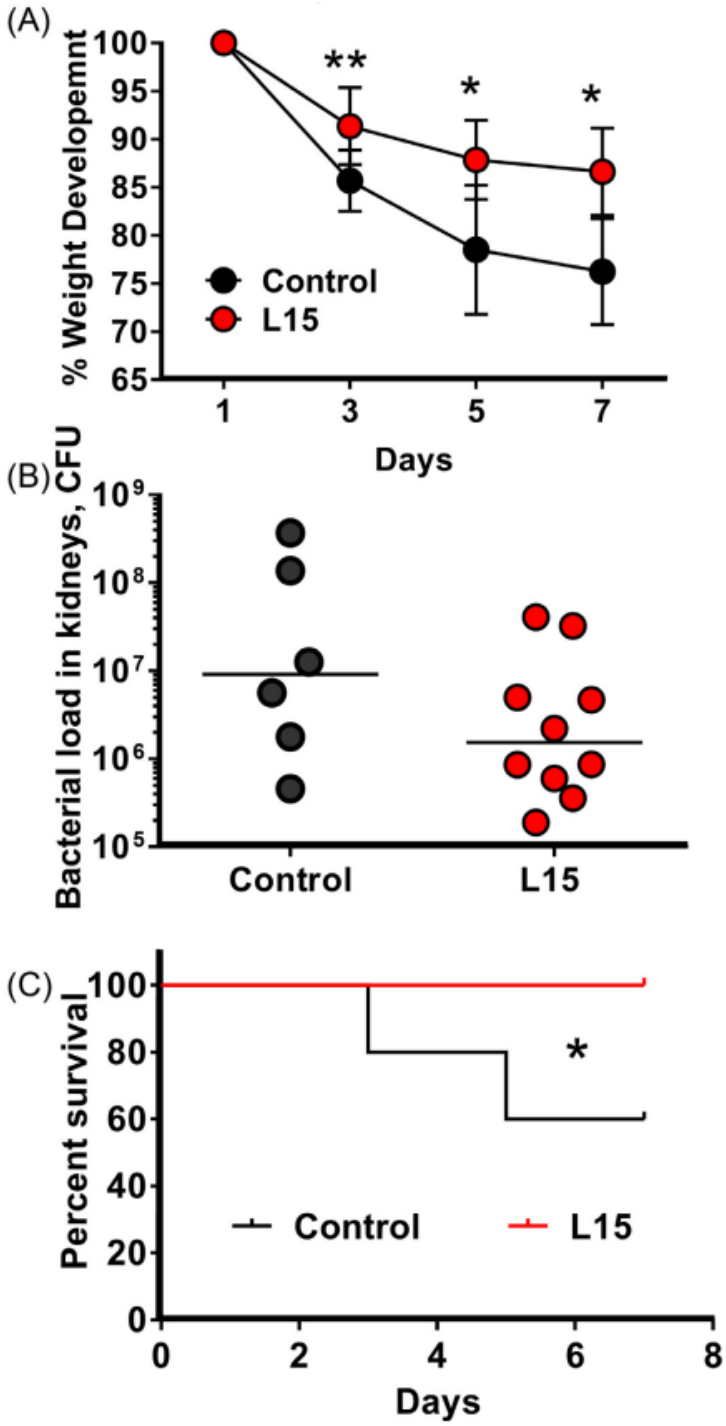

Fig. 6. **L15 treatment ameliorates systemic *S. aureus* infection in mice.** NMRI mice were intraperitoneally treated with L15 (10 mg/kg) or PBS (control) starting two hours before intravenous inoculation of *S. aureus* Newman strain ($2x10^6$ CFU/mouse). Treatment with peptides or PBS was then continued every day, twice/day, until animals were euthanized on day 7. (**A**) Weight development over the seven-day monitoring. (**B**) Bacterial load in kidneys (CFU) on day 7 post-infection (n=10 (4 died)). (**C**) Mortality of mice infected with *S. aureus* Newman. P-values determined using Mann-Whitney U-test with data expressed as the mean ± standard error of the mean (A) or median (B). * $p < 0.05$, ** $p < 0.01$.

L15 and L13 influence the response of innate immune cells to *S. aureus*. To understand the molecular basis of the protective effect of L15 and L13 we carried out immune stimulation studies with human peripheral blood mononuclear cells (PBMCs) from buffy coat blood samples of healthy donors. We tested the ability of the two peptides to induce IL-6, IL10, IL-12p70, IL12-p40, IL-23, TNFα, IL-1ß, IL-1RA, IP-10 and TARC. L15 was relatively inert with respect to cytokine inducing activity in PBMCs (**Fig. S3**).

We then stimulated *S. aureus* USA300 infected PBMCs from four to five healthy donors with L15 or L13 (20 and 30 µM, respectively) and compared it to the unstimulated USA300 infected PBMCs. It turned out that both peptides significantly increased IL-6 (n=5) but not TNF-alpha production (n=4) (**Fig. 7A and B**). Geldanamycin (5 µM) inhibited both the production of IL-6 and TNF-alpha in infected PBMCs. Later, we examined whether the peptides affected phagocytosis of *S. aureus*. The phagocytosis was performed in $CD14^+$ monocytes purified from PBMCs (n=4). The assay revealed that both peptides significantly decreased phagocytosis of *S.aureus* into $CD14^+$ monocytes: L15 by about 22.6 ± 7.67% and L13 by about 62.0 ± 6.80% (**Fig. 7C**). Geldanamycin (5 µM) showed no significant impact on phagocytosis.

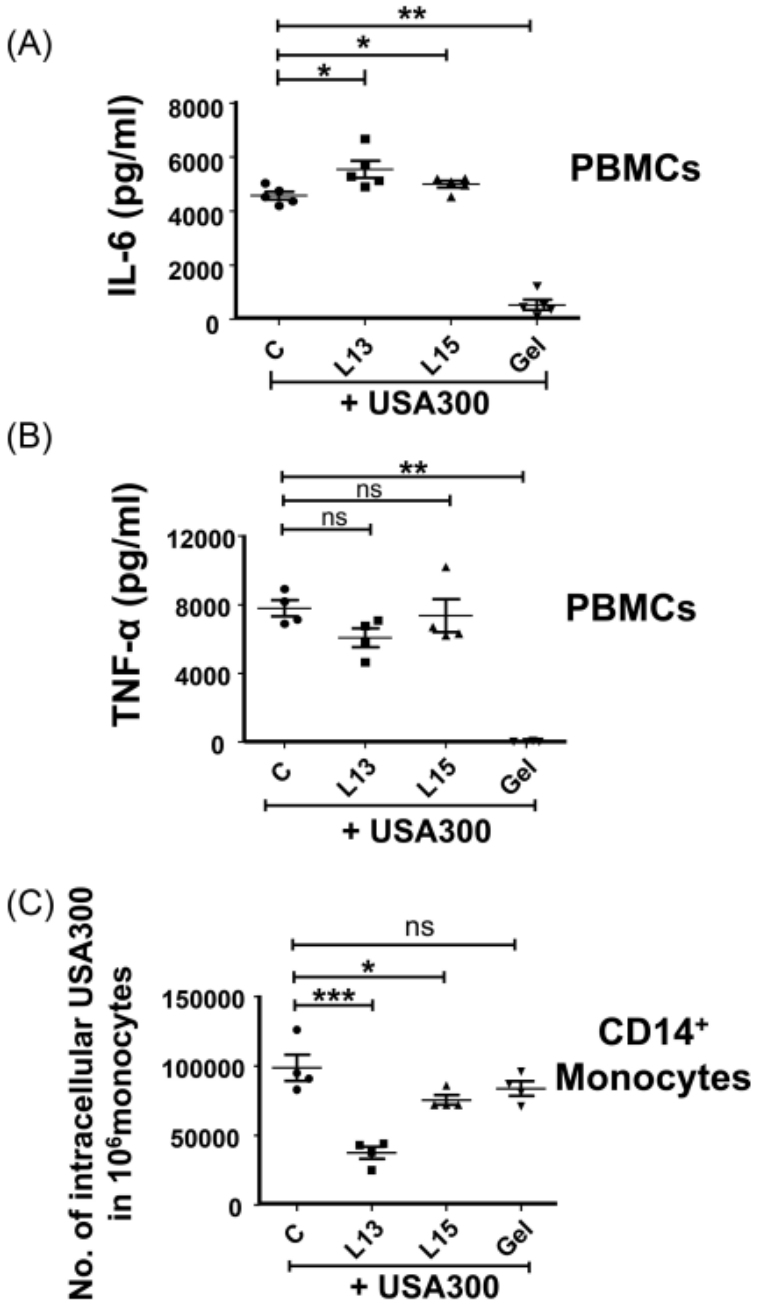

Fig. 7. Influence of L13 and L15 on the response of host innate immune cells. Release of IL-6 (**A**) and TNF-alpha (**B**) in the supernatant of *S. aureus*-infected PBMCs was assayed by ELISA 20 h after stimulation with L13 or L15 or geldanamycin. C indicates control cells without peptide pretreatment. Samples from 4 donors were carried out in triplicate. (**C**) Effect of L15 and L13 on *S. aureus* USA300 phagocytosis by primary human $CD14^+$ monocytes; control (C) was without peptide pretreatment. Samples from 4 donors were carried out in duplicate. Error bars represent SEM. Statistic significances were calculated between the peptide treated cells compared to control (C) by using one-way ANOVA analysis with Tukey's multiple comparison test: *p< 0.05, **p<0.01, ***p<0.001, ns > 0.05.

Multiple sequence alignment identifies Lpl1 homologs in other species. We also investigated in which microorganisms Lpl1 homologs occur. Protein BLAST analysis revealed that Lpl1 proteins with high similarity are present not only in different staphylococcal species but also in different unrelated bacterial species (**Fig. 8**). Lpl1 homologs from *Staphylococcus hyicus*, *Staphylococcus schweitzeri*, and *Staphylococcus argenteus* showed identities of 88%, 97%, and 88%, respectively, and the corresponding L15 and L13 homologous sequences in these lipoproteins were identical. The Lpl1-homolog was also found in some *Staphylococcus epidermidis* strains, however, the corresponding L15 sequence was not exactly the same. *Listeria monocytogenes* had an Lpl1 homolog with a sequence similarity of 80 % and *Ligilactobacillus ruminis* with 74 %. Even Gram-negative species such as *Escherichia coli*, *Klebsiella pneumoniae*, and *Pseudomonas aeruginosa* had a very similar lipoprotein with percent sequence similarity of 75, 90, and 85, respectively. Interestingly, the corresponding L15 sequence of *P. aeruginosa* was identical to that of *S. aureus*. Lpl1 protein was blasted against all organisms. We obtained similarities only against bacteria and within the bacteria only against these pathogenic species. The limitation to these species suggests that Lpl protein plays an important role in the pathogenicity and/or fitness of these bacteria, which should be further investigated.

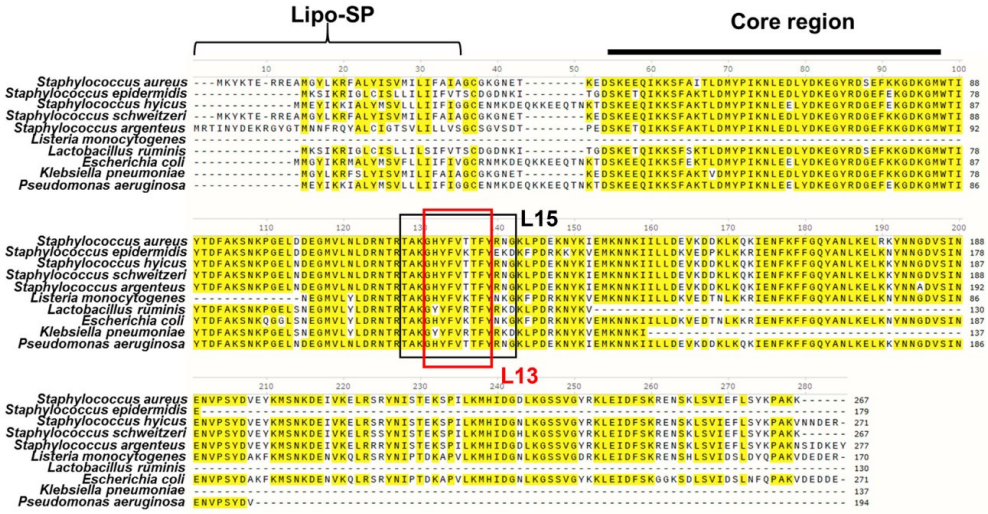

Fig. 8. Multiple sequence alignments of Lpl1 from *S. aureus* USA300 with other bacteria. These include *Staphylococcus epidermidis* SE62, *Staphylococcus hyicus* NCTC 8294, *Staphylococcus schweitzeri* NCTC 13712, *Staphylococcus argenteus* B3-25B, *Listeria monocytogenes* ATCC 15313, *Ligilactobacillus ruminis* ATCC 27780, *Escherichia coli* NCTC 9001, *Klebsiella pneumoniae* NCTC 9633 and *Pseudomonas aeruginosa* PA216. The lipoprotein signal peptide is indicated by the bracket, the conserved core region by the bar and the L15 sequence is boxed.

Discussion

Hsp90 is a molecular chaperone that ensures cellular proteostasis by folding, stabilizing, activating and degrading over 400 client proteins (23). There exist two isoforms, Hsp90α and β, however, because of the structural and functional similarity the name HSP90 is normally used for both (23). Normally, Hsp90α localizes in the cytoplasm but it can be secreted under stress such as reactive oxygen species, heat, hypoxia, irradiation, or tissue injury (24). The extracellular form, eHsp90α, has been shown to enhance cell motility and support wound healing (25). Due to its ability to affect numerous client proteins, inhibition of Hsp90 is regarded as an attractive approach for cancer treatment (26). Therefore, any new compound that interacts with and alters the activity of Hsp90 is regarded with great interest.

The well-studied geldanamycin (14, 15) and our L15 and L13 peptides have one thing in common, namely binding to Hsp90. This was the reason why we always included geldanamycin as a control in our studies. However, beyond the binding to Hsp90 the similarities become less pronounced. For example, Lpl1 increased both the internalisation of *S. aureus* by host cells and F-actin levels, whereas geldanamycin decreased the internalisation and F-actin levels by about the same factor suggesting that they bind to different sites of Hsp90 (13).

In the search for Lpl1 domains that interacted with Hsp90α, we found 2 peptides, L15 and L13, which interacted with Hsp90α but, unlike the parent protein Lpl1, decreased the internalisation of *S. aureus* into host cells, similar to geldanamycin does. L15 and L13 are part of a ß-sheet domain in Lpl1 as illustrated in **Fig. 1B, C**. The previously described L27 peptide (38 aa long) is localized in the C-terminal alpha-helical and loop structures part of Lpl1 and activates, like the parent protein Lpl1, the internalisation of *S. aureus*. Hsp90 comprises three main conserved domains, the N-terminal domain (NTD), C-terminal domain (CTD), and middle domain (MD) each performing a specific function (23). While geldanamycin is known to bind to the N-terminal NTD domain thereby inhibiting the ATPase activity that is necessary to regulate Hsp90 conformation (27, 28), we currently do not know how or where L13/L15 interact with Hsp90.

Owing to the significant roles of protein kinases and phosphatases in cellular regulation (29) we also investigated whether L15 or L13 exerted an effect on total ATPase activity in HaCaT cells. However, we could not detect any significant inhibition by L15 or L13 and assumed that Hsp90 ATPase activity is not significantly affected (**Fig. S4**). Most likely the peptides bind to a different site on Hsp90 than geldanamycin.

Similar to geldanamycin, L15 and L13 inhibit F-actin formation and *S. aureus* internalisation in host cells (**Fig. 2 and Table 1**).

Since geldanamycin is more cytotoxic than L15 and L13 we took care of using it at the subinhibitory concentration of 5 µM, while L15 and L13 were used at concentrations of ≈ 20 and 30 µM, respectively. In both the *G. mellonella* and the mouse model, L15 reduced the lethality of *S. aureus,* by about 30% in the insect model and about 40% in the mouse model (**Fig. 5 and 6**). In the insect model the peptides were added immediately before infection with *S. aureus*. In the mouse model, L15 was added one hour before the infection with *S. aureus* and at daily time intervals, similar to classical antibiotic treatment. This positive effect, shows that the peptides act not only at the cellular level but also in animal models.

In order to reduce the lethality of *S. aureus,* we speculated that a) L15 and L13 inhibited growth and expression of virulence factors of *S. aureus* or b) they strengthened the host defense or c) both.

At the concentrations used, L15 and L13 neither inhibit the viability of host cells (**Fig. S1A, B**) nor the growth or hemolytic activity of *S. aureus* (**Fig. S2A, B**). But, it was observed that the peptides L15 and L13, can interact directly not only to Hsp90α, but also to the Lpl1 (**Fig. 3A,B**).

We also believe that they strengthen host defenses through their interaction with Hsp90. However, there might be also a third mechanism. In the blood stream there are abundant neutrophils who can sense, engulf, and kill the bacteria. The inhibitory effect of L15 on bacterial internalization in keratinocytes and monocytes may also apply to the endothelial cells. In the bacteremia model, less internalized bacteria upon L15 treatment may result in higher number of bacteria in the blood stream that are more susceptible to immune killing which may lead to less focal infection in the vital organs.

How the defense is strengthened is not completely clear. However, insects and mammalians have one defense system in common, namely the innate immune system (30). Both peptides are relatively inert with respect to cytokine inducing activity in PBMCs (**Fig. S3**). However, *S. aureus* infected PBMCs that were pretreated with L13 and L15 showed an increase in IL-6 production (**Fig. 7A**), and in primary human monocytes pretreatment with L13 or L15 decreased the *S. aureus* internalization (**Fig. 7C**). In the latter case, the peptides could compete with the Lpl proteins on the surface of *S. aureus* for binding to the Hsp90 receptor or bind directly to the Lpl preventing them from interacting with Hsp90 (**Fig. 3A and B**). Both could lead to neutralization of the Lpl proteins, and this in turn could lead to reduced pathogenicity. This would be consistent with our previous results showing that deletion of the *lpl* genes significantly reduces the pathogenicity of *S. aureus* in a mouse kidney abscess model (8).

Hsp90 and related heat shock proteins are also involved in host defence (31). Hsp90 induces the adaptive immunity by activation of antigen presenting cells and dendritic cells. And the related heat shock protein, GRP94 (gp96), shows the same domain structure as Hsp90 and also binds geldanamycin. It is the most abundant glycoprotein in the ER hence known as endoplasmin. The remarkable feature of GRP94 is that some of its client proteins are important components of the immune system such as TLR1, 2, 4 and MHC class II (32-35). In fact, GRP94 (GP96) is the master chaperone for Toll-like receptors and is important in the innate function of macrophages (36).

Conclusion

Any compound that interacts with Hsp90 and thereby exerts an effect on cellular physiology is of particular interest. The Lpl1-derived small peptides, L15 and L13, not only impact the cytoskeleton and the associated internalization of *S. aureus* by the host cells *in vitro*. They also exert an effect in both insect and mammalian models by reducing the lethality of *S. aureus* infection. How this happens is still unclear, however, we envisage two scenarios: a) binding of the peptides to Hsp90 and related Hsp proteins engages the innate immune system in such a way that it responds faster or more strongly to *S. aureus* infection, or b) binding of the peptides to Lpl1 interferes the binding of the membrane-anchored Lpl proteins of *S. aureus*. Indeed,

we found that the peptides also interact with Lpl1. This indicates that the peptides bind to both Lpl1 and Hsp90. We now hypothesize that the L15/L13-induced reduction in virulence of *S. aureus* is due to interaction with both the Lpl protein and Hsp90. Whether both interactions or only one of them affects virulence will have to be further investigated. In this work, we also demonstrate that rationally selected peptides of a cell surface-bound virulence factor can turn out to be promising drugs.

Acknowledgements

This work was supported by infrastructural funding from the Deutsche Forschungsgemeinschaft (DFG), Cluster of Excellence EXC 2124 - Controlling Microbes to Fight Infections - 390838134. Minh-Thu Nguyen acknowledges the Innovative Medizinische Forschung (IMF) Grant provided by the Medical Faculty Münster (number NG 122106). We thank Dr. J. Rheinwald for providing us with the N/TERT-1 cell line. We are also thankful to Libera Lo Presti for the proof reading and editing of the manuscript. A priority patent has been filed for L13 and L15 under the application number EP21217169.8.

Author Contributions

FG, AVA and SBH designed the study. AVA performed most of the experiments. AJ (under the supervision of TJ) conducted the mice studies. MTN carried out the phagocytosis experiments. LW (guided by SBH), MTN and CB performed the immune stimulation assays. PT contributed to the initial experiments. HK synthesised some of the peptides. MN and BM performed quality control (MS, NMR) of the peptides. AVA and KS carried out the interaction studies. FG, AVA, SBH and AL analysed the data. FG and AVA wrote the manuscript. MTN, SBH and TJ edited the manuscript.

Conflict of interest

The authors declare no conflict of interest.

References

1. Hirschhausen, N., Schlesier, T., Schmidt, M. A., Götz, F., Peters, G., and Heilmann, C. (2010) A novel staphylococcal internalization mechanism involves the major autolysin Atl and heat shock cognate protein Hsc70 as host cell receptor. *Cellular Microbiology* **12**, 1746-1764
2. Sinha, B., François, P. P., Nüße, O., Foti, M., Hartford, O. M., Vaudaux, P., Foster, T. J., Lew, D. P., Herrmann, M., and Krause, K. H. (1999) Fibronectin-binding protein acts as *Staphylococcus aureus* invasin via fibronectin bridging to integrin α5β1. *Cellular Microbiology* **1**, 101-117
3. Nguyen, M. T., and Götz, F. (2016) Lipoproteins of Gram-Positive Bacteria: Key Players in the Immune Response and Virulence. *Microbiol Mol Biol Rev* **80**, 891-903
4. Buddelmeijer, N. (2015) The molecular mechanism of bacterial lipoprotein modification--how, when and why? *FEMS Microbiol Rev* **39**, 246-261
5. Shahmirzadi, S. V., Nguyen, M. T., and Götz, F. (2016) Evaluation of *Staphylococcus aureus* Lipoproteins: Role in Nutritional Acquisition and Pathogenicity. *Front Microbiol* **7**, 1404
6. Nguyen, M. T., Hanzelmann, D., Härtner, T., Peschel, A., and Götz, F. (2016) Skin-Specific Unsaturated Fatty Acids Boost the *Staphylococcus aureus* Innate Immune Response. *Infect Immun* **84**, 205-215
7. Diep, B. A., Gill, S. R., Chang, R. F., Phan, T. H., Chen, J. H., Davidson, M. G., Lin, F., Lin, J., Carleton, H. A., Mongodin, E. F., Sensabaugh, G. F., and Perdreau-Remington, F. (2006) Complete genome sequence of USA300, an epidemic clone of community-acquired meticillin-resistant Staphylococcus aureus. *Lancet* **367**, 731-739
8. Nguyen, M. T., Kraft, B., Yu, W., Demicrioglu, D. D., Hertlein, T., Burian, M., Schmaler, M., Boller, K., Bekeredjian-Ding, I., Ohlsen, K., Schittek, B., and Götz, F. (2015) The vSaα Specific Lipoprotein Like Cluster (lpl) of *S. aureus* USA300 Contributes to Immune Stimulation and Invasion in Human Cells. *PLoS Pathog* **11**, e1004984
9. Nguyen, M. T., Peisl, L., Solari, F. B., Luqman, A., and Götz, F. (2018) Toll-Like Receptor 2 and Lipoprotein-Like Lipoproteins Enhance *Staphylococcus aureus* Invasion in Epithelial Cells. *Infect Immun* **86**
10. Nguyen, M. T., Deplanche, M., Nega, M., Le Loir, Y., Peisl, L., Götz, F., and Berkova, N. (2016) *Staphylococcus aureus* Lpl Lipoproteins Delay G2/M Phase Transition in HeLa Cells. *Front Cell Infect Microbiol* **6**, 201
11. Deplanche, M., Filho, R. A., Alekseeva, L., Ladier, E., Jardin, J., Henry, G., Azevedo, V., Miyoshi, A., Beraud, L., Laurent, F., Lina, G., Vandenesch, F., Steghens, J. P., Le Loir, Y., Otto, M., Götz, F., and Berkova, N. (2015) Phenol-soluble modulin alpha induce G2/M phase transition delay in eukaryotic HeLa cells. *FASEB journal : official publication of the Federation of American Societies for Experimental Biology* **pii: fj.14-260513**
12. Alekseeva, L., Rault, L., Almeida, S., Legembre, P., Edmond, V., Azevedo, V., Miyoshi, A., Even, S., Taieb, F., Arlot-Bonnemains, Y., Le Loir, Y., and Berkova, N. (2013) *Staphylococcus aureus*-induced G2/M phase transition delay in host epithelial cells increases bacterial infective efficiency. *PLoS One* **8**, e63279
13. Tribelli, P. M., Luqman, A., Nguyen, M. T., Madlung, J., Fan, S. H., Macek, B., Sass, P., Bitschar, K., Schittek, B., Kretschmer, D., and Götz, F. (2020)

Staphylococcus aureus Lpl protein triggers human host cell invasion via activation of Hsp90 receptor. *Cellular Microbiology* **22**, 13111
14. Miyata, Y. (2005) Hsp90 inhibitor geldanamycin and its derivatives as novel cancer chemotherapeutic agents. *Curr Pharm Des* **11**, 1131-1138
15. Blagosklonny, M. V. (2002) Hsp-90-associated oncoproteins: multiple targets of geldanamycin and its analogs. *Leukemia* **16**, 455-462
16. Dickson, M. A., Hahn, W. C., Ino, Y., Ronfard, V., Wu, J. Y., Weinberg, R. A., Louis, D. N., Li, F. P., and Rheinwald, J. G. (2000) Human keratinocytes that express hTERT and also bypass a p16 INK4a -enforced mechanism that limits life span become immortal yet retain normal growth and differentiation characteristics. *Molecular and Cellular Biology* **20**, 1436-1447
17. Nguyen, M. T., Kraft, B., Yu, W., Demicrioglu, D. D., Hertlein, T., Burian, M., Schmaler, M., Boller, K., Bekeredjian-Ding, I., Ohlsen, K., Schittek, B., and Götz, F. (2015) The vSaα specific lipoprotein like cluster (lpl) of *S. aureus* USA300 contributes to immune stimulation and invasion in human cells. *PLoS Pathogens* **11**, 1004984
18. Nguyen, M. T., Schellerhoff, L. H., Niemann, S., Schaumburg, F., and Herrmann, M. (2022) Quiescence of Human Monocytes after Affinity Purification: A Novel Method Apt for Monocyte Stimulation Assays. *Biomolecules* **12**
19. Luqman, A., Muttaqin, M. Z., Yulaipi, S., Ebner, P., Matsuo, M., Zabel, S., Tribelli, P. M., Nieselt, K., Hidayati, D., and Götz, F. (2020) Trace amines produced by skin bacteria accelerate wound healing in mice. *Communications Biology* **3**, 1-10
20. Saising, J., Nguyen, M. T., Härtner, T., Ebner, P., Al Mamun Bhuyan, A., Berscheid, A., Muehlenkamp, M., Schäkermann, S., Kumari, N., Maier, M. E., Voravuthikunchai, S. P., Bandow, J., Lang, F., Brötz-Oesterhelt, H., and Götz, F. (2018) Rhodomyrtone (Rom) is a membrane-active compound. *Biochimica et Biophysica Acta - Biomembranes* **1860**, 1114-1124
21. Baek, M., DiMaio, F., Anishchenko, I., Dauparas, J., Ovchinnikov, S., Lee, G. R., Wang, J., Cong, Q., Kinch, L. N., Schaeffer, R. D., Millan, C., Park, H., Adams, C., Glassman, C. R., DeGiovanni, A., Pereira, J. H., Rodrigues, A. V., van Dijk, A. A., Ebrecht, A. C., Opperman, D. J., Sagmeister, T., Buhlheller, C., Pavkov-Keller, T., Rathinaswamy, M. K., Dalwadi, U., Yip, C. K., Burke, J. E., Garcia, K. C., Grishin, N. V., Adams, P. D., Read, R. J., and Baker, D. (2021) Accurate prediction of protein structures and interactions using a three-track neural network. *Science* **373**, 871-876
22. Smits, J. P. H., Niehues, H., Rikken, G., Van Vlijmen-Willems, I. M. J. J., Van De Zande, G. W. H. J. F., Zeeuwen, P. L. J. M., Schalkwijk, J., and Van Den Bogaard, E. H. (2017) Immortalized N/TERT keratinocytes as an alternative cell source in 3D human epidermal models. *Scientific Reports* **7**, 1-14
23. Hoter, A., El-Sabban, M. E., and Naim, H. Y. (2018) The HSP90 Family: Structure, Regulation, Function, and Implications in Health and Disease. *Int J Mol Sci* **19**
24. Jackson, S. E. (2013) Hsp90: structure and function. *Top Curr Chem* **328**, 155-240
25. Li, W., Sahu, D., and Tsen, F. (2012) Secreted heat shock protein-90 (Hsp90) in wound healing and cancer. *Biochim Biophys Acta* **1823**, 730-741

26. Sanchez, J., Carter, T. R., Cohen, M. S., and Blagg, B. S. J. (2020) Old and New Approaches to Target the Hsp90 Chaperone. *Curr Cancer Drug Targets* **20**, 253-270
27. Gorska, M., Popowska, U., Sielicka-Dudzin, A., Kuban-Jankowska, A., Sawczuk, W., Knap, N., Cicero, G., and Wozniak, F. (2012) Geldanamycin and its derivatives as Hsp90 inhibitors. *Front Biosci (Landmark Ed)* **17**, 2269-2277
28. Grenert, J. P., Sullivan, W. P., Fadden, P., Haystead, T. A., Clark, J., Mimnaugh, E., Krutzsch, H., Ochel, H. J., Schulte, T. W., Sausville, E., Neckers, L. M., and Toft, D. O. (1997) The amino-terminal domain of heat shock protein 90 (hsp90) that binds geldanamycin is an ATP/ADP switch domain that regulates hsp90 conformation. *J Biol Chem* **272**, 23843-23850
29. Cheng, H. C., Qi, R. Z., Paudel, H., and Zhu, H. J. (2011) Regulation and function of protein kinases and phosphatases. *Enzyme Res* **2011**, 794089
30. Sheehan, G., Garvey, A., Croke, M., and Kavanagh, K. (2018) Innate humoral immune defences in mammals and insects: The same, with differences? *Virulence* **9**, 1625-1639
31. Calderwood, S. K., Gong, J., and Murshid, A. (2016) Extracellular HSPs: The Complicated Roles of Extracellular HSPs in Immunity. *Front Immunol* **7**, 159
32. Schaiff, W. T., Hruska, K. A., Jr., McCourt, D. W., Green, M., and Schwartz, B. D. (1992) HLA-DR associates with specific stress proteins and is retained in the endoplasmic reticulum in invariant chain negative cells. *J Exp Med* **176**, 657-666
33. Randow, F., and Seed, B. (2001) Endoplasmic reticulum chaperone gp96 is required for innate immunity but not cell viability. *Nat Cell Biol* **3**, 891-896
34. Mesquita, F. S., Brito, C., Mazon Moya, M. J., Pinheiro, J. C., Mostowy, S., Cabanes, D., and Sousa, S. (2017) Endoplasmic reticulum chaperone Gp96 controls actomyosin dynamics and protects against pore-forming toxins. *EMBO Rep* **18**, 303-318
35. Staron, M., Yang, Y., Liu, B., Li, J., Shen, Y., Zuniga-Pflucker, J. C., Aguila, H. L., Goldschneider, I., and Li, Z. (2010) gp96, an endoplasmic reticulum master chaperone for integrins and Toll-like receptors, selectively regulates early T and B lymphopoiesis. *Blood* **115**, 2380-2390
36. Yang, Y., Liu, B., Dai, J., Srivastava, P. K., Zammit, D. J., Lefrancois, L., and Li, Z. (2007) Heat shock protein gp96 is a master chaperone for toll-like receptors and is important in the innate function of macrophages. *Immunity* **26**, 215-226

Chapter 5

Acetate sensing by GPR43 alarms neutrophils and protects from severe sepsis

Katja Schlatterer[1,2,3], Christian Beck[1,2,3], Ulrich Schoppmeier[2,3,4], Andreas Peschel[1,2,3]*, Dorothee Kretschmer[1,2,3]

[1] Interfaculty Institute for Microbiology and Infection Medicine Tübingen (IMIT), Infection Biology, University of Tübingen, Auf der Morgenstelle 28, 72076 Tübingen, Germany

[2] German Center for Infection Research, partner site Tübingen, Germany

[3] Cluster of Excellence EXC 2124 Controlling Microbes to Fight Infections, Tübingen, Germany

[4] Interfaculty Institute for Microbiology and Infection Medicine Tübingen (IMIT), Medical Microbiology and Hygiene, University of Tübingen, Elfriede-Aulhorn-Straße 6, 72076 Tübingen, Germany

*Corresponding author:
Andreas Peschel
andreas.peschel@uni-tuebingen.de
Phone +49 7071 2975937
Fax +49 7071 295937

Published: Schlatterer, K., Beck, C., Schoppmeier, U., Peschel, A., and Kretschmer, D. (2021) Acetate sensing by GPR43 alarms neutrophils and protects from severe sepsis. *Communications Biology* **4**, 928

Abstract

Bacterial sepsis is a major cause of mortality resulting from inadequate immune responses to systemic infection. Effective immunomodulatory approaches are urgently needed but it has remained elusive, which targets might be suitable for intervention. Increased expression of the G-protein-coupled receptor GPR43, which is known to govern intestinal responses to acetate, has been associated with sepsis patient survival but the mechanisms behind this observation have remained unclear. We show that elevated serum acetate concentrations prime neutrophils in a GPR43-dependent fashion, leading to enhanced neutrophil chemotaxis, oxidative burst, cytokine release and upregulation of phagocytic receptors. Consequently, acetate priming improved the capacity of human neutrophils to eliminate methicillin-resistant *Staphylococcus aureus*. Acetate administration increased mouse serum acetate concentrations and primed neutrophils. Notably, it rescued wild-type mice from severe *S. aureus* sepsis and reduced bacterial numbers in peripheral organs by several magnitudes. Acetate treatment improved the sepsis course even when applied several hours after onset of the infection, which recommends GPR43 as a potential target for sepsis therapy. Our study indicates that the severity of sepsis depends on transient neutrophil priming by appropriate blood acetate concentrations. Therapeutic interventions based on GPR43 stimulation could become valuable strategies for reducing sepsis-associated morbidity and mortality.

Introduction

Bacterial infections represent a major cause for severe diseases whose therapy is complicated by worldwide increasing rates of antibiotic resistance (1). Disseminated bacterial bloodstream infections represent a frequent complication, leading to life-threatening sepsis and septic shock with multi-organ failure (2). Sepsis is a common reason for intensive-care unit admission also in high-income countries, causing for instance 750,000 cases per year with an estimated death rate of about 30% in the United States (2, 3). The bacterial pathogen *Staphylococcus aureus* is one of the most frequent causative agents of sepsis (4, 5). Many of these infections are caused by methicillin-resistant *S. aureus* (MRSA) strains, which can be treated only with limited efficacy by some last-resort antibiotics (6). Sepsis-related pathology results from insufficient or dysregulated immune responses involving multiple immune cells and signaling pathways, the complex interplay of which limits our understanding and

the development of effective preventive or therapeutic interventions (7). Accordingly, the therapy of sepsis has not made major progress in the last decades and new approaches that modulate systemic immune responses in suitable ways are urgently needed (8).

Bacterial infections are primarily contained by neutrophil granulocytes, potent phagocytic cells and the most abundant leukocytes in the bloodstream (9, 10). Neutrophils express various well-studied pattern recognition receptors including Toll-like receptors (TLRs) (11) and formyl-peptide receptors (FPRs) (12) on their surface, in order to detect 'microbe-associated molecular pattern' (MAMP) molecules, hallmark signals for invasive infections (13). FPRs belong to the family of G-protein coupled receptors, members of which sense for instance chemokines or bacterial products such as formylated peptides (12) and phenol-soluble modulin peptides (14-16). Stimulation of various GPCR can establish a 'primed' state, which allows neutrophils to trigger a maximal antimicrobial response upon further pro-inflammatory stimulation (17). The role of neutrophil priming and activation in sepsis remains elusive – activated neutrophils are essential for pathogen elimination, in particular by release of reactive oxygen species (ROS), but exuberant and prolonged release of ROS can contribute to multi-organ failure (18, 19).

Neutrophils also express GPR43, a GPCR that recognizes the short-chain fatty acids (SCFA) acetate, propionate, and butyrate (20). GPR43 is expressed for instance on enterocytes (21) and is known to have a critical role in monitoring intestinal SCFA levels with critical consequences for chronic metabolic and inflammatory disorders such as obesity, gout, or colitis (22). In contrast, far less is known about the consequences of GPR43 activation in neutrophils. Increased expression of GPR43 on blood cells is linked to enhanced survival of septic patients (23), strongly suggesting that this receptor plays a critical role in the host defense against systemic infections. However, if and how GPR43 activation of neutrophils may influence the outcome of severe sepsis has remained unclear. Among the potential GPR43 agonists, only acetate can reach concentrations in human serum that would be sufficient to activate GPR43 (24, 25). However, serum acetate levels vary strongly according to individual nutritional and metabolic properties (0.02 - 2 mM) (24, 26) with an average concentration of ca. 0.050 (27) and it remains elusive under which conditions GPR43 may prime or activate neutrophils or not. Moreover, the acetate concentrations required for activation of GPR43 are high enough to affect the pH of

culture media and the functions of human cells, which may have contributed to inconsistent reports about either pro- or anti-inflammatory roles of GPR43 in neutrophils (28, 29).

We demonstrate that GPR43 can prime neutrophils to enhance their capacity to eliminate bacterial pathogens. Average serum acetate concentrations were not sufficient to achieve full priming, but interventional acetate injection led to strongly improved capacities of mice to cure *S. aureus* infections in a GPR43-dependent fashion, even when applied several hours after onset of the infection.

Results

GPR43 activation by acetate primes neutrophils

GPR43 is highly expressed on the surface of neutrophils (20), suggesting a role in infection control. An essential feature of the host defence of neutrophils is the generation of ROS, which are required for bacterial killing. To analyse if GPR43 can shape neutrophil ROS production, we monitored oxidative burst upon GPR43 activation by the natural ligand acetate or the synthetic specific agonist 4-chloro-α-(1-methylethyl)-N-2-thiazolylbenzeneacetamide) (4-CMTB) (30). Since acetate has the capacity to alter the medium pH and thereby cause unintended activation of other receptors, we used pH-neutralized, buffered sodium acetate solutions and confirmed that the medium pH did not change. While GPR43 activation failed to induce ROS generation in the absence of other stimuli, it enhanced the oxidative burst induced by bacterial ligands of FPR1 (Fig.1 a-c and Suppl. Fig.1a) or FPR2 (Suppl. Fig.1a), by endogenous ligands for platelet-activating factor or C5a receptors (PAFR or C5aR, respectively) (Suppl. Fig.1a), or by live, serum-opsonized *S. aureus* cells (Suppl. Fig.1 b, c). Acetate enhanced ROS generation at concentrations above 0.5 mM (Fig. 1a), which is far above the average but within the wide range of the reported variable human serum concentration. Serum acetate concentrations can reach up to 2 mM depending on the nutritional and metabolic status or, for instance, in the portal venous system (24, 31). The acetate-mediated effect was dependent on GPR43 as it could be completely blocked by the GPR43-specific antagonist (*S*)-3-(2-(3-chlorophenyl) acetamido)-4-(4-(trifluoromethyl)phenyl) butanoic acid (CATPB) (32) (Fig. 1b, c, Suppl. Fig. 1a, c). Thus, GPR43 activation strongly increases the oxidative burst in neutrophils in combination with other pro-inflammatory GPCR

agonists. This behaviour is a hallmark of agents that can prime neutrophils and it is known to be associated with phosphorylation of the NADPH oxidase subunit p47^{phox} at serine position 345 (33). Indeed, GPR43 activation by acetate triggered p47^{phox} S345 phosphorylation (Fig. 1d, Suppl. Fig. 1d), thereby confirming that GPR43 activation primes neutrophils.

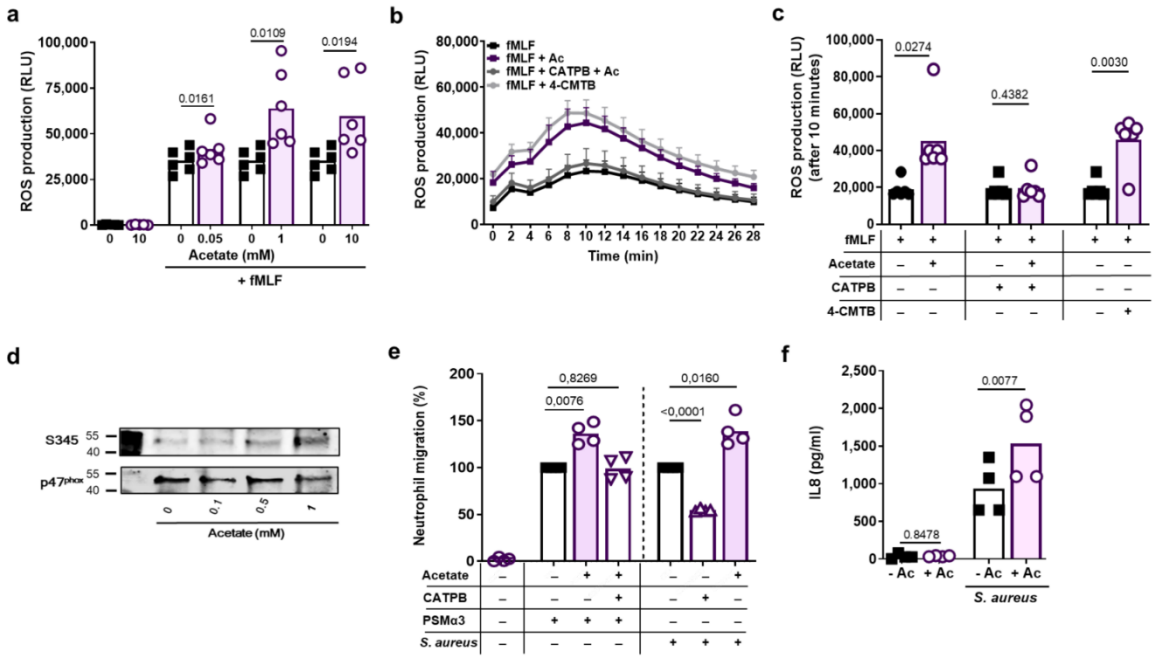

Figure 1: Acetate primes neutrophils in a GPR43-dependent manner.

Acetate enhanced the oxidative burst induced by (a) the FPR1 ligand fMLF (500 nM), which could be inhibited by the GPR43 antagonist CATPB (b). The same effect was caused by the synthetic GPR43 ligand 4-CMTB. ROS production was monitored by measuring relative luminescence units (RLU) emitted by ROS-responsive luminol (c). Incubation of neutrophils with acetate induced the priming-associated phosphorylation of the NADPH oxidase subunit p47phox at serine position 345 (S345) (d). Migration of neutrophils towards the bacteria-derived chemoattractant FPR2 ligand PSMα3 (500 nM) or towards live S. aureus cells (e), as well as release of the chemokine IL-8 in response to S. aureus challenge (both MOI of 1) were enhanced upon neutrophil priming with 1 mM acetate (Ac) (f). Data in panels a, c, e and f represent means of n=6 (a, c) and n=4 (e, f) independent experiments. Data in panel b represent mean ± SEM of n=7 independent experiments. *, $P < 0.05$; **, $P < 0.01$ ***, $P < 0.001$, significant difference versus the indicated or non-acetate treated control (0 or - Ac) as calculated by paired two-tailed Student's t test (a, c, f) or one-way ANOVA with Dunnett's multiple comparisons test (e). d shows one representative experiment out of three.

Next, we explored whether acetate sensing by GPR43 influences neutrophil migration. As for the oxidative burst, acetate alone did not induce migration of neutrophils but enhanced FPR2-dependent migration. Furthermore, neutrophil

chemotaxis elicited by *S. aureus* USA200 (34) cells or by USA200 culture filtrates could be partially inhibited by CATPB, which is in agreement with the documented secretion of substantial acetate amounts by *S. aureus* (Fig. 1e, Suppl. Fig. 2a, b) (35). Similar findings were obtained when analysing the IL-8 cytokine secretion by neutrophils after stimulation with acetate in combination with various other GPCR or with toll-like receptor (TLR) ligands. Acetate alone failed to induce IL-8 release and did not influence IL-8RA/ IL-8RB expression (Suppl. Fig. 2c) but enhanced the IL-8 secretion capacities of live serum-opsonized *S. aureus* cells or of FPR2, FPR1, TLR2, or TLR4 ligands (Fig. 1f, Suppl. Fig. 2d, e). This enhanced autocrine IL-8 release could be due to the neutrophil activation status leading to increased intracellular Ca^{2+} levels, or enhanced phagocytosis of *S. aureus*, two processes, which are known to be associated with increased IL-8 release (36, 37).

Acetate priming augments *S. aureus* phagocytosis and killing by human neutrophils

Neutrophil priming is usually associated with an increase in surface expression of opsonic receptors (38). To investigate if GPR43 ligands also have such an influence, the abundance of complement and Fc receptors on neutrophils before and after acetate stimulation was compared. In contrast to the above-described assays, acetate led to upregulation of complement receptors CD11b (CR3) and CD35 (CR1), and of Fc receptor CD16 (FcyRIII) even in the absence of other MAMPs or endogenous GPCR agonists (Fig. 2a). This response could be blocked by CATPB

indicating that it depended on GRP43 (Suppl. Fig. 2f).

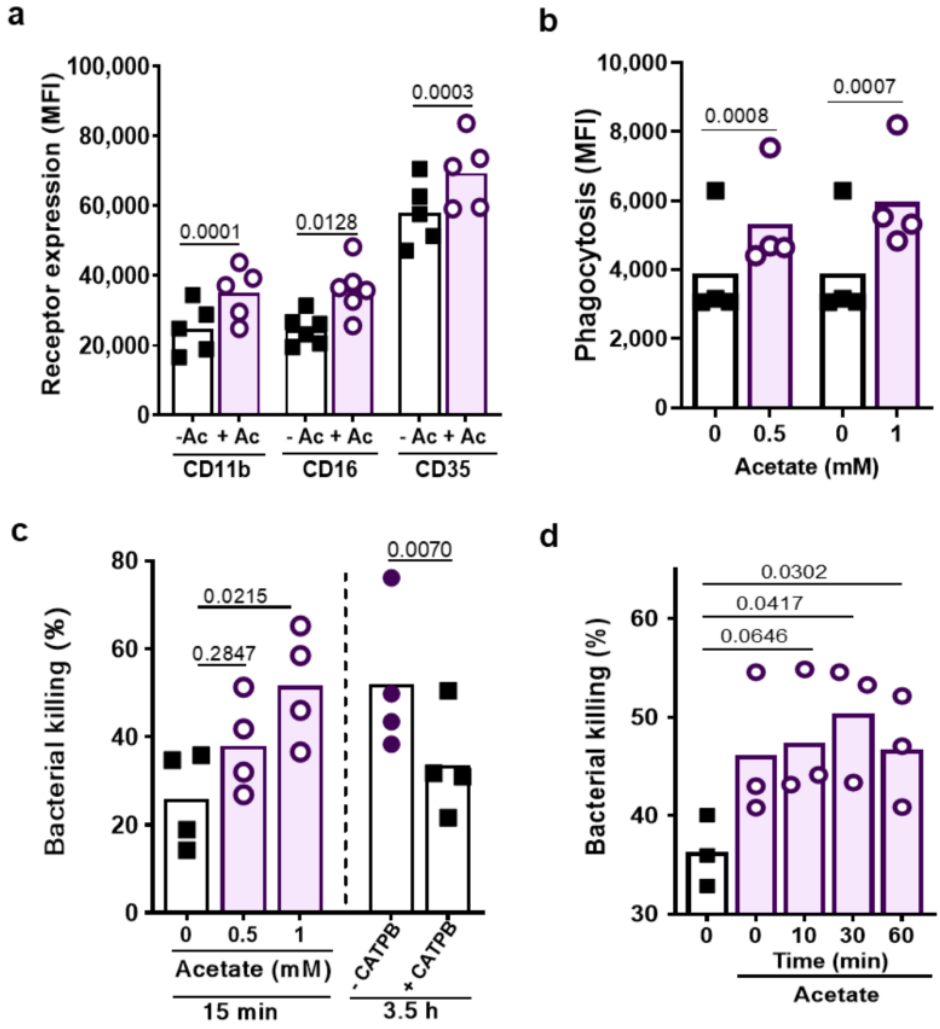

Figure 2: Acetate priming enhances phagocytosis and killing of *S. aureus* by human neutrophils.

(a) 1 mM acetate (Ac) increased the neutrophil expression of complement (CD11b and CD35) and Fcγ (CD16) receptors given as mean fluorescence intensity (MFI) measured by flow cytometry. (b) Incubation of neutrophils for 15 minutes with the indicated acetate concentrations increased the phagocytic capacity as well as (c,) the ability to kill *S. aureus* (MOI of 1) during a 15-minutes incubation period. Bacterial killing is expressed as dead vs. input bacterial counts (%). (c) CATPB-mediated GPR43 inhibition decreased the neutrophil capacity to kill *S. aureus* after 3.5 h co-incubation (MOI 1). (d) Addition of 1 mM acetate (Ac) at the indicated time points after the start of the *S. aureus* killing assay still improved the ability of neutrophils to kill bacteria. Data in panel a and c represent means from n=4, in panel b means from n=5 and in panel d means from n=3 independent experiments. *, $P < 0.05$; **, $P < 0.01$ ***, $P < 0.001$, significant difference versus the indicated condition as calculated by the paired two-tailed Student's *t* test (a, b), or one way ANOVA with Dunnett's multiple comparisons test (c and d).

Upregulation of opsonin receptors should increase the phagocytosis capacity of neutrophils. Indeed, 15-minutes pre-incubation of human neutrophils with acetate led to significantly enhanced phagocytosis of serum-opsonized *S. aureus* USA200 (Fig. 2b). This finding, together with the strongly increased oxidative burst suggested that GPR43 stimulation should improve the capacity of neutrophils to kill bacteria. Indeed, 10-min preincubation of neutrophils with acetate led to 25.7% stronger killing of serum-opsonized *S. aureus* (Fig. 2c). *S*imilar observations were made with the bacterial pathogens *Enterococcus faecalis, Listeria monocytogenesis,* and *Staphylococcus epidermidis* (Suppl. Fig. 2g) indicating that acetate priming has a general promoting impact on neutrophil phagocytosis. In agreement with the major role of NADPH oxidase in the antimicrobial activity of neutrophils, *S. aureus* killing was strongly reduced by treatment with the NADPH oxidase inhibitor diphenyleniodonium (DPI) (Suppl. Fig. 2h). When acetate was added to neutrophils at the same time as the opsonized bacteria or even 60 min later, improved killing could still be observed (Fig. 2d) suggesting that neutrophil priming via GPR43 can help to control invading pathogens even after the onset of an infection. *S. aureus* and several other bacterial species release high levels of acetate as an intermediary product of their energy metabolism (39). When live *S. aureus* cells were co-cultivated with neutrophils for 3.5 hours, they survived significantly better in the presence of the GPR43 inhibitor CATPB indicating that the sensing of *S. aureus*-produced acetate may be a prerequisite for efficient elimination of the bacteria by neutrophils (Fig. 2c). In agreement with the GPR43-dependence of acetate-promoted neutrophil *S. aureus* killing, acetate did not inhibit but even slightly improved growth of *S. aureus* (Suppl. Fig. 2i).

Intraperitoneal injection of acetate increases serum acetate levels and primes neutrophils

To analyze if acetate also primes neutrophils of mice in an *in-vivo* setting, we injected mice intraperitoneally (i.p.) with acetate dissolved in PBS or with the same volume of PBS and analyzed blood acetate levels, neutrophil surface markers, and neutrophil capacity to generate ROS six hours later (Fig. 3a). The serum of PBS-treated mice contained on average 341 ± 39.9 µM acetate. 30 min after i.p. injection of 500 mg/kg sodium acetate, the serum acetate concentration raised to 766 ± 34.8 µM (Fig. 3b). Neutrophils from acetate-treated mice showed enhanced expression of

complement receptor CD11b (CR3) and Fc receptor CD16/32 (Fig. 3c) and significantly enhanced oxidative burst after stimulation with the synthetic protein kinase C activator phorbol-12-myristat-13-acetat (PMA) six hours after infection compared to PBS-treated mice (Fig. 3d). Acetate had a significant impact on neutrophil opsonin receptor expression at six hours after acetate injection although the serum acetate concentration had already normalized at this time point (Fig. 3b). Thus, mouse neutrophils are primed by acetate in a similar way as human neutrophils and maintain the primed state for several hours.

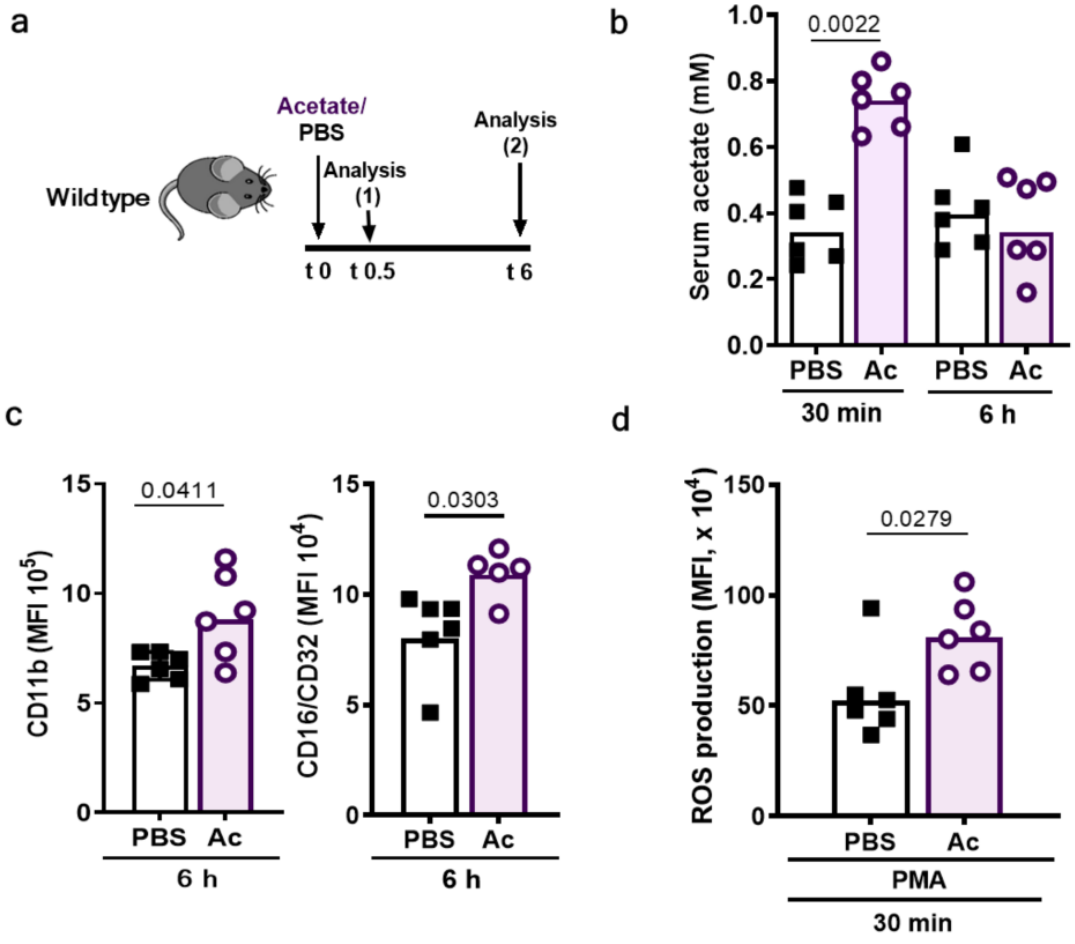

Figure 3: Intraperitoneal acetate injection increases serum acetate levels and primes neutrophils in mice.

(a) Mice received an intra-peritoneal acetate (Ac) injection (500 mg/kg) followed by analysis of blood acetate concentrations (isolated from the tail vein) and neutrophil phenotypes 30 minutes and six hours after injection. (b) Acetate (Ac) i.p. injection caused a two-fold serum acetate increase 30 minutes after injection and normal serum acetate levels were restored after six hours. (c) Neutrophils isolated from mice treated with acetate showed enhanced complement (CD11b) and Fcγ

(CD16/CD32) receptor expression compared to PBS-treated mice. (d) *In-vivo* acetate (Ac) injection caused increased ROS production upon stimulation with phorbol-12-myristat-13-acetate (PMA). Data in all panels represent geometric means from six animals. *, $P < 0.05$; **; $P < 0.01$ significant difference versus the indicated condition as calculated by Mann-Whitney-U test.

Intraperitoneal acetate treatment did not alter the basal numbers of neutrophil and monocytes, neither in the blood nor in the peritoneum (Suppl. Fig. 3a-c). However, when mice were i.p.-infected by *S. aureus* USA200 30 minutes after the animals had received acetate rather than PBS i.p., neutrophil numbers in the peritoneum were significantly increased six hours later (Fig. 4 A, B). This difference was not observed in GPR43$^{-/-}$ mice indicating that it resulted from GPR43-mediated acetate priming. Only a small fraction of the inoculated bacteria was recovered from the peritoneum after six hours (Suppl. 3d), whereas the majority had spread to the liver (Fig. 4c) and other peripheral organs (Suppl. Fig. 3d). Wild-type and GPR43$^{-/-}$ mice had comparable basic acetate concentrations in their sera (Suppl. Fig. 4a). PBS-treated wild-type mice had slightly higher peritoneal neutrophil numbers and lower *S. aureus* CFUs in the liver than GPR43$^{-/-}$ mice (Fig. 4b, c), suggesting that the basal serum concentrations of acetate led to a weak priming level in the presence of a functional GPR43, which was strongly augmented by increasing the serum acetate concentration.

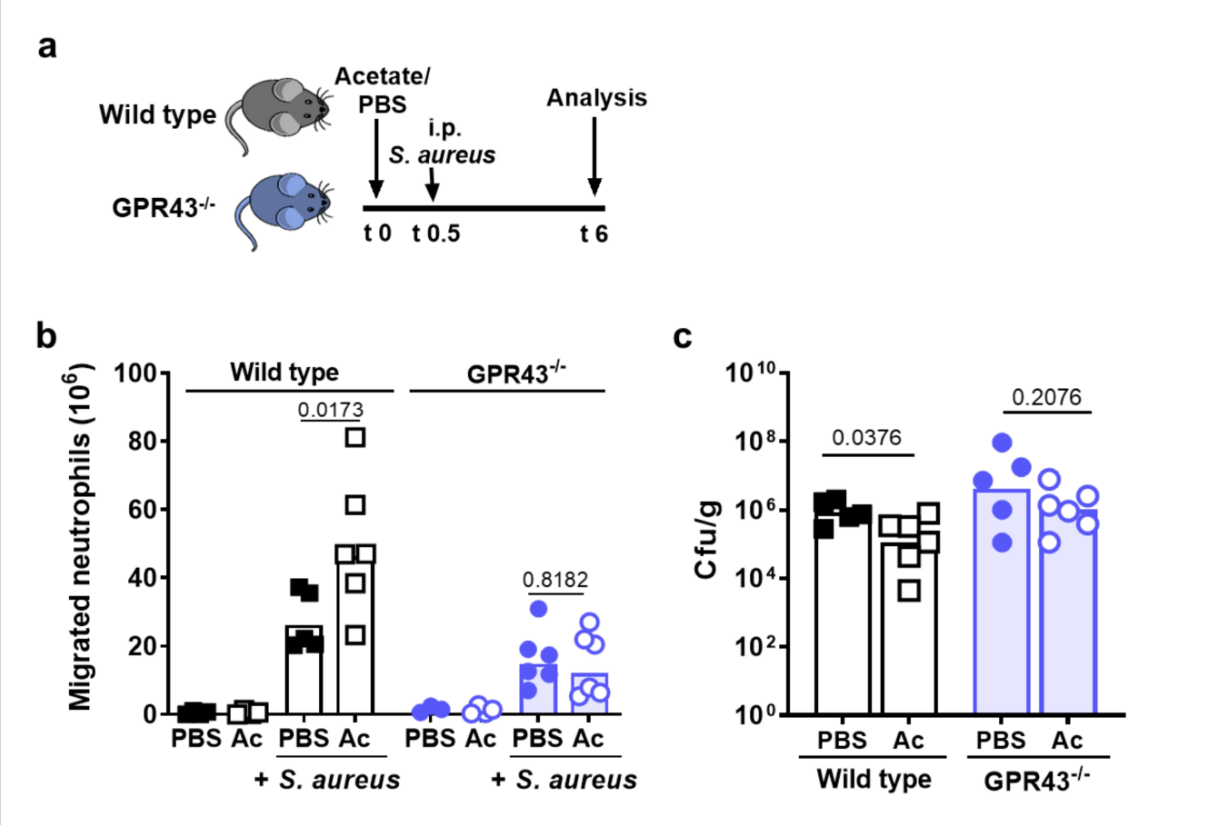

Figure 4: Intraperitoneal acetate injection enhances neutrophil influx and decreases bacterial loads in a mouse peritoneal infection model.

(a) In the murine peritonitis model, mice were pre-treated with acetate (Ac) or PBS 30 minutes prior to intra-peritoneal *S. aureus* injection. (b) Acetate (Ac) treatment resulted in enhanced $CD45^{+}Ly6G^{+}$ neutrophil migration into the peritoneum compared to PBS-treated wild-type mice (black symbols) six hours after infection. $GPR43^{-/-}$ mice (blue symbols) showed reduced overall neutrophil migration into the peritoneum with no beneficial effect of acetate treatment. (c) Acetate-treated wild-type mice showed slightly reduced bacterial loads in the liver, whereas acetate treatment of $GPR43^{-/-}$ mice did not influence bacterial loads. Data in panel b and c represent geometric means from six animals. $*P < 0.05$ significant difference versus the indicated PBS or wild-type control as calculated by Mann-Whitney-U test.

GPR43-dependent acetate priming prevents severe courses of *S. aureus* sepsis

The finding that acetate levels and neutrophil priming state were increased after i.p. acetate injection on a systemic level raised the question, whether intraperitoneal acetate injection could also help to cure disseminated bacterial infections. *S. aureus* USA200 was injected into the bloodstream of wild-type and $GPR43^{-/-}$ mice 30 min after intraperitoneal application of acetate or PBS (Fig. 5a). Whereas PBS-treated wild-type mice developed signs of severe disease and rapidly lost weight, the

acetate-treated wild-type mice were less sick and lost much less weight. In contrast, treatment of GPR43$^{-/-}$ mice with acetate did not influence weight loss (Fig. 5b, Suppl. Fig. 4b, c).

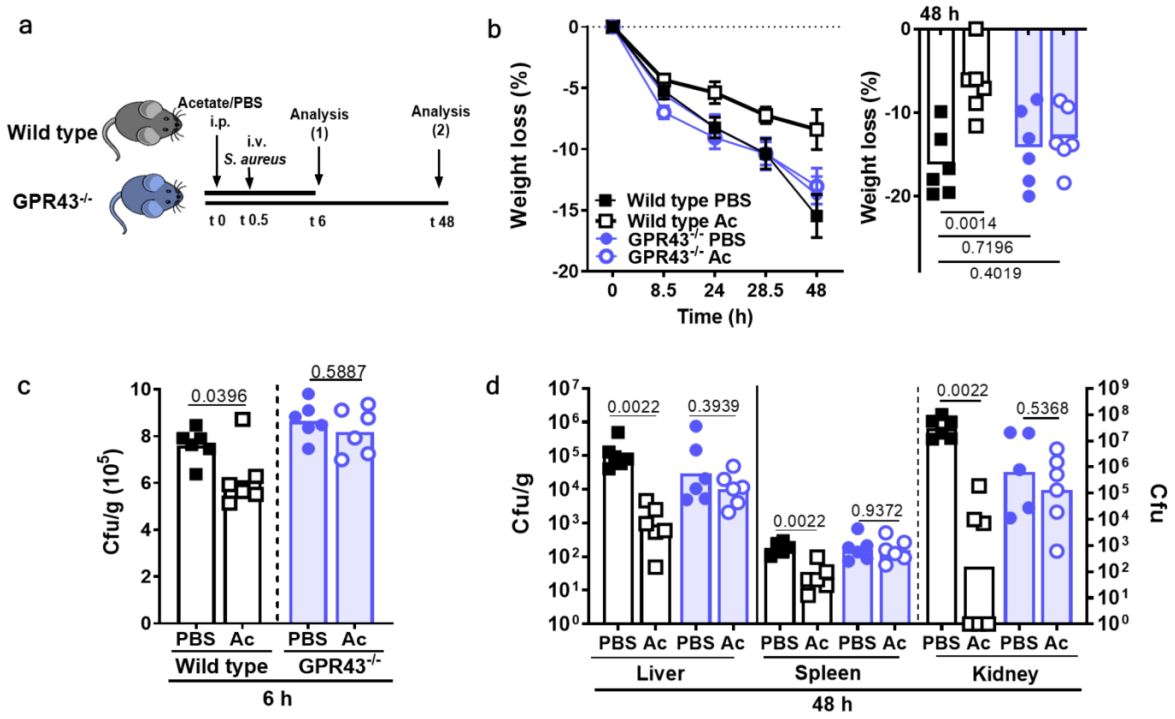

Figure 5: GPR43-dependent acetate priming is beneficial during *S. aureus* bloodstream infection.

(a) Treatment of mice with acetate (Ac) 30 minutes prior to *S. aureus* i.v. injection resulted in (b) decreased weight loss in wild-type mice (black symbols) but not in GPR43$^{-/-}$ mice (blue symbols). (c) Six hours after infection onset, bacterial loads were slightly reduced in the liver of acetate-treated wild-type mice (black), whereas acetate showed no such effect in GPR43$^{-/-}$ mice (blue). (d) After 48 hours, acetate (Ac) treatment prior to the onset of bloodstream infection resulted in drastically decreased bacterial loads in the liver, spleen, and kidney in wild-type mice, while no such difference was observed in GPR43$^{-/-}$ mice (blue). Data in b – e panels represent geometric means or geometric means ± SEM (b) from six animals. *, $P < 0.05$; **, $P < 0.01$ significant difference versus the indicated PBS control as calculated by one-way ANOVA with Dunnett's multiple comparisons test (b) and Mann-Whitney-U test (c and d).

Six hours after infection, most of the injected bacteria were found in the liver, which is in agreement with previous studies demonstrating that the liver has a primordial role in early stages of *S. aureus* bloodstream infections. Notably, the bacterial numbers were significantly lower in the livers of acetate-treated wild-type mice, while acetate had no notable effect on the *S. aureus* population in GPR43$^{-/-}$ mice indicating that

GPR43 activation contributes to bacterial clearance from the bloodstream (Fig. 5c). At 48 hours after infection, most of the bacteria had disappeared from the liver but the acetate-treated animals still had significantly lower *S. aureus* numbers compared to the mock-treatment in the liver (Fig. 5d). Whereas a similar situation was found in the spleen, the vast majority of the bacteria could be isolated from the kidneys. Here, the i.p. application of acetate led to a five-orders-of-magnitude reduced *S. aureus* density in wild-type animals (Fig. 5d). Again, acetate had no significant impact on bacterial numbers in GPR43$^{-/-}$ mice indicating that the strong acetate-mediated improvement of the infection outcome depended on GPR43.

I.p. acetate treatment had no effect on the basal cytokine levels 30 min or six hours after application (Suppl. Fig. 5a, b). However, acetate-treated mice had slightly increased serum levels of the pro- and anti-inflammatory cytokine IL-6 (46 ± 10 µg/ml) and of the chemokines MIP-2 (CXCL2; 53 ± 4 µg/ml) and MCP-1 (CCL2; 590 ± 80 µg/ml) compared to PBS-treated mice six hours after infection, probably as a consequence of the GPR43-dependent boost of anti-infective host defense (Fig. 6a). Likewise, neutrophils from acetate-treated mice exhibited increased intrinsic ROS production (Fig. 6c). In contrast, acetate application had no impact on serum cytokine and chemokine levels of GPR43$^{-/-}$ mice (Fig. 6a). At 48 hours after infection, the differences in cytokine patterns between acetate and PBS treatment had reversed. The recovery of acetate-treated wild-type animals was reflected by significantly lower concentrations of the cytokines IL-6 and TNF-α, two major mediators of sepsis-associated exuberant inflammation (7), which were at high levels in the mock-treated wild-type animals (IL-6, 194,6 ± 29 µ/ml ;TNF-α, 76 ± 10 µg/ml) (Fig. 6b, Suppl. Fig. 5c). Likewise, the chemokines MIP-2, MCP-1, and KC were reduced in acetate-treated wild-type animals. The lack of any significant differences in cytokine or chemokine levels between acetate or mock-treated GPR43$^{-/-}$ mice confirmed that the presence of both, GPR43 and sufficient amounts of its agonist acetate, can prevent severe courses of sepsis in mice (Fig. 6b).

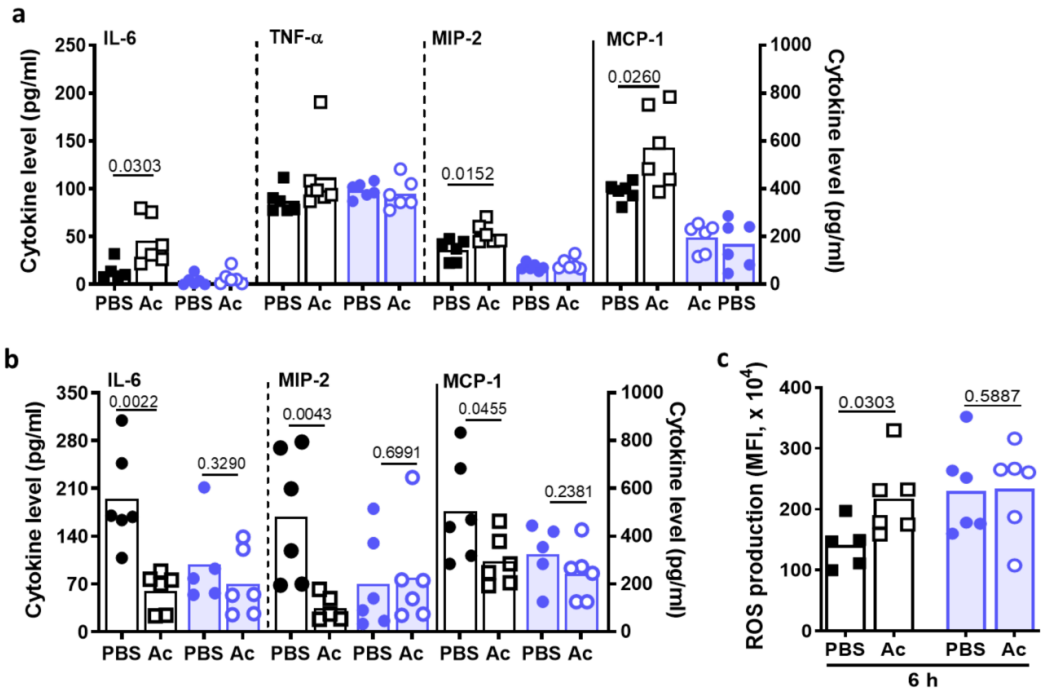

Figure 6: Intraperitoneal acetate priming promotes cytokine and ROS release during mouse bloodstream infection.

(a) Treatment of wild-type mice (black symbols) with acetate prior to an *S. aureus* bloodstream infection, i.v. injection induces an initial increase in serum IL-6, MIP-2 and MCP-1 levels measured after six hours. (b) 48 hours after induction of a bloodstream infection, the cytokine levels in acetate-treated (Ac) wild-type but not in GPR43$^{-/-}$ mice were significantly decreased compared to PBS-treated mice, which is in line with the decreased disease severity. (c) This was accompanied by increased intrinsic ROS production by neutrophils from acetate-treated (Ac) wild-type mice, while acetate treatment had no such effect in GPR43$^{-/-}$ mice (blue symbols). Data in all panels represent geometric means from six animals. *, $P < 0.05$; **, $P < 0.01$ significant difference versus the indicated PBS control as calculated by Mann-Whitney-U test.

Acetate improves sepsis outcome independently of the application route and even when applied after the onset of infection

To analyse if also oral application of acetate could improve sepsis outcome, acetate was added to the drinking water (neutralized to avoid rejection by mice), five days before mice were infected i.v. with S. aureus (Suppl. Fig. 6a). 48 hours later we found significant less bacterial numbers in the spleen of acetate-treated wild-type mice compared to the control mice. A similar trend was seen in the kidneys, which, however, did not reach significance (Suppl. Fig. 6b). Notably, oral acetate administration led to significantly reduced weight loss in case of the acetate-fed wild-

type mice, but no such influence of acetate on GPR43$^{-/-}$ following infection by S. aureus compared to control-fed animals (Suppl. Fig. 6c, d). Only acetate-fed animals had increased serum acetate levels, which reached concentrations of 580 +/- 150 µM (Suppl. Fig. 6e). These data indicate that acetate can prevent systemic S. aureus infections in similar ways if administered orally or intraperitoneally.

The fact that the severe course of sepsis could be prevented by the presence of sufficiently high acetate concentrations in serum at the time point of S. aureus entry into the bloodstream raised the question, whether an interventional application of acetate after infection onset could still help to treat the disease. To assess this possibility wild-type and GPR43$^{-/-}$ mice were i.v.-infected with S. aureus and were six hours later treated via the intraperitoneal route with acetate or PBS (Fig. 7a). Already after two days of infection, the acetate treatment showed a slightly positive impact on the infection course (Suppl. Fig. 6f). To monitor the full course of infection, the infection period was extended to four days and a lower infection dose was used than in the previous experiments to avoid excessive weight loss and mortality. Indeed, acetate-treated wild-type mice lost weight only during the first day but rapidly gained weight at later time points after infection, whereas PBS-treated mice did not recover from sepsis (Fig. 7b). This was accompanied by decreased bacterial loads in the liver of acetate vs. PBS-treated mice at four days after infection (Fig. 7c). Together, these date indicate that the application of acetate could be an effective treatment option for sepsis even after the onset of an infection.

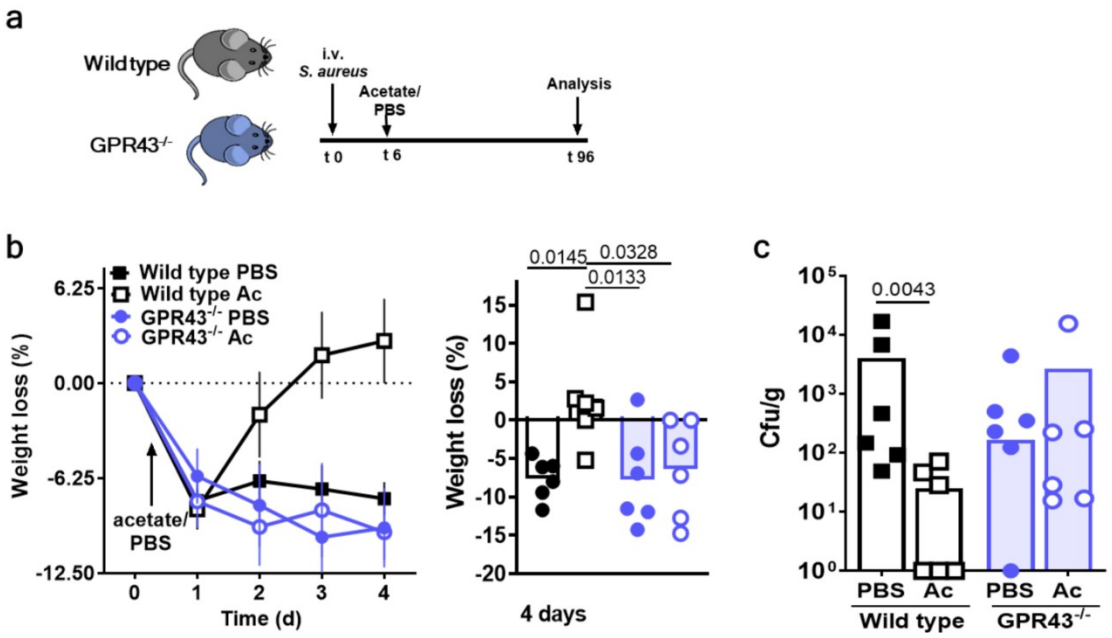

Figure 7: Acetate treatment after infection onset improves sepsis outcome.
(a) Mice were treated with acetate (Ac) in PBS or an equal volume of PBS six hours after the onset of an *S. aureus* bloodstream infection, and septic wild-type (black symbols) and GPR43$^{-/-}$ (blue symbols) mice were monitored for four days. (b) Acetate-treated wild-type mice regained weight more rapidly than PBS-treated wild-type mice. (c) This was accompanied by a reduced bacterial load in the liver when compared to PBS-treated septic mice. GPR43$^{-/-}$ mice displayed similar bacterial loads in the liver compared to PBS-treated wild-type mice (c). Acetate (Ac) treatment showed no effect in GPR43$^{-/-}$ mice. Data in panel b - d represent geometric means or geometric means ± SEM (b) from six animals. *, $P < 0.05$; **, $P < 0.01$ significant difference versus the indicated condition as calculated by one-way ANOVA with Dunnett's multiple comparisons test (b) or by Mann-Whitney-U test (c).

Discussion

The pathophysiology of sepsis involves both, hyper-inflammatory and anti-inflammatory dysfunctions, which shape the course of the diseases in different phases and in different tissues. The dichotomy of these processes has made it extraordinarily difficult to identify suitable molecular targets for the prevention and therapy of sepsis and dozens of clinical trials with multiple immunomodulatory drugs have shown no efficacy or led even to aggravation of the disease (8). Neutrophils are major players in the immunopathology of sepsis and either exuberant, persistent activation or dampened, insufficient antimicrobial responses have been identified as major reasons for the failure of neutrophils to clear bloodstream infections (40, 41). Neutrophils can be stimulated by microbial or endogenous agonists in multiple ways,

leading to different levels of priming or activation (42). A high percentage of primed neutrophils can prevent bacterial infections even in neutropenic patients (43, 44). The extent and duration of priming may be crucial for the capacity of neutrophils to ameliorate or aggravate the disease. Our study demonstrates that activation of neutrophils via GPR43 leads to transient priming and improved capacities to ingest and kill bacterial invaders, which was reflected by substantially better resolution of sepsis in a mouse infection model. GPR43 has been extensively studied in the context of intestinal microbiome-host interaction (45) but has not been added to the list of potential targets for the treatment of sepsis. Nevertheless, a retrospective study has demonstrated that increased GPR43 expression in whole-blood samples of septic patients correlates with increased sepsis survival (23), and GPR43 activation has been found to be beneficial for the treatment of lung infections (46, 47).

GPR43 seems to have a crucial role in neutrophil immune responses since it is highly expressed on human and mouse neutrophils, which distinguishes it from the two additional SCFA receptors GPR41 and GPR40 (20) that are predominantly found on enteroendocrine cells, enteric neurons, pancreatic beta cells, and in various regions of the human brain (48). We demonstrate that acetate treatment primes neutrophils in a GPR43-dependent manner leading to enhanced neutrophil chemotaxis, bacterial killing as well as improved resolution of inflammation and sepsis outcome. Among the three GPR43 agonists, acetate, propionate, and butyrate, only acetate can usually be found in the blood at concentrations near the effective concentration of approximately 0.5 mM (49). However, serum acetate concentrations vary strongly and may lead to full GPR43 priming only in certain instances. Nevertheless, even average serum acetate amounts may cause a basal level of neutrophil priming even in the absence of acetate injection. In accord with this assumption, we found that wild-type mice had a general tendency to cope better with *S. aureus* sepsis than GPR43$^{-/-}$ mice. Increasing the serum acetate concentration by i.p. injection or addition to drinking water of sodium acetate had a transient, yet profound impact on neutrophil ROS production, serum cytokine levels, and bacterial clearance in peripheral organs. Some incidental reports support the positive role of acetate in the control of infections. Local SCFA treatment has been found to reduce the diameter of MRSA skin abscesses in mice (50). Moreover, clinical data have shown that septic patients treated with volume substitutes that contain acetate show less mortality than patients treated with substitutes lacking acetate (51).

Multiple processes can influence the concentration of acetate in human serum and other body fluids. The major acetate sources seem to be food intake and intestinal bacterial microbiome members, which produce SCFAs as fermentation products (52). Under certain conditions such as phases of high alcohol consumption (26), starvation, or diabetes also the liver produces acetate (48). Moreover, some pathogens including *S. aureus* produces acetate during substrate level phosphorylation in case of carbon overflow (53, 54), suggesting that GPR43 might activate neutrophils in response to local bacterial metabolic activity. A recent study found that neutrophils from GPR43$^{-/-}$ mice were less capable of clearing bacterial pneumonia than wild-type mice even when the animals had not been treated with acetate (46). It is possible that the local acetate release by the pathogen (55) and specific dietary conditions led to a sufficiently high acetate concentration in the lung to allow GPR43-dependent host defence even in the absence of interventional acetate treatment while during systemic infection the bacteria-produced acetate cannot accumulate locally.

Our study indicates that the severity of sepsis in mice depends critically on transient neutrophil priming, which can be shaped by elevating serum acetate concentrations. Acetate had a strong positive impact on *S. aureus* sepsis if applied before or after the onset of infection and even if it was orally applied, indicating that it could be of used in a prophylactic or therapeutic fashion. A recently reported synthetic GPR43 agonist that enhanced the response of human neutrophils to acetate could become an attractive lead compound for future GPR43-targeting drugs (56). Since acetate priming enabled neutrophils to better eliminate several unrelated bacteria, GPR43-based interventions might be of help for a wide range of sepsis-causing pathogens. It has been shown that the intestinal microbiome compositions play a central role in sepsis (57). One of the crucial hallmarks of a health-promoting microbiome dominated by Firmicutes and Bacteroidetes is the production of high amounts of SCFA such as acetate (58, 59). The combined effects of artificial nutrition and sustained exposure to antibiotics in severely ill patients can lead to the disruption of a health-promoting gut microbiome (60). Fecal microbiome transplantation (FMT) as a potential therapy could be an option. However, such an approach needs extreme caution as a recent report demonstrated the transmission of multi-drug-resistant organism via FMT, which subsequently caused lethal bacteremia (61). The precise

optimization of microbiome composition to increase the content of SCFA-producing commensals would be preferable but will require extensive research efforts.
Our data suggest that the direct application of acetate to patients receiving enteral nutrition or i.v. in case of parenteral nutrition could become a therapeutic option also in non-invasive ways by supplying acetate-rich food or a fiber-rich diet, which enhances the production of SCFAs by fermenting gut microbiota members such as Firmicutes and Actinobacteria species (62).

Methods

Material

Sodium acetate (Sigma Aldrich) stock solution was pH-adjusted to 7.2 ± 0.5 in order to avoid unspecific cellular responses to altered pH values. Formylated PSMα3 (fMEFVAKLFKFFKDLLGFLGNN) peptide was kindly provided by S. Stevanović (University Tubingen). N-Formyl-Met-Leu-Phe (fMLF) and phorbol 12-myristate 13-acetate (PMA) were purchased from Sigma Aldrich, P_2CysK_4 and LPS from Invivogen, rhC5a from R&D, and platelet-activating factor (PAF) from Biomol. The GPR43 agonist 4-CMTB and the GPR43 antagonist CATPB were synthesized by EMC (Tübingen).

Bacteria

S. aureus stain USA200 (UAMS-1) was kindly provided by K. Bayles (University of Nebraska) (34). *L. monocytogenes* (ATCC19118), *E. faecalis* (BK4684) (63) and *S. epidermidis* (Tü3298) (64) were utilized for neutrophil killing experiments. All bacteria were inoculated at OD_{600} 0.1 in tryptic soy both (TSB) or lysogeny broth (LB, only *S. epidermidis*) and grown for four hours under aerobic conditions (medium to flask ratio 1:5) followed by three washing steps with PBS. For optimal recognition by neutrophils, bacteria were opsonized with 10% pooled normal human serum (NHS) for 60 min and, if not otherwise mentioned, bacteria and neutrophils were used at a ratio of 1:1 (MOI of 1). Bacterial culture filtrates were obtained by centrifugation and subsequent filtration through a 0.2-µm pore size filters (Merck).

Neutrophil isolation

Human neutrophils were isolated by standard ficoll/histopaque gradient centrifugation (14). If not otherwise mentioned neutrophils were suspended in RPMI with 5% human serum albumin, 2% HEPES, and 1% pyruvate. For inhibition of GPR43, neutrophils were incubated with 2.5 µM CATPB for 10 minutes. Blood was kindly donated by healthy volunteers (age 20-50) upon informed consent.

ROS production and chemotaxis

ROS production by human neutrophils was measured over a time period of one hour by monitoring luminol-amplified chemiluminescence using 282 µM luminol (Sigma Aldrich). If not otherwise mentioned, neutrophils were incubated with 1 mM acetate for 10 minutes and subsequently stimulated with fMLF (500 nM), PSMα3 (500 nM), PAF (2 µM), C5a (100 ng/ml) or opsonized live *S. aureus* bacteria (MOI 2).

For the analysis of the chemotactic capacities of different stimuli, neutrophils were loaded with 3 µM 2',7'-bis-(2-carboxyethyl)-5-(and-6)-carboxyfluorescein, acetoxymethyl ester (BCECF-AM, Molecular Probes). The migration along gradients of the indicated stimuli were monitored using 3-µm polycarbone trans-well membranes (Greiner). The chemotactic index was calculated as the percentage of total cells migrated to the lower chamber and corrected by the buffer control. PSMα3 and fMLF were applied at a concentrations of 375 nM and 10 nM, respectively and live opsonised *S. aureus* USA200 with an MOI of 1. The GPR43 agonist 4-CMTB (EMC, Tübingen) was used at a final concentration of 1 µM.

Western Blot

Neutrophils were incubated with the indicated acetate concentrations for 15 minutes followed by lysis with immunoprecipitation (IP)-lysis buffer (ThermoFisher). The subsequent immunoprecipitation was performed using the Dynabead Protein G IP Kit (ThermoFisher). Briefly, a mouse anti-human $p47^{phox}$–specific monoclonal antibody (BD Bioscience) was bound to the protein G beads for 15 minutes under constant shaking (350 rpm). After washing, dynabeads were added to the cell lysis and incubated for 15 minutes followed by washing, addition of elution and SDS-PAGE sample buffer, and denaturation for 5 minutes at 99°C. Samples were subjected to a standard 4-20%-SDS PAGE gel (BioRad). Proteins were blotted to a nitrocellulose

membrane and $p47^{phox}$ and $p47^{phox}$ S345 were visualized using mouse anti-human $p47^{phox}$ (BD) and rabbit anti-human p47phox S345 (Invitrogen) antibodies. Secondary antibodies were IRDye 680CW anti-rabbit and IRDye 800CW anti-mouse from Licor. Protein bands were detected with the Licor Odyssey CLx.

Surface receptor analysis and phagocytosis

Neutrophils were stimulated for 60 minutes with 1 mM acetate, followed by 45 minutes staining with antibodies directed against the different surface receptors. As positive control for analysis of IL-8 receptor downregulation, 250 nM fMLF was used. Anti-CD35-PE (clone E11, Miltenyi), anti-CD16-PE (clone 3G8, BD Bioscience), anti-CD11b-PE (clone ICRF44, BD Bioscience), anti-hCXCR1/IL8-RA-PE (clone 42705, R&D) and anti-hCXCR2-RB-PE (clone 242216, R&D) were used at a 1:40 dilution (Suppl. Fig. 7a). Prior to measurement with the FACSCalibur (BD), neutrophils were fixed with 3.7% formaldehyde for 20 minutes.

For the phagocytosis assay, bacteria from an overnight culture were washed and stained with 10 µM CFSE (Sigma Aldrich) for 60 minutes. CFSE-stained bacteria were opsonized for 60 minutes with 10% human pooled serum (University Hospital Tübingen). Neutrophils were pre-incubated with the indicated acetate concentration for 30 minutes before incubation with bacteria at an MOI of 1 for further 30 minutes. Neutrophils were fixed with 3.7% formaldehyde for 20 minutes prior to measurement with the FACSCalibur (BD). This assay measures in principle both, extracellular, neutrophil-adherent and intracellular bacteria. However, our previous control experiments using an agent that quenches extracellular fluorescence have demonstrated that the vast majority of neutrophil-associated opsonized *S. aureus* are indeed intracellular after only a few seconds (65).

Bacterial killing

Bacteria from a four-hour culture grown in TSB were washed and opsonized with 10% pooled human serum (University Hospital Tübingen) for 60 minutes at 37°C. Neutrophils were stimulated with the indicated concentration of acetate or buffer for 30 minutes prior or post incubation with bacteria (MOI of 1). For inhibition of the NADPH oxidase, neutrophils were pre-incubated with 5 µM dibenziodolium chloride (DPI) for 20 min prior to incubation with bacteria. The numbers of surviving bacteria

were detected by determination of the colony-forming units (CFUs) per ml. Bacterial survival was calculated in relation to a bacterial control without neutrophils.

Cytokine detection

The release of IL-8 from neutrophils was measured with a human IL-8/CXCL8 ELISA Kit (R&D). Primary neutrophils were stimulated with 1 or 10 mM acetate 30 minutes prior to incubation with the indicated secondary stimuli for further 4.5 hours. Stimuli were used at the following concentrations: PSMα3 500 nM; fMLF 500 nM; P_2Cysk_4 200 ng/ml; LPS 100 nM; opsonized USA200 bacteria at MOI of 1. Human IL-8 detection in the cellular supernatant was performed according to the IL-8 ELISA vendor's manual. Cytokines in mouse serum were detected using the Bioplex Mouse Cytokine Assay (BioRad) and BioRad Multiplex Instrument.

Mouse infection assay

All experimental procedures involving mice were carried out according to protocols approved by the Animal Ethics Committees of the Regierungspräsidium Tübingen (IMIT1/17 and IMIT1/18). $Gpr43^{-/-}$ mice were kindly provided by Stephan Offermanns and have been previously described (66) and bred in the animal facility of the University Hospital of Tübingen. C57BL/6N mice (Envigo/Netherlands) were used as wild-type control mice. Mice were bred under specific pathogen-free conditions under 22°C, 50%-55% relative humidity and 12 h/12 h light/dark cycle conditions.

For *in-vivo* analysis of the acetate effect on neutrophils, six to eight weeks-old female C57BL/6N mice were i.p. injected with 500 mg/kg sodium acetate in PBS (pH 7.2) or with PBS (pH 7.2). 30 minutes after injection, blood was drawn to analyse serum acetate concentrations, blood leukocyte counts, cytokine levels, and ROS production by leukocytes. ROS production was determined in whole blood by staining with 5 µM DCFDA (Sigma Aldrich) for 10 minutes prior to erythrocyte lysis using a solution of 155 mM NH_4Cl, 10 mM $KHCO_3$, and 0.1 mM EDTA with a pH of 7.4. After DCFDA incubation, neutrophils were stimulated with RPMI or 200 nM PMA for 10 minutes. Serum acetate levels were measured using the Acetate Colorimetric Assay Kit (Sigma Aldrich). Blood was centrifuged for 10 minutes with 500 g to obtain mouse serum. In order to decrease cell debris, the mouse sera were cleared using a 10-kDa centrifugation cartridge. The acetate measurement was performed according to the vendors' instructions. Blood leucocyte counts were determined by antibody staining

and subsequent flow cytometry using a FACS LSR Fortessa X-20 (BD). Neutrophils were stained with Ly6G (APC, clone REA526) and CD45 (APC or PE, clone REA737, monocytes with CD14 (PE, clone REA934) and CD45 (APC, clone REA526) (all Miltenyi). For the cytokine detection, mouse blood was obtained by cardiac puncture and incubation with heparin for 30 minutes. Serum was gained by centrifugation and was rapidly frozen at -80°C before analysis with a Bio-plex Mouse Cytokine Assay (BioRad) according to the vendor's instruction. Briefly, mouse sera were diluted 1 to 4 and measured using a Bio-plex Pro Mouse Cytokine 8-plex Assay kit including TNF-alpha, MIP-2, MCP-1 and IL-6.

Six hours after acetate or PBS treatment, mice were euthanized and the surface receptor expression of peripheral blood leukocytes was determined. For this purpose, erythrocytes were lysed and leukocytes were stained with monoclonal antibodies specific for mouse CD45, Ly6G (APC, clone REA526), CD14 (PE, clone REA934), CD16/32 (PE, clone REA370), or CD11b (PE, clone REA592) (all Miltenyi). Ly6G was used as neutrophil marker (Suppl. Fig.7b). The staining was analysed by a FACS LSR Fortessa X-20 (BD).

In the mouse sepsis model, 1 x 10^7 (48h) or 2.5 x 10^6 (4 days) colony-forming units (cfu) of *S. aureus* USA200 were injected intra-venously into six to eight-weeks old female C57BL/6N wild-type or GPR43$^{-/-}$ mice. Acetate treatment occurred 30 minutes prior or six hours after *S. aureus* infection by i.p. injection of 500 mg/kg sodium acetate in PBS or the same volume of PBS. Six hours, 48 hours, or four days after infection, mice were euthanized with CO_2. Subsequently, CFUs in organs were determined by plating serial dilutions on agar plates and leukocytes were stained for ROS production and receptor expression as described above. Leukocyte staining was determined with a FACS LSR Fortessa X-20 (BD). For the cytokine detection mouse serum was obtained and rapidly stored at -80°C before analysis with a Bioplex Mouse Cytokine Assay (BioRad) according to vendors' instruction.

For the mouse peritonitis model, six- to eight- weeks-old female C57BL/6N wild-type and GPR43$^{-/-}$ mice were treated with 500 mg/kg acetate in PBS or PBS. 30 minutes after treatment, 5 x 10^8 CFUs of *S. aureus* USA200 were injected in the peritoneum. At six hours after infection mice were euthanized with CO_2 and peritoneal exudates were collected and leukocytes stained as described above. The numbers of immigrated cells were detected by counting in the peritoneal exudates.

For the non-invasive acetate application model, six- to eight weeks-old female C57BL/6N wild-type and GPR43$^{-/-}$ mice were fed for 7 days with 150 mM sodium acetate (pH 7.3) or 150 mM sodium chloride (control) in drinking water. Mice were given *ad-libidum* access to drinking water. Five days after treatment begin, 1 x 10^7 CFUs of *S. aureus* USA200 were injected i.v. to induce sepsis. 48 hours or four days after infection, mice were euthanized with CO_2. Subsequently, *S. aureus* CFUs in organs were determined by plating serial dilutions on agar plates.

Statistics and Reproducibility

Statistical analysis was performed using Graph Pad Prism 8.0. (GraphPad Software, La Jolla, USA). Normal distributions were analyzed by two-tailed Student's t test or Mann-Whitney-U test to compare two data groups unless otherwise stated. For comparison of more than two data groups, one-way ANOVA with Dunnett's multiple comparisons test was used. For each figure, the replicate number n is indicated in the figure legend and represents the number of independently performed biological replicates.

Data availability

The authors declare that the main data supporting the findings of this study are available within the article and its Supplementary Information files (Supplementary Data 1). All other data are available from the corresponding author on reasonable request.

References

1. E. Tacconelli *et al.*, Surveillance for control of antimicrobial resistance. *Lancet Infect Dis* **18**, e99-e106 (2018).
2. K. E. Rudd *et al.*, Global, regional, and national sepsis incidence and mortality, 1990-2017: analysis for the Global Burden of Disease Study. *Lancet* **395**, 200-211 (2020).
3. D. C. Angus *et al.*, Epidemiology of severe sepsis in the United States: analysis of incidence, outcome, and associated costs of care. *Crit Care Med* **29**, 1303-1310 (2001).

4. A. S. Lee *et al.*, Methicillin-resistant Staphylococcus aureus. *Nat Rev Dis Primers* **4**, 18033 (2018).
5. S. Y. Tong, J. S. Davis, E. Eichenberger, T. L. Holland, V. G. Fowler, Jr., Staphylococcus aureus infections: epidemiology, pathophysiology, clinical manifestations, and management. *Clin Microbiol Rev* **28**, 603-661 (2015).
6. H. S. Sader, M. Castanheira, J. M. Streit, R. K. Flamm, Frequency of occurrence and antimicrobial susceptibility of bacteria isolated from patients hospitalized with bloodstream infections in United States medical centers (2015-2017). *Diagn Microbiol Infect Dis* **95**, 114850 (2019).
7. I. Rubio *et al.*, Current gaps in sepsis immunology: new opportunities for translational research. *Lancet Infect Dis* **19**, e422-e436 (2019).
8. R. Davies, K. O'Dea, A. Gordon, Immune therapy in sepsis: Are we ready to try again? *J Intensive Care Soc* **19**, 326-344 (2018).
9. S. D. Kobayashi, N. Malachowa, F. R. DeLeo, Neutrophils and Bacterial Immune Evasion. *J Innate Immun* **10**, 432-441 (2018).
10. H. L. Malech, F. R. Deleo, M. T. Quinn, The role of neutrophils in the immune system: an overview. *Methods Mol Biol* **1124**, 3-10 (2014).
11. K. Futosi, S. Fodor, A. Mocsai, Neutrophil cell surface receptors and their intracellular signal transduction pathways. *Int Immunopharmacol* **17**, 638-650 (2013).
12. E. Weiss, D. Kretschmer, Formyl-Peptide Receptors in Infection, Inflammation, and Cancer. *Trends Immunol* **39**, 815-829 (2018).
13. N. W. M. de Jong, K. P. M. van Kessel, J. A. G. van Strijp, Immune Evasion by Staphylococcus aureus. *Microbiol Spectr* **7** (2019).
14. D. Kretschmer *et al.*, Human formyl peptide receptor 2 senses highly pathogenic Staphylococcus aureus. *Cell Host Microbe* **7**, 463-473 (2010).
15. T. Lammermann, W. Kastenmuller, Concepts of GPCR-controlled navigation in the immune system. *Immunol Rev* **289**, 205-231 (2019).
16. D. A. Bloes, D. Kretschmer, A. Peschel, Enemy attraction: bacterial agonists for leukocyte chemotaxis receptors. *Nat Rev Microbiol* **13**, 95-104 (2015).
17. J. El-Benna *et al.*, Priming of the neutrophil respiratory burst: role in host defense and inflammation. *Immunol Rev* **273**, 180-193 (2016).
18. K. L. Vogt, C. Summers, A. M. Condliffe, The clinical consequences of neutrophil priming. *Curr Opin Hematol* **26**, 22-27 (2019).

19. X. F. Shen, K. Cao, J. P. Jiang, W. X. Guan, J. F. Du, Neutrophil dysregulation during sepsis: an overview and update. *J Cell Mol Med* **21**, 1687-1697 (2017).
20. E. Le Poul *et al.*, Functional characterization of human receptors for short chain fatty acids and their role in polymorphonuclear cell activation. *J Biol Chem* **278**, 25481-25489 (2003).
21. M. H. Kim, S. G. Kang, J. H. Park, M. Yanagisawa, C. H. Kim, Short-chain fatty acids activate GPR41 and GPR43 on intestinal epithelial cells to promote inflammatory responses in mice. *Gastroenterology* **145**, 396-406 e391-310 (2013).
22. Z. Ang, J. L. Ding, GPR41 and GPR43 in Obesity and Inflammation - Protective or Causative? *Front Immunol* **7**, 28 (2016).
23. Z. J. Carr *et al.*, Increased whole blood FFA2/GPR43 receptor expression is associated with increased 30-day survival in patients with sepsis. *BMC Res Notes* **11**, 41 (2018).
24. R. H. Richards, J. A. Dowling, H. J. Vreman, C. Feldman, M. W. Weiner, Acetate levels in human plasma. *Proc Clin Dial Transplant Forum* **6**, 73-79 (1976).
25. G. Milligan, B. Shimpukade, T. Ulven, B. D. Hudson, Complex Pharmacology of Free Fatty Acid Receptors. *Chem Rev* **117**, 67-110 (2017).
26. H. Nuutinen, K. Lindros, P. Hekali, M. Salaspuro, Elevated blood acetate as indicator of fast ethanol elimination in chronic alcoholics. *Alcohol* **2**, 623-626 (1985).
27. C. D. Tollinger, H. J. Vreman, M. W. Weiner, Measurement of acetate in human blood by gas chromatography: effects of sample preparation, feeding, and various diseases. *Clin Chem* **25**, 1787-1790 (1979).
28. M. A. Vinolo *et al.*, Short-chain fatty acids stimulate the migration of neutrophils to inflammatory sites. *Clin Sci (Lond)* **117**, 331-338 (2009).
29. M. Li, B. van Esch, P. A. J. Henricks, G. Folkerts, J. Garssen, The Anti-inflammatory Effects of Short Chain Fatty Acids on Lipopolysaccharide- or Tumor Necrosis Factor alpha-Stimulated Endothelial Cells via Activation of GPR41/43 and Inhibition of HDACs. *Front Pharmacol* **9**, 533 (2018).
30. Y. Wang *et al.*, The first synthetic agonists of FFA2: Discovery and SAR of phenylacetamides as allosteric modulators. *Bioorg Med Chem Lett* **20**, 493-498 (2010).

31. J. H. Cummings, E. W. Pomare, W. J. Branch, C. P. Naylor, G. T. Macfarlane, Short chain fatty acids in human large intestine, portal, hepatic and venous blood. *Gut* **28**, 1221-1227 (1987).
32. L. B. Bindels, E. M. Dewulf, N. M. Delzenne, GPR43/FFA2: physiopathological relevance and therapeutic prospects. *Trends Pharmacol Sci* **34**, 226-232 (2013).
33. P. M. Dang *et al.*, A specific p47phox -serine phosphorylated by convergent MAPKs mediates neutrophil NADPH oxidase priming at inflammatory sites. *J Clin Invest* **116**, 2033-2043 (2006).
34. M. Sassi, D. Sharma, S. R. Brinsmade, B. Felden, Y. Augagneur, Genome Sequence of the Clinical Isolate Staphylococcus aureus subsp. aureus Strain UAMS-1. *Genome Announc* **3** (2015).
35. G. A. Somerville, R. A. Proctor, At the crossroads of bacterial metabolism and virulence factor synthesis in Staphylococci. *Microbiol Mol Biol Rev* **73**, 233-248 (2009).
36. S. Brechard, J. L. Bueb, E. J. Tschirhart, Interleukin-8 primes oxidative burst in neutrophil-like HL-60 through changes in cytosolic calcium. *Cell Calcium* **37**, 531-540 (2005).
37. E. Weiss, K. Schlatterer, C. Beck, A. Peschel, D. Kretschmer, Formyl-Peptide Receptor Activation Enhances Phagocytosis of Community-Acquired Methicillin-Resistant Staphylococcus aureus. *J Infect Dis* **221**, 668-678 (2020).
38. I. Miralda, S. M. Uriarte, K. R. McLeish, Multiple Phenotypic Changes Define Neutrophil Priming. *Front Cell Infect Microbiol* **7**, 217 (2017).
39. A. J. Wolfe, The acetate switch. *Microbiol Mol Biol Rev* **69**, 12-50 (2005).
40. M. A. Kovach, T. J. Standiford, The function of neutrophils in sepsis. *Curr Opin Infect Dis* **25**, 321-327 (2012).
41. J. M. Patel *et al.*, Sepsis Induces a Dysregulated Neutrophil Phenotype That Is Associated with Increased Mortality. *Mediators Inflamm* **2018**, 4065362 (2018).
42. K. L. Vogt, C. Summers, E. R. Chilvers, A. M. Condliffe, Priming and de-priming of neutrophil responses in vitro and in vivo. *Eur J Clin Invest* **48 Suppl 2**, e12967 (2018).
43. N. Fine *et al.*, Primed PMNs in healthy mouse and human circulation are first responders during acute inflammation. *Blood Adv* **3**, 1622-1637 (2019).

44. S. Uchiyama *et al.*, Interferon alpha-Enhanced Clearance of Group A Streptococcus Despite Neutropenia. *J Infect Dis* **214**, 321-328 (2016).
45. K. M. Maslowski *et al.*, Regulation of inflammatory responses by gut microbiota and chemoattractant receptor GPR43. *Nature* **461**, 1282-1286 (2009).
46. I. Galvao *et al.*, The Metabolic Sensor GPR43 Receptor Plays a Role in the Control of Klebsiella pneumoniae Infection in the Lung. *Front Immunol* **9**, 142 (2018).
47. K. H. Antunes *et al.*, Microbiota-derived acetate protects against respiratory syncytial virus infection through a GPR43-type 1 interferon response. *Nat Commun* **10**, 3273 (2019).
48. C. Tang, S. Offermanns, FFA2 and FFA3 in Metabolic Regulation. *Handb Exp Pharmacol* **236**, 205-220 (2017).
49. D. Bolognini, A. B. Tobin, G. Milligan, C. E. Moss, The Pharmacology and Function of Receptors for Short-Chain Fatty Acids. *Mol Pharmacol* **89**, 388-398 (2016).
50. S. Jeong, H. Y. Kim, A. R. Kim, C. H. Yun, S. H. Han, Propionate Ameliorates Staphylococcus aureus Skin Infection by Attenuating Bacterial Growth. *Front Microbiol* **10**, 1363 (2019).
51. A. Perner *et al.*, Hydroxyethyl starch 130/0.42 versus Ringer's acetate in severe sepsis. *N Engl J Med* **367**, 124-134 (2012).
52. P. Louis, H. J. Flint, Formation of propionate and butyrate by the human colonic microbiota. *Environ Microbiol* **19**, 29-41 (2017).
53. D. D. Marshall, M. R. Sadykov, V. C. Thomas, K. W. Bayles, R. Powers, Redox Imbalance Underlies the Fitness Defect Associated with Inactivation of the Pta-AckA Pathway in Staphylococcus aureus. *J Proteome Res* **15**, 1205-1212 (2016).
54. G. A. Somerville *et al.*, Correlation of acetate catabolism and growth yield in Staphylococcus aureus: implications for host-pathogen interactions. *Infect Immun* **71**, 4724-4732 (2003).
55. R. Y. Huang, D. Raymond Herr, S. Moochhala, Manipulation of Alcohol and Short-Chain Fatty Acids in the Metabolome of Commensal and Virulent Klebsiella pneumoniae by Linolenic Acid. *Microorganisms* **8** (2020).

56. J. Martensson *et al.*, Neutrophil priming that turns natural FFA2R agonists into potent activators of the superoxide generating NADPH-oxidase. *J Leukoc Biol* **104**, 1117-1132 (2018).
57. B. H. Singer *et al.*, Bacterial Dissemination to the Brain in Sepsis. *Am J Respir Crit Care Med* **197**, 747-756 (2018).
58. A. Zaborin *et al.*, Membership and behavior of ultra-low-diversity pathogen communities present in the gut of humans during prolonged critical illness. *mBio* **5**, e01361-01314 (2014).
59. X. Zhao *et al.*, Sensitive and Simplified Detection of Antibiotic Influence on the Dynamic and Versatile Changes of Fecal Short-Chain Fatty Acids. *PLoS One* **11**, e0167032 (2016).
60. W. D. Miller, R. Keskey, J. C. Alverdy, Sepsis and the Microbiome: A Vicious Cycle. *J Infect Dis* 10.1093/infdis/jiaa682 (2020).
61. Z. DeFilipp, P. P. Bloom, E. L. Hohmann, F. M. T. S. Group, Drug-Resistant Bacteremia after Fecal Microbiota Transplant. Reply. *N Engl J Med* **382**, 1961-1962 (2020).
62. F. Fava, L. Rizzetto, K. M. Tuohy, Gut microbiota and health: connecting actors across the metabolic system. *Proc Nutr Soc* 10.1017/S0029665118002719, 1-12 (2018).
63. D. A. Bloes, M. Otto, A. Peschel, D. Kretschmer, Enterococcus faecium stimulates human neutrophils via the formyl-peptide receptor 2. *PLoS One* **7**, e39910 (2012).
64. J. C. Moran, M. J. Horsburgh, Whole-Genome Sequence of Staphylococcus epidermidis Tu3298. *Genome Announc* **4** (2016).
65. L. V. Collins *et al.*, Staphylococcus aureus strains lacking D-alanine modifications of teichoic acids are highly susceptible to human neutrophil killing and are virulence attenuated in mice. *J Infect Dis* **186**, 214-219 (2002).
66. C. Tang *et al.*, Loss of FFA2 and FFA3 increases insulin secretion and improves glucose tolerance in type 2 diabetes. *Nat Med* **21**, 173-177 (2015).

Acknowledgments. We thank Cosima Hirt, Cordula Gekeler and Darya Belikova for technical support, Stefan Offermanns for kindly providing the GPR43-/- mice, as well as Stefan Stevanović for synthesizing PSM peptides. This study was funded by grants from the German Research Foundation (SFB685 to A. P. and TRR34 and

TR156, project ID 246807620, to D. K. and A. P.) and the German Center for Infection Research (DZIF) to A.P. and D.K. The authors acknowledge infrastructural support by the Cluster of Excellence EXC2124 Controlling Microbes to Fight Infections, project ID 390838134.

Author contributions. K.S and D. K. designed the experiments; K. S., C. B., and D. K. performed the experiments; U.S. analyzed data and calculated statistics; K.S., A. P., and D. K. edited the manuscript and interpreted the data.

Competing Interests. The authors declare no conflict of interest.

Chapter 6

Inhibition of the ATP synthase sensitizes *Staphylococcus aureus* towards human antimicrobial peptides

Liping Liu[1], Christian Beck[2], Katrine Nøhr-Meldgaard[1], Andreas Peschel[2], Dorothee Kretschmer[2], Hanne Ingmer[1*] & Martin Vestergaard[1]

1. Department of Veterinary and Animal Sciences, Faculty of Health and Medical Sciences, University of Copenhagen, Stigbøjlen 4, DK-1870 Frederiksberg C, Denmark.
2. Department of Infection Biology, Interfaculty Institute for Microbiology and Infection Medicine Tübingen (IMIT), University of Tübingen, Auf der Morgenstelle 28, 72076 Tübingen, Germany.

* Corresponding author: Hanne Ingmer (hi@sund.ku.dk)

Key words: *Staphylococcus aureus,* antimicrobial peptides, defensins, intrinsic resistance and ATP synthase

Running title: Sensitizing *S. aureus* to human antimicrobial peptides.

Published: Liu, L., Beck, C., Nøhr-Meldgaard, K., Peschel, A., Kretschmer, D., Ingmer, H., and Vestergaard, M. (2020) Inhibition of the ATP synthase sensitizes Staphylococcus aureus towards human antimicrobial peptides. *Scientific Reports* **10**, 11391

Abstract

Antimicrobial peptides (AMPs) are an important part of the human innate immune system for protection against bacterial infections, however the AMPs display varying degrees of activity against *Staphylococcus aureus*. Previously, we showed that inactivation of the ATP synthase sensitizes *S. aureus* towards the AMP antibiotic class of polymyxins. Here we wondered if the ATP synthase similarly is needed for tolerance towards various human AMPs, including human β-defensins (hBD1-4), LL-37 and histatin 5.

Importantly, we find that the ATP synthase mutant (*atpA*) is more susceptible to killing by hBD4, hBD2, LL-37 and histatin 5 than wild type cells, while no changes in susceptibility was detected for hBD3 and hBD1. Administration of the ATP synthase inhibitor, resveratrol, sensitizes *S. aureus* towards hBD4-mediated killing. Neutrophils rely on AMPs and reactive oxygen molecules to eliminate bacteria and the *atpA* mutant is more susceptible to killing by neutrophils than the WT, even when the oxidative burst is inhibited.

These results show that the staphylococcal ATP synthase enhance tolerance of *S. aureus* towards some human AMPs and this indicate that inhibition of the ATP synthase may be explored as a new therapeutic strategy that sensitizes *S. aureus* to naturally occurring AMPs of the innate immune system.

Introduction

Bacterial pathogens that cause disease in humans remain a serious threat to public health and antibiotics are still our primary weapons in treating many bacterial diseases. The ability to eradicate bacterial infections is however challenged by development of resistance for every type of antibiotic introduced to the clinic (1). The majority of the new small molecule antibiotics in clinical development are however inhibiting the same targets as already marketed antibiotics (2). As an alternative to small molecule antibiotics, antimicrobial peptides (AMPs) are also explored in clinical trials, however most of the AMPs are only tested for topical applications due to toxicity issues and low metabolic stability (3). Here we propose a new strategy to combat bacterial infections, namely to sensitize bacteria to the naturally occurring antimicrobial peptides of the human body and hence boosting the antibacterial capabilities of the innate immune system to eradicate bacterial infections.

Humans are continuously exposed to numerous, and potentially pathogenic, microorganisms, where the innate immune system provides the first line of defense. AMPs constitute an important defense mechanism of the innate immune system against invading microorganisms, due to their antimicrobial and immune stimulatory properties (4, 5). In humans, several classes of AMPs have been identified, such as α- and β-defensins, the cathelicidin LL-37 and histatins (5). The α-defensins consist of six members, which are divided into human neutrophil peptides (HNP1-4) and human α-defensin 5 and 6 (HD5 and HD6). HNP1-4 are highly concentrated in the granules of neutrophils, but are also expressed in monocytes, lymphocytes and natural killer cells. HD5 and HD6 are primarily expressed in Paneth cells of the small intestine (4). The β-defensins consist of four members (hBD1-4) and are primarily secreted by mucosal surface epithelia, e.g. by keratinocytes in the human skin (6). Histatins comprise a family of cationic, histidine-rich peptides that are present in human saliva and are important for maintaining oral health by limiting infections in the oral cavity (5). Several histatins have been characterized, however histatin 5 displays the strongest antimicrobial activity (5). LL-37 is an antimicrobial peptide that belongs to the cathelicidin family and is expressed in various epithelial- (e.g. keratinocytes) and immune cells (e.g. neutrophils and macrophages) (7). The bactericidal activities of many AMPs have generally been attributed to pore formation in bacterial cytoplasmic membranes, however this mode of action may be too simplistic (8, 9).

The bactericidal activity of hBD3 has for example been associated with lipid II binding, leading to inhibition of cell wall biosynthesis (10) and some AMPs also have intracellular targets (11). Many antimicrobial peptides display a net positive charge, which is important in the initial electrostatic attraction to negatively charged bacterial phospholipid membranes and negatively charged teichoic acids on the surface of Gram positive bacteria, e.g. *Staphylococcus aureus* (11).

S. aureus is a common colonizer of the human body (6), where approximately 30-50% of healthy adults transiently carry this species and approximately 20% are persistently colonized (12). The skin, nose and intestinal tract are important ecological niches for *S. aureus* carriage (13). Topical colonization with *S. aureus* imposes a risk for subsequent infections, if the skin or mucosal barriers are breached and enables transmission of *S. aureus* cells to the adjacent tissues or the bloodstream (12). *S. aureus* is an opportunistic pathogen that may cause life-threatening diseases, such as sepsis, endocarditis and pneumonia (12). Even though keratinocytes express various antimicrobial peptides, such as hBD1-4 and LL-37, *S. aureus* frequently colonizes human skin (6). Among the human β-defensins, only hBD3 displays potent bactericidal activity against *S. aureus* at physiological conditions (14-16), and keratinocytes are dependent on hBD3 for killing of *S. aureus* (17). However, it is incompletely understood, why the remaining β-defensins display limited anti-staphylococcal activity. This indicates that sensitizing *S. aureus* towards the innate immune system AMPs may potentially facilitate eradication of colonizing *S. aureus*.

Multiple factors affect bacterial susceptibility towards AMPs, such as cell membrane composition, cell surface charge and transmembrane potential (8). The positive charge of many AMPs facilitates the interaction with negatively charged bacterial envelopes (11). A common resistance mechanism exploited by bacteria is to reduce the net negative charge of the cell envelope, for example by lysinylation of phospholipids (18) and D-alanylation of teichoic acids in *S. aureus* (19). Curiously, deficiency of wall teichoic acids selectively confers reduced susceptibility to hBD3, while not affecting susceptibility to LL-37 and HNP1-3 (20). The transmembrane potential affects the ability of cationic AMPs to permeabilize membranes (8, 21), where an inside-negative transmembrane potential facilitates insertion of some cationic AMPs into bacterial membranes (8). Interference with the electron transport

chain by inactivation of menaquinone- (*men* mutants) or hemin (*hem* mutants) biosynthesis pathways leads to membrane depolarization in *S. aureus* and in the appearance as small colony variants (SCVs) on agar plates (22). Electron transport chain SCVs have been associated with reduced susceptibility towards multiple AMPs, including hBD2-3 (23), thrombin-induced platelet microbicidal protein (24) and nisin (24). We recently reported that inactivation of genes encoding for multiple subunits of the ATP synthase sensitizes *S. aureus* towards polymyxins (25), a class of cationic AMPs that is used for treatment of Gram-negative infections (26). The ATP synthase basically serves two physiological functions, first being synthesis of ATP from ADP and inorganic phosphate by using energy from the proton motive force. Secondly, during conditions with a low proton-motive force the ATP synthase can work in reverse as an ATPase and thereby contributes to the establishment of a cross-membrane proton gradient through ATP hydrolysis (27). In *S. aureus*, the ATP synthase is primarily used to hydrolyze ATP for maintaining the cross-membrane proton gradient both under fermentative and respiratory conditions (28). ATP synthase inactivation in *S. aureus* leads to hyper-polarization of the membrane (25, 28), which was hypothesized to be the mechanism for sensitizing ATP synthase mutants towards polymyxins (25).

Several molecules have been shown to inhibit the ATP synthase in different species (29). For example inhibition of the ATP synthase with oligomycin A sensitizes *S. aureus* towards polymyxin B (25) and aminoglycosides (30). However, oligomycin A displays similar 50% inhibitory concentration (IC_{50}) between *S. aureus* and human mitochondrial ATP synthases (31), and cannot be used clinically due to toxicity issues (32). Resveratrol is a widely used nutraceutical that has been shown to bind to the bovine ATP synthase in the F_1-domain (33) and also binds reversibly to the ATP synthase in *E. coli*, partially inhibiting both ATP hydrolysis and ATP synthesis (34). Co-administration of resveratrol sensitizes *S. aureus* towards aminoglycosides (30). However, resveratrol is readily metabolized following oral administration, which probably only enables topical use (35).

Since ATP synthase inactivation sensitizes *S. aureus* towards polymyxins, we hypothesize that this strategy also can sensitize *S. aureus* towards various human AMPs. Potentiation of human AMPs that are currently ineffective against *S. aureus* may potentially become a new therapeutic strategy, where treatment relies on

deprivation of AMP resistance mechanisms and hence boosting of the naturally occurring AMPs of the innate immune system.

Materials and Methods

Bacterial strains, growth conditions and chemicals

The *Staphylococcus aureus* JE2 wild type (WT) strain and derivative mutants used in this study are highlighted in Table 1. Antimicrobial peptides used in this study included histatin-5 (Innovagen, Sweden), LL-37 (Isca Biochemicals, United Kingdom) and hBD1-4 (Innovagen, Sweden), as well as polymyxin B Etests (bioMérieux, France). We used the ATP synthase inhibitor resveratrol (Santa Cruz Biotechnology). Bacterial strains were routinely cultured at 37 °C in tryptic soy broth (TSB) or on tryptic soy agar (TSA).

Table 1 - Strains and mutants used.

Organism	Description and genotype	Source
S. aureus	JE2, CA-MRSA USA300	
S. aureus	JE2 *menD*::ΦNΣ	(60)
S. aureus	JE2 *atpA*::ΦNΣ	(60)
S. aureus	JE2 *atpB*::ΦNΣ	(60)
S. aureus	JE2 *atpG*::ΦNΣ	(60)
S. aureus	*atpA*$^{+}$ - Strain with allelic exchange of the transposon insertion (*atpA*::ΦNΣ) with the intact *atpA* gene	(25)

Antimicrobial susceptibility assays

Microdilution

The minimum inhibitory concentration for resveratrol was determined using a two-fold broth microdilution assay in TSB (100 µl) with an initial inoculum of approximately $5x10^5$ cells/ml. MIC was determined upon incubation at 37 °C for 24 h.

Etest

The MIC for polymyxin B was determined using Etest (bioMérieux, France) in the absence and in the presence of sub-inhibitory concentrations (0.0625x – 0.25x MIC) of resveratrol or menadione (1 µg/ml, Sigma). From overnight cultures, strains were

diluted to approximately 10^8 CFU/ml and then distributed on TSA plates using a sterile cotton swab. MIC was determined upon incubation at 37 °C for 24 h.

Bacterial cell survival assays

From overnight cultures of *S. aureus* JE2 and mutants, 10 µl was diluted into 990 µl fresh TSB medium in a falcon tube and grown for 2 h for the cells to reach early exponential phase. After 2 h the cultures were re-suspended in 10 mM sodium phosphate buffer (pH 7.4), termed NaPi (Medicago, Sweden). Cells were subsequently diluted in NaPi to approximately $5 \cdot 10^5$ CFU/ml, and combined with antimicrobial peptides and resveratrol when indicated, to a final volume of 100 µl and incubated in 96-well plates with shaking for 2 h at 37 °C. Bacteria were plated for CFU on TSA plates. Following overnight incubation at 37 °C for 24 h, viable cells were enumerated and relative cell survival was calculated as $CFU_{\text{with peptide}}/CFU_{\text{without peptide}}$ at 2 h post-exposure. Values provided are the mean ± SEM derived from at least three independent biological replicates.

Isolation of PMNs from human blood

Blood was collected from healthy adult volunteers and written informed consent was given. Isolation of neutrophils was performed following the procedure described in (36). All methods were carried out in accordance with relevant guidelines and regulations. The institutional review board (IRB) of the University of Tübingen approved the study and all adult subjects provided informed consent. This study was done in accordance with the ethics committee of the medical faculty of the University of Tübingen that approved the study, Approval number 015/2014 BO2. Briefly, heparinized blood was diluted 1:1 (v/v) with PBS containing 0.5% BSA and 2mM EDTA and layered onto a gradient of Biocoll (density, 1.077 g/ml; Biochrom) and Histopaque (density, 1.119 g/ml; Sigma). After centrifugation for 20 min at 380 x g, neutrophils were collected from the Histopaque phase. Cells were subjected to a brief hypotonic shock with ultrapure-water containing 155 mM ammonium chloride, 1 mM potassium hydrogen carbonate and 0.1 mM EDTA at pH 7.4, washed, and suspended at 2.5 x 10^6 cells/ml in RPMI containing 200 mg/ml HSA, 2 mM glutamine, 2mM sodium pyruvate and 10 mM HEPES.

Phagocytosis of *S. aureus* by neutrophils

Starter cultures of *S. aureus* JE2 and its respective *atpA* mutant were grown in TSB medium overnight. Main cultures were subsequently inoculated at an OD_{600} of 0.1 and grown to an OD of 1. 10^9 CFU of WT and *atpA* mutant cells were adjusted in PBS, stained with 10 µM carboxyfluorescein succinimidyl ester (CFSE) for 1 h at 37 °C and subsequently washed 3 times with PBS. 10^8 CFU/ml were opsonized with 10% normal human serum (NHS) in RPMI for 1 h at 37 °C. To check for correct CFUs, the dilution was plated onto TSA agar plates. 2.5 x 10^6 previously isolated PMNs were seeded in a 96 well round-bottom plate and challenged with opsonized WT and *atpA* mutant *S. aureus* JE2 at a MOI of 1. Incubation was performed for 20 min or 1 hour at 37°C. After incubation, the plate was centrifuged at 300 x g for 10 min, and the pellet was fixed with 3.7% formaldehyde for 20 min in the dark. The fixed cells were then washed and suspended in PBS. The samples were analyzed with a BD FACSCalibur by measuring 5000 events for each sample.

Killing of *S. aureus* by neutrophils

Starter cultures of *S. aureus* JE2 and its respective *atpA* mutant were grown in TSB medium overnight. Main cultures were subsequently inoculated at an OD_{600} of 0.1 and grown to an OD of 1. 10^9 CFU of WT and *atpA* mutant cells were adjusted in PBS medium, then washed and resuspended in PBS. 10^8 CFU/ml were opsonized with 10% normal human serum (NHS) in RPMI for 1 h at 37 °C. 2.5 x 10^6 previously isolated PMNs were seeded in 96 well round-bottom plates and challenged with opsonized WT and *atpA* mutant *S. aureus* JE2 at a MOI of 1. Incubation was performed for 1 h at 37 °C in a 96 well round-bottom plate and inoculation controls were included. After incubation, the plate was centrifuged at 300 x g for 10 min, the supernatants were collected, and the remaining neutrophil pellets were lysed using cold ddH_20 for 10 min on a rocker. The lysed neutrophils and remaining bacteria were resuspended and pooled with the previously collected supernatants. Dilutions of 10^{-2} were plated on TSA plates with an Eddy Jet 2W and incubated overnight at 37 °C. Values provided are the mean ± SEM derived from at least three independent biological replicates.

Statistics

The data were analyzed in GraphPad Prism 7 (GraphPad Software Inc.) using paired t-tests or one-way analysis of variance (ANOVA) with a *post hoc* analysis of Dunnett's multiple comparison tests. Log-transformed data was used for bacterial survival. $P < 0.05$ (*), $P < 0.01$ (**) and $P < 0.001$ (***).

Results

ATP synthase mutants are more susceptible to hBD2 and hBD4

Since inactivation of the ATP synthase increases susceptibility of *S. aureus* towards the antimicrobial peptides, polymyxins (25), we wondered if inactivation of the ATP synthase also sensitizes *S. aureus* towards AMPs of the human innate immune system. Therefore, bacterial killing of the WT *S. aureus* JE2 and isogenic *atpA* (ATP synthase subunit alpha) transposon mutant was assessed following 2 h exposure to human cationic AMPs, comprising histatin-5, LL-37 and hBD1-4 at the concentrations highlighted in Figure 1a. The *atpA* mutant was more susceptible to hBD4 and hBD2 compared with the WT (Figure 1a). The *atpA* mutant displayed a 63-fold greater reduction in viable cells compared with WT upon treatment with hBD4. For hBD2, the *atpA* mutant displayed a 5-fold greater reduction in viable cells compared with WT. A minor increase in bactericidal activity against the *atpA* mutant was detected for histatin-5 and LL-37, whereas no differences between WT and *atpA* survival were detected upon treatment with hBD1 nor hBD3.

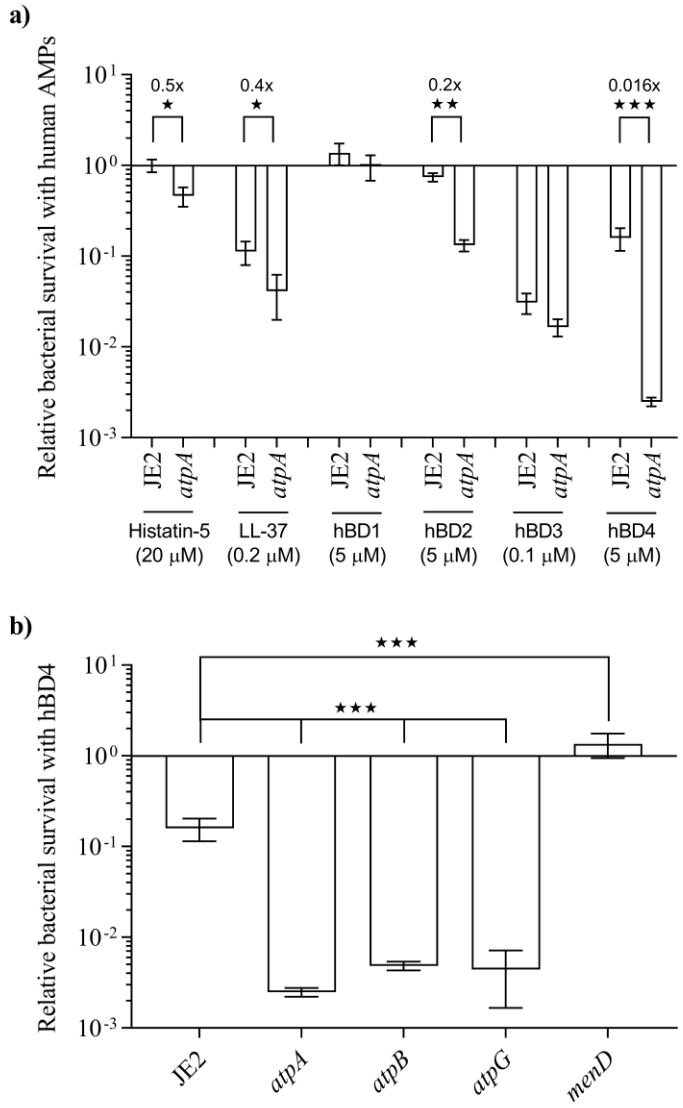

Figure 1 – **ATP synthase mutants are more susceptible to specific human AMPs than the WT.** (a) The susceptibilities to the different AMPs assayed are presented as the relative survival following 2 h exposure at the indicated AMP concentrations for JE2 (WT) and *atpA* mutant. (b) Survival of ATP synthase mutants (*atpA*, *atpB* and *atpG*) and *menD* mutant following 2 h exposure to hBD4 (5 μM). Each survival value provided is the mean ± SEM derived from at least three independent measurements. ★ $p<0.05$, ★★ $p<0.01$ and ★★★ $p<0.001$.

We assessed hBD4-mediated killing of other ATP synthase mutants, namely *atpB* (ATP synthase subunit A) and *atpG* (ATP synthase subunit gamma) and both mutants displayed increased susceptibility to hBD4, similarly to the *atpA* mutant (Figure 1b).

Since the *atpA* mutant has a hyperpolarized membrane (25), we also assessed hBD4 susceptibility of the *menD* transposon mutant, which has a depolarized membrane (37). The *menD* mutant was indeed more tolerant to hBD4 compared with WT, as no reduction in viable cell count was observed following 2 h exposure to hBD4 at 5 µM (Figure 1b), suggesting that the magnitude of the membrane potential is an important determinant for hBD4 susceptibility.

Similarly we observed this correlation between magnitude of membrane potential and polymyxin B susceptibility, where the *menD* mutant was more resistant towards polymyxin B compared with the WT (Supplementary Table S1). The *menD* mutant is auxotrophic for menadione and supplementation with the compound re-sensitized the *menD* mutant to polymyxin B (Supplementary Table S1).

Taken together, inactivation of the ATP synthase sensitizes *S. aureus* to specific human AMPs and the magnitude of the membrane potential correlates with hBD4 susceptibility. This correlation also applies more broadly to include the non-human AMP, polymyxin B.

The ATP synthase inhibitor resveratrol sensitizes S. aureus towards hBD4

Resveratrol is a putative ATP synthase inhibitor in *S. aureus* (30) and therefore, we assessed if resveratrol could sensitize *S. aureus* JE2 towards hBD4. Resveratrol has growth-inhibitory properties with a MIC of 256 µg/ml, but at a sub-inhibitory concentration (0.125x MIC) it had no impact on *S. aureus* viability (Figure 2). Importantly, however, when supplemented in combination with hBD4, resveratrol increased killing of WT *S. aureus* by 20-fold compared with hBD4 alone.

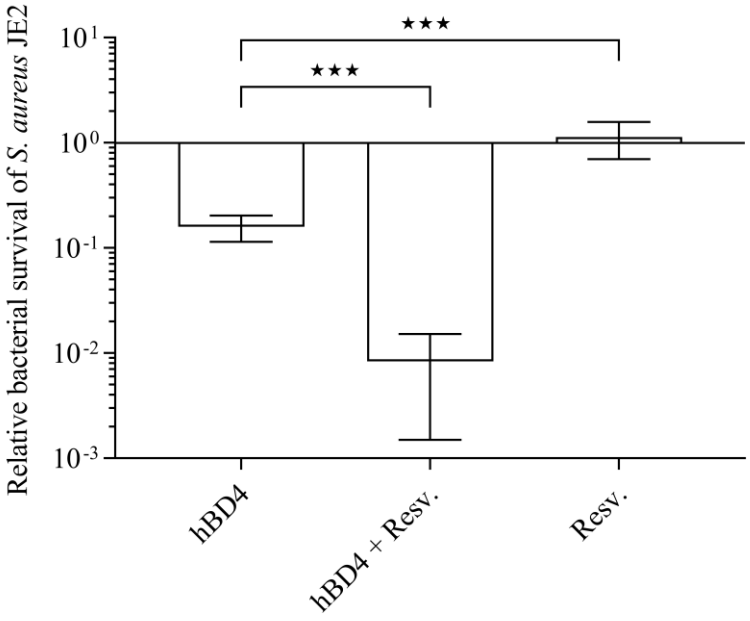

Figure 2 – Resveratrol sensitizes *S. aureus* to hBD4.

Survival of *S. aureus* JE2 was assessed for resveratrol (32 µg/ml) and hBD4 (5 µM), either alone or in combination. Each value provided is the mean ± SEM derived from at least three independent measurements. ★ p<0.05, ★★ p<0.01 and ★★★ p<0.001.

Similarly, supplementation of resveratrol at sub-inhibitory concentrations (0.0625x – 0.25x MIC) sensitized *S. aureus* JE2 to polymyxin B (Supplementary Table S2).
These result suggests that ATP synthase inhibition with resveratrol may be an attractive approach to sensitize *S. aureus* towards hBD4.

The *atpA* mutant is more susceptible to killing by human neutrophils

Log-phase bacteria of the WT and *atpA* mutant were opsonized with pooled normal human serum, phagocytosed by neutrophils, and subsequently incubated for one hour before determination of surviving cells. The *atpA* mutant was more susceptible to neutrophil killing than the WT and after one hour of incubation with neutrophils, only 39.2% of the *atpA* cells survived compared with 49.9% for the WT (P = 0.006) (Figure 3). The uptake of the strains into the neutrophils was similar (Data not shown), suggesting that the increased killing of the *atpA* is due to antimicrobial activities of the neutrophils and not due to alterations in phagocytosis rates.

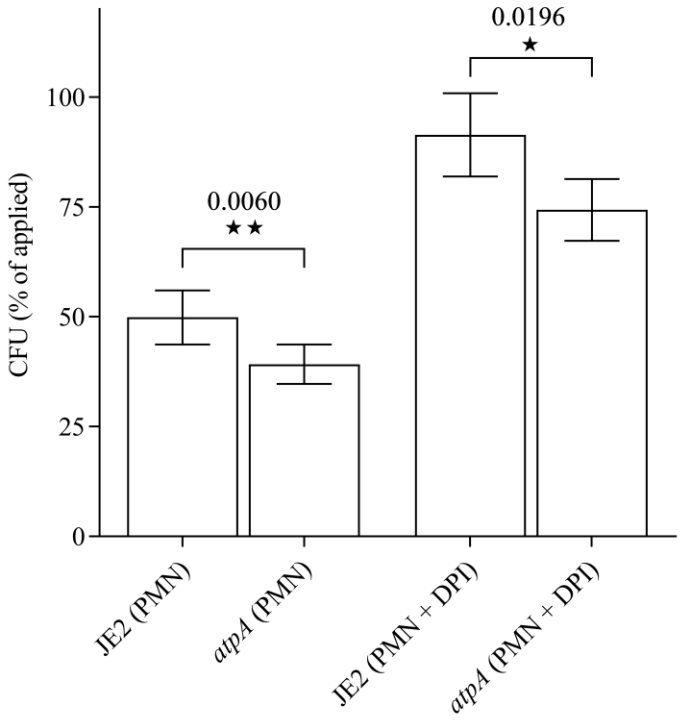

Figure 3 – Neutrophil-mediated killing of *S. aureus*.
The percentage of viable opsonized WT and *atpA* mutant cells following incubation with neutrophils (PMN) for 1 h. Surviving cells are expressed in percentage of the initial counts. Diphenyleneiodonium (DPI) is a NADPH oxidase inhibitor. Each value provided is the mean ± SEM derived from at least seven independent measurements. ★ $p<0.05$, ★★ $p<0.01$ and ★★★ $p<0.001$.

As neutrophils normally use both, oxygen-dependent and non-oxygen-dependent killing mechanisms, including antimicrobial peptides (38), we compared survival of *atpA* and WT in neutrophils treated with the NADPH oxidase inhibitor diphenyleneiodonium (DPI), which suppresses the formation of reactive oxygen species (18). Suppression of the oxidative burst limited killing of *S. aureus* (Figure 3). After one hour incubation only 74.3% of the *atpA* cells survived in DPI-treated neutrophils, compared to 91.4% for the WT (P = 0.0196) (Figure 3). These data suggest that the *atpA* mutant is more susceptible towards the oxygen-independent antimicrobial activities of neutrophils.

Discussion

Antimicrobial peptides are an important part of the innate immune system and the AMPs display activity against a wide range of bacterial-, fungal- and viral species (6). Several human AMPs however display low inhibitory activity against *S. aureus* (14). For example, the human β-defensins 1-4 are produced by keratinocytes and are key in protecting against skin infections (6). hBD3 displays greater bactericidal activity against *S. aureus* than the other β-defensins (14-16), and hBD3 is important for keratinocytes in killing *S. aureus* (17). Production of AMPs in the skin and in the nasal passages plays a major role in preventing *S. aureus* persistent colonization and people with defects in hBD3 production have enhanced nasal colonization of *S. aureus* (39). Our results point to a novel type of antimicrobial therapy, whereby the susceptibility of the pathogen is enhanced towards the natural human antimicrobial peptides. Here we demonstrate the potential for *S. aureus*, but it may be applicable to other human pathogens.

The energetic state of bacterial membranes can affect the susceptibility towards AMPs in different bacterial species (8) and for some conventional classes of antibiotics as well, i.e. aminoglycosides (40). Recently, we demonstrated that ATP synthase mutants of *S. aureus* become more sensitive towards polymyxins (25). ATP synthase inactivation confers hyperpolarization of the membrane (25, 28) and larger membrane potentials can facilitate AMP insertion into membranes (8). In this study, we demonstrate that the activities of certain human AMPs are affected by the magnitude of the membrane potential. ATP synthase mutants have a hyperpolarized membrane (25, 28) and become more sensitive towards hBD2 and hBD4 and to a minor degree towards LL-37 and histatin-5 (Figure 1a). Contrarily, a *menD* mutant with a depolarized membrane is less sensitive towards hBD4 (Figure 1b).

Our finding that membrane depolarization protects *S. aureus* from hBD4-mediated killing corroborate previous studies demonstrating that *S. aureus* SCVs are less susceptible to different AMPs. For *S. aureus*, electron-transport chain deficient mutants are less susceptible to killing by thrombin-induced PMP-1 (tPMP-1) (41), nisin (24), lactoferrin B (42) and human AMPs, including hBD2, hBD3 and LL-37 (23). Another study, with genetically defined *menD* and *hemB* mutants in different *S. aureus* genetic backgrounds did however not observe changes in susceptibility to LL-37 (43). Killing by the human neutrophil defensin 1 (hNP-1) is similar in WT and

mutants with impaired electron transport chains (24, 41, 44). These observations indicate that membrane potential changes only affect the activity of specific AMPs.

It has been suggested that membrane depolarization and subsequently increased tolerance towards AMPs of the innate immune system is a survival strategy that enables intracellular persistence of *S. aureus* in eukaryotic cells (45). Here we demonstrate that inactivation of the ATP synthase contrarily sensitizes *S. aureus* to neutrophil-killing (Figure 3). The increased susceptibility to neutrophil-killing is also evident when the oxidative burst is suppressed (Figure 3), suggesting that this effect is mediated by increased susceptibility to AMPs produced by neutrophils (38).

It is not only in *S. aureus* that AMP sensitivity is modulated by the magnitude of the membrane potential. In *E. coli*, inactivation of the ATP synthase also leads to hyperpolarization of the membrane (46) and ATP synthase mutants are more sensitive to colistin (47) and aminoglycosides (40, 47). Deletion of the gene *phoP* in *E. coli* conferred hyperpolarization of the membrane and a concomitant increase in activity of polymyxin B, while collapsing the proton gradient with the protonophore carbonyl cyanide *m*-chlorophenyl hydrazone (CCCP) abrogated this effect (48). Dissipation of membrane potential with CCCP also impaired killing of *E. coli* with the AMP indolicidin (49). For *Salmonella enterica* Typhimurium, impairment of the electron transport chain reduces AMP activity, e.g. a *hemB* mutant displays a 4-fold increase in MIC for colistin (50). Even respiration-deficient mutants of the fungus *Candida albicans* experience reduced sensitivity to histatin-5 and chemical inhibition of the electron transport chain with sodium azide or CCCP treatment also protects *C. albicans* against histatin-5 killing (51, 52).

The ATP synthase may potentially be targeted to facilitate killing by AMPs of the innate immune system and hence be essential under *in vivo* conditions. By employing the Tn-seq methodology, the ATP synthase has been identified in several studies as essential during *in vivo* conditions, such as in abscess formation or osteomyelitis, while the ATP synthase is dispensable during growth in laboratory medium (53-55). Recently, Grosser and colleagues demonstrated that an ATP synthase mutant indeed is severely attenuated in a murine skin abscess model (28). ATP synthase inactivation confers pleiotropic effects, including attenuated growth under anaerobic conditions, increased sensitivity towards peroxide and nitric oxide stresses (28). Whether virulence attenuation of the ATP synthase mutant in the

murine skin abscess model is mediated by a single phenotypic trait or a combination thereof remain unexplored in the study (28) and here we provide an additional phenotype that may contribute to the attenuated virulence, namely increased sensitivity of *S. aureus* to different AMPs of the innate immune system.

Inhibition of the ATP synthase may potentially have therapeutic value either as a monotherapy or in combination with AMPs or aminoglycosides. Many ATP synthase inhibitors have been identified (29), however several of these, e.g. oligomycin A, are not selective for bacterial ATP synthases and also blocks human mitochondrial ATP synthases (31). The ATP synthase has been clinically validated as a druggable target in recent years with the antibiotic bedaquiline that selectively inhibits ATP synthases of Mycobacteria (56). We demonstrated that the ATP synthase inhibitor resveratrol, a commonly used nutraceutical (57), sensitizes *S. aureus* towards hBD4 (Figure 2). Resveratrol has previously been assessed for clearance of acne skin lesions (58) and has recently been shown to reduce abscess formation by *S. aureus* when used as a monotherapy (59). It will be important in future animal experiments to elucidate, whether resveratrol in combination with human defensins are superior in treating topical *S. aureus* infections compared with the respective monotherapies.

It is encouraging that bacterial ATP synthases are sufficiently different from human ATP synthases, which enables identification of selective bacterial ATP synthase inhibitors that are not toxic to human cells (32). Selective staphylococcal ATP synthase inhibitors may provide a novel class of antibacterial therapies that is based on sensitizing *S. aureus* towards the AMPs of the innate immune system. Additionally, such inhibitors can be adjuvants that potentiate the activity of conventional antibiotics, such as aminoglycosides and polymyxins (25, 30). Several AMPs are in clinical development (3), whose activity potentially also can be enhanced by co-administration of ATP synthase inhibitors.

In summary, we have investigated the possibility of sensitizing *S. aureus* towards human AMPs by targeting the ATP synthase and our results suggest that it may be a novel strategy for development of new antimicrobial therapeutics.

Funding information

The work is funded by the Danish Research Council for Independent Research, Technology and Production nr. 12-127417 for HI and of the German Center of Infection Research to DK and AP.

Author contributions

MV, AP, DK and HI conceived and designed the study. Experiments were performed by MV, LL, KNM and CB. All authors contributed in analysis of data and writing of the manuscript. All authors read and approved the final manuscript.

Conflict of interest

None to declare.

References

1. Lewis, K. (2013) Platforms for antibiotic discovery. *Nature reviews Drug discovery* **12**, 371-387
2. Butler, M. S., Blaskovich, M. A., and Cooper, M. A. (2016) Antibiotics in the clinical pipeline at the end of 2015. *The Journal of Antibiotics*
3. Mahlapuu, M., Håkansson, J., Ringstad, L., and Björn, C. (2016) Antimicrobial peptides: an emerging category of therapeutic agents. *Frontiers in cellular and infection microbiology* **6**, 194
4. Hancock, R. E., Haney, E. F., and Gill, E. E. (2016) The immunology of host defence peptides: beyond antimicrobial activity. *Nature Reviews Immunology* **16**, 321
5. De Smet, K., and Contreras, R. (2005) Human antimicrobial peptides: defensins, cathelicidins and histatins. *Biotechnology letters* **27**, 1337-1347
6. Otto, M. (2010) *Staphylococcus* colonization of the skin and antimicrobial peptides. *Expert review of dermatology* **5**, 183-195
7. Xhindoli, D., Pacor, S., Benincasa, M., Scocchi, M., Gennaro, R., and Tossi, A. (2016) The human cathelicidin LL-37—A pore-forming antibacterial peptide and host-cell modulator. *Biochimica et Biophysica Acta (BBA)-Biomembranes* **1858**, 546-566
8. Yeaman, M. R., and Yount, N. Y. (2003) Mechanisms of antimicrobial peptide action and resistance. *Pharmacological reviews* **55**, 27-55
9. Omardien, S., Brul, S., and Zaat, S. A. (2016) Antimicrobial activity of cationic antimicrobial peptides against gram-positives: current progress made in understanding the mode of action and the response of bacteria. *Frontiers in cell and developmental biology* **4**, 111
10. Sass, V., Schneider, T., Wilmes, M., Körner, C., Tossi, A., Novikova, N., Shamova, O., and Sahl, H.-G. (2010) Human β-defensin 3 inhibits cell wall biosynthesis in Staphylococci. *Infection and immunity* **78**, 2793-2800
11. Andersson, D. I., Hughes, D., and Kubicek-Sutherland, J. Z. (2016) Mechanisms and consequences of bacterial resistance to antimicrobial peptides. *Drug Resistance Updates* **26**, 43-57
12. Lowy, F. D. (1998) *Staphylococcus aureus* infections. *New England Journal of Medicine* **339**, 520-532

13. Gordon, R. J., and Lowy, F. D. (2008) Pathogenesis of methicillin-resistant *Staphylococcus aureus* infection. *Clinical infectious diseases* **46**, S350-S359
14. Midorikawa, K., Ouhara, K., Komatsuzawa, H., Kawai, T., Yamada, S., Fujiwara, T., Yamazaki, K., Sayama, K., Taubman, M. A., and Kurihara, H. (2003) *Staphylococcus aureus* susceptibility to innate antimicrobial peptides, β-defensins and CAP18, expressed by human keratinocytes. *Infection and immunity* **71**, 3730-3739
15. Chen, X., Niyonsaba, F., Ushio, H., Okuda, D., Nagaoka, I., Ikeda, S., Okumura, K., and Ogawa, H. (2005) Synergistic effect of antibacterial agents human β-defensins, cathelicidin LL-37 and lysozyme against *Staphylococcus aureus* and *Escherichia coli*. *Journal of dermatological science* **40**, 123-132
16. Kubicek-Sutherland, J. Z., Lofton, H., Vestergaard, M., Hjort, K., Ingmer, H., and Andersson, D. I. (2016) Antimicrobial peptide exposure selects for *Staphylococcus aureus* resistance to human defence peptides. *Journal of Antimicrobial Chemotherapy*, dkw381
17. Kisich, K. O., Howell, M. D., Boguniewicz, M., Heizer, H. R., Watson, N. U., and Leung, D. Y. (2007) The constitutive capacity of human keratinocytes to kill *Staphylococcus aureus* is dependent on β-defensin 3. *Journal of Investigative Dermatology* **127**, 2368-2380
18. Peschel, A., Jack, R. W., Otto, M., Collins, L. V., Staubitz, P., Nicholson, G., Kalbacher, H., Nieuwenhuizen, W. F., Jung, G., and Tarkowski, A. (2001) *Staphylococcus aureus* resistance to human defensins and evasion of neutrophil killing via the novel virulence factor MprF is based on modification of membrane lipids with l-lysine. *The Journal of experimental medicine* **193**, 1067-1076
19. Peschel, A., Otto, M., Jack, R. W., Kalbacher, H., Jung, G., and Götz, F. (1999) Inactivation of the *dlt* operon in *Staphylococcus aureus* confers sensitivity to defensins, protegrins, and other antimicrobial peptides. *Journal of Biological Chemistry* **274**, 8405-8410
20. Koprivnjak, T., Weidenmaier, C., Peschel, A., and Weiss, J. P. (2008) Wall teichoic acid deficiency in *Staphylococcus aureus* confers selective resistance to mammalian group IIA phospholipase A2 and human β-defensin 3. *Infection and immunity* **76**, 2169-2176

21. Kagan, B. L., Selsted, M. E., Ganz, T., and Lehrer, R. I. (1990) Antimicrobial defensin peptides form voltage-dependent ion-permeable channels in planar lipid bilayer membranes. *Proceedings of the National Academy of Sciences* **87**, 210-214
22. Proctor, R. A., Von Eiff, C., Kahl, B. C., Becker, K., McNamara, P., Herrmann, M., and Peters, G. (2006) Small colony variants: a pathogenic form of bacteria that facilitates persistent and recurrent infections. *Nature Reviews Microbiology* **4**, 295-305
23. Gläser, R., Becker, K., von Eiff, C., Meyer-Hoffert, U., and Harder, J. (2014) Decreased susceptibility of *Staphylococcus aureus* small-colony variants toward human antimicrobial peptides. *Journal of Investigative Dermatology* **134**, 2347-2350
24. Koo, S.-P., Bayer, A. S., Sahl, H.-G., Proctor, R. A., and Yeaman, M. R. (1996) Staphylocidal action of thrombin-induced platelet microbicidal protein is not solely dependent on transmembrane potential. *Infection and immunity* **64**, 1070-1074
25. Vestergaard, M., Nøhr-Meldgaard, K., Bojer, M. S., Nielsen, C. K., Meyer, R. L., Slavetinsky, C., Peschel, A., and Ingmer, H. (2017) Inhibition of the ATP Synthase Eliminates the Intrinsic Resistance of *Staphylococcus aureus* towards Polymyxins. *mBio* **8**, e01114-01117
26. Zavascki, A. P., Goldani, L. Z., Li, J., and Nation, R. L. (2007) Polymyxin B for the treatment of multidrug-resistant pathogens: a critical review. *Journal of antimicrobial chemotherapy* **60**, 1206-1215
27. Deckers-Hebestreit, G., and Altendorf, K. (1996) The F0F1-type ATP synthases of bacteria: structure and function of the F0 complex. *Annual review of microbiology* **50**, 791-824
28. Grosser, M. R., Paluscio, E., Thurlow, L. R., Dillon, M. M., Cooper, V. S., Kawula, T. H., and Richardson, A. R. (2018) Genetic requirements for *Staphylococcus aureus* nitric oxide resistance and virulence. *PLoS pathogens* **14**, e1006907
29. Hong, S., and Pedersen, P. L. (2008) ATP synthase and the actions of inhibitors utilized to study its roles in human health, disease, and other scientific areas. *Microbiology and Molecular Biology Reviews* **72**, 590-641

30. Nøhr-Meldgaard, K., Ovsepian, A., Ingmer, H., and Vestergaard, M. (2018) Resveratrol enhances the efficacy of aminoglycosides against *Staphylococcus aureus*. *International Journal of Antimicrobial Agents*
31. Balemans, W., Vranckx, L., Lounis, N., Pop, O., Guillemont, J., Vergauwen, K., Mol, S., Gilissen, R., Motte, M., and Lançois, D. (2012) Novel antibiotics targeting respiratory ATP synthesis in Gram-positive pathogenic bacteria. *Antimicrobial agents and chemotherapy* **56**, 4131-4139
32. Haagsma, A. C., Abdillahi-Ibrahim, R., Wagner, M. J., Krab, K., Vergauwen, K., Guillemont, J., Andries, K., Lill, H., Koul, A., and Bald, D. (2009) Selectivity of TMC207 towards mycobacterial ATP synthase compared with that towards the eukaryotic homologue. *Antimicrobial agents and chemotherapy* **53**, 1290-1292
33. Gledhill, J. R., Montgomery, M. G., Leslie, A. G., and Walker, J. E. (2007) Mechanism of inhibition of bovine F1-ATPase by resveratrol and related polyphenols. *Proceedings of the National Academy of Sciences* **104**, 13632-13637
34. Dadi, P. K., Ahmad, M., and Ahmad, Z. (2009) Inhibition of ATPase activity of *Escherichia coli* ATP synthase by polyphenols. *International Journal of Biological Macromolecules* **45**, 72-79
35. Vestergaard, M., and Ingmer, H. (2019) Antibacterial and antifungal properties of resveratrol. *International journal of antimicrobial agents*
36. Troelstra, A., Giepmans, B. N., Van Kessel, K. P., Lichenstein, H. S., Verhoef, J., and Van Strijp, J. A. (1997) Dual effects of soluble CD14 on LPS priming of neutrophils. *Journal of leukocyte biology* **61**, 173-178
37. Vestergaard, M., Paulander, W., Leng, B., Nielsen, J. B., Westh, H. T., and Ingmer, H. (2016) Novel Pathways for Ameliorating the Fitness Cost of Gentamicin Resistant Small Colony Variants. *Frontiers in Microbiology* **7**
38. Amulic, B., Cazalet, C., Hayes, G. L., Metzler, K. D., and Zychlinsky, A. (2012) Neutrophil function: from mechanisms to disease. *Annual review of immunology* **30**, 459-489
39. Zanger, P., Nurjadi, D., Vath, B., and Kremsner, P. G. (2011) Persistent nasal carriage of *Staphylococcus aureus* is associated with deficient induction of

human β-defensin 3 after sterile wounding of healthy skin *in vivo*. *Infection and immunity* **79**, 2658-2662

40. Lobritz, M. A., Belenky, P., Porter, C. B., Gutierrez, A., Yang, J. H., Schwarz, E. G., Dwyer, D. J., Khalil, A. S., and Collins, J. J. (2015) Antibiotic efficacy is linked to bacterial cellular respiration. *Proceedings of the National Academy of Sciences* **112**, 8173-8180
41. Yeaman, M. R., Bayer, A. S., Koo, S.-P., Foss, W., and Sullam, P. M. (1998) Platelet microbicidal proteins and neutrophil defensin disrupt the *Staphylococcus aureus* cytoplasmic membrane by distinct mechanisms of action. *The Journal of clinical investigation* **101**, 178-187
42. Samuelsen, Ø., Haukland, H. H., Kahl, B. C., Von Eiff, C., Proctor, R. A., Ulvatne, H., Sandvik, K., and Vorland, L. H. (2005) *Staphylococcus aureus* small colony variants are resistant to the antimicrobial peptide lactoferricin B. *Journal of Antimicrobial Chemotherapy* **56**, 1126-1129
43. Zhang, P., Wright, J. A., Tymon, A., and Nair, S. P. (2017) Bicarbonate induces high-level resistance to the human antimicrobial peptide LL-37 in *Staphylococcus aureus* small colony variants. *Journal of Antimicrobial Chemotherapy* **73**, 615-619
44. Sadowska, B., Bonar, A., von Eiff, C., Proctor, R. A., Chmiela, M., Rudnicka, W., and Różalska, B. (2002) Characteristics of *Staphylococcus aureus* isolated from airways of cystic fibrosis patients, and their small colony variants. *FEMS Immunology & Medical Microbiology* **32**, 191-197
45. Kahl, B. C. (2014) Small colony variants (SCVs) of *Staphylococcus aureus* – a bacterial survival strategy. *Infection, Genetics and Evolution* **21**, 515-522
46. Jensen, P. R., and Michelsen, O. (1992) Carbon and energy metabolism of *atp* mutants of *Escherichia coli*. *Journal of bacteriology* **174**, 7635-7641
47. Liu, A., Tran, L., Becket, E., Lee, K., Chinn, L., Park, E., Tran, K., and Miller, J. H. (2010) Antibiotic sensitivity profiles determined with an *Escherichia coli* gene knockout collection: generating an antibiotic bar code. *Antimicrobial agents and chemotherapy* **54**, 1393-1403
48. Alteri, C. J., Lindner, J. R., Reiss, D. J., Smith, S. N., and Mobley, H. L. (2011) The broadly conserved regulator PhoP links pathogen virulence and membrane potential in *Escherichia coli*. *Molecular microbiology* **82**, 145-163

49. Falla, T. J., Karunaratne, D. N., and Hancock, R. E. (1996) Mode of action of the antimicrobial peptide indolicidin. *Journal of Biological Chemistry* **271**, 19298-19303
50. Pränting, M., and Andersson, D. I. (2010) Mechanisms and physiological effects of protamine resistance in *Salmonella enterica* serovar Typhimurium LT2. *Journal of antimicrobial chemotherapy* **65**, 876-887
51. Gyurko, C., Lendenmann, U., Troxler, R. F., and Oppenheim, F. G. (2000) *Candida albicans* mutants deficient in respiration are resistant to the small cationic salivary antimicrobial peptide histatin 5. *Antimicrobial agents and chemotherapy* **44**, 348-354
52. Koshlukova, S. E., Lloyd, T. L., Araujo, M. W., and Edgerton, M. (1999) Salivary histatin 5 induces non-lytic release of ATP from *Candida albicans* leading to cell death. *Journal of Biological Chemistry* **274**, 18872-18879
53. Ibberson, C. B., Stacy, A., Fleming, D., Dees, J. L., Rumbaugh, K., Gilmore, M. S., and Whiteley, M. (2017) Co-infecting microorganisms dramatically alter pathogen gene essentiality during polymicrobial infection. *Nature microbiology* **2**, 17079
54. Wilde, A. D., Snyder, D. J., Putnam, N. E., Valentino, M. D., Hammer, N. D., Lonergan, Z. R., Hinger, S. A., Aysanoa, E. E., Blanchard, C., and Dunman, P. M. (2015) Bacterial hypoxic responses revealed as critical determinants of the host-pathogen outcome by TnSeq analysis of *Staphylococcus aureus* invasive infection. *PLoS pathogens* **11**, e1005341
55. Valentino, M. D., Foulston, L., Sadaka, A., Kos, V. N., Villet, R. A., Santa Maria, J., Lazinski, D. W., Camilli, A., Walker, S., and Hooper, D. C. (2014) Genes contributing to *Staphylococcus aureus* fitness in abscess-and infection-related ecologies. *MBio* **5**, e01729-01714
56. Mahajan, R. (2013) Bedaquiline: first FDA-approved tuberculosis drug in 40 years. *International Journal of Applied and Basic Medical Research* **3**, 1
57. Aschemann-Witzel, J., and Grunert, K. G. (2015) Resveratrol food supplements: a survey on the role of individual consumer characteristics in predicting the attitudes and adoption intentions of US American and Danish respondents. *BMC Public Health* **15**, 110

58. Fabbrocini, G., Staibano, S., De Rosa, G., Battimiello, V., Fardella, N., Ilardi, G., La Rotonda, M. I., Longobardi, A., Mazzella, M., and Siano, M. (2011) Resveratrol-containing gel for the treatment of acne vulgaris. *American Journal of Clinical Dermatology* **12**, 133-141

59. Duan, J., Li, M., Hao, Z., Shen, X., Liu, L., Jin, Y., Wang, S., Guo, Y., Yang, L., and Wang, L. (2018) Subinhibitory concentrations of resveratrol reduce alpha-hemolysin production in *Staphylococcus aureus* isolates by downregulating *saeRS*. *Emerging microbes & infections* **7**, 1-10

60. Fey, P. D., Endres, J. L., Yajjala, V. K., Widhelm, T. J., Boissy, R. J., Bose, J. L., and Bayles, K. W. (2013) A genetic resource for rapid and comprehensive phenotype screening of nonessential *Staphylococcus aureus* genes. *MBio* **4**, e00537-00512

Chapter 7

Formyl-Peptide Receptor Activation Enhances Phagocytosis of Community-Acquired Methicillin-Resistant *Staphylococcus aureus*

Weiß E[1], Schlatterer K[1], Beck C[1], Peschel A[1], Kretschmer D[1].

[1] Infection Biology, Interfaculty Institute for Microbiology and Infection Medicine Tübingen, University of Tübingen, Tübingen, Germany.

Published: Weiß, E., Schlatterer, K., Beck, C., Peschel, A., and Kretschmer, D. (2020) Formyl-Peptide Receptor Activation Enhances Phagocytosis of Community-Acquired Methicillin-Resistant Staphylococcus aureus. *J Infect Dis* **221**, 668-678

Abstract

Background

Formyl-peptide receptors (FPRs) are important pattern recognition receptors that sense specific bacterial peptides. Formyl-peptide receptors are highly expressed on neutrophils and monocytes, and their activation promotes the migration of phagocytes to sites of infection. It is currently unknown whether FPRs may also influence subsequent processes such as bacterial phagocytosis and killing. *Staphylococcus aureus*, especially highly pathogenic community-acquired methicillin-resistant *S aureus* strains, release high amounts of FPR2 ligands, the phenol-soluble modulins.

Methods

We demonstrate that FPR activation leads to upregulation of complement receptors 1 and 3 as well as FCγ receptor I on neutrophils and, consequently, increased opsonic phagocytosis of *S aureus* and other pathogens.

Results

Increased phagocytosis promotes killing of *S aureus* and interleukin-8 release by neutrophils.

Conclusions

We show here for the first time that FPRs govern opsonic phagocytosis. Manipulation of FPR2 activation could open new therapeutic opportunities against bacterial pathogens.

Introduction

Staphylococcus aureus is a major human pathogen that causes a variety of diseases, including local skin infections, sepsis, endocarditis, pneumonia, and toxic shock syndrome [1]. Various host cell types are involved in the early defense against *S aureus*. Activation of keratinocytes leads to the release of inflammatory cytokines and antimicrobial peptides (AMPs), which can directly kill *S aureus*. Neutrophils are the most frequent leukocytes involved in innate immune response [2]. Neutrophils constitute the first line of defense against invading microorganisms, representing approximately 50% to 70% of the circulating human leukocytes. In response to chemotactic signals, neutrophils rapidly migrate from the bloodstream into tissues [3]. *Staphylococcus aureus* releases a number of chemotactic microbe-associated molecular pattern molecules, including formylated peptides [4] and phenol-soluble modulins (PSMs) [5] that activate human neutrophil formyl-peptide receptor (FPR) 1 and 2, respectively [6]. It is interesting to note that highly pathogenic community-acquired methicillin-resistant *S aureus* (CA-MRSA) strains release remarkably high amounts of these PSMs [7].

In addition to their ability to recruit human neutrophils, FPR ligands of *S aureus* also induce the release of reactive oxygen species (ROS) [8], AMPs, and chemokines [9] from neutrophils, as well as the receptor-independent formation of neutrophil extracellular traps [10]. Whether the activation of FPRs on the surface of human neutrophils also regulates *S aureus* phagocytosis by these professional phagocytes remains unknown.

Human neutrophils express 2 complement receptors (CR1 and CR3) on their surface that recognize pathogens opsonized by complement factor C3b [11]. Pathogens opsonized by immunoglobulin (Ig)G antibodies are recognized by FCγ receptors

(FCγR) on the surface of neutrophils. Normal peripheral blood neutrophils express FCγRII and FCγRIIIB, as well as FCγRI during systemic infections and sepsis [11–13]. The recognition of opsonized pathogens by complement and FCγR is mandatory for phagocytosis. *Staphylococcus aureus* uses several strategies to avoid phagocytosis. For example, staphylococcal protein A binds to the Fc region of IgG antibodies and prevents the recognition of bacteria by FCγR [14].

Phagocytosis is not only necessary to initiate the intracellular killing of pathogens, it also triggers the release of chemokines by neutrophils [15,16] and monocytes [17,18]. Kang et al [18] showed that the numbers of *S aureus* cells phagocytosed by human monocytes correlates with the concentration of interleukin [IL]-8 released by these cells. Interleukin-8 is an intermediate chemokine that recruits neutrophils from the bloodstream into tissues, whereas end-target chemoattractants such as fMLF guide neutrophils within the tissues to the infection site [19]. Thus, phagocytosis represents an important enhancer of the recruitment of neutrophils to the infection site. Interleukin-8 also has a critical influence on the efficiency of bacterial killing during infection. Blocking of the IL-8 receptor CXCR1 decreases the macrophage ability to clear staphylococcal infections, probably via attenuating proinflammatory cytokine production [20]. In this study, we evaluated the role of FPR1 and FPR2 activation during the phagocytosis and killing of *S aureus* by neutrophils. We show that stimulation of these 2 receptors greatly enhances phagocytosis of *S aureus* and of various other pathogenic bacteria. Our results demonstrate for the first time that FPR activation leads not only to higher expression of CR1, but also of FCyRI and CR3. Furthermore, we show that phagocytosis enhanced by the FPR ligands leads to augmentation of IL-8 release by human neutrophils followed by increased neutrophil recruitment compared with phagocytosis without FPR stimulation. In addition, enhanced phagocytosis leads to enhanced bacterial killing depending on the numbers of bacteria phagocytized by neutrophils.

Material and Methods

Isolation of Human Neutrophils

Human neutrophils were isolated from healthy blood donors by density gradient centrifugation as previously described [5].

Phagocytosis Assay

Staphylococcus aureus strain USA300 [21], *Staphylococcus epidermidis* 1457 [22], *Staphylococcus lugdunensis* IVK28 [23], and a clinical *Listeria monocytogenes* isolate (from the strain collection of the diagnostics unit of the Medical Microbiology and Hygiene department, University of Tübingen) were grown overnight in tryptic soy broth (TSB) medium, whereas *Escherichia coli* BK2324 [24] was grown in Lennox broth medium. Bacteria were labeled with carboxyfluorescein diacetate succinimidyl ester (CFSE) (Sigma-Aldrich), heat-inactivated for 20 minutes at 70°C, and opsonized with 10% human pooled serum (Hospital Tübingen) in Roswell Park Memorial Institute (RPMI) medium for 1 hour at 37°C. Opsonized bacteria and human neutrophils were seeded into a 96-well plate at a ratio of 5 bacteria per neutrophil (multiplicity of infection [MOI] of 5). Formyl-peptide receptor ligands (fMLF from Sigma-Aldrich; PSM peptides were kindly provided by Stefan Stevanovic, Immunology Department, University of Tübingen) were added at the indicated concentrations. After incubating for 1 hour at 37°C, the neutrophils were fixed with 3.7% formaldehyde. To inhibit the FPRs, the neutrophils were incubated with 1.25 μg/mL CHIPS (kindly provided by Kok van Kessel, Bacterial Infections and Immunity Department, University of Utrecht) or 22.5 μM WRW_4 (synthesized by EMC Microcollections) for 20 minutes at room temperature prior to phagocytosis. The fluorescence intensity of the neutrophils was determined using a BD FACSCalibur instrument, and the phagocytic index (= %CFSE-positive neutrophils × CFSE fluorescent mean) was calculated. The index describes the fluorescence per cell as a relative indicator for how many bacteria per cell were phagocytosed (mean fluorescence of the positives).

Expression of Complement Receptor and FCγ Receptor

Neutrophils were seeded into a 96-well-plate and stimulated with fMLF or PSM peptides at the indicated concentrations for 1 hour. Subsequently, the supernatant

was discarded, and the neutrophils were incubated with PE-labeled antibodies against CD11b (BD Pharmingen), CD35 (Miltenyi Biotech), CD64 (Miltenyi Biotech), or an IgG isotype control (Miltenyi Biotech) for 30 minutes on ice. Next, the neutrophils were fixed with 3.7% formaldehyde, and the fluorescence intensity of the neutrophils was determined using a BD FACSCalibur instrument, and the mean fluorescence intensity (= %PE-positive neutrophils × PE fluorescent mean) was calculated.

Phagocytosis Assay with Blocking Antibodies

Neutrophils were seeded into a 96-well plate and stimulated with 500 nM fMLF or PSMα3 for 30 minutes. LEAF-purified antihuman antibodies from BioLegend (CD11b clone ICRF44 [10 µg/mL]; CD35 clone E11 [20 µg/mL]; CD64 clone 10.1 [2.5 µg/mL]) were used to functionally block the complement receptor and FCγR for 15 minutes. Subsequently, CFSE-labeled bacteria were added as described in the phagocytosis assay. After incubating for 1 hour at 37°C, the neutrophils were fixed with 3.7% formaldehyde, the fluorescence intensity of the neutrophils was determined using a BD FACSCalibur, and the phagocytic index was calculated.

Interleukin-8 Release

Neutrophils were incubated with opsonized or unopsonized heat-inactivated USA300 at an MOI of 5 and 50 nM fMLF or 1 µM PSMα3 for 5 hours at 37°C. To inhibit the FPRs, neutrophils were incubated with 1.25 µg/mL CHIPS or 22.5 µM WRW_4 for 20 minutes at room temperature prior to phagocytosis. The supernatants were collected, and released IL-8 was measured using an enzyme-linked immunosorbent assay kit (R&D Systems) according to the manufacturer's instructions.

Chemotaxis Assay

Neutrophils were labeled with BCECF, AM (Life Technologies) and seeded into 3-µm pore-sized ThinCerts (Greiner Bio-One). The compartments below the cell culture inserts contained the neutrophil supernatants stimulated for IL-8 release. After 2 hours, the cell culture inserts were removed, and the fluorescence intensity of the migrated neutrophils in the lower compartments was measured using a BMG Labtech CLARIOstar plate reader. The percentages of migrated neutrophils were calculated

compared with a positive control, where the neutrophils were seeded into the lower compartment.

Bacterial Killing Assay

Staphylococcus aureus strains USA300 or USA300ΔαβδΔ were grown overnight in TSB medium. Next, the bacteria were washed 3 times with phosphate-buffered saline and opsonized with 10% human pooled serum (Hospital Tübingen) in RPMI for 1 hour at 37°C. For the bacterial killing assay in the presence of FPR ligands, the neutrophils and bacteria were seeded in a 24-well plate at an MOI of 0.1 and incubated for 60 minutes with 500 nM fMLF or 1 µM PSMα3. For the bacterial killing assay in the presence of the FPR-inhibitors, neutrophils were incubated with 1.25 µg/mL CHIPS or 22.5 µM WRW_4 for 20 minutes at room temperature in a 24-well plate with bacteria at an MOI of 0.1 and incubated for 60 minutes. For the kinetic analysis, neutrophils and bacteria were seeded in a 24-well plate at the indicated MOIs.

After 1 hour, 100 µL of each sample was collected, and the neutrophils were lysed with ddH_2O for 15 minutes at 4°C, 1000 rpm. Serial dilutions of the samples were plated on TSA plates using an IUL EDDY Jet 2 spiral plater. On the following day, the colony-forming units (CFUs) were counted with an IUL Flash & Go instrument. For the bacterial killing assay with USA300 and USA300ΔαβδΔ, neutrophils were incubated with opsonized bacteria at the indicated MOI for 2 hours in a 96-well plate. After lysis of neutrophils, serial dilutions of the samples were plated on TSA plates and CFUs were counted as described previously.

Statistics

Statistical analyses were performed using Graph Pad Prism 6.01. A 2-tailed *t* test was used to compare 2 data groups, and multiple groups were compared using two-way analysis of variance.

Ethics Statement

Blood was collected from healthy adult volunteers and written informed consent was given. The institutional review board of the University of Tübingen approved the study and all adult subjects provided informed consent. This study was done in accordance with the ethics committee of the medical faculty of the University of Tübingen that approved the study (Approval number 015/2014 BO2).

Results

Formyl-peptide receptor ligands enhance bacterial phagocytosis by human neutrophils

Short formylated peptides and PSMs were previously shown to be ligands for FPR1 and FPR2, respectively [5, 25]. Neutrophils respond to these ligands primarily by migrating to sites of infection. Because the primary task of neutrophils is to phagocytose pathogens, we evaluated whether the activation of FPRs also affects the uptake of the CA-MRSA USA300 strain. To investigate this possibility, the phagocytosis of serum-opsonized USA300 by human neutrophils that were simultaneously stimulated with different FPR ligands was analyzed. We found that fMLF, a potent ligand of the human FPR1, induced a dose-dependent increase in USA300 phagocytosis (Figure 1A). Furthermore, different α-type PSMs (PSMα2, PSMα3, and δ-toxin) also enhanced phagocytosis (Figure 1A). The inhibition of FPR1 with CHIPS or of FPR2 with WRW_4 showed that the increased phagocytosis through fMLF or α-type PSM stimulation was FPR1- or FPR2-dependent, respectively (Figure 1B and C).

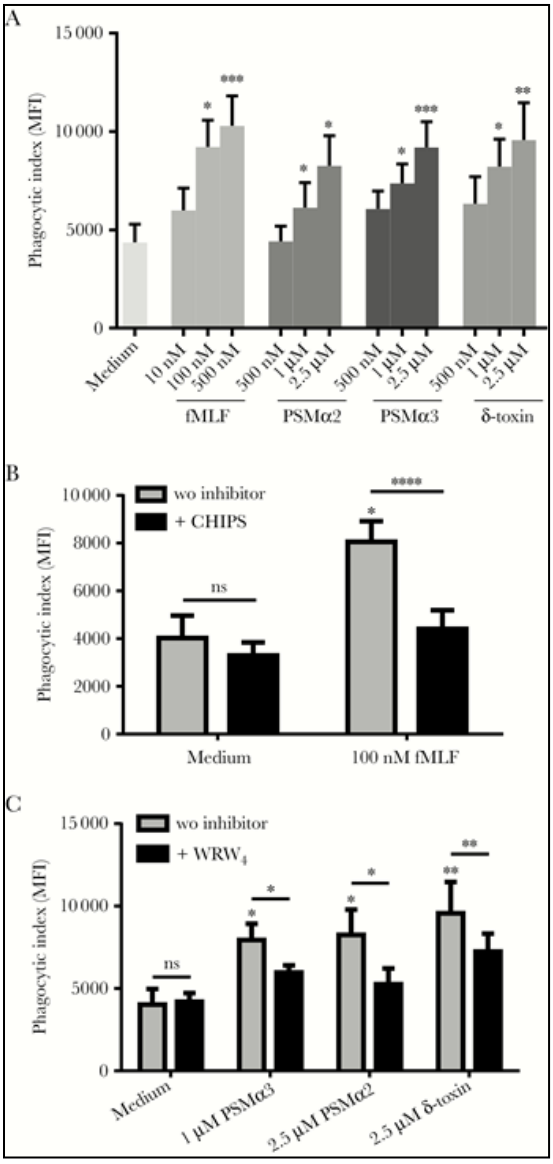

Figure 1. Formyl-peptide receptor (FPR) ligands enhance the phagocytosis of USA300 by human neutrophils receptor-dependent. (A) fMLF, phenol-soluble modulin (PSM) α 2, PSMα3, and δ-toxin induce an increase in the phagocytosis of *Staphylococcus aureus* USA300 by human neutrophils in a concentration-dependent manner. The enhanced phagocytosis promoted by (B) fMLF was blocked by the FPR1 inhibitor CHIPS (1.25 μg/mL), and the increased phagocytosis promoted by (C) α-type PSMs was blocked by the FPR2 inhibitor WRW_4 (22.5 μM). The data represent the means ± standard error of the mean of at least 3 independent experiments. *, $P < .05$, **, $P < .01$, ***, $P < .001$, ****, $P < .0001$, and ns = not significantly different vs the corresponding medium control calculated by Student's *t* test (A) or vs inhibitor-treated cells calculated by two-way analysis of variance (B and C). MFI, mean fluorescence intensity.

To determine whether the increase of *S aureus* phagocytosis by human neutrophils stimulated with FPR ligands was specific for *S aureus* or may be a common mechanism relevant for all bacteria, the phagocytosis assay was repeated with the Gram-positive bacteria *S epidermidis*, *S lugdunensis*, *L monocytogenes* and *E coli*. For all of the tested bacteria, we observed increased phagocytosis when neutrophils were costimulated with FPR ligands compared with unstimulated neutrophils (Figure 2). Thus, the augmented phagocytosis induced by FPR ligands is a common mechanism for different types of bacteria.

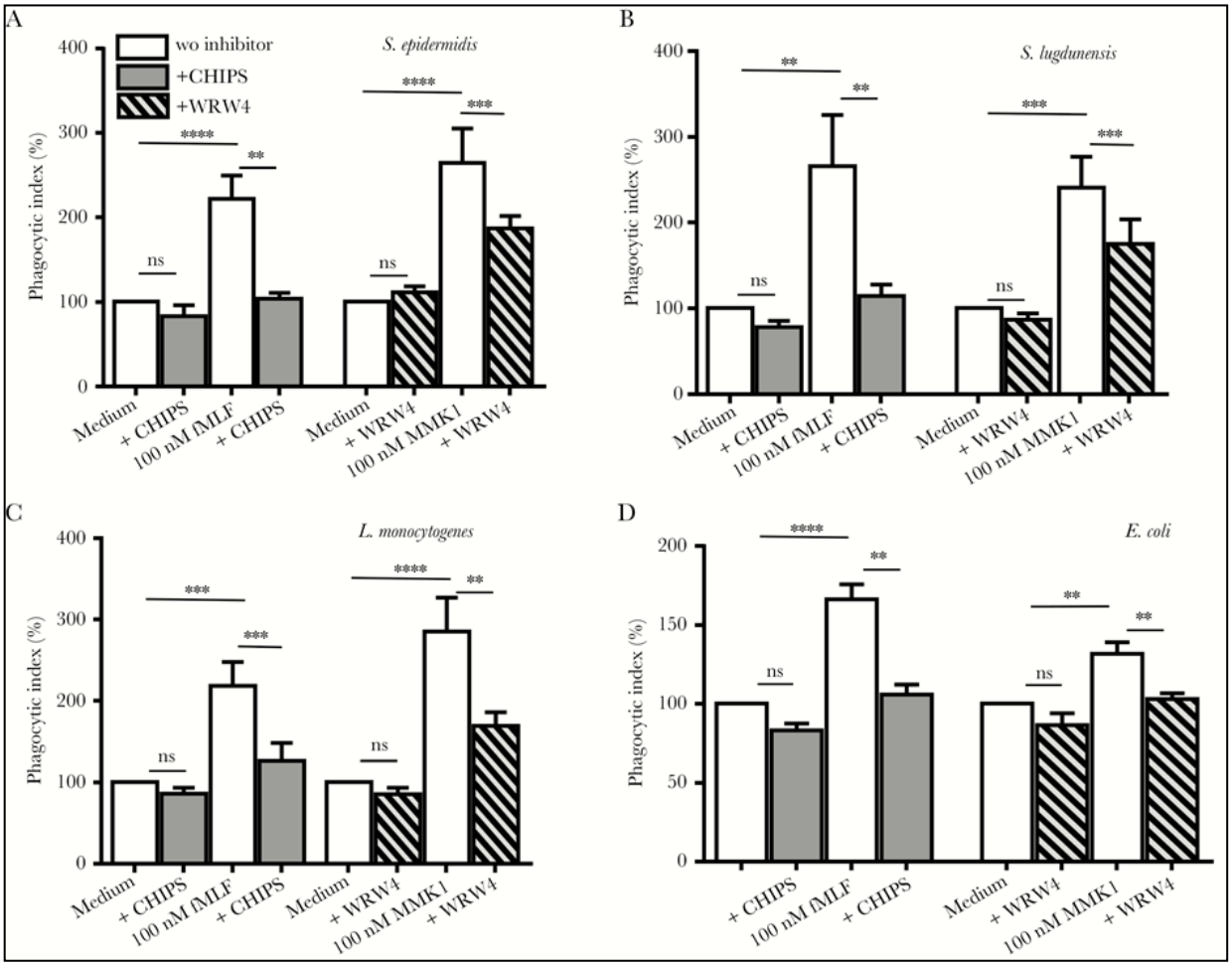

Figure 2. Phagocytosis of Gram-positive and Gram-negative bacteria by human neutrophils is enhanced by formyl-peptide receptor ligands. Phagocytosis of (A) *Staphylococcus epidermidis*, (B) *Staphylococcus lugdunensis*, (C) *Listeria monocytogenes*, and (D) *Escherichia coli* was enhanced by fMLF or MMK1 and could be inhibited by CHIPS or WRW_4, respectively. The data represent means ± standard error of the mean of at least 3 independent experiments. **, $P < .01$, ***, $P < .001$, ****, $P < .0001$, and ns = not significantly different vs the corresponding medium control or inhibitor-treated cells calculated by two-way analysis of variance.

Complement receptors and FCγRI are responsible for the increased phagocytosis

To elucidate whether the receptors mediating the recognition of opsonized particles are involved in the observed enhancement of phagocytosis, the expression of complement and FCγR upon addition of FPR ligands or inhibitors was analyzed. CD11b is part of CR3, which recognizes C3b-opsonized pathogens. In addition to CR3, neutrophils express a second complement receptor, CR1 (CD35), which also recognizes C3b. Pathogens opsonized with IgG antibodies are recognized by FCγR. Peripheral blood neutrophils express FCγRII (CD32) and FCγRIIIB (CD16). During systemic infections and sepsis, FCγRI (CD64) is also expressed [13, 14].

These results show that the stimulation of neutrophils by the FPR1 ligand fMLF or the FPR2 ligand PSMα3 led to significantly increased expression of CD11b, CD35, and CD64 (Figure 3) but not of FCγR CD16 or CD32 (Supplementary Figure 1). The upregulation could be completely inhibited by preincubating neutrophils with the FPR1 inhibitor CHIPS or the FPR2 inhibitor WRW_4, demonstrating that this process is FPR dependent (Figure 3). To correlate the increased expression of complement receptors and FCγRI in response to the FPR ligands with the enhanced phagocytosis of USA300 under these conditions, the phagocytosis assay with function-blocking antibodies directed against the involved complement receptors and FCγRI was repeated. The results show that the combined blocking of CD11b with either CD35 or CD64 almost completely abrogated the enhanced phagocytosis promoted by the FPR ligands (Figure 3D and Supplementary Figure 2). Thus, FPR ligands of *S aureus* induce the enhanced expression of complement receptors and of FCγRI on the surface of neutrophils, which leads to an increased uptake of bacteria by these professional phagocytes.

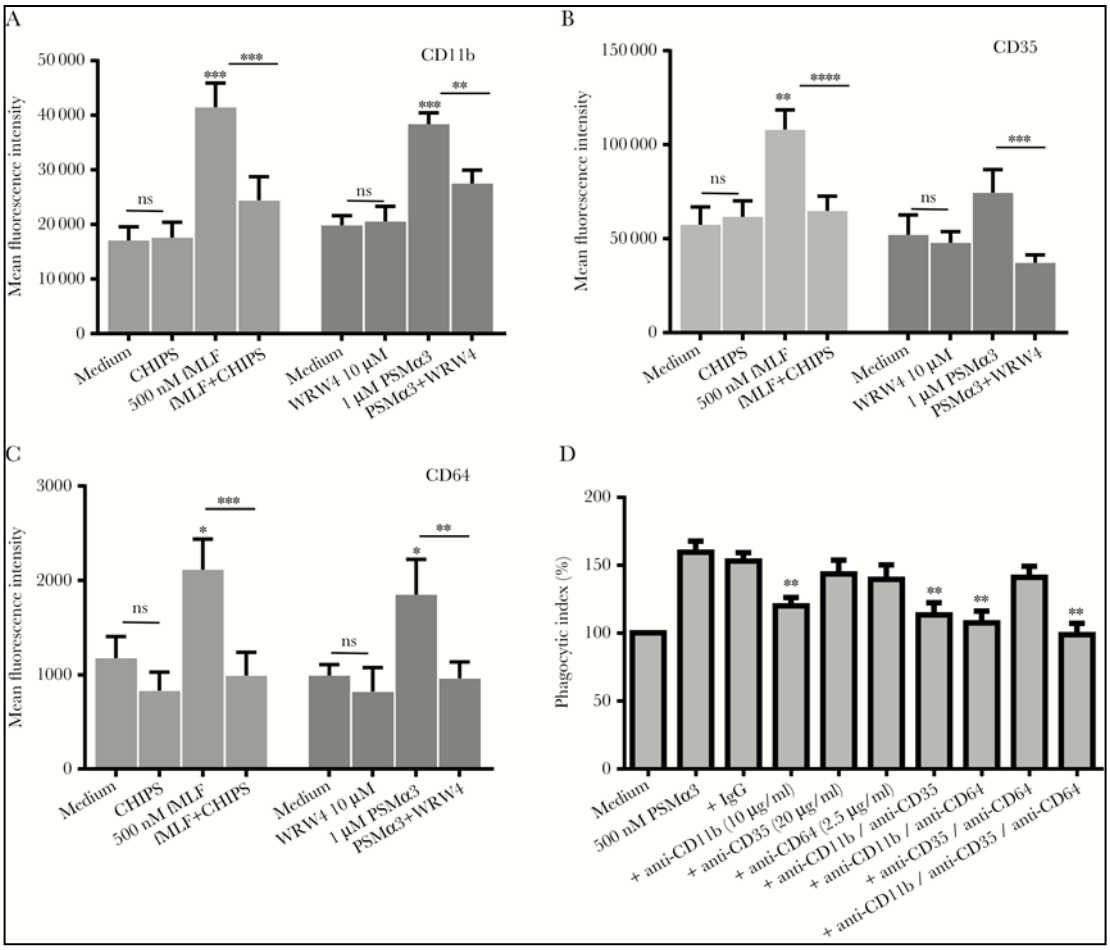

Figure 3. Enhanced phagocytosis by formyl-peptide receptor (FPR)2 ligand is complement receptor- and FCγRI-dependent. The enhanced expression of (A) CD11b, (B) CD35, and (C) CD64 by phenol-soluble modulin (PSM)α3 was FPR1- or FPR2-dependent. The data represent means ± standard error of the mean (SEM) of at least 3 independent experiments. *, $P < .05$; **, $P < .01$; ***, $P < .001$; ****, $P < .0001$. ns = not significantly different vs the corresponding medium control or inhibitor-treated cells calculated by two-way analysis of variance. The incubation of human neutrophils with (D) PSMα3 led to enhanced phagocytosis of USA300, which could be blocked by antibodies against CD11b, CD35, and/or CD64. The data represent the means ± SEM of at least 3 independent experiments. *, $P < .05$ and **, $P < .01$ vs the corresponding medium control calculated by Student's *t* test.

Formyl-Peptide Receptor Activation and Phagocytosis Synergistically Amplify Interleukin-8 Release

Subsequently, we wanted to know what the consequences of the enhanced phagocytosis are. Phagocytosis of opsonized *S aureus* led to a significantly increased amount of IL-8 released by neutrophils compared with unopsonized bacteria (Figure 4A–D). Moreover, stimulation of neutrophils with FPR ligands during the process of *S aureus* phagocytosis led to a synergistic release of IL-8 compared with neutrophils incubated with opsonized bacteria or FPR ligands alone (Figure 4A and B). This effect was phagocytosis-dependent, because it was not observed with unopsonized bacteria (Figure 4C and D).

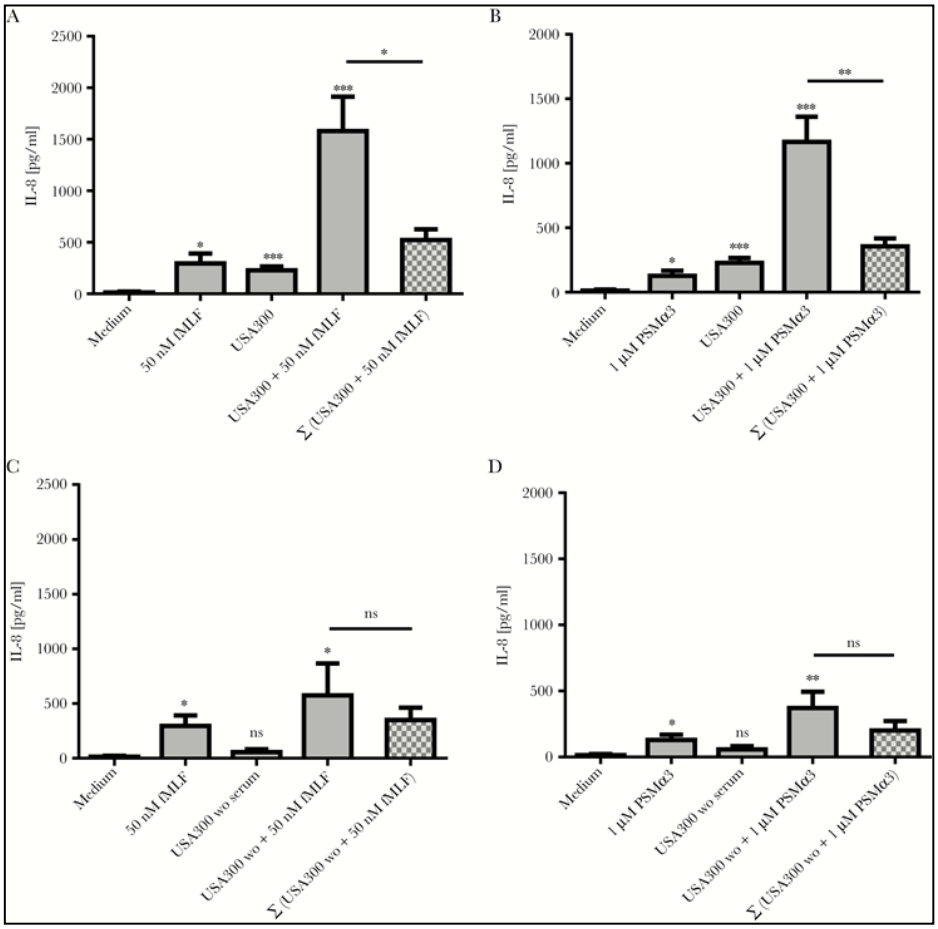

Figure 4. Enhanced phagocytosis promoted by formyl-peptide receptor ligands leads to synergistic interleukin (IL)-8 release. Stimulation of human neutrophils with (A) fMLF or (B) phenol-soluble modulin (PSM)α3 during phagocytosis of USA300 resulted in a synergistic release of IL-8. (C and D) The synergistic release of IL-8 was abrogated using unopsonized bacteria. The data represent means ± standard error of the mean of at least 3 independent experiments. *, $P < .05$, **, $P < .01$, ***, $P < .001$, and ns = not significantly different vs the corresponding medium control or as indicated calculated by two-way analysis of variance.

To determine whether the released IL-8 leads to increased neutrophil recruitment, the supernatants of neutrophils that had been costimulated with FPR ligands during phagocytosis to elicit neutrophil chemotaxis were used. Supernatants of neutrophils that had been incubated with unopsonized bacteria induced almost no neutrophil migration (Figure 5A and B). However, supernatants of FPR-stimulated and phagocytosing neutrophils induced significantly higher neutrophil migration compared with those collected from neutrophils stimulated only with either FPR ligands or phagocytosed bacteria (Figure 5A and B). Thus, these data demonstrated that FPR ligands induce a synergistic release of IL-8 during the phagocytosis of bacteria, resulting in significantly increased neutrophil migration to the site of infection.

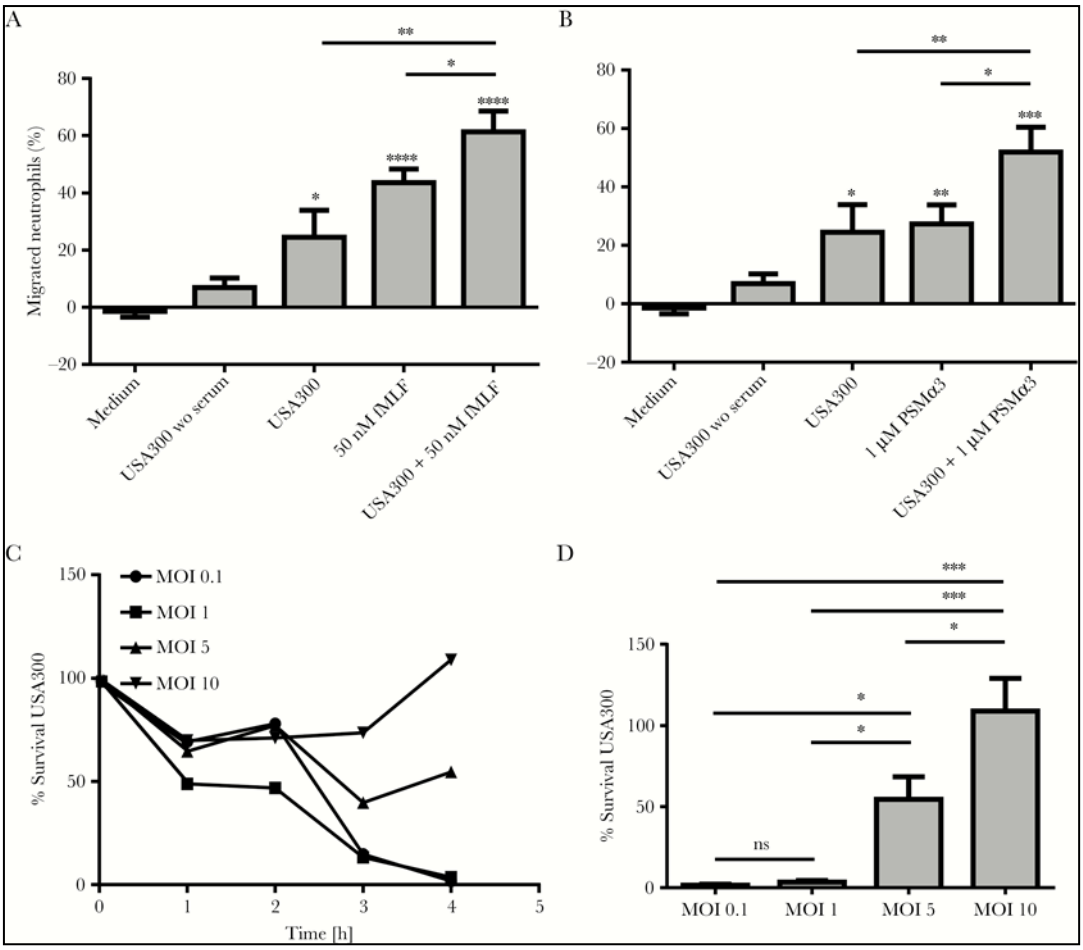

Figure 5. Phagocytosis-induced synergistic interleukin (IL)-8 release leads to significantly increased migration of human neutrophils followed by increased killing of USA300. The synergistic release of IL-8 by (A) fMLF or (B) phenol-soluble modulin (PSM)α3 resulted in significantly increased migration of neutrophils. (C) The killing of USA300 over time depended on the ratio of neutrophils and bacteria. (D) After 4 hours, all bacteria were killed if neutrophils outnumbered bacteria. At higher multiplicity of

infection (MOI) values, the bacteria survived neutrophil killing. The data represent the means ± standard error of the mean of at least 3 independent experiments. *, $P < .05$, **, $P < .01$, ***, $P < .001$, ****, $P < .0001$, and ns = not significantly different vs the corresponding medium control or as indicated calculated by two-way analysis of variance.

Enhanced *Staphylococcus aureus* phagocytosis leads to higher bacterial killing

Phagocytosis of bacterial pathogens leads to the generation of ROS, the fusion of granules with the phagosome, and the release of AMPs, proteases, and degradative enzymes into the phagosome, which is necessary for the killing of bacteria. We next evaluated whether the significant increase in neutrophil migration observed after stimulating the phagocytosis of *S aureus* using different FPR ligands has an effect on bacterial killing by human neutrophils. Therefore, human neutrophils were challenged with USA300 at different multiplicities of infection values for approximately 4 hours and determined bacterial and neutrophil survival at different time points. The results showed that approximately 50% of the bacterial cells were killed by human neutrophils during the first 2 hours irrespective of the MOI used (Figure 5C), whereas a clear difference in neutrophil survival was observed already after 1 hour of coincubation of opsonized bacteria and neutrophils. If bacteria outnumbered neutrophils, a rapid destruction of neutrophils occurred (Supplementary Figure 3), probably as a result of the *S aureus* PSMs and leukocidins, whereas when neutrophils outnumbered bacteria, the neutrophils remained intact (Supplementary Figure 3). After 4 hours, the destruction of neutrophils by high MOIs led to bacterial proliferation (Figure 5C and D). Under conditions in which the neutrophils were still intact after 2 hours (at MOI 0.1), bacteria were killed 2 hours later (Figure 5C and D and Supplementary Figure 3).

At low MOI values, FPR ligands led to an increase in the killing of *S aureus* by human neutrophils (Figure 6A). In contrast, inhibition of FPR1 and FPR2 by CHIPS and WRW_4, respectively, resulted in increased survival of USA300 (Figure 6B). Beneficial effects of FPR ligands on bacterial killing were abolished after prolonged incubation with higher numbers of bacteria (Figure 6C), whereas under these conditions inhibition of FPRs led to reduced *S aureus* survival probably because more neutrophils remained intact and could not be destroyed by high numbers of toxin-producing *S aureus* (Figure 6D).

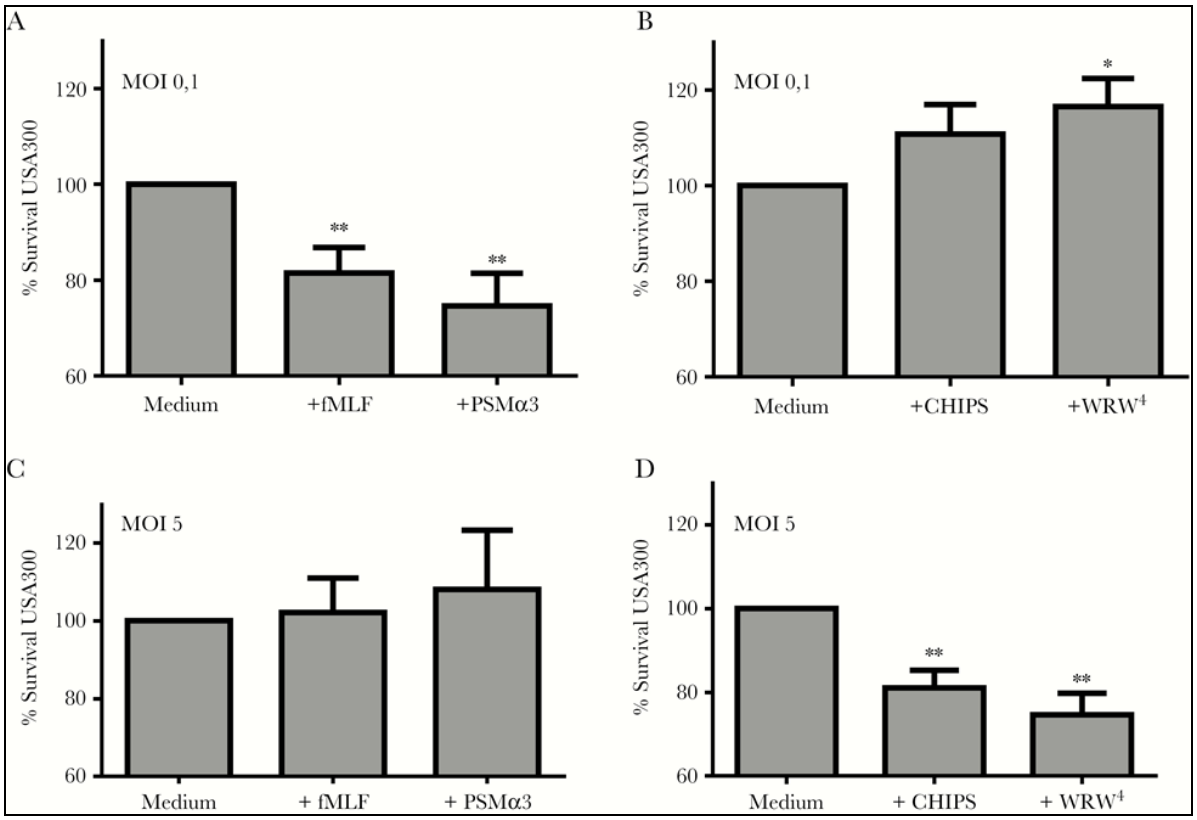

Figure 6. Enhanced phagocytosis could be beneficial for *Staphylococcus aureus* killing or survival. Human neutrophils were incubated for 1 hour with (A) formyl-peptide receptor (FPR) ligands (500 nM fMLF or 1 μM phenol-soluble modulin [PSM] α 3) or (B) FPR inhibitors (1.25 μg/mL CHIPS or 22.5 μM WRW_4) during the killing of USA300. (A) The FPR ligands were beneficial for the immune system at low multiplicity of infection (MOI) values, whereas (B) FPR inhibitors were beneficial for *S aureus* at low MOI values. (C) The FPR ligands led to decreased bacterial killing at high MOI values and at later time points, whereas (D) FPR inhibitors were beneficial for immune system at high MOI values. The data represent the means ± standard error of the mean of at least 3 independent experiments. *, $P < .05$ and **, $P < .01$ vs the corresponding medium control calculated by Student's *t* test.

Discussion

Neutrophils represent the first line of defense during infections and are professional phagocytes of the innate immune system. In this study, we showed that FPR ligands play an important role in the phagocytosis of Gram-positive and Gram-negative bacteria by human neutrophils. The stimulation of FPRs resulted in increased complement and FCγR expression on the surface of neutrophils, resulting in increased bacterial phagocytosis. The results of a study performed in the early 1990s showed that the stimulation of human neutrophils with fMLF enhances CR1

expression and phagocytosis, with the authors speculating that increased CR1 expression is required but not sufficient for the enhanced phagocytosis [26]. In the current study, we demonstrated that besides increased CR1 expression, CR3 and FCγRI are also responsible for the enhanced phagocytosis, because blocking of these receptors abrogated this effect (Figure 7).

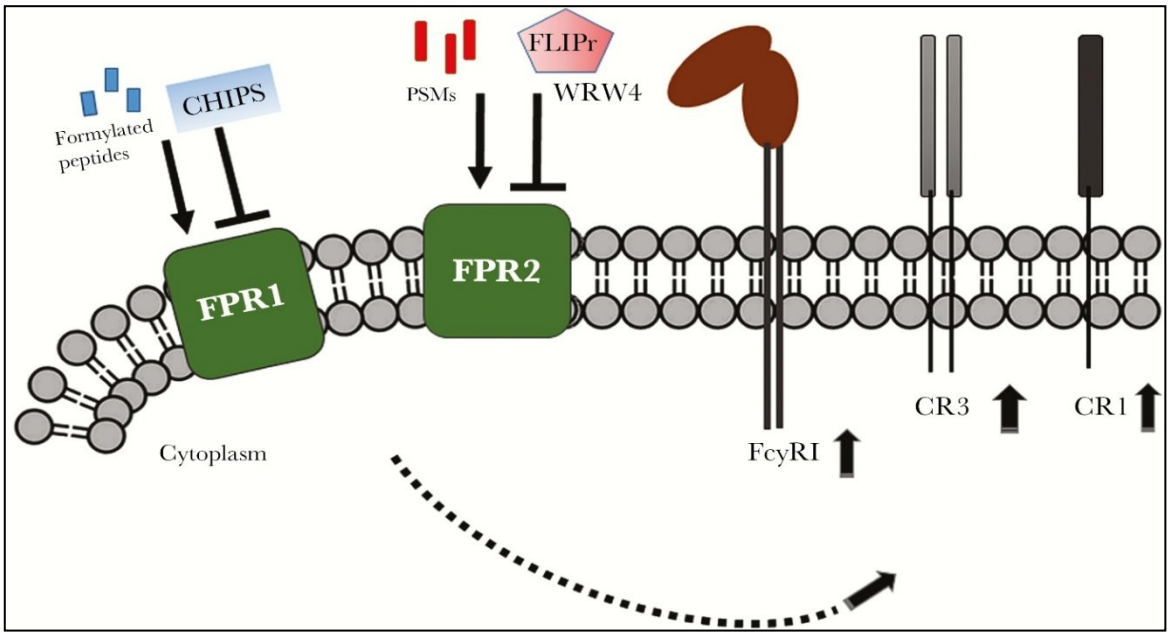

Figure 7. Proposed mechanism of enhanced phagocytosis by formyl-peptide receptor (FPR) ligands. Formylated peptides and phenol soluble modulins (PSMs) activate FPR1 and FPR2, respectively. Activation of FPRs leads to enhanced expression of Fcγ-receptor (FCγRI) as well as complement receptor CR1 and CR3. Inhibition of FPR1 by CHIPS, a staphylococcal-derived inhibitor of FPR1, or FPR2 by WRW_4, a synthetic inhibitor of FPR2 (as well as FLIPr, a staphylococcal-derived inhibitor of FPR2), prevents upregulation of these receptors. Upregulation of CR1, CR3, and FCγRI leads to enhanced phagocytosis of opsonized bacteria.

Phagocytosis results in the release of the chemokine IL-8 by neutrophils and monocytes [15, 16, 18]. In this study, we showed that FPR activation during phagocytosis results in a synergistic release of IL-8, which leads to significantly enhanced recruitment of neutrophils. Phagocytosis and FPR activation both induce activation of the transcription factor nuclear factor (NF)-κB, which results in the expression of IL-8 [27, 28]. The activation of different receptors that all activate NF- κ B was previously shown to result in the synergistic activation of this transcription factor, with phosphorylation of different serine residues of p65 also shown to be involved in this process [28]. The enhanced IL-8 release suggests that a stronger

neutrophil recruitment but also IL-8-mediated neutrophil activation improve the infection outcome. Neutrophils isolated from the lung of patients with chronic obstructive pulmonary disease, bronchiectasis, or cystic fibrosis express less CXCR1 and show strongly reduced capacities to kill *Pseudomonas aeruginosa* after IL-8 stimulation, compared with neutrophils from healthy controls [29]. The enhanced phagocytosis of bacteria upon activation of FPRs may result in increased bacterial killing within neutrophils. The results of our study show that the process of killing is not as straightforward as previously thought as indicated by the complex interactions of the ligand responses. We showed that the ratio of bacteria to neutrophils (multiplicity of infection) has an impact on the outcome of bacterial elimination in vitro and a rapid recruitment of neutrophils to the infection site can disrupt the progression of the infection. This hypothesis is supported by the fact that low MOIs of *L monocytogenes* in a systemic infection model can be eradicated by neutrophils, whereas high MOIs lead to neutrophils exhaustion and bacterial overgrowth [30].

Thus, our data suggest that *S aureus* may inadvertently induce phagocytosis through FPR2 activation by PSMs and may use some neutrophils that remain intact but cannot kill bacteria efficiently thereby promoting persistence. It seems that neutrophils represent a privileged site for *S aureus* in the bloodstream during severe infections providing a mechanism to acquire nutrients and to infect distant sites. Better killing of only a high MOI of a PSM deletion mutant compared with the PSM producing wild type by neutrophils supports this hypothesis (Supplemental Figure 4). This is further supported by the fact that *S aureus* strains from patients with persistent bacteraemia are associated with enhanced survival of bacteria in neutrophils and increased bacterial resistance to neutrophil-derived AMPs. *Staphylococcus aureus* has evolved many strategies to resist AMPs and ROS within the phagosome [14] and to lyse neutrophils from within [31–33]. Staphylococcal PSMs play a crucial role in the destruction of the phagosome from within, whereas the bicomponent pore-forming toxin LukAB destroys the cytoplasmic membrane of host cells [31]. These results may result from a threshold concentration of leukocidins required to destroy neutrophils and release nutrients that the bacteria can use for multiplication. Only a certain number of *S aureus* cells, which reached a high MOI, may be able to produce such leukocidin concentrations. If the threshold leukocidin concentration is not reached, neutrophils will succeed in the competition with *S*

aureus. These assumptions suggest that *S aureus* could promote phagocytosis to better multiply after destruction of neutrophils.

Furthermore, the phagocytosis of *S aureus* also results in an upregulation of the "don't eat me signal" protein CD47 on the surface of neutrophils, preventing the uptake of bacteria-containing neutrophils by macrophages [34]. Whether FPR stimulation or simultaneous FPR activation and phagocytosis influence CD47 expression needs to be analyzed. The hypothesis that *S aureus* uses neutrophils to disseminate to distant organs and induce systemic infections [35–37] is further supported by studies showing that neutropenic cancer patients, who have decreased numbers of neutrophils, are less often affected by *S aureus* bacteremia compared with Gram-negative bacteremia [38, 39]. In contrast, neutropenic cancer patients are more often affected by polymicrobial infections [38]. In addition, nonneutropenic cancer patients affected by *S aureus* bacteremia develop more frequently severe sepsis or septic shock and metastatic infections, and the overall mortality of these patients is significantly higher than that of neutropenic cancer patients [39]. However, whether FPR2 activation during severe *S aureus* infection in vivo leads to less bacterial dissemination needs to be investigated in more detail in the future.

Conclusion

In summary, our results demonstrate that FPRs play an important role in the phagocytosis of bacteria. Most importantly, enhanced phagocytosis leads to enhanced bacterial killing depending on the numbers of bacteria phagocytosed by neutrophils. Formyl-peptide receptors could be a central target for therapeutic intervention to upregulate the neutrophil capacity for phagocytosis and for preventing the development of sepsis. Whether the resolution of local infections exhibiting low numbers of *S aureus* cells could be therapeutically supported by the administration of FPR ligands have to be investigated in the future.

Acknowledgments. We thank Cordula Gekeler for technical support and Stefan Stevanovic who kindly provided us with the synthetic phenol-soluble modulin peptides.

*Author contributions***.** E. W. and D. K. designed the experiments; E. W., K. S., C. B., and D. K. performed the experiments; and E. W., A. P., and D. K. edited the manuscript and interpreted the data.

*Financial support***.** This study was funded by grants from the German Research Foundation (SFB685, TRR156, and SFB766 [to A. P.] and TRR34 [to D. K. and A. P.]).

Potential conflicts of interest. All authors: No reported conflicts of interest. All authors have submitted the ICMJE Form for Disclosure of Potential Conflicts of Interest.

References

1. Lowy FD. Staphylococcus aureus infections. N Engl J Med 1998; 339:520–32.
2. Bitschar K, Wolz C, Krismer B, Peschel A, Schittek B. Keratinocytes as sensors and central players in the immune defense against Staphylococcus aureus in the skin. J Dermatol Sci 2017; 87:215–20.
3. Kolaczkowska E, Kubes P. Neutrophil recruitment and function in health and inflammation. Nat Rev Immunol 2013; 13:159–75.
4. Bufe B, Schumann T, Kappl R, et al. Recognition of bacterial signal peptides by mammalian formyl peptide receptors: a new mechanism for sensing pathogens. J Biol Chem 2015; 290:7369–87.
5. Kretschmer D, Gleske AK, Rautenberg M, et al. Human formyl peptide receptor 2 senses highly pathogenic Staphylococcus aureus. Cell Host Microbe 2010; 7:463–73.
6. Kretschmer D, Rautenberg M, Linke D, Peschel A. Peptide length and folding state govern the capacity of staphylococcal β-type phenol-soluble modulins to activate human formyl-peptide receptors 1 or 2. J Leukoc Biol 2015; 97:689–97.
7. Wang R, Braughton KR, Kretschmer D, et al. Identification of novel cytolytic peptides as key virulence determinants for community-associated MRSA. Nat Med 2007; 13:1510–4.
8. Liles WC, Thomsen AR, O'Mahony DS, Klebanoff SJ. Stimulation of human neutrophils and monocytes by staphylococcal phenol-soluble modulin. J Leukoc Biol 2001; 70:96–102.
9. Weiss E, Hanzelmann D, Fehlhaber B, et al. Formyl-peptide receptor 2 governs leukocyte influx in local Staphylococcus aureus infections. FASEB J 2018; 32:26–36.

10. Björnsdottir H, Dahlstrand Rudin A, Klose FP, et al. Phenol-soluble modulin α peptide toxins from aggressive Staphylococcus aureus induce rapid formation of neutrophil extracellular traps through a reactive oxygen species-independent pathway. Front Immunol 2017; 8:257.
11. van Kessel KP, Bestebroer J, van Strijp JA. Neutrophil-mediated phagocytosis of Staphylococcus aureus. Front Immunol 2014; 5:467.
12. Hoffmann JJ. Neutrophil CD64: a diagnostic marker for infection and sepsis. Clin Chem Lab Med 2009; 47:903–16.
13. Wang X, Li ZY, Zeng L, et al. Neutrophil CD64 expression as a diagnostic marker for sepsis in adult patients: a meta-analysis. Crit Care 2015; 19:245.
14. Spaan AN, Surewaard BG, Nijland R, van Strijp JA. Neutrophils versus Staphylococcus aureus: a biological tug of war. Annu Rev Microbiol 2013; 67:629–50.
15. Arnold R, König W. Interleukin-8 release from human neutrophils after phagocytosis of Listeria monocytogenes and Yersinia enterocolitica. J Med Microbiol 1998; 47:55–62.
16. Bazzoni F, Cassatella MA, Rossi F, Ceska M, Dewald B, Baggiolini M. Phagocytosing neutrophils produce and release high amounts of the neutrophil-activating peptide 1/interleukin 8. J Exp Med 1991; 173:771–4.
17. Friedland JS, Constantin D, Shaw TC, Stylianou E. Regulation of interleukin-8 gene expression after phagocytosis of zymosan by human monocytic cells. J Leukoc Biol 2001; 70:447–54.
18. Kang HJ, Ha JM, Kim HS, Lee H, Kurokawa K, Lee BL. The role of phagocytosis in IL-8 production by human monocytes in response to lipoproteins on Staphylococcus aureus. Biochem Biophys Res Commun 2011; 406:449–53.
19. Heit B, Tavener S, Raharjo E, Kubes P. An intracellular signaling hierarchy determines direction of migration in opposing chemotactic gradients. J Cell Biol 2002; 159:91–102.
20. Bishayi B, Nandi A, Dey R, Adhikary R. Expression of CXCR1 (IL-8 receptor A) in splenic, peritoneal macrophages and resident bone marrow cells after acute live or heat killed Staphylococcus aureus stimulation in mice. Microb Pathog 2017; 109:131–50.

21. Diep BA, Otto M. The role of virulence determinants in community-associated MRSA pathogenesis. Trends Microbiol 2008; 16:361–9.
22. Mack D, Siemssen N, Laufs R. Parallel induction by glucose of adherence and a polysaccharide antigen specific for plastic-adherent Staphylococcus epidermidis: evidence for functional relation to intercellular adhesion. Infect Immun 1992; 60:2048–57.
23. Zipperer A, Konnerth MC, Laux C, et al. Human commensals producing a novel antibiotic impair pathogen colonization. Nature 2016; 535:511–6.
24. Bloes DA, Otto M, Peschel A, Kretschmer D. Enterococcus faecium stimulates human neutrophils via the formyl-peptide receptor 2. PLoS One 2012; 7:e39910.
25. Boulay F, Tardif M, Brouchon L, Vignais P. The human N-formylpeptide receptor. Characterization of two cDNA isolates and evidence for a new subfamily of G-protein-coupled receptors. Biochemistry 1990; 29:11123–33.
26. Ogle JD, Noel JG, Sramkoski RM, Ogle CK, Alexander JW. Effects of chemotactic peptide f-Met-Leu-Phe (FMLP) on C3b receptor (CR1) expression and phagocytosis of microspheres by human neutrophils. Inflammation 1990; 14:337–53.
27. McDonald PP, Cassatella MA. Activation of transcription factor NF-kappa B by phagocytic stimuli in human neutrophils. FEBS Lett 1997; 412:583–6.
28. Chen LY, Pan WW, Chen M, et al. Synergistic induction of inflammation by bacterial products lipopolysaccharide and fMLP: an important microbial pathogenic mechanism. J Immunol 2009; 182:2518–24.
29. Hartl D, Latzin P, Hordijk P, et al. Cleavage of CXCR1 on neutrophils disables bacterial killing in cystic fibrosis lung disease. Nat Med 2007; 13:1423–30.
30. Navarini AA, Lang KS, Verschoor A, et al. Innate immune-induced depletion of bone marrow neutrophils aggravates systemic bacterial infections. Proc Natl Acad Sci U S A 2009; 106:7107–12.
31. Münzenmayer L, Geiger T, Daiber E, et al. Influence of Sae-regulated and Agr-regulated factors on the escape of Staphylococcus aureus from human macrophages. Cell Microbiol 2016; 18:1172–83.

32. DuMont AL, Yoong P, Surewaard BG, et al. Staphylococcus aureus elaborates leukocidin AB to mediate escape from within human neutrophils. Infect Immun 2013; 81:1830–41.
33. Surewaard BG, de Haas CJ, Vervoort F, et al. Staphylococcal alpha-phenol soluble modulins contribute to neutrophil lysis after phagocytosis. Cell Microbiol 2013; 15:1427–37.
34. Greenlee-Wacker MC, Rigby KM, Kobayashi SD, Porter AR, DeLeo FR, Nauseef WM. Phagocytosis of Staphylococcus aureus by human neutrophils prevents macrophage efferocytosis and induces programmed necrosis. J Immunol 2014; 192:4709–17.
35. Gresham HD, Lowrance JH, Caver TE, Wilson BS, Cheung AL, Lindberg FP. Survival of Staphylococcus aureus inside neutrophils contributes to infection. J Immunol 2000; 164:3713–22.
36. Lehar SM, Pillow T, Xu M, et al. Novel antibody-antibiotic conjugate eliminates intracellular S. aureus. Nature 2015; 527:323–8.
37. Thwaites GE, Gant V. Are bloodstream leukocytes Trojan Horses for the metastasis of Staphylococcus aureus? Nat Rev Microbiol 2011; 9:215–22.
38. Velasco E, Byington R, Martins CA, Schirmer M, Dias LM, Gonçalves VM. Comparative study of clinical characteristics of neutropenic and non-neutropenic adult cancer patients with bloodstream infections. Eur J Clin Microbiol Infect Dis 2006; 25:1–7.
39. Venditti M, Falcone M, Micozzi A, et al. Staphylococcus aureus bacteremia in patients with hematologic malignancies: a retrospective case-control study. Haematologica 2003; 88:923–30.

Chapter 8

The Mechanism behind Bacterial Lipoprotein Release: Phenol-Soluble Modulins Mediate Toll-Like Receptor 2 Activation via Extracellular Vesicle Release from *Staphylococcus aureus*

Katja Schlatterer,[a] Christian Beck,[a] Dennis Hanzelmann,[a] Marco Lebtig,[a] Birgit Fehrenbacher,[b] Martin Schaller,[b] Patrick Ebner,[c] Mulugeta Nega,[c] Michael Otto,[d] Dorothee Kretschmer,[#a] and Andreas Peschel[#a]

a Department of Infection Biology, Interfaculty Institute for Microbiology and Infection Medicine Tübingen (IMIT), University of Tübingen, Tübingen, Germany

b Electron-Microscopy, Department of Dermatology, University Hospital Tübingen, Tübingen, Germany

c Department of Microbial Genetics, Interfaculty Institute for Microbiology and Infection Medicine Tübingen (IMIT), University of Tübingen, Tübingen, Germany

d Pathogen Molecular Genetics Section, Laboratory of Bacteriology, National Institute of Allergy and Infectious Diseases, National Institutes of Health, Bethesda, Maryland, USA

#Contributed equally.

Address correspondence to Dorothee Kretschmer, dorothee.kretschmer@uni-tuebingen.de

Published: Schlatterer, K., Beck, C., Hanzelmann, D., Lebtig, M., Fehrenbacher, B., Schaller, M., Ebner, P., Nega, M., Otto, M., Kretschmer, D., and Peschel, A. (2018) The Mechanism behind Bacterial Lipoprotein Release: Phenol-Soluble Modulins Mediate Toll-Like Receptor 2 Activation via Extracellular Vesicle Release from Staphylococcus aureus. *mBio* **9**

ABSTRACT

The innate immune system uses Toll-like receptor (TLR) 2 to detect conserved bacterial lipoproteins of invading pathogens. The lipid anchor attaches lipoproteins to the cytoplasmic membrane and prevents their release from the bacterial cell envelope. How bacteria release lipoproteins and how these molecules reach TLR2 remain unknown. *Staphylococcus aureus* has been described to liberate membrane vesicles. The composition, mode of release, and relevance for microbe-host interaction of such membrane vesicles have remained ambiguous. We recently reported that *S. aureus* can release lipoproteins only when surfactant-like small peptides, the phenol-soluble modulins (PSMs), are expressed. Here we demonstrate that PSM peptides promote the release of membrane vesicles from the cytoplasmic membrane of *S. aureus* via an increase in membrane fluidity, and we provide evidence that the bacterial turgor is the driving force for vesicle budding under hypotonic osmotic conditions. Intriguingly, the majority of lipoproteins are released by *S. aureus* as components of membrane vesicles, and this process depends on surfactant-like molecules such as PSMs. Vesicle disruption at high detergent concentrations promotes the capacity of lipoproteins to activate TLR2. These results reveal that vesicle release by bacterium-derived surfactants is required for TLR2-mediated inflammation.

INTRODUCTION

The innate immune system uses pattern recognition receptors (PRRs) such as the Toll-like receptors (TLRs) to detect conserved microbe-associated molecular pattern molecules (MAMPs) as a hallmark for the presence of invading pathogens (1). TLR2 is the major mammalian PRR that senses the presence of *Staphylococcus aureus*, one of the most frequent and aggressive bacterial causes of wound, soft tissue, lung, and bloodstream infections (2). TLR2 senses bacterial lipoproteins, the characteristic lipid anchor of which is absent from human molecules. *S. aureus* uses a large panel of lipoproteins, most of which are components of ATP-binding cassette (ABC) import systems (3). The lipid anchor attaches lipoproteins to the outer surface of the cytoplasmic membrane, which ensures an appropriate localization in the bacterial cell

envelope but also prevents their release and detection by TLR2. How bacteria release lipoproteins and how they reach TLR2 have remained incompletely understood.

We recently reported that *S. aureus* releases substantial amounts of lipoproteins into culture supernatants only when surfactant-like small peptides, the phenol-soluble modulins (PSMs), are strongly expressed (4). PSMs have direct proinflammatory and leukocyte-recruiting activity through activation of the human and mouse formyl-peptide receptor (FPR) 2, a G-protein-coupled receptor (5, 6). Moreover, PSMs can modulate host membrane functions, including the cytolysis of human cells, at high concentrations (7, 8). Therefore, PSMs are among the most critical and aggressive *S. aureus* virulence factors. *S. aureus* produces seven to eight different PSMs, including the short α-type PSMs (PSMα1 to -4 and the δ-toxin) and the twice-as-long β-type PSMs (PSMβ1 and -2) (9). An additional α-type PSM, PSMmec, is encoded on the mobile genetic element SCCmec type II and III of some methicillin-resistant *S. aureus* (MRSA) strains (10). Interestingly, PSMα1-4 and δ-toxin are abundant on the *S. aureus* cell surface (11). This feature demonstrates that PSMs interact not only with the eukaryotic cell envelope but also with the PSM producer's own membrane. We have also previously shown that PSMs mobilize lipoproteins from the cytoplasmic membrane of *S. aureus* (4), but the precise mechanism has remained unclear.

TLR2 activation by *S. aureus* lipoproteins can contribute to massive inflammation (4) but can also elicit anti-inflammatory responses (12) in a context-dependent, only partially elucidated way. TLR2-deficient mice are more susceptible to death from systemic *S. aureus* infections (4), and *S. aureus* mutants without lipoproteins have abrogated virulence (13). However, *S. aureus* can modulate the release and activity of lipoproteins through several mechanisms. While many commensal bacteria produce highly active lipoproteins, *S. aureus* and the opportunistic pathogen *Staphylococcus epidermidis* incorporate a third long-chain fatty acid into their lipoproteins, which reduces the TLR2-stimulating capacity of lipoproteins (14). Many *S. aureus* strains produce SSL3, a specific inhibitor of TLR2 (15). Moreover, the release of lipoproteins is controlled by the quorum-sensing Agr regulation system, which modulates the expression of lipoprotein-releasing PSM peptides (4).

S. aureus has recently been found to release membrane vesicles (MVs), which can stimulate TLR2 and contribute to inflammation, for instance, in the skin (16,–18). However, it is unclear whether such MVs contain a relevant percentage of *S. aureus* lipoproteins, and the molecular mechanisms responsible for vesicle release remain unknown.

We demonstrate here that PSM peptides promote the release of MVs from the cytoplasmic membrane of *S. aureus* by increasing membrane fluidity, and we provide evidence that bacterial turgor is the driving force for vesicle budding under hypotonic osmotic conditions. Most of the lipoproteins released by *S. aureus* are embedded in MVs, which, when disrupted by high detergent concentrations, show higher capacity to activate TLR2.

RESULTS

Lipoproteins and PSMs released by *S. aureus* are associated with high-molecular-weight aggregates.

PSMs might release lipoproteins from the cytoplasmic membrane of *S. aureus* either as individual molecules with hydrophobic fatty acid chains that are shielded by amphipathic PSM peptides or embedded into larger aggregates, which may be kept together by hydrophobic interactions. To discriminate between these two possibilities, the culture filtrates of *S. aureus* USA300 wild type, which contain large amounts of lipoproteins, and of the isogenic PSM mutant, which releases only residual amounts of lipoproteins, were size-fractioned using centrifugal concentrator cartridges with a molecular weight cutoff of 100 kDa. *S. aureus* lipoproteins and PSM peptides have masses of 33 to 37 (19) and 2.2 kDa (7), respectively, and would be found in the 100-kDa fraction if they were not associated with larger aggregates.

Most of the proteins in *S. aureus* culture filtrates were found in the flowthrough (<100-kDa) fraction, indicating that the majority of secretory proteins do not form larger aggregates (Fig. 1A). However, the PSM mutant contains approximately 15-fold less protein in the high-molecular-weight (>100-kDa) fraction than the wild type (Fig. 1A), indicating that *S. aureus* releases proteins embedded in larger aggregates in a PSM-dependent fashion.

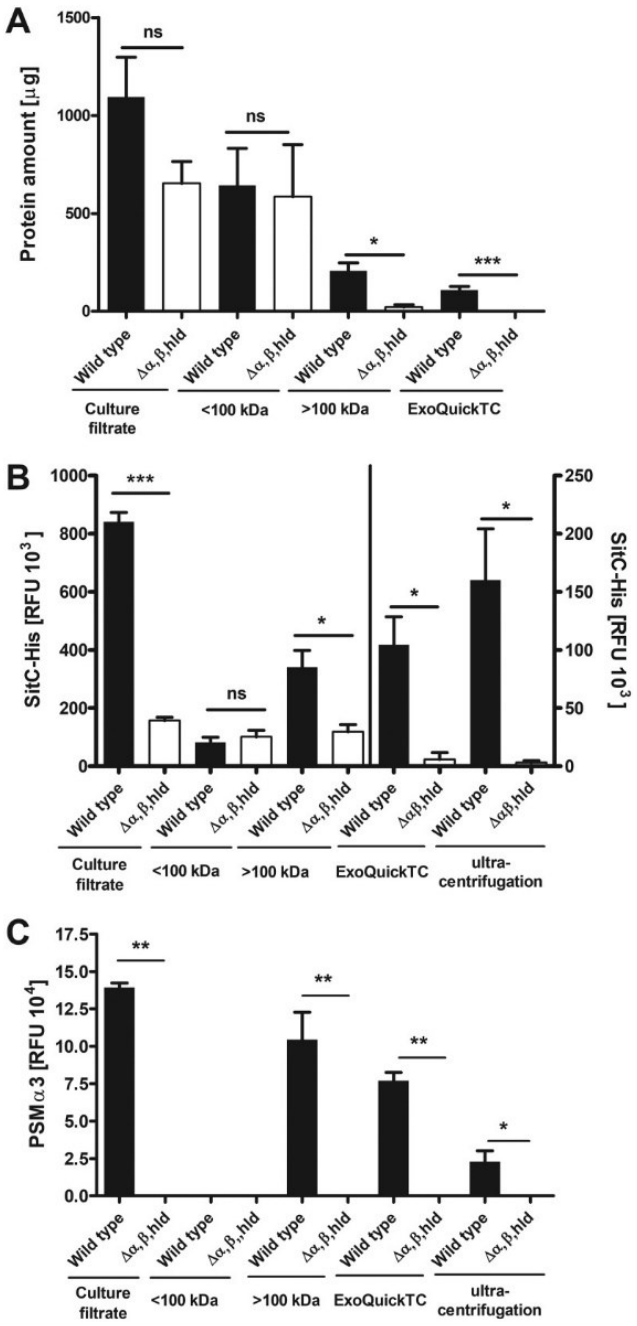

Fig.1: Detection of proteins, SitC, and PSMα3 in different wild-type and PSM mutant (Δ*α,β,hld*) fractions. Culture filtrates were fractioned with 100-kDa centrifugal concentrator cartridges. Fractions were analyzed for protein amounts (A) and amounts of both the model lipoprotein SitC (B) and PSMα3 (C). Culture filtrates, low-molecular-weight (<100-kDa), and high-molecular-weight (>100-kDa) fractions as well as membrane vesicles (MVs) isolated by gradient ultracentrifugation and ExoQuickTC were analyzed. Data represent means ± SEMs from at least three independent experiments. ns, not significant; *, $P < 0.05$; **, $P < 0.01$; ***, $P < 0.001$, significant difference versus USA300 wild type as calculated by the unpaired, two-tailed Student *t* test.

When the size-fractioned culture filtrates from *S. aureus* were analyzed for amounts of the model lipoprotein SitC (18 , 19), using a USA300 strain expressing SitC with a C-terminally linked His tag (SitC-His), most SitC was detected in the high-molecularweight fraction of the wild type, whereas all fractions of the PSM mutant contained only small amounts of SitC (Fig. 1B). This finding is in agreement with our previous report on the essential role of PSMs for lipoprotein release (4) and indicates that most SitC is enclosed in high-molecular-weight aggregates. Furthermore, the amount of PSM 3 in the different fractions was analyzed by immunoblotting, and PSM 3 was also detected mostly in the > 100-kDa fraction of the wild type (Fig. 1C). This finding indicates that PSMs do not only mobilize lipoproteins but also remain associated with them in large aggregates.

***S. aureus*-released lipoproteins are components of membrane vesicles.**

Since the aggregates containing *S. aureus* lipoproteins were found to be over 100 kDa in size, it is possible that these aggregates are large hydrophobic structures like membrane vesicles (MVs), which were previously reported to show a size range of 20 to 130 nm (16). To analyze if the *S. aureus* lipoproteins in culture supernatants are indeed embedded in MVs, the high-molecular-weight fractions of *S. aureus* USA300 and the isogenic PSM mutant (Δα,β,*hld*) were additionally enriched for MVs by MV-precipitation reagent (ExoQuickTC) or density gradient ultracentrifugation (OptiPrep) (Fig.2A), which have been reported to facilitate the isolation of MVs. The wild-type fraction, which was enriched via ExoQuickTC, contained approximately 50% of the protein amount found in the high-molecular-weight fraction, while no proteins could be found in the corresponding fraction from the PSM mutant (Fig.1A). Fractions isolated by density gradient ultracentrifugation also showed decreased protein amounts in the PSM mutant fraction compared to the wild type (see Fig.S1A in the supplemental material).

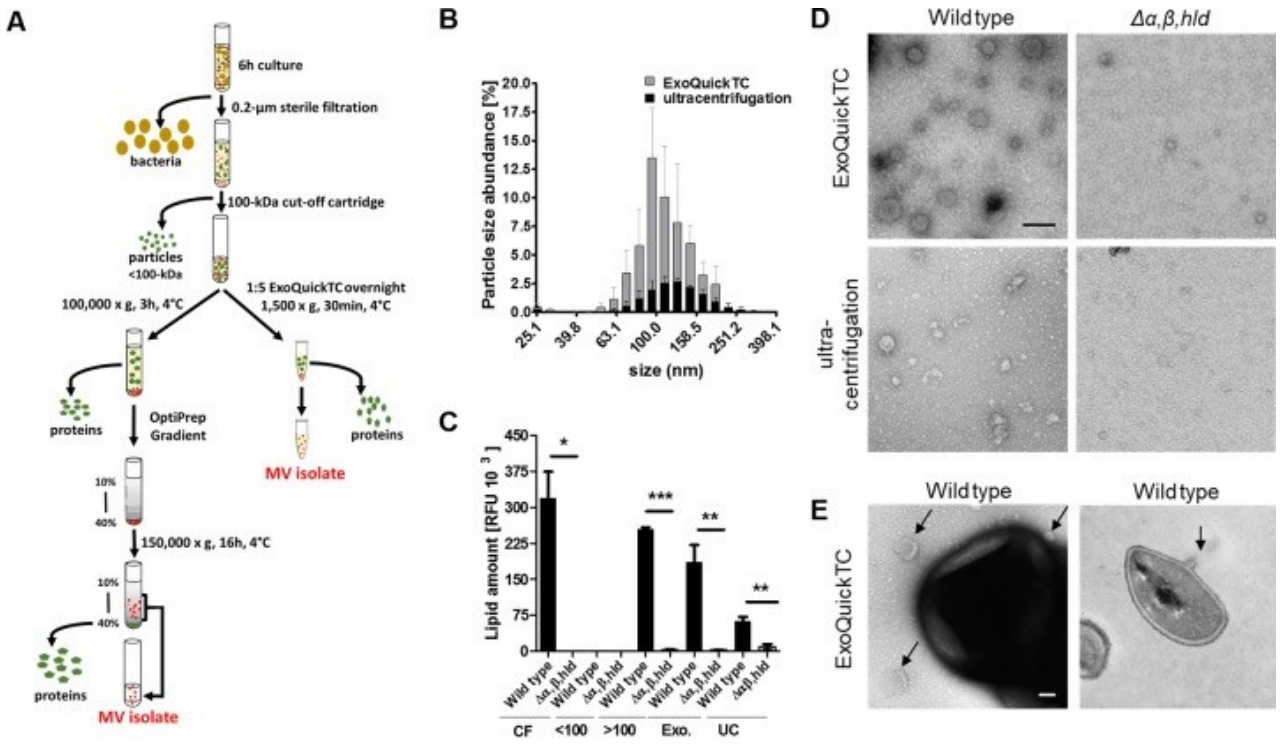

Fig.2: *S. aureus* MV biogenesis is PSM dependent regardless of the MV isolation method. (A) Schematic representation of the vesicle isolation using the ExoQuickTC kit and gradient ultracentrifugation. (B) Particle size analysis via dynamic light scattering in wild-type MVs isolated by ExoQuickTC and gradient ultracentrifugation. (C) Lipid amount (FM4-64 dye) in culture filtrates (CF) and low-molecular-weight (<100-kDa), high-molecular-weight (>100-kDa), and MV fractions isolated via ExoQuickTC (Exo.) and gradient ultracentrifugation (UC). (D) Electron microscopic (TEM) images of wild-type and *Δα,β,hld* MVs after isolation with the ExoQuickTC isolation kit and OptiPrep gradient ultracentrifugation (scale bar, 0.1 µm). (E) TEM images of USA300 wild-type bacteria and associated membrane vesicles (indicated by black arrows) in a negative-stained and an ultrathin section (scale bar, 0.1 µm). Data in panel B represent means and data in panel C represent means ± SEMs from at least three independent experiments. *, $P < 0.05$; **, $P < 0.01$; ***, $P < 0.001$, significantly different versus USA300 wild type, as calculated by the unpaired, two-tailed Student *t* test. Data in panels D and E show one representative example.

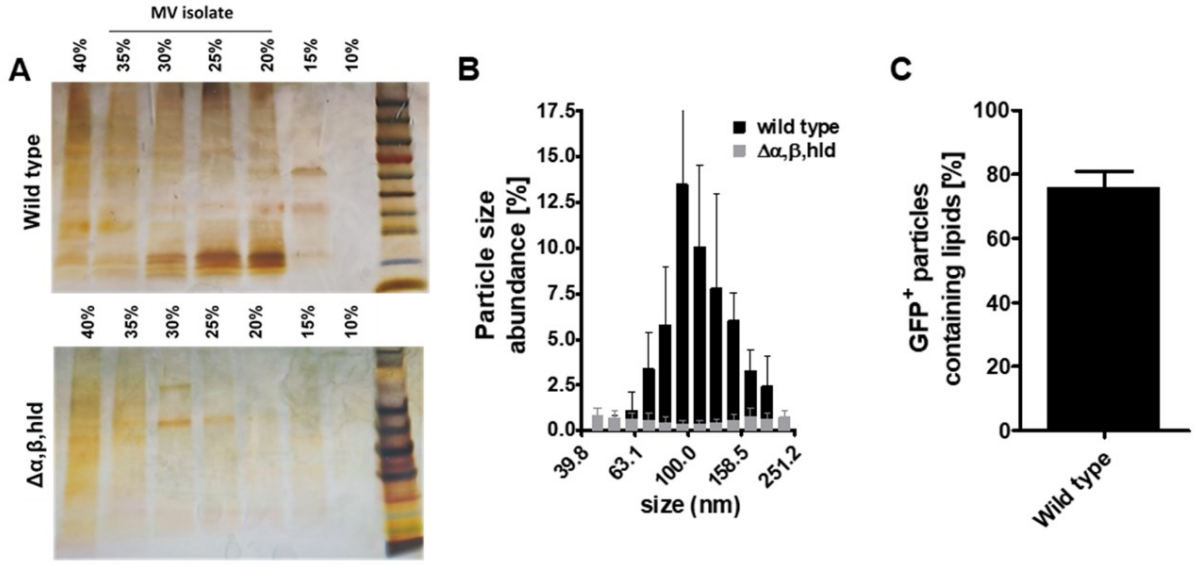

Fig.S1: Determination of protein amounts, MV size, and cargo in MV isolates of wild-type and Δ*α,β,hld* strains. (A) Silver staining of MV isolates from USA300 pTX SitC-His and Δ*α,β,hld* pTX SitC-His recovered via OptiPrep gradient ultracentrifugation. Fractions showing similar protein patterns (35 to 20% OptiPrep) were pooled and referred to as MV isolates. (B) Particle size analysis via dynamic light scattering in wild-type and PSM mutant MVs isolated by ExoQuickTC. (C) Flow cytometric analysis of GFP-positive particles additionally positive for lipids (FM4-64) after isolation from USA300 carrying the pTX143-S3-GFP plasmid. Data in panels B and C represent means from at least three independent experiments. Data in panel A show one representative of at least three independent experiments.

The particle sizes in the MV-containing fractions gained by both isolation methods were determined by dynamic light scattering analysis and were found to be in the range of 60 to 200 nm with a maximum around 100 nm (Fig.2B and Fig.S1B), which is similar to the reported sizes of *S. aureus* MVs. Furthermore, by using transmission electron microscopy (TEM), we observed vesicles with average diameters of 80 to 100 nm in wild type but not in PSM mutant fractions prepared via OptiPrep or ExoQuickTC (Fig.2D). Moreover, individual *S. aureus* cells were found to constrict MV-like structures (Fig.2E).

The presence of membrane lipids is a hallmark for MVs. Although microscopically, more MVs are visible in wild-type than in PSM mutant MV preparations, it is difficult to quantify vesicles by TEM. We used a specific fluorescent membrane dye (FM4-64) to quantify the amount of lipids in the MV and size-separated fractions. All fractions

containing MVs exhibit substantial FM4-64 signals. Moreover, the significantly decreased amounts of lipids in all fractions of the PSM mutant compared with the wild type (Fig.2C) match the results from protein detection and TEM analysis. Additionally, MVs could be analyzed by flow cytometry upon staining with FM4-64 in wild-type ExoQuickTC vesicle isolates but not in isolates from the PSM mutant (*Δα,β,hld*) or a mutant lacking only PSMα1 to -4 (Δ*psmα1-4*) (Fig.3A). Likewise, in USA300 Δ*agr* and the *agr*-deficient laboratory strain SA113, which do not express PSMs, MV release was substantially reduced (Fig.3A). Addition of synthetic PSMα3 to the PSM mutant culture, or complementation of SA113 with a plasmid carrying *psmα1-4*, successfully restored the release of MVs (Fig.3A), confirming the PSMα1 to -4-dependent MV biogenesis in *S. aureus*. Altogether, this corroborates recent findings on the PSM-promoted release of proteins, lipids, nucleic acids, and ATP from *S. aureus* cells (16).

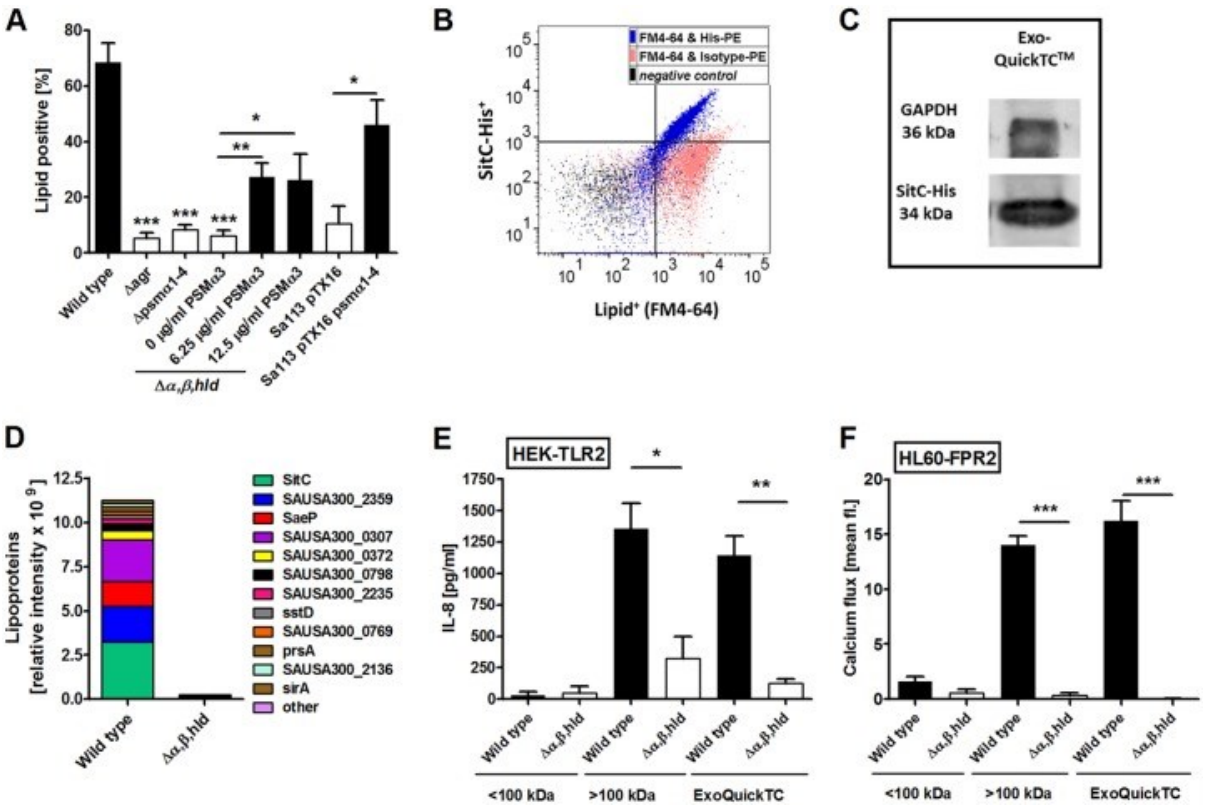

Fig. 3: Composition and host-activating capacity of MVs isolated from wild-type and Δ*α,β,hld* bacterial cultures. (A) Flow cytometry analysis of MVs recovered from strains without PSM expression such as USA300 Δ*agr*, USA300 Δ*psmα1-4*, the PSM mutant (*Δα,β,hld;* lacking all PSMs), or the *agr*-deficient laboratory strain SA113 revealed substantially reduced MV amounts. Addition of synthetic PSMα3 to the PSM mutant culture, or complementation of SA113 with a plasmid carrying *psmα1-4*, successfully restored the release of MVs. (B) Lipid membrane (FM4-64$^+$)-positive particles from USA300 Δ*spa* pTX SitC-His are also SitC-His positive when analyzed by flow cytometry. (C) Immunoblotting of wild-type ExoQuickTC-isolated MVs detecting the cytoplasmic protein glyceraldehyde-3-phosphate dehydrogenase (GAPDH) and the model lipoprotein SitC. (D) Proteomic analysis reveals the presence of other lipoproteins in addition to SitC in wild-type ExoQuickTC-isolated MVs. (E) Larger-than-100-kDa and MV fractions from wild type can activate TLR2-transfected HEK293 cells, resulting in the secretion of IL-8 cytokines. All <100-kDa fractions as well as all Δ*α,β,hld* fractions fail to induce a strong IL-8 secretion. (F) Wild-type MV and high-molecular-weight (>100-kDa) fractions induce calcium influx in FPR2-transfected HL60 cells. All other fractions fail to induce calcium influx. Data in panels A, E, and F represent means ± SEM from at least three independent experiments. *, $P < 0.05$; **, $P < 0.01$; ***, $P < 0.001$, significant difference versus USA300 wild type, as calculated by the unpaired (A) or paired (E and F) two-tailed Student *t* test. Data in panel D represent means of three independent experiments, and data in panels B and C are each representative of three independent experiments.

To analyze the presence of SitC and PSMs in *S. aureus*-released MVs, the vesicle preparations were also subjected to immunoblotting. Indeed, SitC and PSMα3 were found in the ExoQuickTC- or OptiPrep-isolated MV fractions of *S. aureus* wild type but not of the PSM mutant (Fig.1B and C and 3D), which confirms that SitC and PSMs do not occur in culture filtrates as individual molecules but as a components of MVs. Using flow cytometry, colocalization of lipid membranes (FM4-64) and SitC (Fig.3B) could be confirmed using a His-tag-specific antibody to detect SitC-His. Since MVs are constricted from the cytoplasmic membrane, they are likely to contain cytoplasmic proteins. In addition to the lipoprotein SitC, the plasmid-expressed cytoplasmic green fluorescent protein (GFP) was also found to colocalize with lipids (Fig.S1C) when analyzed by flow cytometry. Immunoblotting of wild-type MV fractions additionally confirm an association of the cytoplasmic protein glycerophosphate dehydrogenase (GAPDH) with MVs (Fig.3C). MV preparations were furthermore subjected to proteomic analysis, and the wild-type MVs were found to contain cytoplasmic proteins and other lipoproteins in addition to SitC (Fig.3D and Data Set S1).

The high-molecular-weight and the MV-enriched fractions were also tested for their TLR2- and FPR2-activating capacities using TLR2-transfected HEK293 cells and FPR2-transfected HL60 cells, respectively. In agreement with the presence of large amounts of lipoproteins and PSMs in high-molecular-weight and MV fractions from the USA300 wild type (Fig.1B and C), high TLR2- and FPR2-stimulating activities were observed in these fractions (Fig.3E and F). In contrast, the same volumes of the MV fractions from the PSM mutant were largely inactive, which is in agreement with the low MV content. Likewise, all analyzed fractions <100 kDa showed only minimal TLR2 or FPR2 activity (Fig.3E and F). Thus, the vast majority of TLR2-activating lipoproteins and FPR2-activating PSMs in S. aureus culture supernatants did not occur as individual molecules but as components of MVs. Altogether, these data confirm that lipoproteins and cytoplasmic proteins in the *S. aureus* culture supernatant are enclosed in MVs.

PSMα3 increases *S. aureus* membrane fluidity and promotes turgor-dependent MV budding.

While eukaryotic cells use sophisticated molecular machines to constrict MVs, no such systems are known in prokaryotes (17). Because PSMs have surfactant-like properties (9), it is tempting to assume that they alter the properties of the *S. aureus* cytoplasmic membrane in a way that favours the spontaneous budding of MVs. A membrane fluidity assay based on the fluorescence of a membrane-integrating fluorescent dye (20) was used to analyze the impact of PSMs on *S. aureus* membrane properties. *S. aureus* wild type exhibited a higher intrinsic membrane fluidity than the PSM mutant (Fig.4A), suggesting that PSMs may increase fluidity. In accordance with this idea, the addition of synthetic PSMs to PSM mutant bacteria also led to increased membrane fluidity. The PSMα peptides, in particular PSMα3 and -α2, had a much stronger impact on membrane fluidity than δ-toxin (Hld) (Fig.4B to E), which is in agreement with the documented, particularly high capacity of PSMα3 to disrupt membranes (7). The lytic effect of PSMs, especially PSMα3, is most likely a result of their strong α-helical and amphipathic structure (7). Analysis of an alanine substitution library of PSMα3 has revealed the importance of the positively charged lysine residues for the lytic capacity of PSMα3 (21). Selected alanine substitution variants of PSMα3 showed an impaired ability to increase the membrane fluidity in comparison to PSMα3, indicating that the amphipathic, α-helical structure is important for the increase in membrane fluidity (Fig.4F).

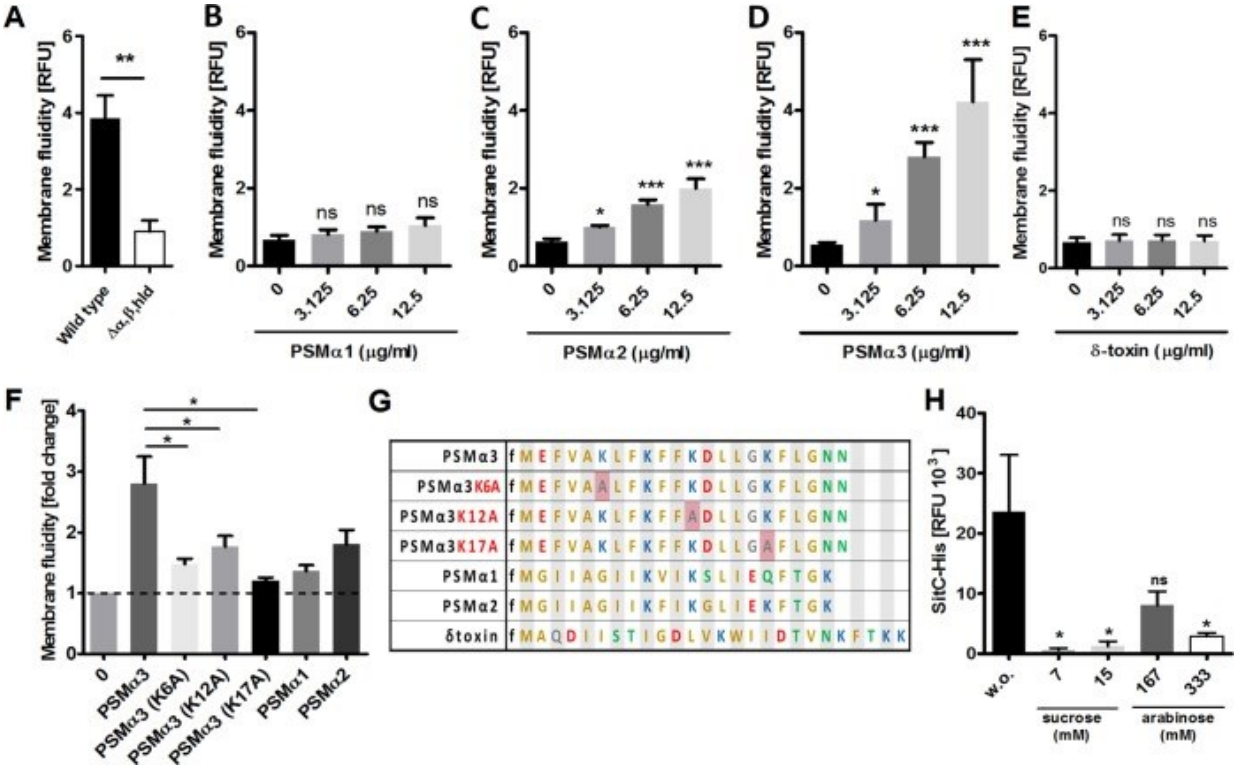

Fig. 4: PSMα3 increases membrane fluidity, while turgor pressure influences vesicle formation. (A) Measurements of membrane fluidity in USA300 wild-type and USA300 Δ*α,β,hld* bacteria containing 10% autologous culture filtrate reveal higher intrinsic fluidity of the wild-type cytoplasmic membrane. (B to E) Membrane fluidity of USA300 Δ*α,β,hld* bacteria after addition of the indicated synthetic PSMs. (F) Amino acid exchanges in the sequence of PSMα3 strongly impair the positive effect of the native PSMα3 on the membrane fluidity. Dashed line represents a fold change of one (base value). (G) Sequences of the synthetic PSMs and the PSMα3 alanine substitution variants. (H) Immunoblot analysis of MV-bound SitC released from USA300 pTX SitC-His after addition of the indicated concentrations of sucrose or arabinose or without (w.o.) addition to the bacterial culture. (A to F) Membrane fluidity was measured as relative fluorescence units (RFU) and calculated as ratio of excimer/monomer RFU of the lipophilic pyrene probe. Data in panels A to F and H represent means ± SEMs from at least three independent experiments; ns, not significant; *, $P < 0.05$; **, $P < 0.01$; ***, $P < 0.001$, significant difference versus untreated bacteria as calculated by the unpaired, two-tailed Student *t* tests.

While increased membrane fluidity can promote vesicle budding (22), the mechanism providing the driving force for this energy-dependent process has remained unknown. *S. aureus* usually encounters hypotonic conditions in human body fluids or in culture media, and it is tempting to assume that turgor pressure may be the driving force for vesicle constriction. To evaluate this hypothesis, *S. aureus* was incubated in the presence of increasing concentrations of the solutes sucrose and arabinose, which do not affect *S. aureus* growth (Fig.S2A) but are thought to decrease the turgor pressure in *S. aureus* cells. Notably, both substances strongly reduced the release of SitC-containing MVs (Fig.4H and Fig.S2B). Thus, a high turgor in addition to a PSM-mediated increase in membrane fluidity is essential for membrane vesicle release by *S. aureus*.

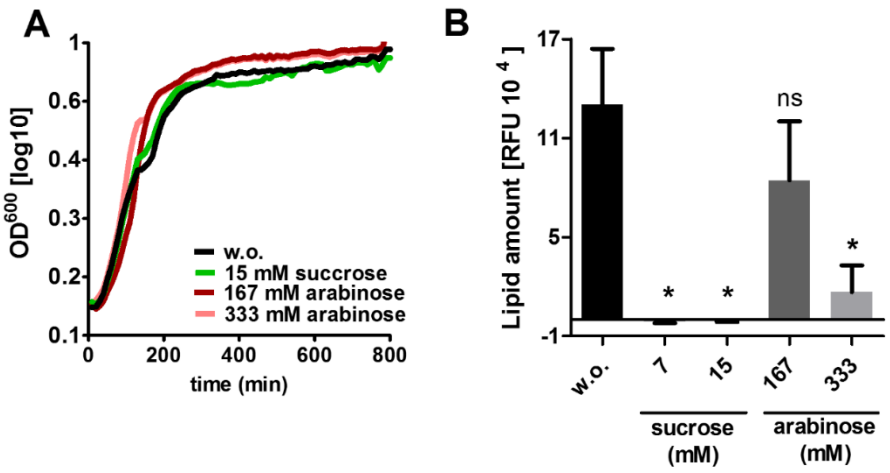

Fig. S2: Influence of turgor pressure on vesicle biogenesis. (A) Growth of USA300 wild type in medium containing the indicated turgor-affecting substances. (B) Lipid amounts in MV isolates recovered from bacteria grown in media containing the indicated turgor-affecting substances. Data in panel A represent means and data in panel B represent means ± SEMs from at least three independent experiments. ns, not significant; *, $P < 0.05$, significant difference versus untreated bacteria as calculated by the unpaired, two-tailed Student *t* tests.

High concentrations of PSMs and other surfactants destroy *S. aureus* membrane vesicles, which promotes the proinflammatory activity of *S. aureus* lipoproteins.

To analyze the stability of lipoprotein- and PSM-containing vesicles, the preparations were treated with the nonionic detergent Triton X-100, with sonication, or with high concentrations of PSMα3. Notably, all treatments led to a decay of FM4-64-positive MV particles, as measured by flow cytometry (Fig.5A) and as verified by TEM (Fig.5B). While PSMs mediate the release of membrane vesicles at low concentrations (<12.5 µg/ml), they were found to destroy them at very high concentrations (>12.5 µg/ml). This phenomenon correlates with the present finding that MVs can mostly be isolated from bacterial cultures at between 6 and 8 hours of cultivation (Fig.5D), when the PSM-controlling quorum-sensing system Agr is most active (23). Under these conditions, the PSMα3 concentration in culture supernatants was below 12.5 µg/ml. After 10 hours of growth, when Agr strongly reduces its activity (23), PSMα3 concentrations reached higher values, and consequently, only small amounts of MVs were found in wild-type culture supernatants (Fig.5D).

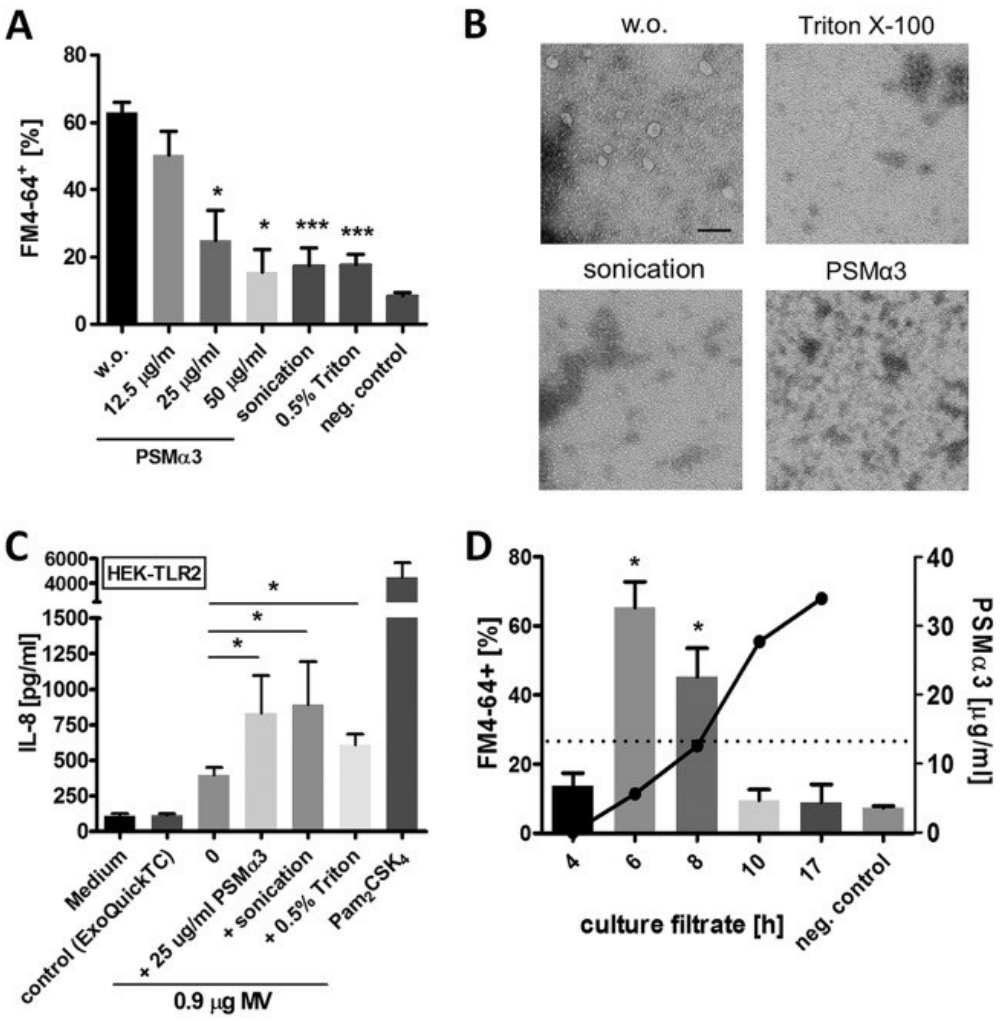

Fig. 5 Role of PSMs in vesicle biogenesis and vesicle disruption. (A) Flow cytometric analysis shows disruption of wild-type membrane vesicles through PSMα3 (>12.5 µg/ml), sonication, or 0.5% Triton X-100. (B) TEM of vesicles disrupted by PSMα3, sonication, or Triton X-100 (scale bar, 0.1 µm). (C) Disrupted membrane vesicles show higher activation of TLR2-transfected HEK293 cells. TLR2 agonist Pam_2CSK_4 (300 ng/ml) was used as a positive control. (D) Membrane vesicle counts from USA300 wild type at different culture time points analyzed by flow cytometry (bars) and the corresponding PSMα3 concentration (dots) in the culture filtrates measured by HPLC (dashed line, 12.5 µg/ml PSMα3). Data in panels A, C, and D represent means ± SEMs from at least three independent experiments. ns, not significant; *, $P < 0.05$; ***, $P < 0.001$, significant difference versus the untreated control (A and C) (w.o. or medium) or negative control (D) as calculated by unpaired (A and D) or paired (C) two-tailed Student's *t* tests. (B) One representative experiment.

The proinflammatory motif of lipoproteins, the characteristic lipid anchor, is buried in the membrane when lipoproteins are embedded in MVs, which raises the question of how lipoproteins can reach TLR2. Vesicle-disrupting surfactants could increase the availability of lipoproteins for TLR2 binding, but they could also cover the hydrophobic fatty acid chains in a way that would abrogate its biological activity. When MV preparations were treated with vesicle-disrupting concentrations of Triton X-100 or PSMα3 or by sonication, their capacity to stimulate TLR2-transfected HEK293 cells was significantly increased (Fig.5C and Fig.S3A), indicating that lipoproteins must be released from MVs to exert their maximal stimulating activity and that surfactants do not abrogate but promote the activity of lipoproteins.

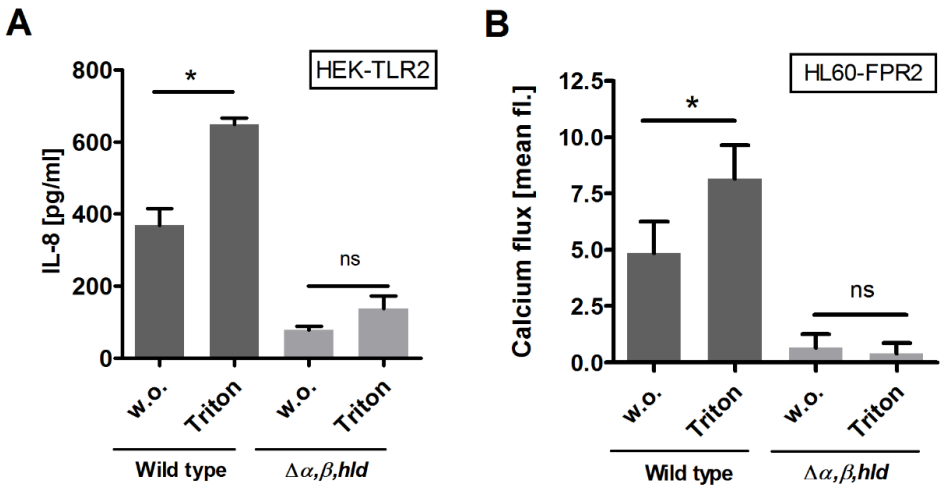

Fig. S3: Stimulation of HEK-TLR2 and HL60-FPR2 cells with Triton X-100-disrupted vesicles. (A) HEK-TLR2 stimulation with intact or with 0.5% Triton X-100-disrupted vesicles (0.5% MV isolation) derived from wild-type and Δ*α,β,hld* mutant cells. TLR2 activation was measured by IL-8 cytokine secretion. (B) Flow cytometric analysis of calcium mobilization in FPR2-transfected HL60 cells after incubation with intact or 0.5% Triton X-100-disrupted vesicles (0.005% MV isolation). Data represent means ± SEMs from at least three independent experiments. ns, not significant; *, $P < 0.05$, significant difference versus untreated vesicles (w.o.) as calculated by the paired, two-tailed Student *t* tests.

DISCUSSION

Lipoproteins are major bacterial MAMPs with particularly important roles in infections caused by Gram-positive bacteria (2, 3), and they can cause exuberant inflammation and contribute to the severity of diseases or orchestrate host defense in a beneficial, sometimes even anti-inflammatory fashion (24). Bacterial pathogens vary strongly in the amounts of lipoproteins that they release (25), and *S. aureus* has been found to modulate TLR2 activation, for instance, by controlling lipoprotein release via the quorum-sensing system Agr (4) or by producing the TLR2-inhibitory protein SSL3 (15). Many aspects of the pathway, from the bacterial release of lipoproteins to their activation of TLR2, have remained unclear. Lipoproteins have difficult physicochemical properties because the hydrophobic fatty acids limit their solubility. Interestingly, the same is true for PSM peptides and their capacity to stimulate FPR2 (8). How lipoproteins are released from bacterial membranes has remained largely unclear, considering that the extraction of fatty acid chains from the cytoplasmic membrane is regarded as an energy-dependent process. PSMs have been found to promote the release of lipoproteins, but the mechanism has remained unknown.

We demonstrate here that lipoproteins are not released as individual molecules but as components of larger MVs. Such vesicles were released only under hypotonic conditions, indicating that strong turgor provides the energy for the constriction of MVs. Factors that impact on peptidoglycan cross-linking, such as autolysins or antibiotics, have been found to influence the amount and size of membrane vesicles probably because they govern the capacity of MVs to penetrate the cell wall (26). The strong curvature that the membrane has to undergo during vesicle budding requires a high level of fluidity. It seems that the surfactant-like properties of PSMs impart the necessary level of fluidity to the membrane, which may explain why MVs are released only in the presence of PSMs and why PSMα s with particularly strong amphipathic properties have the highest MV-releasing capacity. It remains to be analyzed how other bacterial, environmental, or host-derived detergents may affect the release of lipoprotein-containing MVs. It should be noted that the membrane-active antibiotic daptomycin has been shown to promote the release of phospholipids from *S. aureus* (17). The release of TLR2 agonists by skin-associated bacteria is thought to contribute to local inflammation, in particular in chronic disorders such as

atopic dermatitis (27). Along this line, *S. aureus*-derived MVs have been shown to cause strong skin inflammation in a mouse model (28). It will be important to analyze how the components of skin lotions and soaps may facilitate lipoprotein release. Extensive use of skin detergents is known to augment skin inflammation in atopic dermatitis (26), which may in part be due to the mobilization of proinflammatory TLR2 agonists.

Detergent-like molecules such as PSMα3 not only promoted release of vesicles from the *S. aureus* cytoplasmic membrane but also induced their disintegration at high concentrations. Notably, vesicle disintegration was accompanied by an increased capacity of lipoproteins to activate TLR2, suggesting that solubilized lipoproteins can reach the ligand binding pocket of TLR2 more easily than membrane-embedded lipoproteins. The activating motif of lipoproteins is the lipid anchor with its fatty acid chains, which is usually not accessible to TLR2 as long as it is attached to the membrane. Surfactant-like molecules may thus be essential for effective TLR2 activation. Bacterial lipopolysaccharide (LPS), the agonist of TLR4, also needs to be released from membranes to exert its proinflammatory activity (29). Accessory host proteins, such as LPS-binding protein (LBP) and CD14, are thought to facilitate the release of LPS from vesicles and promote their integration into TLR4 (29, 30). Of note, LBP, CD14, and CD36 have also been implicated in TLR2 activation (30,–32), which raises the possibility that these or further, yet-to-be-identified host proteins can contribute to the membrane vesicle extraction of lipoproteins. Some reports have also described the fusion of bacterial MVs with host cells (28), which could transfer lipoproteins into host cytoplasmic membranes and allow them to reach TLR2 by lateral diffusion.

The release of MVs by *S. aureus* and other bacteria has been reported by several laboratories in the past, and some described TLR2-dependent proinflammatory properties of such structures, which is in agreement with our findings (16, 28). Different methods have been described for MV isolation, including precipitation by high-speed centrifugation (33), density gradient centrifugation, and size exclusion centrifugation (18). We compared density gradient centrifugation with a new, particularly convenient method, based on the MV isolation reagent ExoQuickTC, which has been developed for preparation of eukaryotic exosomes (34). We

demonstrate that ExoQuickTC preparations yield very similar results in several microscopy, flow cytometry, and bioactivity-based assays and lead to even higher MV yields than density gradient centrifugation. Thus, the new technique may strongly facilitate future research on bacterial MVs and on the potential application of MVs for vaccination purposes (35). Some previous studies have attributed cytotoxic properties to *S. aureus* MVs (16), which may be due to vesicle-associated PSM peptides. Some have also reported the presence of secretory toxins in MVs, such as γ-hemolysin, leucocidin D, and exfoliative toxin C (36), which is unexpected because the content of vesicles should be derived from the bacterial cytoplasm. However, even secretory proteins could remain associated with the membranes of MVs. Careful evaluation of the purity and absence of cell debris will be important for future studies on the molecular properties of bacterial MVs.

Our findings suggest that PSMs may use two different strategies to exit bacterial cells—the previously described Pmt ABC transporter, probably taking PSMs up from the membrane and excreting them as free molecules (37), and the release of PSM-containing MVs. Our study also underscores the crucial roles of PSMs in the release of membrane-embedded and cytoplasmic proteins ranging from the mobilization of protein-containing MVs to the disintegration of vesicles at high concentrations, which leads to the release of free lipoproteins and cytoplasmic proteins. The release of cytoplasmic proteins by Gram-positive bacteria, some of which have moonlighting activities when they are extracellular, has been documented in several studies (18). The surfactant-promoted release of membrane vesicles may represent the major pathway for their release.

MATERIALS AND METHODS

Bacterial cultivation and preparation of culture filtrates.

Bacterial strains (see TableS1 in the supplemental material) were maintained on sheep blood tryptic soy agar plates. Hemolysis on blood agar plates and RNAIII expression were monitored to confirm functional Agr systems and toxin production in *S. aureus* USA300. All bacteria were grown in tryptic soy broth (TSB) or in TSB without glucose supplemented with 0.5% xylose (*S. aureus* USA300 pTX SitC-His strains). Bacterial cultures were supplemented with the appropriate antibiotics and

grown in flasks on a 37°C shaker, and culture supernatants were obtained by centrifugation of 6-h or 10-h cultures by filtration through 0.2-µm-pore-size filters.

Vesicle isolation from bacterial culture filtrates.

To obtain size-separated culture supernatants, sterile-filtered culture supernatants from late exponential growth phase (6 h) of *S. aureus* USA300 were transferred onto 100-kDa centrifugal concentrator cartridges (Vivaspin 20; Sartorius) and centrifuged at 3,000 × *g*. The >100-kDa fraction was resuspended in 1 ml PBS or TSB. For vesicle isolation with the ExoQuickTC kit (EQPL10TC; System Bioscience), the over-100-kDa culture filtrate fractions were incubated overnight at 4°C with ExoQuickTC at a ratio of 5:1. Vesicles were then pelleted by centrifugation at 1.500 rpm for 30 min and resuspended in 1 ml fresh PBS (Fig.2A).

For vesicle isolation by OptiPrep (D1556, Sigma-Aldrich) density gradient ultracentrifugation, the >100-kDa fraction was resuspended in PBS, and the vesicles were pelleted by ultracentrifugation (3 h, 100,000 × *g*, 4°C) using a T29 rotor (ThermoFisher). The pellet was then resuspended in 40% OptiPrep and overlaid with OptiPrep dilutions ranging from 35% to 10%. The gradient was centrifuged in a SW40 rotor (Beckmann) for 16 h at 139,000 × *g*. The different density fractions were then collected, and the fractions (35% to 20%) that showed a similar protein pattern by silver staining (Fig.S1A) were pooled. These pooled fractions were concentrated using a 100-kDa concentrator cartridge and further referred to as MV isolates (Fig.2A).

Lipid and protein quantification.

The fluorescent membrane dye FM4-64 (Life Technologies) was used to quantify the lipid amount in culture filtrates, size-separated culture filtrate fractions, or vesicle isolates from *S. aureus* USA300 wild type and USA300 Δ*α,β,hld*. The different fractions were stained at 37°C for 5 to 10 min with FM4-64 at a final concentration of 5 µg/ml, and lipid positivity was detected using the fluorescence microplate reader CLARIOStar (BMG Labtech). Determination of the protein amount was performed using a Bradford assay according to the manufacturer's manual (Bio-Rad protein assay kit).

Silver staining was used to detect smaller protein amounts in MVs isolated by OptiPrep ultracentrifugation. SDS-PAGE was performed as described below, and the total MV isolate was applied to an SDS gel. A silver staining kit (Bio-Rad) was used according to the manufacturer's instructions.

Negative staining for transmission electron microscopy (TEM).

MV isolates were gained as described above. ExoQuickTC pellets were resuspended in 20 µl PBS, and pooled fractions from OptiPrep were concentrated to a final volume of 50 µl. All samples were fixed with 1:1 Karnovsky's fixative. Suspensions were placed directly onto a glow-discharged electron microscopy (EM) grid. After adsorption, the grids were washed in double-distilled water and negatively stained with 1% uranyl acetate. The grids were examined using a Zeiss Libra 120 transmission electron microscope (Carl Zeiss, Oberkochen, Germany) operated at 120 kV. Original magnification was 1:25,000.

Bacterial cultures were grown for 6 h, diluted 1:1,000, and centrifuged at 4,700 × *g* for 10 min. Bacteria were fixed with Karnovsky's fixative for 24 h at 4°C. Postfixation bacteria were placed in 1.0% osmium tetroxide containing 1.5% K-ferrocyanide in 0.1 M cacodylate buffer for 2 h. Blocks were embedded in glycide ether and cut using an ultramicrotome (Ultracut; Reichert, Vienna, Austria). Ultrathin sections (30 nm) were mounted on copper grids and analyzed using a Zeiss Libra 120 transmission electron microscope (Carl Zeiss, Oberkochen, Germany) operating at 120 kV.

Dynamic light scattering for size analysis.

Size determination of isolated vesicles was performed using dynamic light scattering analysis with a Zetasizer Nano ZS (Malvern Instruments) according to the manufacturer's instructions.

SitC, PSMα3, and cytoplasmic protein detection.

To induce SitC expression in *S. aureus* USA300 pTX SitC-His, bacteria were cultivated in TSB without glucose containing 0.5% xylose. Bacterial cultures were adjusted to densities of OD_{600} of 0.1 and cultivated for appropriate times in flasks under agitation at 37°C. For turgor modulation, bacterial cultures were supplemented

with the indicated percentage of sucrose or arabinose. MVs were obtained by centrifugation, as described above, and used for detection of SitC-His or PSMα3 by immunoblotting. A volume corresponding to 50 µg of total protein was concentrated with 10 µl Strataclean resin beads (Agilent Technologies) and loaded onto Mini-Protean TGX precast protein gels (Bio-Rad). SitC detection was performed as described recently (4) using mouse anti-5His-IgG from Qiagen (0.2-mg/ml stock solution diluted 1:1,000). Goat anti-mouse-IgG IRDye680 or IRDye800 purchased from Li-Cor (0.2-mg/ml stock solution diluted 1:10,000 in Tris-buffered saline [TBST] with 2% BSA) was used as secondary antibody. PSMα3 probes were prepared as described for SitC-His, but the probes were loaded on 10% to 20% Tris-glycine minigels (Novex) and detected using anti-PSMα3 serum (isolated by M. Otto) and mouse anti-rabbit-IgG IRDye800 from Li-Cor (0.2-mg ml^{-1} stock solution diluted 1:10,000). Samples used for the detection of the cytoplasmic protein GAPDH in ExoQuickTC-isolated vesicles were prepared as described for the SitC sample preparation. GAPDH was detected using a specific primary antibody (α-GAPDH [38]) and a secondary anti-rabbit-IgG IRDye680 antibody. All bands on the membranes were visualized by Li-Cor Reader.

Quantitative label-free proteomics.

Three biological replicates of ExoQuickTC-isolated MVs from USA300 wild type or PSM mutant were analyzed. Volumes corresponding to similar protein amounts in all MV isolates were measured by Bradford assay and used for protein precipitation with 10% ice-cold trichloroacetic acid (TCA) overnight at 4°C. After centrifugation at 13,200 rpm at 4°C for 15 min, the supernatants were discarded, and the precipitated proteins were air-dried. Nano-liquid chromatography–tandem mass spectrometry analysis was performed as described recently (4). Briefly, dried proteins were dissolved in a buffer containing 6 M urea, 2 M thiourea, and 10 mM Tris at pH 8.0 and digested in solution with trypsin. Peptide mixtures from the samples were separated on an EasyLC nano-high-performance liquid chromatograph (Proxeon Biosystems) coupled to a linear trap quadrupole (LTQ) Orbitrap Elite mass spectrometer (Thermo Fisher Scientific). Acquired mass spectrometry spectra were processed as described previously (4). Differences of single proteins between the wild type and PSM mutant are listed in Data Set S1.

Stimulation of HEK-TLR2 cells.

HEK293 cells stably transfected with the human TLR2 genes were purchased from Invivogen. HEK-TLR2 cells were cultivated in 75-cm^2 culture flasks using 20 ml of growth medium (Dulbecco's modified Eagle's medium [DMEM], 10% fetal calf serum [FCS], 20 mM l-glutamine, 100 µg/ml Normocin, and 10 µg/ml blasticidin). Cells were stimulated as described previously (4).

Calcium mobilization in HL60-FPR2 cells.

HL60 cells stably transfected with human FPR2/ALX have been recently described (5). These cells were grown in RPMI medium (Biochrom) supplemented with 10% FCS (Sigma-Aldrich), 20 mM HEPES (Biochrom), penicillin (100 units/ml), streptomycin (100 µg/ml) (Gibco), 1× GlutaMAX (Gibco), and G418 (Biochrom) at a final concentration of 1 mg/ml. Calcium fluxes were analyzed by stimulating cells loaded with Fluo-3-AM (Molecular Probes), and the fluorescence was monitored with a FACSCalibur flow cytometer (Becton, Dickinson), as recently described (39).

FACS analysis.

Membrane vesicle isolates from late-exponential-growth-phase (6-h) cultures were stained with 5 µg/ml FM4-64 (Life Technologies) for 20 min at 37°C and analyzed with a BD Bioscience LSRFortessa. SitC-His was detected in vesicle isolates from USA300 *Δspa* using a His-PE antibody (BioLegend), and the staining was controlled using the corresponding PE isotype control (BioLegend). For analysis of cytoplasmic GFP, vesicles were isolated from USA300 containing the pTX143-S3 GFP plasmid. The correlation of FM4-64-positive events with total events was used to calculate the vesicle concentrations in the samples. FlowJo V10 was used for the data analysis.

Membrane fluidity assay.

Overnight cultures of USA300 wild type and USA300 Δ*α,β,hld* were adjusted to an OD_{600} of 0.2 in Iscove's modified Dulbecco's medium (IMDM; Gibco) and stained for 20 min at 37°C with fluorescent lipid reagent supplied in the membrane fluidity kit (ab189819; Abcam). The stained bacteria were centrifuged for 10 min at 5,000 × *g* and resuspended in PBS with 0.2% glucose. Next, the bacteria were incubated with

indicated stimuli for 10 min. Formylated PSM peptides (PSMα1, PSMα2, PSMα3, and δ-toxin [*hld*]) with the recently published sequences (7) were kindly provided by Stefan Stevanović (Department of Immunology, University of Tübingen, Germany). Membrane fluidity was analyzed in the fluoreader CLARIOstar (BMG Labtech) according to the manual instructions. A ratio between the emission maxima of the excimer (470 nm) and the monomer (400 nm) was calculated, which is equivalent to the relative membrane fluidity.

HPLC analysis of PSM peptides.

The *S. aureus* strain USA300 wild type was grown in TSB at 37°C. Samples were collected at different time points and centrifuged for 10 min at 4,700 × *g* and 4°C. Supernatants were collected by sterile filtration through 0.2-µm filters and concentrated 5 times using a SpeedVac vacuum concentrator. PSM peptides were separated from the supernatant by reversed-phase chromatography using an XBridge C_8 5-µm, 4.6 - by 150-mm column (Waters). A linear gradient from 0.1% TFA (buffer A) in water to acetonitrile containing 0.08% TFA (buffer B) for 15 min with an additional 5 min of 100% buffer B at a flow rate of 1 ml/min was used, and a 50-µl sample volume was injected. Peaks were detected at 210 nm. A PSMα3 standard curve was used to calculate the PSMα3 amounts.

Statistics.

Statistical analysis was performed using GraphPad Prism 5.0. The unpaired two-tailed Student *t* test was used to compare two groups unless otherwise noted. Data represent the mean and SEM from at least three independent experiments unless stated otherwise.

ACKNOWLEDGMENTS

We thank Sebastian Kuhn and Cordula Gekeler for technical support; Stefan Stevanović, who kindly provided us with the synthetic PSM peptides; Andreas Kappler, who provided access to the Zetasizer Nano; and Mirita Franz-Wachtel for performing the proteomic analysis.

This study was supported by grants from the German Research Council SFB685 to A.P., PE 805/5-2 to A.P., TRR34 to D.K., TRR156, GRK1708 to A.P., and SFB766 to A.P. and by the Intramural Research Program, NIAID, NIH (project ZIA AI000904), to M.O.

mBio 9:e01851-18. https://doi.org/10.1128/mBio.01851-18.

REFERENCES

1. Kawai T, Akira S. 2011. Toll-like receptors and their crosstalk with other innate receptors in infection and immunity. Immunity 34:637–650. doi:10.1016/j.immuni.2011.05.006.
2. Nguyen MT, Gotz F. 2016. Lipoproteins of Gram-positive bacteria: key players in the immune response and virulence. Microbiol Mol Biol Rev 80:891–903. doi:10.1128/MMBR.00028-16.
3. Nakayama H, Kurokawa K, Lee BL. 2012. Lipoproteins in bacteria: structures and biosynthetic pathways. FEBS J 279:4247–4268. doi:10.1111/febs.12041.
4. Hanzelmann D, Joo HS, Franz-Wachtel M, Hertlein T, Stevanovic S, Macek B, Wolz C, Gotz F, Otto M, Kretschmer D, Peschel A. 2016. Toll-like receptor 2 activation depends on lipopeptide shedding by bacterial surfactants. Nat Commun 7:12304. doi:10.1038/ncomms12304.
5. Kretschmer D, Gleske AK, Rautenberg M, Wang R, Koberle M, Bohn E, Schoneberg T, Rabiet MJ, Boulay F, Klebanoff SJ, van Kessel KA, van Strijp JA, Otto M, Peschel A. 2010. Human formyl peptide receptor 2 senses highly pathogenic Staphylococcus aureus. Cell Host Microbe 7:463–473. doi:10.1016/j.chom.2010.05.012.
6. Weiss E, Hanzelmann D, Fehlhaber B, Klos A, von Loewenich FD, Liese J, Peschel A, Kretschmer D. 2018. Formyl-peptide receptor 2 governs leukocyte

influx in local Staphylococcus aureus infections. FASEB J 32:26–36. doi:10.1096/fj.201700441R.

7. Wang R, Braughton KR, Kretschmer D, Bach TH, Queck SY, Li M, Kennedy AD, Dorward DW, Klebanoff SJ, Peschel A, DeLeo FR, Otto M. 2007. Identification of novel cytolytic peptides as key virulence determinants for community-associated MRSA. Nat Med 13:1510–1514. doi:10.1038/nm1656.
8. Kretschmer D, Rautenberg M, Linke D, Peschel A. 2015. Peptide length and folding state govern the capacity of staphylococcal beta-type phenol-soluble modulins to activate human formyl-peptide receptors 1 or 2. J Leukocyte Biol 97:689–697. doi:10.1189/jlb.2A0514-275R.
9. Peschel A, Otto M. 2013. Phenol-soluble modulins and staphylococcal infection. Nat Rev Microbiol 11:667–673. doi:10.1038/nrmicro3110.
10. Queck SY, Khan BA, Wang R, Bach TH, Kretschmer D, Chen L, Kreiswirth BN, Peschel A, Deleo FR, Otto M. 2009. Mobile genetic element-encoded cytolysin connects virulence to methicillin resistance in MRSA. PLoS Pathog 5:e1000533. doi:10.1371/journal.ppat.1000533.
11. Kizaki H, Omae Y, Tabuchi F, Saito Y, Sekimizu K, Kaito C. 2016. Cell-surface phenol soluble modulins regulate Staphylococcus aureus colony spreading. PLoS One 11:e0164523. doi:10.1371/journal.pone.0164523.
12. Skabytska Y, Wolbing F, Gunther C, Koberle M, Kaesler S, Chen KM, Guenova E, Demircioglu D, Kempf WE, Volz T, Rammensee HG, Schaller M, Rocken M, Gotz F, Biedermann T. 2014. Cutaneous innate immune sensing of Toll-like receptor 2-6 ligands suppresses T cell immunity by inducing myeloid-derived suppressor cells. Immunity 41:762–775. doi:10.1016/j.immuni.2014.10.009.
13. Schmaler M, Jann NJ, Ferracin F, Landolt LZ, Biswas L, Gotz F, Landmann R. 2009. Lipoproteins in Staphylococcus aureus mediate inflammation by TLR2 and iron-dependent growth in vivo. J Immunol 182:7110–7118. doi:10.4049/jimmunol.0804292.
14. Nguyen MT, Uebele J, Kumari N, Nakayama H, Peter L, Ticha O, Woischnig AK, Schmaler M, Khanna N, Dohmae N, Lee BL, Bekeredjian-Ding I, Gotz F. 2017. Lipid moieties on lipoproteins of commensal and non-commensal

staphylococci induce differential immune responses. Nat Commun 8:2246. doi:10.1038/s41467-017-02234-4

15. Bardoel BW, Vos R, Bouman T, Aerts PC, Bestebroer J, Huizinga EG, Brondijk TH, van Strijp JA, de Haas CJ. 2012. Evasion of Toll-like receptor 2 activation by staphylococcal superantigen-like protein 3. J Mol Med 90:1109–1120. doi:10.1007/s00109-012-0926-8.
16. Gurung M, Moon DC, Choi CW, Lee JH, Bae YC, Kim J, Lee YC, Seol SY, Cho DT, Kim SI, Lee JC. 2011. Staphylococcus aureus produces membrane-derived vesicles that induce host cell death. PLoS One 6:e27958. doi:10.1371/journal.pone.0027958.
17. Pader V, Hakim S, Painter KL, Wigneshweraraj S, Clarke TB, Edwards AM. 2016. Staphylococcus aureus inactivates daptomycin by releasing membrane phospholipids. Nat Microbiol 2:16194. doi:10.1038/nmicrobiol.2016.194.
18. Brown L, Wolf JM, Prados-Rosales R, Casadevall A. 2015. Through the wall: extracellular vesicles in Gram-positive bacteria, mycobacteria and fungi. Nat Rev Microbiol 13:620–630. doi:10.1038/nrmicro3480.
19. Kurokawa K, Lee H, Roh KB, Asanuma M, Kim YS, Nakayama H, Shiratsuchi A, Choi Y, Takeuchi O, Kang HJ, Dohmae N, Nakanishi Y, Akira S, Sekimizu K, Lee BL. 2009. The triacylated ATP binding cluster transporter substrate-binding lipoprotein of Staphylococcus aureus functions as a native ligand for Toll-like receptor 2. J Biol Chem 284:8406–8411. doi:10.1074/jbc.M809618200.
20. Vida TA, Emr SD. 1995. A new vital stain for visualizing vacuolar membrane dynamics and endocytosis in yeast. J Cell Physiol 128:779–792.
21. Cheung GY, Kretschmer D, Queck SY, Joo H-S, Wang R, Duong AC, Nguyen TH, Bach T-HL, Porter AR, DeLeo FR. 2014. Insight into structure-function relationship in phenol-soluble modulins using an alanine screen of the phenol-soluble modulin (PSM) α3 peptide. FASEB J 28:153–161. doi:10.1096/fj.13-232041.
22. Schwechheimer C, Kuehn MJ. 2015. Outer-membrane vesicles from Gram-negative bacteria: biogenesis and functions. Nat Rev Microbiol 13:605. doi:10.1038/nrmicro3525.

23. Cheung GY, Wang R, Khan BA, Sturdevant DE, Otto M. 2011. Role of the accessory gene regulator agr in community-associated methicillin-resistant Staphylococcus aureus pathogenesis. Infect Immun 79:1927–1935. doi:10.1128/IAI.00046-11.
24. Biedermann T, Skabytska Y, Kaesler S, Volz T. 2015. Regulation of T cell immunity in atopic dermatitis by microbes: the yin and yang of cutaneous inflammation. Front Immunol 6:353. doi:10.3389/fimmu.2015.00353.
25. Hilmi D, Parcina M, Stollewerk D, Ostrop J, Josten M, Meilaender A, Zaehringer U, Wichelhaus TA, Bierbaum G, Heeg K, Wolz C, Bekeredjian-Ding I. 2014. Heterogeneity of host TLR2 stimulation by Staphylococcus aureus isolates. PLoS One 9:e96416. doi:10.1371/journal.pone.0096416.
26. Deguchi H, Aoyama R, Takahashi H, Isobe Y, Tsutsumi Y. 2015. Harmful effects of synthetic surface-active detergents against atopic dermatitis. Case Rep Dermatol Med 2015:898262. doi:10.1155/2015/898262.
27. Kaesler S, Volz T, Skabytska Y, Koberle M, Hein U, Chen KM, Guenova E, Wolbing F, Rocken M, Biedermann T. 2014. Toll-like receptor 2 ligands promote chronic atopic dermatitis through IL-4-mediated suppression of IL-10. J Allergy Clin Immunol 134:92–99. doi:10.1016/j.jaci.2014.02.017
28. Jun SH, Lee JH, Kim SI, Choi CW, Park TI, Jung HR, Cho JW, Kim SH, Lee JC. 2017. Staphylococcus aureus-derived membrane vesicles exacerbate skin inflammation in atopic dermatitis. Clin Exp Allergy 47:85–96. doi:10.1111/cea.12851.
29. Vesy CJ, Kitchens RL, Wolfbauer G, Albers JJ, Munford RS. 2000. Lipopolysaccharide-binding protein and phospholipid transfer protein release lipopolysaccharides from gram-negative bacterial membranes. Infect Immun 68:2410–2417. doi:10.1128/IAI.68.5.2410-2417.2000.]
30. Ranoa DR, Kelley SL, Tapping RI. 2013. Human lipopolysaccharide-binding protein (LBP) and CD14 independently deliver triacylated lipoproteins to Toll-like receptor 1 (TLR1) and TLR2 and enhance formation of the ternary signaling complex. J Biol Chem 288:9729–9741. doi:10.1074/jbc.M113.453266.
31. Nakata T, Yasuda M, Fujita M, Kataoka H, Kiura K, Sano H, Shibata K. 2006. CD14 directly binds to triacylated lipopeptides and facilitates recognition of the

lipopeptides by the receptor complex of Toll-like receptors 2 and 1 without binding to the complex. Cell Microbiol 8:1899–1909. doi:10.1111/j.1462-5822.2006.00756.x.

32. Hoebe K, Georgel P, Rutschmann S, Du X, Mudd S, Crozat K, Sovath S, Shamel L, Hartung T, Zahringer U, Beutler B. 2005. CD36 is a sensor of diacylglycerides. Nature 433:523–527. doi:10.1038/nature03253.
33. Lee J, Lee EY, Kim SH, Kim DK, Park KS, Kim KP, Kim YK, Roh TY, Gho YS. 2013. Staphylococcus aureus extracellular vesicles carry biologically active beta-lactamase. Antimicrob Agents Chemother 57:2589–2595. doi:10.1128/AAC.00522-12.
34. Helwa I, Cai J, Drewry MD, Zimmerman A, Dinkins MB, Khaled ML, Seremwe M, Dismuke WM, Bieberich E, Stamer WD. 2017. A comparative study of serum exosome isolation using differential ultracentrifugation and three commercial reagents. PLoS One 12:e0170628. doi:10.1371/journal.pone.0170628.
35. Wang X, Thompson CD, Weidenmaier C, Lee JC. 2018. Release of Staphylococcus aureus extracellular vesicles and their application as a vaccine platform. Nat Commun 9:1379. doi:10.1038/s41467-018-03847-z.
36. Jeon H, Oh MH, Jun SH, Kim SI, Choi CW, Kwon HI, Na SH, Kim YJ, Nicholas A, Selasi GN, Lee JC. 2016. Variation among Staphylococcus aureus membrane vesicle proteomes affects cytotoxicity of host cells. Microb Pathog 93:185–193. doi:10.1016/j.micpath.2016.02.014.
37. Chatterjee SS, Joo HS, Duong AC, Dieringer TD, Tan VY, Song Y, Fischer ER, Cheung GY, Li M, Otto M. 2013. Essential Staphylococcus aureus toxin export system. Nat Med 19:364–367. doi:10.1038/nm.3047.
38. Ebner P, Rinker J, Nguyen MT, Popella P, Nega M, Luqman A, Schittek B, Di Marco M, Stevanovic S, Gotz F. 2016. Excreted cytoplasmic proteins contribute to pathogenicity in Staphylococcus aureus. Infect Immun 84:1672–1681. doi:10.1128/IAI.00138-16.
39. de Haas CJ, Veldkamp KE, Peschel A, Weerkamp F, Van Wamel WJ, Heezius EC, Poppelier MJ, Van Kessel KP, van Strijp JA. 2004. Chemotaxis inhibitory protein of Staphylococcus aureus, a bacterial antiinflammatory agent. J Exp Med 199:687–695. doi:10.1084/jem.20031636.

Chapter 9

Appendix – Human IgG increases intracellular killing of *Staphylococcus aureus* in neutrophils

Unpublished data generated during the PHD:

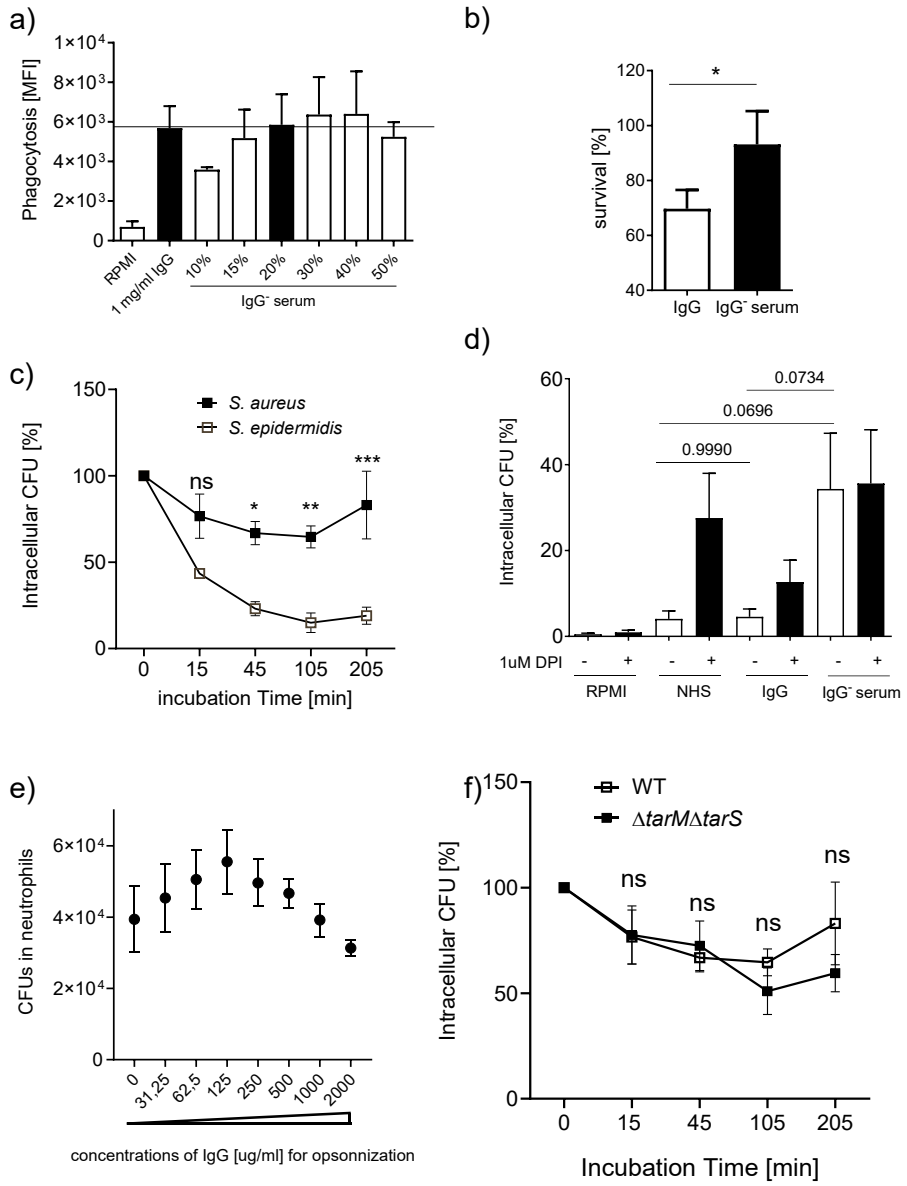

Appendix 1: **Intracellular survival of *Staphylococcus aureus* in neutrophils increases in absence of serum IgG. a)** Neutrophil phagocytosis of *S. aureus* (NRS384 (USA300); 1h hour incubation time; MOI2) was measured via flow cytometry by detecting CFSE-labelled intracellular

bacteria. Opsonization with pooled human IgG (Sigma) or with serum depleted of IgG (IgG$^-$ serum; Molecular Innovations) results in efficient uptake of *S. aureus* compared to the non-opsonized control bacteria (RPMI). Opsonization with 1 mg/ml of human IgG showed similarly efficient phagocytosis as opsonization with 20% IgG depleted serum. **b)** Neutrophil killing of S*. aureus* (NRS384; 1 hour incubation time; MOI2) was analysed by plating of surviving bacteria after neutrophil challenge. *S. aureus* killing is low when opsonized with 20% IgG depleted serum (IgG$^-$ serum), while opsonization with 1 mg/ml pooled human IgG resulted in killing of approximately 30% of the applied *S. aureus* (NRS384). **c)** Intracellular survival of *S. aureus* (NRS384) compared to *S. epidermidis* (1457) after opsonization with normal human serum. Neutrophils and bacteria were mixed and incubated for 15 minutes (MOI2), then the remaining extracellular bacteria were lysed with lysostaphin (t=0) and intracellular survival was monitored over time by neutrophil lysis and plating. While *S. aureus*, can survive in the neutrophils over time, *S epidermidis* is more efficiently cleared. **d)** Intracellular survival of *S. aureus* was evaluated after opsonization with different serum components (NRS384; MOI2; 1 hour incubation time), either without opsonization (RPMI), with 10% normal human serum (NHS), pooled human IgG (1mg/ml IgG) or 20% IgG depleted serum (IgG$^-$ serum). Neutrophils and bacteria were mixed and incubated for 1 hour (MOI2), then the remaining extracellular bacteria were lysed with lysostaphin (2U/ml). Intracellular CFU was determined by lysing the neutrophils and plating on TSA plates. While, due to inefficient phagocytosis, unopsonized bacteria were nearly absent from inside neutrophils, low numbers of NHS and IgG opsonized bacteria were recovered, while high numbers could be recovered after opsonization with IgG depleted serum. Addition of 1 µM diphenyleneiodonium chloride (DPI), an inhibitor of the NADPH-oxidase, and therefore of neutrophil mediated ROS production, resulted in increased survival of NHS or IgG opsonized bacteria in neutrophils. **e)** Different concentrations of pooled human IgG were titrated into 20% IgG depleted serum (IgG$^-$ serum) and used for opsonization of *S. aureus* (NRS384). Neutrophils and bacteria were mixed and incubated for 1 hour (MOI2), then the remaining extracellular bacteria were lysed with lysostaphin. While low concentrations of IgG increase the number of bacteria recovered from within the neutrophils (probably due to an increase in phagocytosis), high concentrations decrease the numbers again. **f)** Intracellular survival of *S. aureus* wildtype (NRS384) compared to the Δ*tarM*Δ*tarS* deletion mutant was assessed after opsonization with normal human serum. Neutrophils and bacteria were mixed and incubated for 15 minutes (MOI2), then the remaining extracellular bacteria were lysed with lysostaphin (t=0) and intracellular survival was monitored over time by neutrophil lysis and plating. Absence of n-acetylglucosamine (GlcNAc) on the WTA of *S. aureus* (NRS384) had no direct effect on the intracellular survival of *S. aureus* over time, if equal CFU of WT or Δ*tarM*Δ*tarS* mutant were intracellular at time point t=0. But the increased neutrophil phagocytosis of WT compared to Δ*tarM*Δ*tarS* mutant (Appendix 3b, Appendix 4f) results in higher intracellular survival of S. aureus WT inside the neutrophils. The data represent the mean ± SEM of at least two independent experiments. With statistical tests, for **b)** Paired T-Test, for **c)** and **f)** 2-way ANOVA and for **d)** Ordinary 1-way ANOVA, statistical significance was determined: not significant (ns), *P < 0.05, **P < 0.01, ***P < 0.001 or p-values are shown.

a)

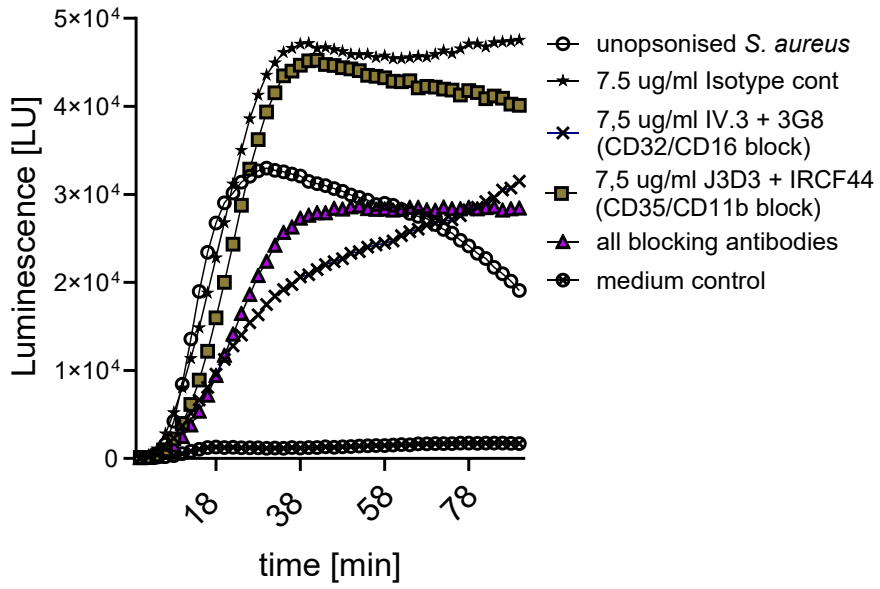

b)

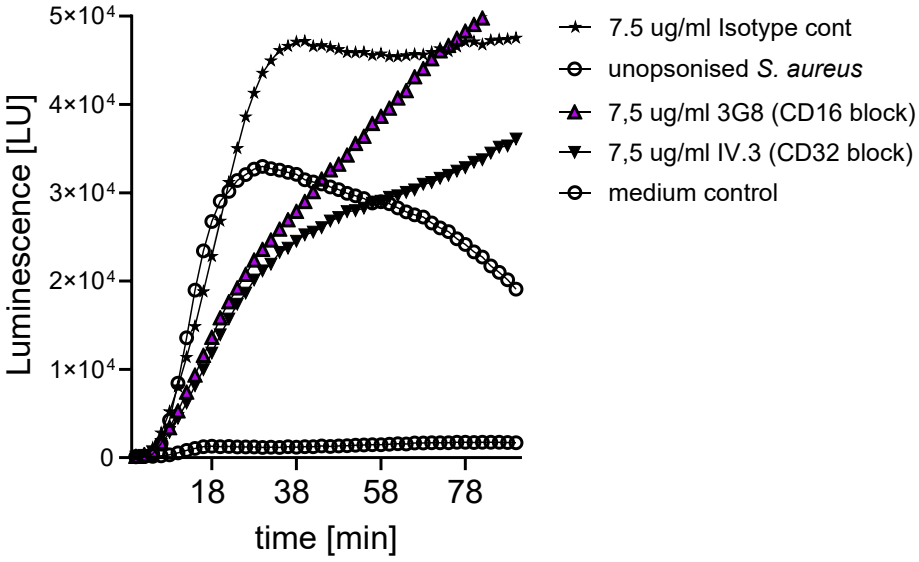

Appendix 2: Opsonization of *S. aureus* with normal human serum leads to a strong neutrophil oxidative burst (MOI2; luminol-based assay) which can be inhibited by blocking FCγ-receptors with blocking antibodies. a) Simultaneous inhibition of FCγ-receptors (CD32/CD16) on neutrophils with blocking antibodies (IV.3/3G8) prior to addition of *S. aureus* opsonized with normal human serum (NHS) inhibits the neutrophil oxidative burst to the level initiated by unopsonized *S. aureus*, while blocking of complement receptors (CD35/CD11b; J3D3/IRCF44) is ineffective. **b)** Blocking individual FCγ-receptors (CD16 with 3G8 antibody or CD32 with IV.3 antibody) on neutrophils shows an inhibitory effect in both cases, which indicates that both receptors might be involved in increasing the oxidative burst of neutrophils. The data represent the mean of two independent experiments.

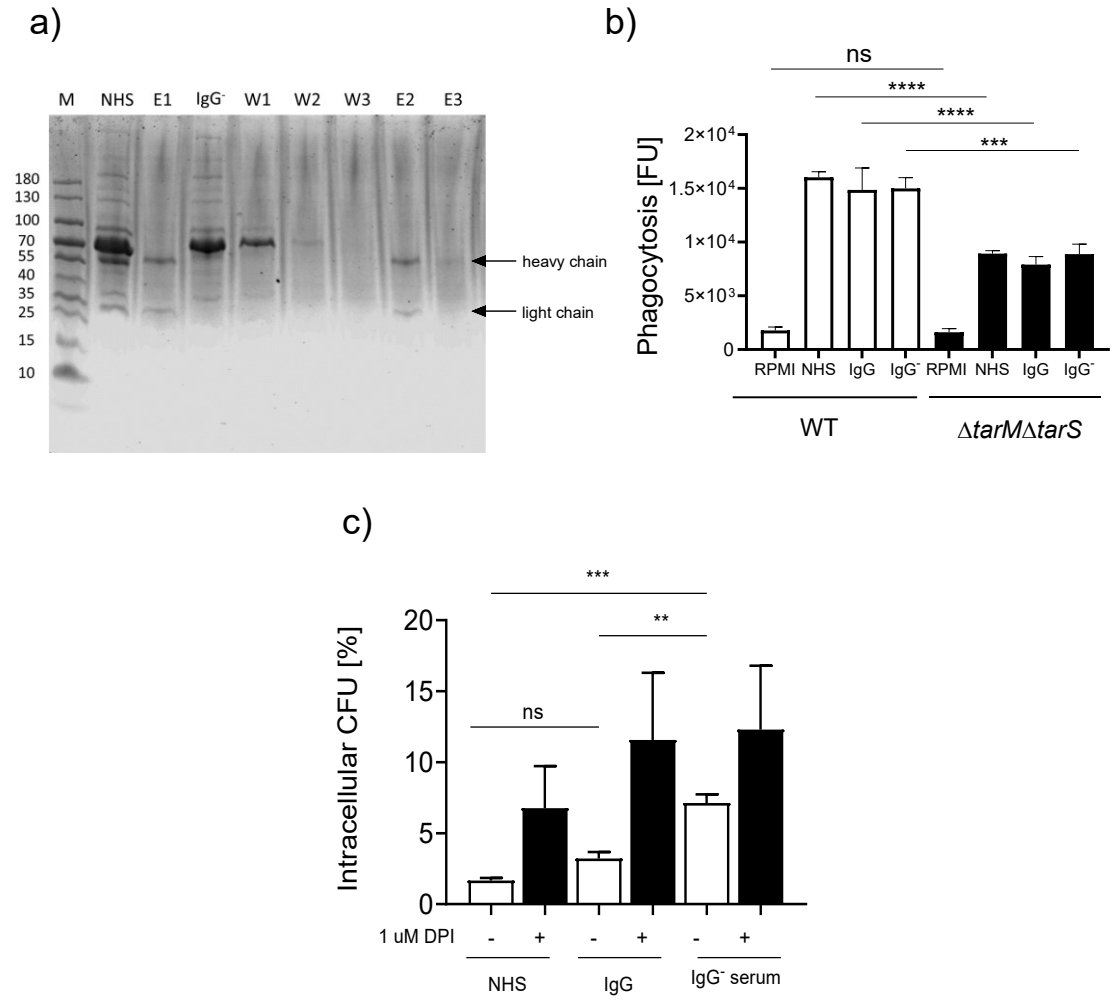

Appendix 3: For further quality control, normal human serum (NHS) was depleted (IgG$^-$) using a commercially available protein A/G column (Thermo Scientific) and an EDTA free 0.1M Phosphate/0.15M sodium chloride buffer. Similar results as in Appendix 1 were obtained. a) SDS page was performed under reducing conditions (5% β-mercaptoethanol) after depletion and elution fractions (E1-E3) and wash fractions (W1-W3) were collected. The amount of eluted IgG (E1-E3) as well as the success in clearing the normal human serum of IgG resulting in IgG depleted serum (IgG$^-$) was evaluated by SDS page. Heavy chains of IgG are found at about 55kDa, light chains at about 27 kDa in the elution fractions and in normal human serum (NHS) before depletion. After depletion, only very faint bands are visible for these sizes in the sample that was IgG depleted (IgG$^-$), showing efficient depletion of IgG. **b)** 20% of NHS, E1 (elution fraction 1) or the IgG depleted fraction (IgG$^-$) were used for opsonization of CFSE-labeled *S. aureus* (NRS384) WT and the respective Δ*tarM*Δ*tarS* mutant. Neutrophil phagocytosis was performed for 1 hour and the efficiency was evaluated by flow cytometry. For all 3 fractions of human serum, similar efficiency of phagocytosis was detected. For all opsonizing serum fractions, phagocytosis was decreased in mutants lacking WTA-GlcNAc. **c)** Intracellular survival was analysed as previously (Appendix 1 d)). Neutrophils and bacteria were mixed and incubated for 1 hour (MOI2), then the remaining extracellular bacteria were lysed with

lysostaphin (2U/ml). Intracellular CFU was determined by lysing the neutrophils and plating on TSA plates. As for IgG depleted serum from Molecular Innovations (Appendix 1), opsonization with serum depleted for IgG resulted in increased survival of *S aureus* WT (NRS384) in neutrophils. Addition of 1 µM diphenyleneiodonium chloride (DPI) increased survival independent of the opsonization state, but the effect was strongest for the IgG containing fraction, suggesting intracellular killing via oxygen radicals. The data represent the mean ± SEM of at least three independent experiments. Ordinary 1-way ANOVA was used to determine statistical significance: not significant (ns), **P < 0.01, ***P < 0.001, ****P < 0.0001.

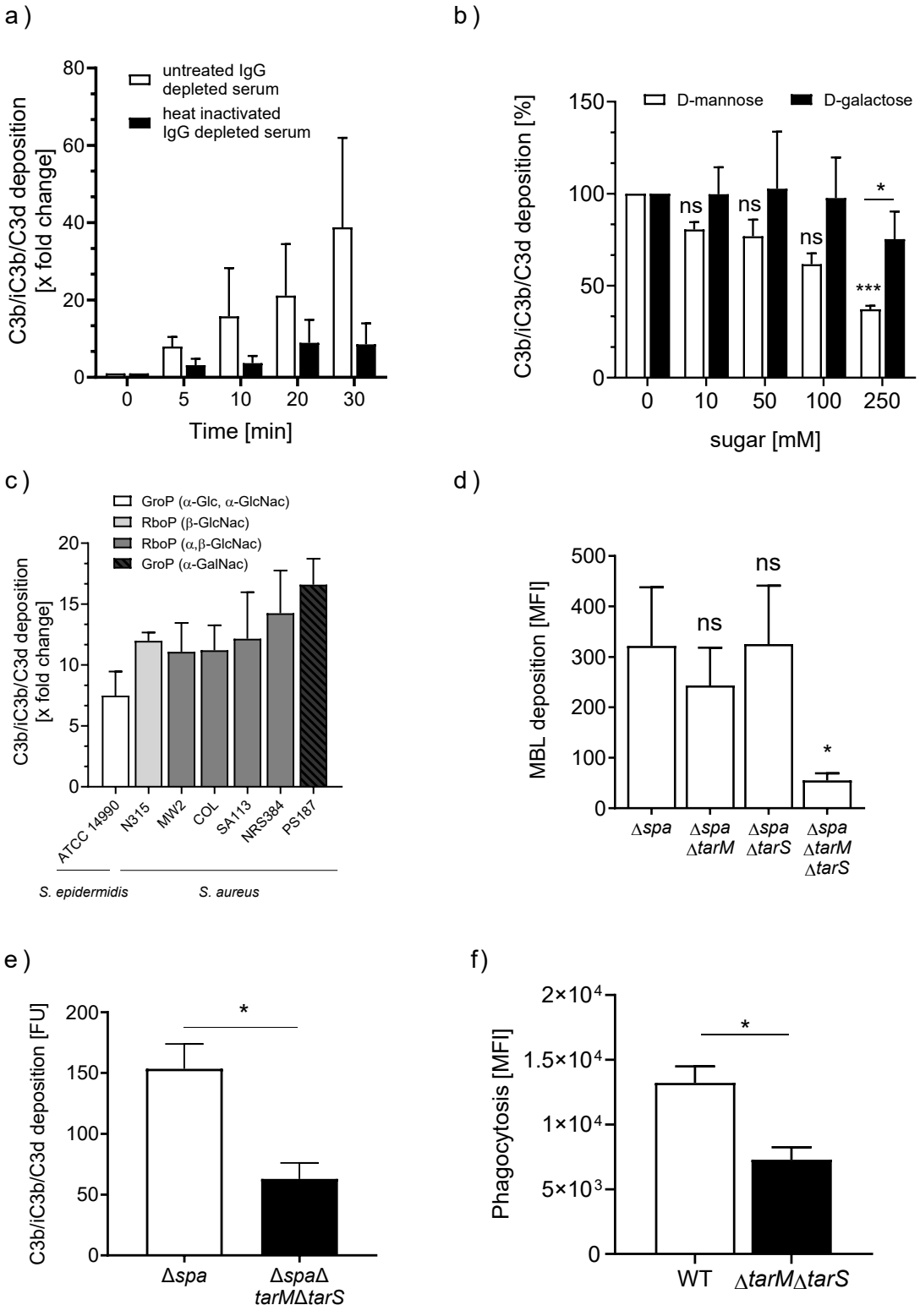

Appendix 4: Complement-dependent C3 deposition from IgG depleted serum (with protein A/G column) depends on MBL binding to n-acetylglucosamine on wall teichoic acid (WTA) and results in efficient opsonophagocytosis. a) C3 deposition (fold change compared to timepoint t=0) on *S. aureus* Δ*spa* during opsonization with IgG depleted serum (2%) was measured at different time

points with and without previous heat inactivation of human serum at 56°C for 30 min, using a FITC labeled anti-C3 complement Fab antibody (Protos Immunoresearch). Complement is active prior to heat inactivation even after IgG depletion. **b)** D-mannose was titrated in different concentrations to IgG depleted serum (2%), which inhibited C3 deposition (30 min incubation time) on *S. aureus* Δ*spa* in a concentration dependent manner. D-galactose was used as control. **c)** C3 deposition from IgG depleted serum (fold change compared to timepoint t=0 (unopsonized); 2% IgG depleted serum; 5 min incubation time) on different strains of *S aureus* and *S. epidermidis* was measured to determine the importance of different WTA types in absence of IgG. *S. epidermidis* ATCC 14990 showed lower deposition of C3 than the tested *S. aureus* strains. **d)** MBL depostition of 100 ng of recombinant MBL (rMBL) was measured using Hyb-131 anti-MBL (2 ng/ul) antibody and a secondary PE-labeled goat-anti mouse antibody. MBL deposition is dependent on the presence of n-acetylglucosamine (GlcNAc) on the wall teichoic acid of *S. aureus* (RN4220) since deletion of the GlcNAc transferases TarS and TarM prevents MBL binding. **e)** C3 deposition from IgG depleted serum (2%; 10 min incubation time) is dependent on the presence of n-acetylglucosamine (GlcNAc) on the wall teichoic acid of *S. aureus* Δ*spa* (NRS384) since deletion of the GlcNAc transferases TarS and TarM prevents efficient C3 deposition. **f)** Neutrophil phagocytosis of *S. aureus* (NRS384) wildtype and Δ*tarM*Δ*tarS* was measured after opsonization with 20% IgG depleted serum (MOI 2, 1hour incubation time). Deletion of the GlcNAc transferases TarS and TarM reduced phagocytosis of *S. aureus* when opsonized with IgG depleted serum. The data represent the mean ± SEM of at least three independent experiments. With statistical tests, for **b)** 2-way ANOVA, **d)** Kruskal-Wallis Test, and **e)** and **f)** Unpaired T-Test, statistical significance was determined: not significant (ns), *P < 0.05, ***P < 0.001 are shown.

Chapter 10

Contribution to publications

Wall teichoic acid substitution with glucose governs phage susceptibility of *Staphylococcus epidermidis*

I did all the experiments and molecular biology (with help from Lara Kränkel, Regine Stemmler and Christoph Mayer), except for the NMR measurement (Cristina De Castro, Anna Notaro), HPLC-MS (Axel Walter, Christoph Mayer) and electron microscopy (Anneli Vollert, Martin Schaller). Andreas Peschel and I wrote the manuscript in a collaborative fashion, with help from Cristina De Castro.

Invasive *Staphylococcus epidermidis* use a unique processive wall teichoic acid glycosyltransferase to evade immune recognition

I performed the IgG binding experiments (figure 1), especially those with the pooled human IgG. I designed figures (figures 1 and 3), wrote material and methods for figure 1 and edited the manuscript.

From a Hsp90 - binding protein to a peptide drug

I isolated PBMCs and helped with the immune stimulation experiments.

Acetate sensing by GPR43 alarms neutrophils and protects from severe sepsis

I assisted in the *in vivo* experiments and edited the manuscript.

Inhibition of the ATP synthase sensitizes *Staphylococcus aureus* towards human antimicrobial peptides

I isolated PMNs and performed the neutrophil killing experiments. (Figure 3)

Formyl-Peptide Receptor Activation Enhances Phagocytosis of Community-Acquired Methicillin-Resistant *Staphylococcus aureus*

I assisted in phagocytosis experiments and contributed to discussions.

The Mechanism behind Bacterial Lipoprotein Release: Phenol-Soluble Modulins Mediate Toll-Like Receptor 2 Activation via Extracellular Vesicle Release from *Staphylococcus aureus*

I isolated membrane vesicles, performed several experiments including the lipoprotein and PSM detection by western blotting, lipid determination and vesicle quantification. I stimulated HEK-TLR2 and HL60-FPR2 cells, measured cytokines, membrane fluidity and performed silver staining. I contributed to writing and editing of the manuscript.

Acknowledgement

I want to thank my supervisor Andreas Peschel for his support and for all the scientific insights he provided to me, while working on this project. Furthermore, I want to thank the PSM-Team for all the great discussions, but also for all the fun that really makes a PHD experience memorable. I am especially grateful to Janes Krusche for his enthusiasm on bacteriophages and wall teichoic acids. I want to particularly thank Regine Stemmler, Axel Walter, Katja Schlatterer and David Gerlach for sharing their thoughts and investing their time.
Many thanks go to my family and close friends, especially to Jerry.